UNIVERSITÀ DEGLI STUDI DI PAVIA

DOTTORATO IN SCIENZE CHIMICHE E FARMACEUTICHE
XXIX CICLO

Coordinatore: Chiar.mo Prof. Mauro Freccero

SILVER NANOPARTICLES FOR ANTIBACTERIAL AND PHARMACEUTICAL APPLICATIONS

Tutore

Chiar.mo Prof. Taglietti Angelo

Tesi di Dottorato di

D'Agostino Agnese

a.a. 2015- 2016

Summary

Note to the reader: in order to make this document more easy to read, the numbering of references, figures, tables and equations is started from the beginning for every independent section (introduction, chapters 2, 3, 4). For the same reasons some repetitions (for example in the experimental sections) were needed.

CHAPTER 1: INTRODUCTION

1.1 Nanotechnology and Nanochemistry

Nanostructures are assemblies of bonded atoms that have dimensions in the range of 1 to 10^2 nanometers (1 nm = 10^{-9} m = 10 Å).[1] Structures in this range of sizes can be considered as exceptionally large, unexceptional, or exceptionally small, depending on one's viewpoint, synthetic and analytical technologies, and interests.

To solid-state physicists, materials scientists and electrical engineers, nanostructures are small. To biologists, nanostructures are familiar objects. A range of biological structures from proteins through viruses to cellular organelles have dimensions of 1-10^2 nm, **Figure 1**. To chemists, nanostructures are large. Considered as molecules, nanostructures require the assembly of groups of atoms numbering from 10^3 to 10^9 and having molecular weights of 10^4 to 10^{10} Daltons.

Developing techniques for synthesizing and characterizing well defined nanostructures has been one of the grand challenges for chemistry since 1990. Actually, nanostructures have presented major unsolved problems in complexity and have required new strategies and technologies for their synthesis and characterization. The stimulus for development and improvement of new strategies for synthesis applicable to nanostructures have so far come primarily from biology.[2]
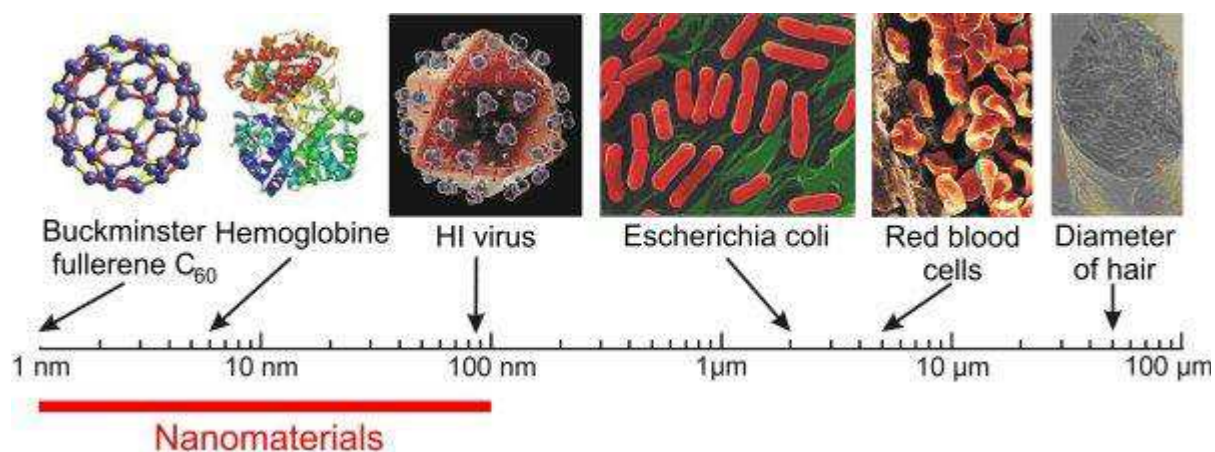
Figure 1 Nanomaterials in comparison with examples of biological entities.

Nanotechnology refers to the branch of science and engineering dedicated to materials, having dimensions in the order of one hundred of nm or less.[3] The term being new, but has been widely used for the development of more efficient technology. In recent years, Nanotechnology has been

---

[1] G.M. Whitesides, J.P. Mathias, C.T. Seto, *Science,* 1991, **254**, 1312.
[2] J.S. Lindsey, *J Chem*, 1991, **15**, 153.
[3] O. Salata, *J Nanobiotechnol.*,2004, **2**, 3.

embraced by industrial sectors due to its applications in the field of electronic storage systems,[4] biotechnology,[5] magnetic separation and preconcentration of target analytes, targeted drug delivery,[6] and vehicles for gene and drug delivery.[7,8] Consequently, with a wide range of applications available, these particles have potential to make a significant impact to the society. Although new, the history of nanomaterials dates long back to 1959, when Richard P. Feynman, a physicist at Cal Tech, forecasted the advent of nanomaterials. In one of his class he said, "There is plenty of room at the bottom," and suggested that scaling down to nanolevel and starting from the bottom was the key to future technology and advancement.[8] Inspired by Richard Feyman, professor Noro Taniguchy from Tokyo University of Science coined the term Nanotechnology in 1974.

One foremost focus of Nanochemistry up to now has consequently been to understand and use the astounding variety of sophisticated strategies and processes encountered in living systems. Nevertheless, Nanochemistry has been appreciated as a subject with very wide-ranging implications, and as one that has ultimately involved many areas: interfaces;[9] functionalization of surfaces;[10] colloid science;[11] molecular recognition;[12,13,14,15]electronics microfabrication;[16] polymer science;[17,18] electrochemistry;[19,20] zeolites and clay chemistry;[21] scanning probe microscopy.[22]

This difference in the physiochemical properties of nanomaterials can be attributed to their high surface-to-volume ratio. Due to these unique properties, they make excellent candidate for biomedical applications as a variety of biological processes occurs at nanometer scale.

At present, two main approaches are used to obtain nanostructures:

1. top-down approach: it is a physical-kind strategy and starts from macroscopic dimensioned materials, and progressively reducing them to nanometric dimensions using lithographic

[4] Y.S. Kang, S. Risbund, J.F. Rabolt, P. Stroeve, *Chem. Mater,* 1996, **8**, 2209.
[5] Q.A. Pankhurst, J. Connolly, S.K. Jones, J. Dobson, *J Phys D Appl Phys*, 2003, **36**, 167.
[6] J. Dobson, *Gene Ther*., 2006, **13**, 283.
[7] S. Rudge, C. Peterson, C. Vessely, J. Koda, S. Stevens, L. Catterall, *J Control Release*., 2001, **74**, 335.
[8] T. Appenzeller, *Science*, 1991, **254**, 1300.
[9] R. Schumacher, *Angew. Chem. Int. Ed. Engl.,*1990, **29**, 329.
[10] S. Ross ,D. Morrison, *Colloidal Systems and Interfaces* (J. Wiley and Sons, New York, 1988).
[11] J.M. Lehn, *Angew, Chem. Int. Ed. Engl.,*1990, **29**, 1304.
[12] A.N. Broerre, A.E. Timbs, R. Koch, *Microelectronic Eng*., 1989, **9**, 187.
[13] G.N. Taylor, M. Omnkaram, L.E. Stiliwagon, *Microelectronic Eng*., 1989, **9**, 513.
[14] A.N. Broers, C.P. Umbach, *J. Vac. Sol. Technol*, 1990, **8**, 1614.
[15] S.D. Berger, J.M. Gibson, *Appi. Phys. Lett*., 1990, **5**, 153.
[16] K.R. Shull, K.I. Winey, E.L. Thomas, E.J. Kramer, *Macromolecules*, 1991, **24**, 2748.
[17] R.M. Penner, M.J. Hobon, T.L. Longin, N.S. Lewis, *Science*, 1990, **250**, 1118.
[18] J.F. Rusling, *Ax. Chem. Res*., 1991, **24**, 75.
[19] G.A. Ozin, A. Kuperman, A. Stein, *Angew. Chem. Int. Ed. Engl*., 1989, **28**, 359.
[20] J.M. Basset, *Angew. Chemn. Int. Ed. Engl.*, 1990, **29**, 805.
[21] K. Kern, *Phys. Rev. Lett*., 1991, **67**, 855.
[22] A. Moel, M.L. Schaftenburg, J.M. Carter, H.L. Smith, *J. Vac. Sal.Technol*., 1990, **138**, 1648.

technologies. With the top-down approach objects' arrays on planar structures can be easily obtained.

2. bottom-up approach: it is a chemical-kind strategy and allows to work in solution to obtain particles with control over shape and dimensions. The bottom up approach relies on interaction between atoms and on the reaction kinetics. It can be used to obtain both spherical and anisotropic clusters.

Approaches to nanostructures based on chemical synthesis are getting exceedingly because this kind of synthesis offers the appeal of a level of control over the selection and placement of individual atoms that is ultimately much higher than that achievable by other methods of fabrication. This increased control over individual nanostructures is accepted at the cost of augmented difficulty in building regular arrays of nanostructures of the type required in microelectronic systems.

Chemical-kind strategy not only used the covalent bond as a required connection between atoms, but also adopt weaker and less directional bonds: ionic bonds, hydrogen bonds, van der Waals interactions to organize atoms, ions, or molecules into structures. Generally accepted name to describe this class of methods is "self-organizing syntheses". Molecular crystals,[23,24,25] liquid crystals,[26] colloids,[27] micelles,[28] emulsions,[29] and self-assembly monolayers[30,31] correspond to examples of types of structures prepared using these techniques. The distinguishing aspect of these methods is self-organization. The molecules or ions adjust their own positions to reach a thermodynamic minimum; the chemist does not specify these positions. Certain of the structures prepared by self-organization are true nanostructures, and they will eventually be incorporated into nanostructure technology.

However one most relevant, to nanostructures, is molecular self-assembly: that is, the spontaneous assembly of molecules into structured, stable, non-covalently joined aggregates.[32] Molecular self-assembly combines features of well-defined molecules of intermediate structural complexity using sequential covalent synthesis; formation of large, stable structurally defined

---

[23] J.D. Wright, *Molecular Crystals* (Cambridge University Press, Cambride, 1987).
[24] ,G.R. Desiraju, *Organic Solids State Chemistry*, (Ed. Elsevier, Amsterdam, 1987).
[25] G.R. Deslraju, *Crystal Engineering: The Design of Organic Solids* (Elsevier, Amsterdam, 1989).
[26] P.J. Coilings, *Liquid Crystals: Nature's Delicate Phase of Matter* (Princeton University Press, New Jersey, 1990).
[27] LE. Brus, *J. Am. Chem. Soc.*, 1990, **112**, 1327.
[28] W.G. Miller, *J. Colloid Interface Sol.*, 1991, **142**, 74.
[29] K. Shinoda, S. Friberg, *Emulsions and Solubilization* (J. Wiley and Sons, New York, 1986).
[30] G.M. Whitesides, *J. Am. Chem. Soc.*, 1989, **111**, 321.
[31] G.M. Whitesides, P.E. Laibinla, *Langmuir*, 1990, **6**, 87.
[32] A. Ulman, *Chem. Rev.*, 1996, **96**, 1533.

aggregates of these molecules using hydrogen bonds, van der Waals interactions, or other non-covalent links; use of multiple copies of one or several of the constituent molecules, or of a polymer, to simplify the synthetic task to make large, structurally well-defined assemblies of atoms. The key to this type of synthesis is to recognize and control the non-covalent interactions between molecules, and to understand and defeat the intrinsically unfavorable entropy involved in bringing many molecules together in a single aggregate. Biology is replete with examples of complex, nanoscale structures formed by self-assembly[33] and living systems have mastered the art of summing many intermolecular interactions rather than covalent between chemical entities to make large ones.

Nanoparticles can be divided in two main groups: organic and inorganic nanoparticles. The former include carbon nanoparticles (fullerenes, polymeric nanoparticles, solid lipid nanoparticles), while the latter includes magnetic nanoparticles, semiconductor nanoparticles, such as titanium dioxide and zinc oxide, and noble metal nanoparticles.

1.1.2 Metallic Nanoparticles

What is fascinating about nanoparticles is that they exhibit completely new or improved properties compared to larger particles of the bulk material and these novel properties are derived due to the variation in specific characteristics such as size, distribution and morphology of the particles. Out of all kinds of nanoparticles, the metallic nanoparticles, including gold, silver, iron, zinc and metal oxide nanoparticles, have shown great promise in terms of biomedical applications, not only due to their large surface area to volume ratio[34] but also because they exhibit different biomedical activities.[35] Moreover, metal nanostructures have been the focus of intensive research in the past several decades due to their potential application in fabricating electronic, optical, optoelectronic, and magnetic devices that may exhibit performance complementary and/or superior to their bulk counterparts.[36] The intrinsic properties of a metal nanostructure can be tailored by controlling its size, shape, composition, and crystallinity.

For these reasons, in recent years Nanotechnology has used metallic nanoparticles in numerous applications in science and technology for the purpose of manufacturing new materials, to be used

[33] B. Alberts, *Molecular Biology of the Cell* (Garland Publishing, New York, ed. 2, 1989).
[34] S.M. Hirst, A.S. Karakoti, R.D. Tyler, N. Sriranganathan, S. Seal, C.M. Reilly, *Small*, 2009, **5**, 2848.
[35] S. Hussain, C. Ferguson, *Emerg. Med. J.*, 2006, **23**, 929.
[36] M.A. Albrecht, C.W. Evans, C.L. Raston, *Green Chem.*, 2006, **8**, 417.

for drug delivery methods,[37] chemical deposition for environmental pollution cleanup,[38] medical imaging,[39] as well as military purposes,[36] just to name a few.

More generally, this type of nanostructure may provide solutions to technological and environmental challenges in the areas of solar energy conversion, catalysis, medicine, and water-treatment, and have a wide range of applications, as in combating microbes,[40] biolabelling,[41] and in the treatment of cancer.[42] Specific surface area is relevant for catalytic activity and properties such as antimicrobial activity.[43]

Generally, the chemical growth of metallic nanometer-sized materials involves the crystallization of a solid phase from a solution. For a particular solvent, there is certain solubility for a solute, whereby addition of any excess solute will result in formation of nanocrystals: this step is called nucleation. So, for nucleation to occur, the solution must be supersaturated: this can be obtained either by directly dissolving the solute at high temperature and then cooling to low temperatures[44] or by adding the necessary reactants to produce a supersaturated solution during the reaction.[45] There are three kind of nucleation: (i) homogeneous nucleation, (ii) heterogeneous nucleation, (iii) secondary nucleation.

Homogeneous nucleation occurs in the absence of a solid interface by combining solute molecules to give nuclei: the driving force is the thermodynamics of the process, in fact the super-saturated solution is not stable in energy. The overall free energy variation is the sum of the free energy due to the formation of a new volume (favorable contribution) and the free energy due to the new surface created (unfavorable contribution).

For spherical particles:

$$\Delta G = -\frac{4}{V}\pi^3 k_B T ln(S) + 4\pi r^2 \gamma$$

where V is the volume of the crystallized species, r is the radius of the nuclei, K_B is the Boltzmann constant, S is the saturation ratio and γ is the surface free energy per unit area. When S > 1, ΔG has a maximum at the critical size r*. This maximum free energy is the activation energy for nucleation, **Figure 2**.

[37] S.V. Vinogradov, *Nanomedicine*, 2010, **5**, 165.

[38] M. Kumar, Y. Ando, *Journal of Nanoscience and Nanotechnology*, 2010, **10**, 3739.

[39] M.S. Muthu, B. Wilson, *Nanomedicine*, 2010, **5**, 169.

[40] F. Furno, K.S. Morley, B. Wong, B.L. Sharp, P.L. Arnold, S.M. Howdle, *J Antimicrob Chemother*, 2004, **54**, 1019.

[41] S. Schultz, D.R. Smith, J.J. Mock, D.A Schultz, *Proc Natl Acad Sci U S A*, 2000, **97**, 996.

[42] S. Gurunathan, K.J. Lee, K. Kalishwararal, S. Sheikpranbabu, R. Vaidyanathan, S.H. Eom, *Biomaterials*, 2009, **30**, 6341.

[43] A. Ivask, A. ElBadawy, C. Kaweeteerawat, D. Boren, H. Fischer, Z. Ji, C.H. Chang, R. Liu, T. Tolaymat, D. Telesca, J.I. Zink, Y. Cohen, P.A. Holden, H.A. Godwin, *ACS Nano*, 2014, **8**, 374.

[44] J. Turkevitch ,P.C. Stevenson, J. Hillier, *Discuss. Faraday Soc.*,1951, **11**, 55.

[45] C.B. Murray, C.R. Kagan, M.G. Bawendi, *Annu. Rev. Mater. Sci.,* 2000, **30**, 545.
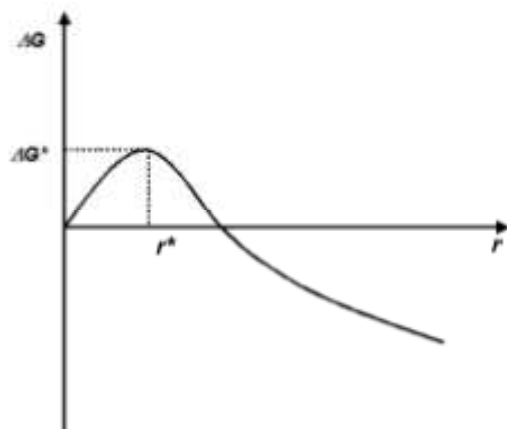
Figure 2 Illustration of the overall free energy ΔG as a function of the growth particle size r.[46]

The critical nuclei size r* can be obtained by setting dΔG/dr = 0.

For a given value of S, all particles with r > r* will grow and all particles with r < r* will dissolve. The higher is the saturation ratio the smaller the critical nuclei size r* is. Homogeneous nucleation continues until the concentration of the reactants drops below the critical level.

Heterogeneous nucleation occurs, with the addition of new material on the pre-formed nuclei. At this stage, the smaller particles grow more rapidly than the larger ones because the free energy driving force is larger for smaller particles than for larger particles, so focusing in size occurs. However, continuing with the reaction, the saturation ratio decreases and consequently r* increases. At this stage the larger particles continue to grow and the smaller one get smaller and finally dissolve: this is the so called "Ostwald ripening" (or defocusing). Once the reaction goes into this stage it is difficult to get monodisperse particles. From an experimental point of view, to obtain monodisperse samples it is necessary either to quickly interrupt the process of growth (for example decreasing temperature) or to provide reactants continuously so to maintain saturation regime during all the reaction.

In addition particles can grow by aggregation with other particles: this process is called secondary growth.

On the other hand, secondary growth is the most important cause of thermodynamic instability in colloidal solution (the rate of particle growth by aggregation is much larger than that by molecular addition). In order to produce stable nanoparticles, usually the synthetic step is followed by a functionalization step (for example by introduction of a protective agent) to stabilize the

---

[46] C. Burda, X. Chen, R. Narayanan, M.A El-Sayed, *Chem. Rev.,* 2005, **105**, 1025.

nanoparticles' surface. Sometimes a protective, "capping" agent can be introduced directly in the synthetic step.[47]

1.2 Silver Nanoparticles (AgNPs)[34,35,36]

Humans have known about the medicinal properties of silver for thousands of years, going back at least as far as ancient Greece, when Hippocrates used the precious metal to heal his patients' wounds and treat their illnesses. In addition, the use of silver plates or vessels dates back from ancient Mesopotamia, or around 2500 B.C., and cultures around the world boast their own long traditions of finely crafted silver utensils. The widespread appearance of silver cooking and eating utensils on the dining tables of history's wealthier classes has spawned more than one idiomatic expression. In the early 19th century, the description "born with a silver spoon in one's mouth" was coined to refer to someone born into wealth and privilege. In fact, the precious metal has been used to treat ailments ranging from skin ulcers to bad breath, as well as to preserve liquids and purify water. The ingestion of too much silver is known to cause a condition called argyria, which turns the skin a blue-gray color permanently. As well-to-do families throughout history have undoubtedly ingested some of the previous metal along with their food and drink, the fact that argyria was typically more common among the upper classes may explain the origins of the term "blue bloods." In classical photography, film is covered with silver compounds, or halides, which set when exposed to light, revealing the captured image. Though it's relatively expensive, a satisfactory substitute has never been found. Until the recent introduction of digital cameras, the use of silver-based film had steadily increased since the early development of photography in the early to mid-19th century. Furthermore, silver has the highest degree of reflectivity of all the elements, and is able to reflect up to 95 percent of visible light. For this reason, it is used extensively in mirrors and other reflective surfaces, including solar panels designed to deflect external heat from the sun in order to maintain internal temperatures. Silver is also often incorporated into automobile windshields and sunglasses, in order to moderate glare.

However, after the 1940s, when doctors began using anti-bacterial drug agents, the medicinal use of silver largely declined, until the 1990's, when there has been a resurgence of the promotion of silver, as a colloidal suspension, as an alternative medicine treatment because of development of microbial resistance towards drugs.

---

[47] M. Benkovičová, K Vegso, P. Siffalovic, M. Jergel, E. Majova, S Luby, A. Sata, *Chemical Papers,* 2013, **67**, 1225.

In particular, the next major milestone for silver has been the engineering of silver nanoparticles (AgNPs). These nanoparticles have multiple functions and have been used in various consumer products such as water purifiers, laundry detergents, and textiles. Extensive research and development has been done to create marketable medical products that utilize the antimicrobial properties of silver nanoparticles in many applications.

As it depends from surface properties, also the biocidal activity of AgNPs will be influenced by their size, shape, and surface coatings. Therefore, the development of AgNPs with well-controlled morphological and physicochemical features for physiological application in humans is necessary to expand their biomedical applications.

1.2.1 Synthesis of AgNPs

The size and shape of nanostructures define and control their unique properties. Many routes have been introduced for the synthesis of silver nanostructures in order to obtain AgNPs with well-controlled morphologies, which can be categorized as: (i) chemical methods;[48] (ii) physical methods;[49] (iii) biological methods.[50]

Chemical methods for the synthesis of AgNPs can be subdivided into chemical reduction,[48] electrochemical techniques,[51] irradiation-assisted chemical methods,[52] and pyrolysis.[53] Synthetic approaches that used chemical reduction in solution usually employ three main components: metal precursors, reducing agents, and stabilizing/capping agents. In this way it is possible to generate elemental Ag from a precursor, the most commonly is silver nitrate $AgNO_3$, and consequently product Ag nanostructures. If we want to synthesize Ag nanostructures with different size and shape, we can mix the Ag precursor with a reducing agent and a colloidal stabilizer under proper conditions. Typically, sodium borohydride, alcohols, sodium citrate, ascorbic acid and hydrazine compounds are used as chemical reducing agents: they reduce the dissolved Ag ions to Ag atoms which grow into small clusters and then nanostructures.[54] In order to stabilize the Ag nanostructures during and after formation, polymers and surfactants are used. In addition, these stabilizers can also play the role to direct particle growth to the desired shapes.

[48] Q. Zhang, N. Li, J. Goebl, Z. Lu, Y. Yin, *J. Am. Chem. Soc.,* 2011, **133**, 18931.
[49] P. Asanithi, S. Chaiyakun, P. Limsuwan, *J. Nanomater.*, 2012, **10**, 96360.
[50] S. Shivaji, S. Madhu, S. Singh, *Process. Biochem.*, 2011, **46**, 1800.
[51] M.V. Roldan, N. Pellegri, O. de Sancti, *J. Nanopart.*, 2013, **10**, 524150.
[52] G.A. Sotiriou, S.E. Pratsinis, *Environ. Sci. Technol.*, 2010, **44**, 5649.
[53] G.A. Sotiriou, A. Teleki, A. Camenzind, F. Krumeich, A. Meyer, S. Panke, S.E. Pratsinis, *Chem. Eng. J.*, 2011, **170**, 547.
[54] C. Yee, M. Scotti, A. Ulman, H. White, M. Rafailovich, J. Sokolov, *Langmuir*, 1999, **15**, 4313.

By contrast, physical methods do not involve toxic chemicals and usually have fast processing time. Such methods include physical vapor condensation,[55] arc-discharge,[56] and direct current (DC) magnetron sputtering.[49] Another advantage of physical methods is that the AgNPs formed have a narrow size distribution;[49] however, a major drawback is their high energy consumption.

In the biological synthesis of AgNPs, the toxic reducing agents and stabilizers are replaced by nontoxic molecules (proteins, carbohydrates, antioxidants, etc.) produced by living organisms, including bacteria, fungi, yeasts, and plants. Biological methods based on microorganisms such as bacteria,[50] fungi,[57] and yeast,[58] have been widely reported. The possible mechanisms of biological synthesis include enzymatic (e.g., NADPH reductase) and nonenzymatic reduction.[59] In general, AgNPs synthesis using plant extracts is the most-used environmentally friendly method of production.

Among chemical reduction approaches, the following method synthesis are the most common.

Citrate reduction

In 1982, Lee and Meisel[60] first reported the synthesis of Ag colloids by reducing $AgNO_3$ with citrate in aqueous solution. This method does not require extensive synthetic laboratory skills, so remains a popular approach to quickly generating Ag colloids. In a typical synthesis, Ag nanoparticles are obtained by adding a set amount of aqueous sodium citrate into a boiling aqueous solution of silver nitrate and waiting for one hour before cooling down the system. The citrate ions serve as both a reducing agent and stabilizer and they may also complex with Ag^+ ions and/or Ag_2^+ dimers in the early stages of the reaction.[61] Even if the process is simple, this synthetic approach tends to produce a very large variety of sizes, from 20 nm until 600 nm, and diversity of shapes, polyhedrons and plates in a single reaction. There are a small number of studies about the mechanism of the citrate reduction reaction. However, thanks to the investigation with ^{1}H NMR of oxidation and decomposition of citrate, the reaction pathway has been observed:[61] typically citrate is oxidized into acetonedicarboxylate, a transitory intermediate, which then decomposes rapidly into acetoacetate. During the reaction formate and/or CO_2 are released as byproducts. A

[55] M.M. Kholoud, A. Eftaiha, A. Al-Warthan, *Arab. J. Chem.*, 2010, **3**, 135.
[56] D.Tiena, K.H. Tsengb, C.Y. Liaob, J.C. Huangb, T.T. Tsung, *J. Alloys Compd.*,2008, **463**, 408.
[57] G. Li, D. He, Y. Qian, B. Guan, S. Gao, Y. Cui, K. Yokoyama, L. Wang, *Int. J. Mol. Sci.*, 2012, **13**, 466.
[58] A. Mourato, M. Gadanho, A.R. Lino, R. Tenreiro, *Bioinorg. Chem. Appl.*, 2011, 546074.
[59] L. Ge, Q. Li, M. Wang, J. Ouyang, X. Li, M. Xing, *Int. J. Nanomed.*, 2014, **9**, 2399.
[60] P.C. Lee, D. Meisel, *J. Phys. Chem.*, 1982, **86**, 339.
[61] Z.S. Pillai, P.V. Kamat, *J. Phys. Chem. B,* 2004, **108**, 945.

few shape-control approaches have been reported by changing the pH of this solution due to the different protonation states associated with citrate ion:[61,62] the reduction rate and consequently the particle morphology depended on the pH of the solution. The reaction was slow, about 2 hours, and the product was primarily triangular plates or polygonal particles at a value of pH lower than six, whereas at higher values of pH, higher than ten, the reaction was complete in a few minutes, and the product was a mixture of spherical and rodlike particles.[63] It has also been demonstrated that it is possible to give a predominant product by adding a small amounts of NaOH during the synthesis, so that pH was increased from 5.5 to 6.5, which is just above the pK_{a3} of citrate ion (6.4). In this way citrate ions were primarily deprotonated and could coordinate to Ag^+ ions more strongly, resulting in a higher-quality product with fewer random aggregates.

Silver mirror reaction

Since the invention of silvered glass mirror by Justus von Liebig[64] in 1835, the Ag mirror reaction has become a popular method for chemical deposition and mass production of Ag coatings on various types of substrates. In this reaction, $AgNO_3$ is used as a precursor to form the Tollens' reagent, $Ag(NH_3)_2OH$, which is subsequently reduced by a sugar (e.g., glucose) or an aldehyde-containing compound to generate elemental Ag:

$$RCHO + 2[Ag(NH_3)_2]^+ + 2OH^- \rightarrow RCOOH + 2Ag + 4NH_3 + H_2O$$
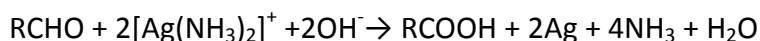
When the reaction is successful, it produces a shiny mirror. Because the reaction can quickly generate a shiny coating on the inner surface of a reaction container (e.g., a test tube), it serves as a popular demonstration of redox reactions and a detection method for aldehyde groups in classrooms.[65] It is also possible to perform the Ag mirror reaction with commercial silvering solutions under sonication to generate stable suspensions of quasi-spherical Ag nanoparticles with a relatively narrow size distribution. However, no shape control has been demonstrated with this technique, limiting its use in the synthesis of high-quality Ag nanostructures. Nevertheless, the Ag mirror reaction is still finding use in a number of applications, including the coating of large objects such as telescopes, the formulation of different types of Ag coating, and the fabrication of smooth micro- or nanostructured Ag surfaces.[66] For example, the reaction has been adapted to prepare Ag

[62] A. Henglein, M. Giersig, *J. Phys. Chem. B*, 1999, **103**, 9533.
[63] X. Dong, X. Ji, H. Wu, L. Zhao, J. Li, W. Yang, *J. Phys. Chem.C*, 2009, **113**, 6573.
[64] L. Justus, *Ann. Chem. Pharm.*, 1856, **98**, 132.
[65] M. Kemp, *J. Chem. Educ.*, 1981, **58**, 655.
[66] L. Shen, J. Ji, J. Shen, *Langmuir*, 2008, **24**, 9962.

alloyed thin films for conventional SPR sensing, as well as smooth films of Ag for use with microcontact printing of alkanethiols.[67] The morphology of these films is typically granular, and as a result, different microstructures and micropatterns, such as leaf or flowerlike fractal structures, can also be created.[68] It is also practical to use the Ag mirror reaction to coat a variety of micro and nanoscale objects with small particles or continuous thin films of Ag, including fiber optic probes, silica beads, polymer capsules, and semiconductor particles for photocatalytic applications.[69]

Polyol process

The polyol process represents a robust and versatile method for generating Ag nanostructures with a wide variety of sizes and shapes.[70] By varying the reaction conditions, such as temperature, reagent concentration, and presence of trace ions, it is possible to achieve a high degree of control over both nucleation and growth and thus the final products. In a typical synthesis, a polyol, such as ethylene glycol, 1,2-propylene glycol, or 1,5-pentanediol, serves as both a solvent and a reducing agent.[71] A capping agent and a Ag precursor are injected into a preheated polyol, and the reduction of Ag^+ ions results in the nucleation and growth of Ag nanostructures. By having a separate reductant and a capping agent, it is possible to have a tighter control over the reaction than is possible in the only citrate-based synthesis. The details of the reduction mechanism have recently been studied for the system based on ethylene glycol.[72] Even if ethylene glycol alone can reduce a typical Ag precursor at an elevated temperature, upon closer investigation the primary reducing agent was found to be glycoaldehyde. This compound forms when ethylene glycol is heated in the presence of oxygen (typically from air). The significant reaction is

$$2HOCH_2CH_2OH + O_2 \rightarrow 2HOCH_2CHO + 2H_2O$$
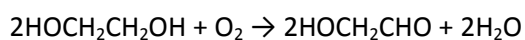
Glycoaldehyde, a stronger reductant than ethylene glycol, is considered to be responsible for the polyol reduction. To confirm the involvement of glycoaldehyde in the reaction, a spectroscopic method has been developed to measure the amount of this intermediate compound by converting glycoaldehyde to glyoxal bis-2,4-dinitrophenylhydrazone, which strongly absorbs light at 570 nm.[72] When oxygen- or air-saturated ethylene glycol was heated at 150 C for 1 h, a clear peak developed

[67] Y. Xia, N. Venkateswaran, D. Qin, J. Tien, G.M. Whitesides, *Langmuir*, 1998, **14**, 363.
[68] L. Qu, L.J. Dai, *Phys. Chem. B*, 2005, **109**, 13985.
[69] S.Q. Wang, H. Zhao, Y. Wang, C.M. Li, Z.H. Chen, V. Paulose, *Appl. Phys. B: Lasers Opt.*, 2008, **92**, 49.
[70] Y. Xia, Y. Xiong, B Lim, S.E. Skrabalak, *Angew. Chem. Int. Ed.*, 2009, **48**, 60.
[71] Y. Sun, Y. Xia, *Science*, 2002, **298**, 2176.
[72] S.E Skrabalak, B.J. Wiley, M. Kim, E. Formo, Y. Xia, *Nano Lett.*, 2008, **8**, 2077.

at this wavelength. When argon-saturated ethylene glycol was tested, however, no such peak was observed. Additionally, the amount of glycoaldehyde present decreased slightly when AgNO$_3$ was added, although the details of this reaction are complicated by the catalytic abilities of Ag nanoparticles.[72] In comparison with the Ag mirror reaction, the polyol process uses a similar reduction scheme but proceeds with a much lower but stable concentration of reductant due to the fact that glycoaldehyde is consumed immediately after its formation. The identification of glycoaldehyde as a reducing agent helps explain the strong temperature dependence of the polyol process. A temperature difference of <5°C can determine the success or failure of a reaction, making precise temperature control critical for achieving good reproducibility. According to this spectroscopic study, the amount of glycoaldehyde increased significantly as the temperature for preheating ethylene glycol was increased from 140 to 160°C. This sensitivity has a great impact on the reduction kinetics of a polyol system and, consequently, the product morphology.

1.2.2 Optical Properties

The intense colors of metal colloids in the visible (Vis) and near infrared regions (NIR) range for Au, Ag and Cu, Li and Al have been very attractive to both researchers and artists.[73] This peculiar feature arises from an optical phenomenon called surface plasmons resonance.[74]

For example, gold colloidal nanoparticles are responsible for the brilliant reds seen in stained glass windows, on the other hand colloidal suspensions of spherical AgNPs are typically yellow. These properties have been of interest for centuries, and scientific research on metal nanoparticles dates at least to Michael Faraday, who was the first that gave a demonstration of this phenomenon in 1857.[75]

It was one of the great triumphs of classical physics when, in 1908, Mie presented a solution to Maxwell's equations[76] that describes the extinction spectra, scattering and absorption of spherical particles of arbitrary size.[77] His theory does an excellent job of predicting the optical properties of spherical particles, spheroids, and infinite cylinders. One of the reasons why Mie's theory has remained important for so long is that it is the only simple, exact solution to Maxwell's equations

[73] P. Mulvaney, *MRS Bull.*, 2001, **26**, 1009.
[74] C. Burda, X. Chen, R. Narayanan, M.A. El-Sayed, *Chem. Rev.,* 2005, **105**, 1025.
[75] M. Faraday,. Philos. *Trans. R. Soc. London*, 1857, **147**, 145.
[76] Maxwell JC., *A treatise on electricity and magnetism*, (Oxford, Clarendon Press 1873).
[77] G. Mie, *Ann Phys*, 1908, **25**, 377.

that is relevant to particles. In addition, most of the standard colloidal preparations yield particles that are approximately spherical, and most of the optical methods for characterizing nanoparticle spectra probe a large ensemble of these particles. This leads to results that can be modeled reasonably well using Mie theory.

The localized surface plasmon resonance of a nanoparticle is responsible for its ability to strongly absorb and scatter light at specific wavelengths.

Plasmonic is related to the localization, guiding, and manipulation of electromagnetic waves beyond the diffraction limit and down to the nanometer-length scale.[78] The key component of a plasmonic phenomenon is a metal, because it is able to support surface plasmon resonances (SPR), which are electromagnetic waves coupled to the collective oscillation of free electron of metal.

When a small spherical metallic nanoparticle is irradiated by light, the oscillating electric field causes the conduction electrons to oscillate coherently. This is schematically illustrated in **Figure 3**.
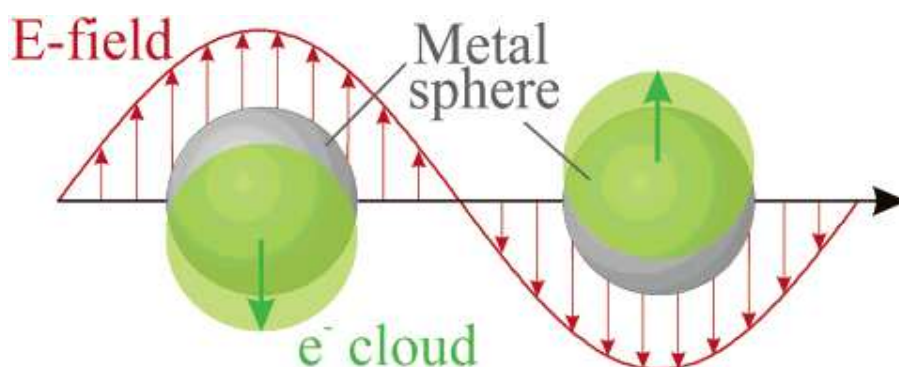
Figure 3 Schematic of plasmon oscillation for a sphere, showing the displacement of the conduction electron charge cloud relative to the nuclei.[79]

When the electron cloud is displaced relatively to the nuclei, a restoring force comes from Coulomb attraction between electrons and nuclei that result in oscillation of the electron cloud relative to the nuclear framework. The oscillation frequency is determined by four factors: the density of electrons, the effective electron mass, and the shape and size of the charge distribution. When this excitation is confined in a nanoparticle, the phenomenon is called localized surface plasmon resonance (LSPR). LSPR can occur only when the incident light can induce a dipole on the surface of the nanoparticle and this is verified only when the particles are smaller than the wavelength of the incident light. These plasmon resonances give rise to surface plasmon

---

[78] D.K. Gramotnev, S.I. Bozhevolnyi, *Nat. Photonics*, 2010, **4**, 83.
[79] K.L. Kelly, E. Coronado, L.L. Zhao, G.C. Schatz, *J. Phys. Chem. B*, 2003, **107**, 668.

absorption bands which, in the case of silver, can be found in the range between 300 and 1200 nm.

Thus, the peaks that define the extinction spectrum of a particular metallic nanoparticle depend on a number of factors, including the size, shape, and dielectric environment of the nanoparticle.[80] For example, if we consider silver nanospheres of less than 40 nm in diameter, this extinction peak is located at ~410 nm, leading to a characteristic yellow color for silver colloids as primarily blue light is absorbed, as reported in **Figure 4**. The sensitivity of the SPR peak position to small changes in the dielectric environment has enabled their use as detectors for low concentrations of biologically interesting molecules.[74]
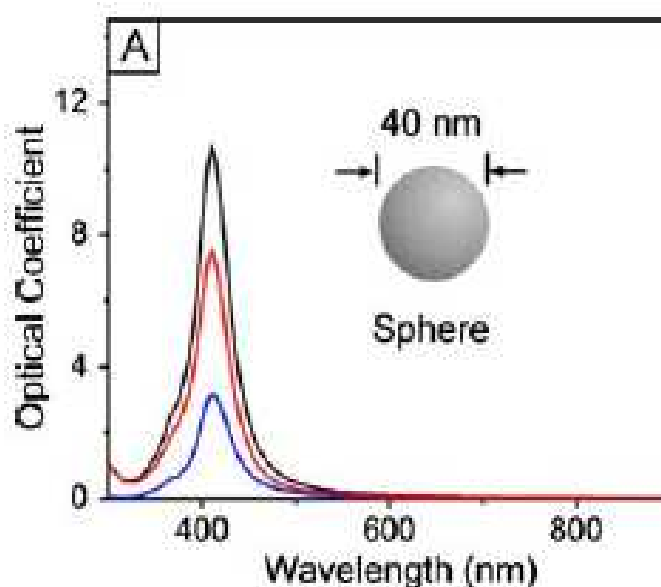
Figure 4 Mie theory was used to calculate the optical response of silver nanoparticles in different shapes in water. Absorption is shown in red, scattering in blue, and extinction in black.[81]

In addition to LSPR effects such as light absorption and scattering, the near-field effects produced close to the surface of particles also have interesting applications. For example, the enhanced electric field around a metal nanoparticle can drastically increase weak Raman signals, even enabling single molecule detection.[82] Silver is especially attractive for surface plasmon applications due to its large enhancement of near fields, in which this enhancement can be an order of

[80] U. Kreibig, M. Vollmer M, *Optical properties of metal clusters*, (Springer, Berlin 1995)
[81] C.M. Cobley, S.E. Skrabalak, D.J. Campbell, Y. Xia, *Plasmonics*, 2009, **4**, 171.
[82] Y.C. Cao, R. Jin, C.A. Mirkin, *Science*, 2002, **297**, 1536.

magnitude greater than what is possible with similar gold nanoparticles.[83] The signal enhancement provided by silver nanoparticles is most pronounced when the LSPR is excited by the incident light under a resonant condition. As a result, there is a strong desire to synthesize silver nanoparticles with specific LSPR properties. Though changing the size of spherical particles can induce small shifts in the LSPR peak position, in theory and in practice, changing the shape of silver nanoparticles provides more versatility. As any change in the shape of the metal particle affects the pattern in which the free electrons are oscillating, the resonant frequencies will change.[80] Control over the size and shape of metal nanoparticles can be achieved also with lithographic methods; however, such techniques are of limited use because of their intrinsic drawbacks such as high costs, poor scalability, and the polycrystallinity of metals deposited by physical or chemical means. Colloidal synthesis, on the other hand, is far less expensive and is capable of providing access to single-crystal nanoparticles in a wide variety of shapes.[84]

1.2.3 Surface Enhanced Raman Scattering

In the 70s of twentieth century, it was discovered that Raman signals could be enhanced at the rough surface of a silver electrode.[85] Since that moment, Surface Enhanced Raman Scattering, SERS, has become a subject of interest in the detection of different kind of species, chemical[86] and biological,[87] for molecular imaging and monitoring of microorganisms,[88] cells,[89] tissues,[90] even for *in vivo* applications.[91] This is due to its high sensitivity, to the intrinsic selectivity given by the spectroscopic fingerprint, to the simple and fast preparation of samples, and, in addition, to the possibility of non-destructive data acquisition.

The enhancement is generally attributed to the electromagnetic field in the proximity of nanostructured metal surfaces.[86]

---

[83] M. Quinten, *Appl Phys B*, 2001, **73**, 245.
[84] B.J. Wiley, Y. Sun, Y. Xia, *Acc Chem Res* , 2007, **40**, 1067.
[85] M. Fleischm., P.J. Hendra, *Chem. Phys. Lett.*, 1974, **26**, 163.
[86] H.B. Zhou, Z.P. Zhang, C.L. Jiang, G.J. Guan, K. Zhang, Q.S. Mei, R.Y. Liu, S.H. Wang, *Anal. Chem.*, 2011, **83**, 6913.
[87] S. Schlucker, *Chemphyschem*, 2009, **10**, 1344.
[88] S. Preciado-Flores, D.A. Wheeler, T.M. Tran, Z. Tanaka, C.Y. Jiang, M. Barboza-Flores, F. Qian, Y. Li, B. Chen, J.Z. Zhang, *Chem. Commun.*, 2011, **47**, 4129.
[89] K.A. Willets, *Anal. Bioanal. Chem.*, 2009, **394**, 85.
[90] L. Sun, K.B. Sung, C. Dentinger, B. Lutz, L. Nguyen, J.W. Zhang, H.Y. Qin, M. Yamakawa, M.Q. Cao, Y. Lu, A.J. Chmura, J. Zhu, X. Su, A.A Berlin, S. Chan, B. Knudsen, *Nano Lett.*, 2007, **7**, 351.
[91] X.M. Qian, X.H. Peng, D.O. Ansari, Q. Yin-Goen, G.Z. Chen, D.M. Shin, L. Yan, A.N. Young, M.D. Wang, S.M. Nie, *Nat. Biotechnol.*, 2008, **26**, 83.

In fact, the Raman effect can be dramatically enhanced if a molecule is attached to or in the immediate proximity of noble metallic (Au, Ag and Cu) surfaces, such as metal colloids[92] consisting of spherical particles, plates, prisms,[93] and stars.[94] These novel SERS active substrates can provide an enhancement factor in the range of 10^3 - 10^6 and, under certain conditions, even up to 10^{15} , allowing to detect single molecules,[95] for different chemical species. The sensitivity of SERS has caused large efforts for the synthesis and fabrication of new and different metallic nanostructures. Two possible mechanisms have been individuated, contributing to the total enhancement in SERS:[96]

1) the electromagnetic enhancement, that arises due to LSPR modes, which can focus light into nanosized volumes, drastically increasing the electromagnetic field intensity near the nanoparticle;

2) the chemical enhancement, which is thought to arise from interactions between the molecule and the nanoparticle as a result of changes to the molecular electronic states. This leads to resonant enhancement from molecular excitations or charge transfers between the molecule and the nanoparticles.

The enhancement obtained with SERS can be quantified and compared with a normal Raman response by calculating the so called Enhancement Factor (EF): there are at least three important and representative definitions of EF.

The Single Molecule Enhancement Factor.

This is the SERS enhancement felt by a given molecule at a specific point. It is, in general, dependent upon the Raman tensor of the probe and its orientation on the SERS substrate and with respect to the local field at that point. It is also dependent upon the orientation of the SERS substrate with respect to the incident laser polarization and direction. Hence, it requires the exact definition of the SERS substrate geometry and the exact position and orientation of the probe on it. Because of these constraints, this definition is much more suited to theoretical estimations of the EF, rather than experimental measurements.

[92] S.E. Bell, N.M.S, Sirimuthu, *J. Am. Chem. Soc.*, 2006, **128**, 15580.
[93] Y. Xia, H.P. Xiao, *J. Raman. Spectrosc*, 2012, **43**, 469.
[94] L. Osinkina, T. Lohmuller, F. Jackel, J. Feldmann, *J. Phys. Chem. C*, 2013, **117**, 22198.
[95] S.M. Nie, S.R. Emery, *Science*, 1997, **275**, 1102.
[96] J.R. Lombardi, R:L. Birke, *Acc. Chem. Res.*, 2009, **42**, 734.

$$SMEF = \frac{I_{SERS}^{SM}}{\langle I_{RS}^{SM} \rangle}$$

where numerator is the SERS intensity of the single molecule (SM) under consideration, whereas denominator is the average Raman intensity per molecule for the same probe. It can be shown that the SMEF defined can be expressed as a ratio of SERS over non-SERS differential cross-sections.

The SERS Substrate Point of View.

For many SERS applications and experiments, the detailed distribution of the SMEF on the substrate, or even its maximum value, is irrelevant because one is mainly dealing with average SERS signals. It is, therefore, equally important to define one or more SERS substrate enhancement factors, which can be used to compare the average SERS enhancements across different substrates. In fact, most studies of SERS EFs, so far, have indeed focused on this aspect. The most widely used definition for the average SERS EF is equation:[97]

$$EF = \frac{I_{SERS}/N_{Surf}}{I_{RS}/N_{Vol}}$$

where N_{Vol} is the average number of molecules in the scattering volume (Vol) for the Raman (non-SERS) measurement, and N_{Surf} is the average number of adsorbed molecules in the scattering volume for the SERS experiments. This is normally taken as representative of a substrate.

The Analytical ChemistryPerspective.

The definitions introduced so far SMEF and SSEF have attempted to emphasize the intrinsic characteristics of the substrate and are not always straightforward for relating to experimental results. For many applications, however, one is mostly concerned with the simple question of how much more signal can be expected. These two components are often treated as independently contributing to the overall effect, with the implication that by properly choosing the experimental parameters, one or more can be ignored. However, the varying experimental conditions can

---

[97] J.A. Dieringer, A.D. McFarland, N.C. Shah, D.A. Stuart, A.V. Whitney, C.R. Yonzon, M.A. Young, X. Zhang, R.P.V. Duyne, *Faraday Discuss.*, 2006, **132**, 9.

influence the relative degree of each enhancement effect and the total enhancement factor. In general, higher enhancement can often be obtained by combining two or more resonances. Each resonance contributes a part of effect on the appearance of the resulting Raman spectrum, and it is necessary to invoke one or more of these resonances to completely describe a particular experiment. On the other hand, it is hard to completely describe all observations of the SERS phenomenon with consideration of all two of these contributions.

For this reason, it has been introduced another definition of the EF, which is fairly intuitive and particularly relevant for analytical chemistry applications. Let us consider an analyte solution with concentration c_{SERS}, which produces a Raman signal I_{RS} under non-SERS conditions. Under identical experimental conditions (laser wavelength, laser power, microscope objective or lenses, spectrometer, etc.), and for the same preparation conditions, the same analyte on a SERS substrate, with possibly different concentration, c_{SERS}, now gives a SERS signal I_{SERS}. The analytical enhancement factor , AEF, can then be defined when the following equation.

$$AEF = \frac{I_{SERS}/c_{SERS}}{I_{RS}/c_{RS}}$$

This definition, although useful for specific practical applications, tends to strongly depend on many factors, in particular, on the adsorption properties and surface coverage, monolayer or multilayer of the probe; SERS does not fully characterize the number of adsorbed molecules. It is also strongly dependent upon the sample preparation procedure for 2D planar substrates (e.g., spin-coating, dipping, or drying). The AEF, in fact, ignores the fact that SERS is a type of surface spectroscopy, which means that only the adsorbed molecules contribute to the signal and that the effect is distance-dependent.[98] For this reason, it is not a good characterization of the SERS substrate itself, and it cannot be used to easily compare the performances of different substrates. However, provided all experimental procedures are clearly stated and sub monolayer coverage is ensured, the AEF represents a simple figure for the SERS EF, whose measurement is easily reproducible. From its definition, it is also clear that the AEF is particularly suited to the case of SERS active liquids (e.g., colloidal suspensions).

From an application point of view, typically SERS uses two strategies, which are illustrated in **Figure 5**.

---

[98] R. Aroca, *Surface Enhanced Vibrational Spectroscopy* (Wiley: Chichester, 2006).
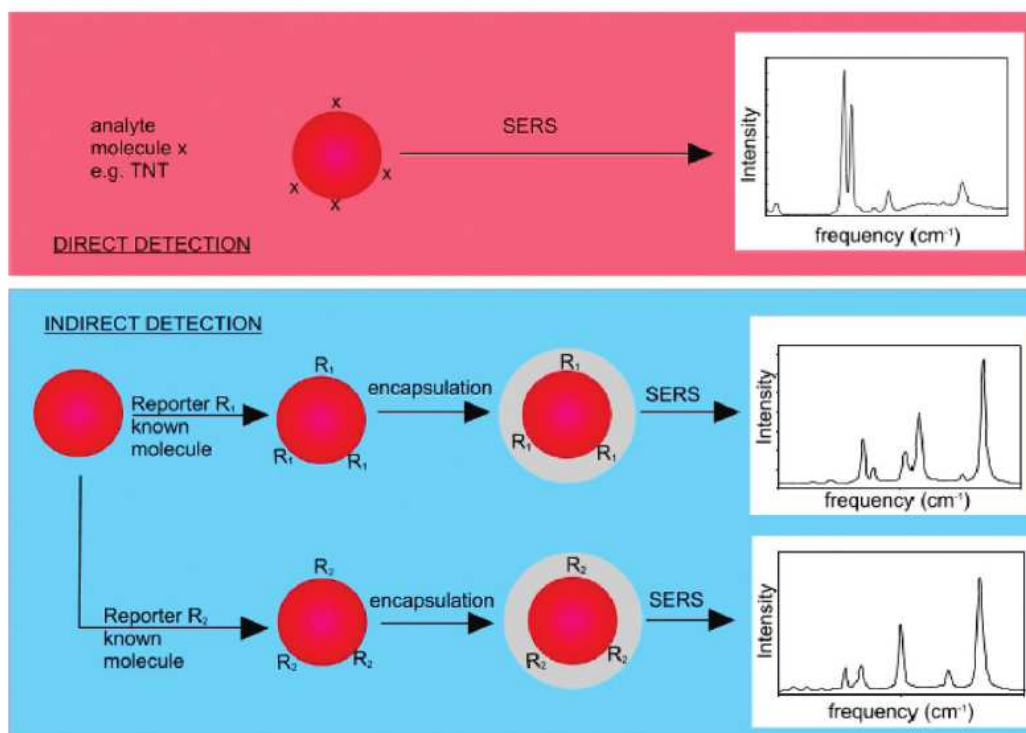
Figure 5 Illustration demonstrating methods used for direct detection via SERS-label-free method (top panel) and preparation of labels for SERS-based indirect detection-label method (bottom panel).[99]

If in the first approach, people try to capture and identify molecules in the local environment for ultrasensitive detection[100]; in the second, people attempt to use SERS "tags" or Raman molecules with specific and strong SERS signals, with a unique SERS spectra, in order to exploit their narrow widths of Raman bands and identify different tags in the same spectrum.[101]

In view of the fact that high enhancement factors are necessary to allow the interesting applications of SERS like single-molecule detection, being able to tune the LSPR peak of silver nanoparticles to the wavelength of the instrument is a powerful tool for the enhancement of SERS signals.

Reproducibility has been difficult in this rapidly growing field as small changes and interactions between the nanoparticles can have extremely large effects on the enhancement factor claim.[82]

[99] R.S. Golightly, W.E. Doering, M.J. Natan, *AcsNano,* 2009, **3**, 2859.

[100] C.L Haynes, C.R. Yonzon, X. Zhang, X., R.P.V Duyne, *J. Raman Spectrosc.* 2005, **36**, 471.

[101] M.Y. Sha, H. Xu, M.J. Natan, R.J. Cromer, *Am. Chem. Soc.*, 2008, **130**, 17214.

1.2.4 Antimicrobial Activity of AgNPs

Colloidal silver has been used commercially for almost 100 years, typically as a biocide. Silver itself has been known for its bactericidal nature and it has been used to cure various diseases since ancient times.

Thanks to the recent improvements of ''bottom-up'' approaches in nanofabrication techniques enabled the design of several type of AgNPs having different and tunable physico-chemical properties (e.g., size, shape, and surface chemistry)[102] , there has been a rebirth of the promotion of AgNPs as an alternative medicine treatment.

Actually, among all the recent non-traditional antibacterial agents, AgNPs have been recognized as optimal candidates for overcoming pathologies previously treated with conventional antibiotics, because of their strong and broad-spectrum antimicrobial features. The huge and constantly increasing amount of literature data available on the synthesis and use of AgNPs (for an example updated to 2012, see figure **Figure 6A)**, confirm these characteristics and their application as antimicrobial agents (see **Figure 6B)**. This latter constitutes about 10% of all the commercial/research uses of AgNPs or silver-based nanocomposites, which leads to an annual worldwide production of nanosilver of ca. 320 tons.[103]

[102] J.A. Dahl, B.L. Maddux, J.E. Hutchison, *Chem. Rev*., 2007, **107**, 2228.
[103] B. Nowack, H.F. Krug, M. Height, *Environ. Sci. Technol*., 2011, **45**, 1177.
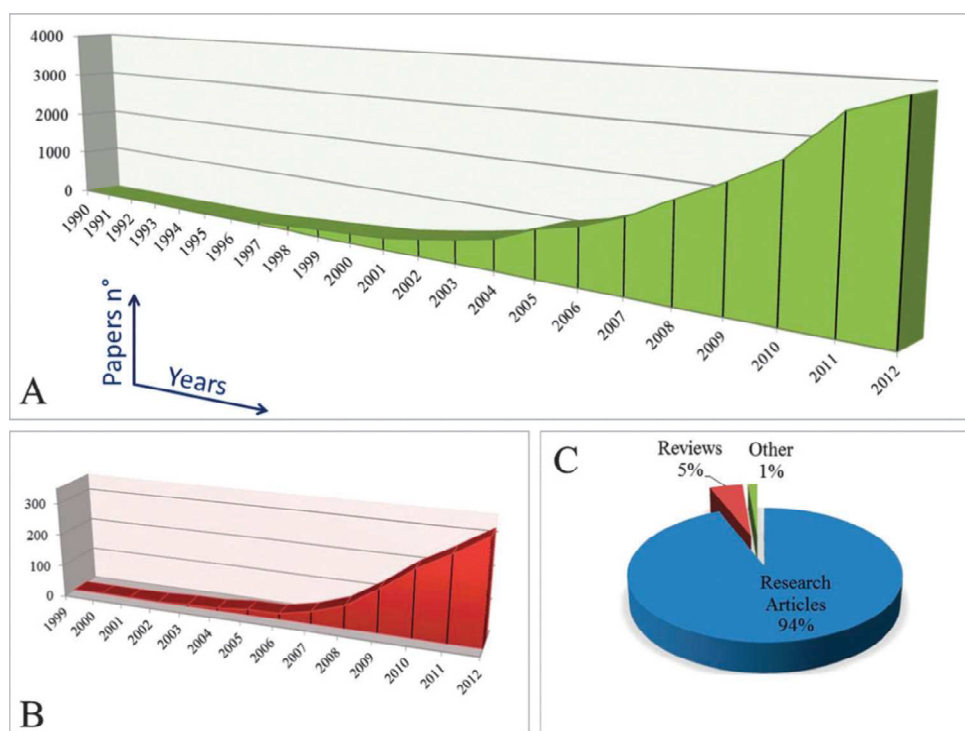
Figure 6 Trend of scientific literature data (updated to 2012) on AgNPs and their application as antimicrobial agents. (A) Number of papers, over time, dealing with synthesis and use of AgNPs (source: Web of Sciences, keywords: ''Silver nanoparticles''). (B) Scientific articles on the application of AgNPs as antimicrobial tools (source: Web of Sciences, keywords: ''Silver nanoparticles'' and ''Bacteria''). The bactericidal effects of AgNPs represent ca. 10% of all the applications of AgNPs. As reported in (C), most of the papers in (B) belong to research articles (about 94%), while only 5% represent review discussions.[104]

At the present time, many products exploit AgNPs and silver nanocomposites as antimicrobial agents: from clothing to household water filters, cosmetics, contraceptives, and even toys.[105]

In addition, several biomedical fields are also taking advantage of nanosilver as a potent antibacterial agent, including dentistry,[106] drug delivery,[107] eye care,[108] orthopedics,[109] pharmaceutics,[110] and surgery.[111]

Although this huge and quite indiscriminate use of Ag nanoproducts, a clear and definitive knowledge of the effects of AgNPs on microorganisms is still lacking. The absence of nanoparticles standard assays and a definitive clarification of molecular mechanisms of action is the key-point of the question. In recent time, some important works have given an explanation and elucidation

[104] L.Rizzello, P.P. Pompa, *Chem. Soc. Rev*., 2014, **43**, 1501.

[105] C. Marambio-Jones, E.M.V. Hoek, *J. Nanopart. Res*.,2010, **12**, 1531.

[106] H.S. Jia, W.S. Hou, L.Q. Wei, B S. Xu, X.G. Liu, *Dent. Mater*., 2008, **24**, 244.

[107] A.G. Skirtach, A.M. Javier, O. Kreft, K. Kohler, A P. Alberola, H. Mohwald, W.J. Parak , G. B. Sukhorukov, *Angew.Chem., Int. Ed.*, 2006, **45**, 4612.

[108] R.E. Weisbarth, *Optometry Vision Sci*., 2007, **84**, 2.

[109] S. Courtney, M. Bettenga, C.M. Agrawal, J.D. Bumgardner, J.L. Ong, *Biomaterials*, 2006, **27**, 5512.

[110] J.R. Morones, A. Camacho- Bragado, X. Gao, H.H. Lar, M.J. Yacaman, *J. Nanobiotechnol.*, 2005, **3**, 6.

[111] K. Galiano, C. Pleifer, K. Engelhardt, G. Brossner, P. Lackner, C. Huck, C. Lass-Florl, A. Obwegeser, *Neurol. Res*., 2008, **30**, 285.

about this topic. For example, Eckhardt et al. provided extensive analyses from a chemical point of view of the interaction of silver at molecular and cellular levels, with a specific focus on the binding with amino acids, enzymes, and DNA and detailed discussion on the biocompatibility of silver for medical devices.[112] Furthermore, biocidal effects of silver in its different structures, specifically as metal, salt and nanoparticles, was accurately reviewed by Chernousova,[113] whilst Lemire[114] gave a focal point on the mechanisms and molecular targets of metals.

Notwithstanding the enormous quantity of important studies, there is still a high level of uncertainty regarding the question "ions or NPs", in other words about mechanism of toxicity concerning the role played by the AgNPs or by the Ag^+ ions, which may be released from the AgNPs surfaces. This topic has been debated for decades and even if it seems to be solved only very recently, is still kept on being an open issue.

Today, it is widely accepted that the crucial cause of toxicity to microorganisms, elicited by AgNPs, is the aerobic release of silver ions, Ag^+, which can be induced by exposing silver to oxygen, as explained by the following equations[115]:

$$4Ag + O_2 \rightarrow 2Ag_2O$$
$$2Ag_2O + 4H^+ \rightarrow 4Ag^+ + 2H_2O$$
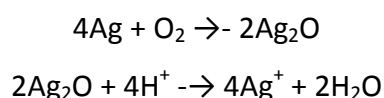
Oxygen molecules promote the formation of silver oxide; this latter is then the foremost cause of Ag^+ ions release, through interaction with H^+ ions. Obviously, acidic conditions induce an overall improved rate of release with respect to neutral pH conditions. Thus, AgNPs have no evident effects on microorganisms under anaerobic condition in which there is no dissolution.

The authors concluded that the AgNPs physico-chemical properties such as size, shape, and charge influence the toxicity only indirectly.[115] For example, very small AgNPs typically exert more prominent toxicity because of their higher surface area and associated faster rate of Ag^+ release, compared to bigger AgNPs. These results explicated some previously uncharacterized aspects of AgNPs bacterial toxicity. Nonetheless, there are still several open questions concerning the mechanisms of ions damage to bacteria, numerous experimental and methodological limits, and request of standardized protocols and reference AgNPs materials.

[112] S. Eckhardt, P.S. Brunetto, J. Gagnon, M. Priebe, B. Giese, K.M. Fromm, *Chem. Rev.*, 2013, **113**, 4708.
[113] S. Chernousova, M. Epple, *Angew. Chem., Int. Ed.*, 2013, **52**, 1636.
[114] J.A. Lemire, J.J. Harrison, R.J. Turner, *Nat. Rev. Microbiol.*, 2013, **11**, 371.
[115] J.Y. Liu, R.H. Hurt, *Environ. Sci. Technol.*, 2010, **44**, 2169.

From a typical molecular microbiology viewpoint, the action mechanism of silver ions and NPs is not completely understood yet. Mostly, there are some hypothesized mechanisms concerning direct Ag^+ induced membrane damage, Ag^+ related ROS production, and cellular uptake of Ag^+ ions, or even poration of membrane due to AgNPs, resulting destruction of ATP production and delaying of DNA replication activities.

In several works,[116,117] the direct membrane damage by Ag^+ ions has been suggested thanks to imaging investigations,[104] in particular with transmission electron microscopy (TEM), which revealed pits or even large holes inside the bacterial membrane.

Furthermore, silver ions may interact with sulfur containing membrane proteins (e.g., with the thiol groups of respiratory chain proteins),[118] causing physical damage to the membrane. In agreement with the hard soft acid-base theory (HSAB), the thiol moiety is a soft and polarizable ligand, namely with a quite large and diffuse distribution of electrons, and with HOMO (highest occupied molecular orbitals) of high energy. Thus, thiol group may bind with high affinity soft cations, such as Ag^+, having a LUMO (low unoccupied molecular orbital) of low energy.[119] Owing to the large size and low charge of the atoms involved in the coordination, and of the small HOMO–LUMO separations between them, a quasi-covalent bond is favorable as compared to ionic bond. Despite sulfur containing membrane peptides and proteins, silver ions may be also implicated in Ag–N and Ag–O bonds,[120] with preferential linear coordination geometry around the Ag^+ ion.

Additionally, numerous other coordination modes of Ag^+–aminoacids/peptides have been proposed from a theoretical[121] and experimental viewpoint,[122] showing, for instance, that histidine has much more affinity to silver compared to cysteine and methionine, which usually considered as the best candidates for binding silver.

All interactions between Ag^+ and membrane proteins may direct, sequentially, to a radical change in membrane permeability, by a progressive release of lipopolysaccharides (LPS) and membrane proteins[123] outcome in the dissipation of proton driving force and reduction of intracellular ATP levels.[124] This may also elicit the intracellular accumulation of Ag^+ ions, and also of some AgNPs,

[116] A. Taglietti, Y.A.D. Fernandez, E. Amato, L. Cucca, G. Dacarro, P. Grisoli, V. Necchi, P. Pallavicini, L. Pasotti, M. Patrini, *Langmuir*, 2012, **28**, 8140.

[117] G.K. Vertelov, Y.A. Krutyakov, O.V. Efremenkova, A.Y. Olenin, G.V. Lisichkin, *Nanotechnology*, 2008, **19**, 355707.

[118] J.R. Morones, J.L. Elechiguerra, A. Camacho, K. Holt, J.B. Kouri, J.T. Ramirez, M.J. Yacaman, *Nanotechnology*, 2005, **16**, 2346.

[119] R.G. Pearson, *J. Am. Chem. Soc.*, 1963, **85**, 3533.

[120] A.G. Orpen, L. Brammer, F.H. Allen, O. Kennard, D.G. Watson, R. Taylor, *J. Chem. Soc., Dalton Trans.,*1989, **1**, 83.

[121] J. Jover, R. Bosque, J. Sales, *Dalton Trans.*, 2008, **45**, 644.

[122] N.C. Kasuga, R. Yoshikawa, Y. Sakai, K. Nomiya, *Inorg.Chem.*, 2012, **51**, 1640.

[123] I. Sondi, B. Salopek-Sondi, *J. Colloid Interface Sci.*, 2004, **275**, 177.

[124] C.N. Lok, C.M. Ho, R. Chen, Q. Y. He, W.Y. Yu, H.Z. Sun,P. K.H. Tam, J F. Chiu, C.M. Che, *J. Proteome Res.*,2006, **5**, 916.

even if this latter evidence has been not often reported. Specifically, intracellular silver ions may bind proteins of the respiratory chains,[125] as a result uncoupling the respiration from the oxidative phosphorylation pathway, that uses energy released by the oxidation of nutrients to produce ATP.[125, 126]

Silver ions were also proposed to increase the frequency of DNA mutation. In particular, investigations based on a combination of FTIR spectroscopy and capillary electrophoresis revealed that guanine N7 and adenine N7 are most favorable binding sites, in DNA, for Ag^+.[127] As well, Ag^+ ions may induce phenomena like cytoplasmic shrinkage, DNA condensation and detachment of cell-wall membrane.[128]

A further mechanism of Ag poisoning may be based on site-specific enzyme inhibition and, above all, ionic mimicry. In this latter case, Ag^+ has been demonstrated to dislocate both Cu and Zn from their coordination site with the superoxide dismutase enzyme (Cu–Zn SOD), with a subsequent inactivation.[129]

The possibility of AgNPs to bind bacteria can be influenced by their surface charge, which may play an important role because of the possibility to give electrostatic interactions.[130] For example, positive surface charge of AgNPs may encourage their binding to bacterial membrane, with a higher local ions release as a consequent of a higher effective dose available. At the same time, thanks to proton motive force that induces a local strong decrease of pH, down to values of 3, close to external membrane of bacteria, silver ions release is strongly promoted.[131]

The toxicity consequences of AgNPs on microorganisms have been also attributed to Ag^+ ions-related ROS production.[132] In fact, the excess of ROS brings to oxidative stress, with additional generation of free radicals that may damage lipids and DNA.[133] Above all, Ag^+ ions may work as a catalyst, generating high levels of ROS in combination with dissolved oxygen molecules. In addition, the free radicals may take place from direct damage of the respiratory chain enzymes carried out by silver. Nevertheless, many research studies on the bactericidal effects of both ROS and also reactive nitrogen species (RSN) remain controversial. Microorganisms have developed

[125] S.Y. Liau, D.C. Read, W.J. Pugh, J R. Furr, A.D. Russell, *Lett. Appl. Microbiol.*, 1997, **25**, 279.

[126] K.B. Holt, A.J. Bard, *Biochemistry*, 2005, **44**, 13214.

[127] H. Arakawa, J.F. Neault, H.A. Tajmir-Riahi, *Biophys. J.*, 2001, **81**, 1580.

[128] E.T. Hwang, J.H. Lee, Y.J. Chae, Y.S. Kim, B.C. Kim, B.I. Sang, M.B. Gu, *Small*, 2008, **4**, 746.

[129] M.R. Ciriolo, P. Civitareale, M.T. Carrı̀, A. De Martino, F. Galiazzo, G. Rotilio, *J. Biol. Chem.*, 1994, **269**, 25783.

[130] M. Raffi, F. Hussain, T.M. Bhatti, J.I. Akhter, A. Hameed, M.M. Hasan, *J. Mater. Sci. Technol.*, 2008, **24**, 192.

[131] Z.M. Xiu, Q.B. Zhang, H.L. Puppala, V.L. Colvin, P.J.J. Alvarez, *Nano Lett.*, 2012, **12**, 4271.

[132] J.S. Kim, E. Kuk, K.N. Yu, J.H. Kim, S.J. Park, H.J. Lee, S.H. Kim, Y.K. Park, Y.H. Park, C.Y. Hwang, Y.K. Kim, Y.S. Lee, D.H. Jeong, M.H. Cho, *J. Nanomed. Nanotechnol.*, 2007, **3**, 95.

[133] A. Nel, T. Xia, L. Madler, N. Li, *Science*, 2006, **311**, 622.

several molecular approaches to challenge the ROS- and RSN-mediated stress, including direct detoxification carried out by enzymes, for instance catalase, superoxide dismutase, and peroxidase, for ROS elimination, and NO reductase, S-nitrosogluthathione reductase and peroxynitrite reductase for RNS detoxification.[134] Moreover, bacteria actively respond to these kind of stress, oxidative and nitrosative, at transcriptional level, by regulating the expression of several proteins such as OxyR, SoxRS, PerR, OhrR, BosR, and NorR, which allow bacteria a high survival probability against stress.[134]

A general scheme in **Figure 7** describes all the proposed effects of AgNPs to microorganism concerning all the current knowledge and studies.
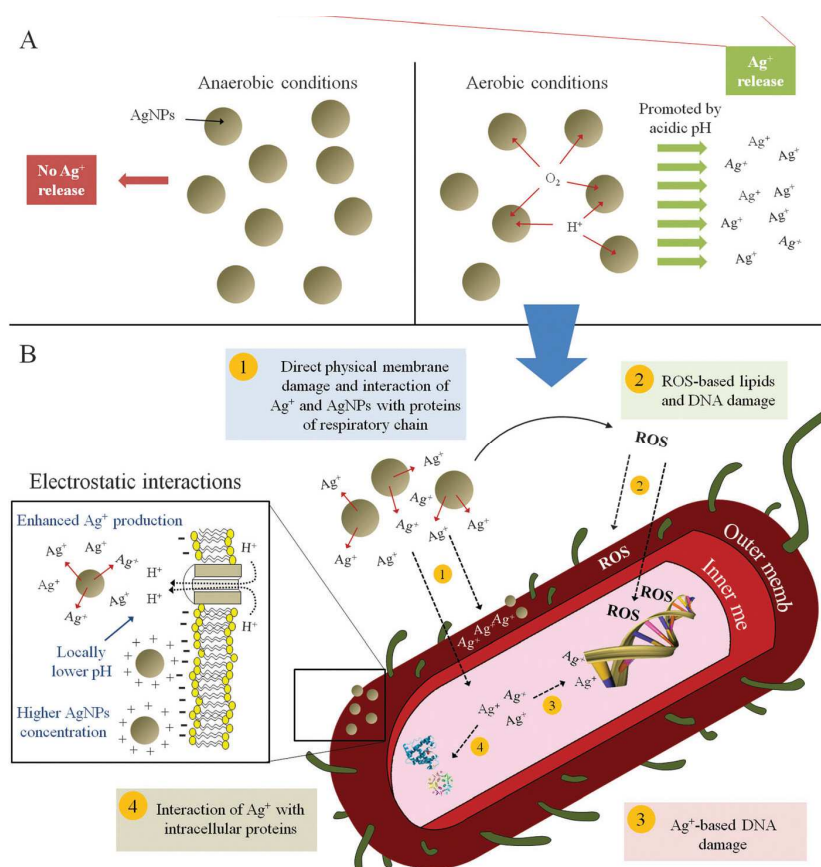
Figure 7 (A) Silver ions release is promoted by acidic and aerobic environment. **(B)** Proposed mechanisms of AgNPs-related toxicity. Silver ions may directly damage bacterial membrane, by blocking the respiratory chain, collapsing the membrane potential and stopping ATP production. Additionally, they may promote the formation of ROS, which then damage both the membrane lipids and DNA. Ag$^+$ ions may bind intracellular proteins and the bacterial chromosome, upon entering the cytosol, thus influencing the metabolic activity and replication. Ag$^+$ uptake can be promoted by membrane damage (although they might enter also through membrane channels). Inset: positively charged AgNPs may be attracted by negatively charged bacterial membrane leading to higher local dose of NPs. Here, the proton motive force takes place, causing a local decrease of pH. This can further promote the dissolution of AgNPs, resulting in a local higher Ag$^+$ concentration. In this picture, a Gram-negative bacterium has been taken as model microorganism.[104]

---

[134] F.C. Fang, *Nat. Rev. Microbiol.*, 2004, **2**, 820.

Size, shape, surface charge, coating, agglomeration and dissolution rate are physicochemical features of AgNPs which are particularly important for determining their biological interactions and impacts. In general, smaller particles have a larger surface area and as a result have greater toxic potential.[135] Moreover, still the shape of silver nanostructures may considerably influence their physical and chemical properties. For this reason, not only silver spherical nanoparticles, but also silver nanoparticles with different shape such as nanowires, nanorods, nanoplates, and nanocubes, have been frequently utilized in the biomedical field.[136] Thus, several researches have been dedicated significant efforts to correlate the physicochemical and morphological properties of AgNPs with their antibacterial effects. Unfortunately, whilst the surface charge seems to play an important role, as it has already explained above, by examining the data available in literature on AgNPs size and shape, a huge disagreement appears. This is primarily owing to the lack of AgNP standards and the absence of standardized protocols and procedures in microbiology assays. About the first point, significant questions have to be overcome in both synthesis processes and nanoparticles characterization approaches. In fact, the synthesis of AgNPs with well-controlled sizes and size distributions in high yield represented an interesting challenge also in the recent past. Their chemical fabrication is, actually, influenced by thermodynamic and kinetic factors, and substantial difficulty remains in capturing the distinct steps of nucleation and growth of AgNPs.[137]

Compared to more standard synthesis processes, where the stabilizing agents are usually polymers,[138] citric acid[139] and thiols,[140], AgNPs–peptide hybrid materials have been demonstrated as most advantageous candidates for applications in medicine, biotechnology, and optical devices.[141] However, it should be considered that most of the literature available on the bactericidal effects of AgNPs is based on their use of with largely uncontrolled properties, in terms of samples highly polydispersed in size and shape. Furthermore, a number of research works made the use of such AgNPs without carrying out any physico-chemical characterizations, hence exacerbating the divergences in the observed results. Indeed, a critical point for reproducible and standardized assays is, therefore, the characterization of AgNPs before any antibacterial tests: AgNPs should be totally characterized both after the synthesis procedure, in aqueous solution, and, therefore, in situ after incubation with the bacterial culture media. The evaluation of the

[135] H.J. Hutchison G, F.M. Christensen , S. Peters , S. Hankin ,V. Stone, *Crit. Rev. Toxicol.*, 2010, **40**, 328.

[136] M. Rycenga, C.M. Cobley, J. Zeng, W. Li, C.H. Moran, Q. Zhang, D. Qin, Y. Xia, *Chem. Rev.*, 2011,**111**, 3669.

[137] C. Burda, X.B. Chen, R. Narayanan, M.A. El-Sayed, *Chem. Rev.*, 2005, **105**, 1025.

[138] S.W. Kim, S. Kim, J.B. Tracy, A. Jasanoff, M.G. Bawendi, *J. Am. Chem. Soc.*, 2005, **127**, 4556.

[139] J.A. Dahl, B.L. S. Maddux, J.E. Hutchison, *Chem. Rev.*,2007, **107**, 2228.

[140]D.I. Gittins, F. Caruso, *ChemPhysChem*, 2002, **3**, 110.

[141] P. Graf, A. Mantion, A. Foelske, A. Shkilnyy, A. Masˇicˊ, A.F. Thu¨nemann, A. Taubert, *Chem.–Eur. J.*, 2009, **15**,5831.

silver nanoparticles physico-chemical properties in biological fluids is not unimportant since bacteriological media may lead to significant changes of the original properties of AgNPs, resulting in the production of new nano-objects with completely different characteristics.[142] For instance, AgNPs may have larger size, different surface charge and coating compared to the as-synthesized AgNPs. In addition, they may undergo important agglomeration/aggregation phenomena. Most of the AgNPs, in fact, are not stable in bacterial culture media, consequently compromising the observed bactericidal effects. Obviously, all these factors may strongly influence the dynamics of ions release, and the effective dose of Ag^+, causing significant irreproducibility in the results.

1.2.4.1 Nosocomial Infections

Infection diseases induced by bacteria persist to be one of the greatest health problems worldwide, upsetting millions of people every year, notwithstanding the current development in drug discovery and pharmaceutical biotechnology

From the late 1800s, bacteria were recognized to be the cause of several human diseases and infections.[104] Since that period, important efforts have been followed on many fronts to realize solutions to this serious concern, including vaccination, improvement of hygienic conditions, and antibiotics development. Antimicrobial drugs, so called "miracle drugs", have saved millions of people and eased several patients affliction from chronic infections since they discovery. All microorganisms exhibit an intrinsic outstanding ability to flout many therapeutic interventions and develop several resistance mechanism against antibiotics because of their fast and easy evolutionary genetic system. For these reasons, healing of their infection is extremely difficult.[143]

Nowadays, the treatment and cure of infectious diseases have been estimated to cost more than 120 billion dollars per year to the U.S. society as direct healthcare expenses. Nevertheless, this corresponds to a large underestimation for the reason that it ignores the disease-associated overheads, above all the long-term care or the treatment of chronic infections, so that, is also expected to rise, due to the constant and dramatic increase in antibiotic resistant bacterial strains. In addition, the healthcare costs associated with the treatment of resistant pathogens consists of ca. $5 billion annually.[144]

Simultaneously, big pharmaceutical companies are losing interest in new antibiotics progress, shifting their principal investments in much more profitable research and development fields. This

[142] A. Lesniak, F. Fenaroli, M.P. Monopoli, K.A.C. Åberg, A. Salvati, *ACS Nano*, 2012, **6**, 5845.
[143] D.I. Andersson, D. Hughes, *Nat. Rev. Microbiol.*, 2010, **8**, 260.
[144] H.W. Boucher, *Clin. Infect. Dis.*, 2010, **50**, S4–S9.

is because such drugs are not so rewarding, in terms of long-term profits, as compared to drugs used for the treatment of chronic diseases (that require long-period therapies). The development of antibiotics is really expensive, as every drug (ca. $1 billion is required to have a new drug in the market), time consuming and risky (the investments require more than 10 years), and is also unappealing because of their too short lifecycle, due to bacterial resistance.

By taking into account all these considerations, scientist are in the presence of one of the greatest health challenges: new smart solutions are required to defeat such constant rise in antibiotic resistance bacteria concerns.[145,146] It is clear that these solutions should combine the possibility of industrial production processes with cheapness and effectiveness.

Biomedical devices have become a fundamental aspect of the human healthcare system. Over the past three decades, the number of artificial hip and knee implants has increased noticeably, and stents, heart valves, vascular grafts and other implanted devices have been used extensively to save lives and to renovate quality of life for many people. In addition, there is also a clinical need for non-implanted, shorter term-usage biomedical devices, such as various catheters and orthopedic fixation screws, among others. As the lifespan increases in industrialized countries, the demand for such biomedical devices continues to increase, and clinicians express their desire for better or longer lasting biomedical devices.[104]

Nosocomial infections due to bacteria attaching and proliferating on surfaces of biomedical devices and implants are a considerable issue in implant surgery as well as with short term biomedical devices.[147]

Nevertheless, there are no analogous premature warning signs of bacterial infection for many implants and devices, for the reason that the outbreak of an infection can be masked by the continuing pain of tissue inflammation after surgery. Frequently, diagnosis of this kind of infection takes places when a full-blown infection has already caused damage to tissue and host organism, and sometimes, reoperation of infected implants has at times led to the death of old patients already weakened by the previous operation or other conditions.

As a consequence, today, healthcare systems attempt to reduce the risk of infection on short-term biomedical devices by prophylactic measures. For example, catheters are replaced at frequent intervals, and such preventative replacement schedules impose considerable costs to the

[145] B. Spellberg, R. Guidos, D. Gilbert, J. Bradley, H.W. Boucher, W.M. Scheld, J.G. Bartlett, J. Edwards Jr, *Clin. Infect. Dis.*, 2008, **46**, 155.
[146] G. Taubes, *Science*, 2008, **321**, 356.
[147] J.W. Costerton, P.S. Stewart, E.P. Greenberg, *Science*, 1999, **284**, 1318.

healthcare system. The problem cannot be addressed as readily with implants. Early-stage infections of implants have significantly reduced thanks to enhanced procedures in sterilization and operating theatres, but delayed infections, for which occurring many weeks or months after operation, have hardly decreased and continue to cause a serious problem. It is supposed that such nosocomial infections do not have origin from surgery but by planktonic bacteria circulating in the vascular system, which may attach on to the implant surface or to incompletely healed wound, multiply and form a biofilms that eventually directs to infection.

What is a biofilm? From a chemical point of view, biofilms consist of a complex mixture of exopoly-saccharides, DNA and catalytic proteins, which are secreted by microorganisms after their adhesion onto surfaces, and whose biological functions are largely unknown.[148] Biologically, it represents an external digestive system that allows extracellular enzymes, secreted by bacteria, to localize in close proximity to cells, allowing the metabolization of the solid biopolymers close to environment.[148] From a physical viewpoint, a biofilm is made up of slime matrix with specific robustness, viscosity and strength that varies depending on the particular strain of microorganism and the specific environmental conditions.[149] Genetically, sessile bacteria have very different profiles of gene and protein expression, compared with their planktonic counter parts.[150]

Therefore, biofilms could represent a complex population of unicellular microorganisms that live, behave and interact with each other and the environment like a quasi-multicellular organism. The biofilm life cycle is reported in **Figure 8**.

[148] H.C. Flemming, J. Wingender, *Nat. Rev. Microbiol.*, 2010, **8**, 623.
[149] I.W. Sutherland, *Trends Microbiol.*, 2001, **9**, 222.
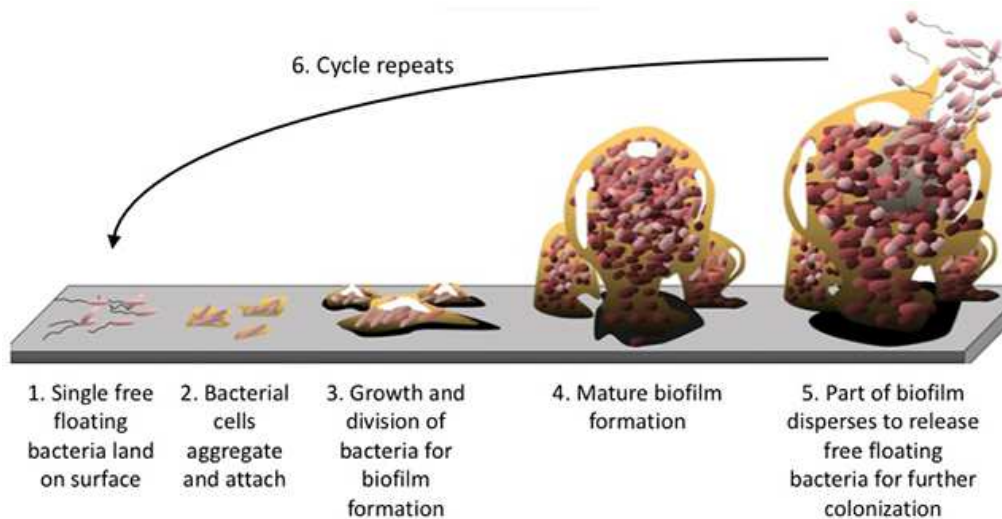[150] K. Sauer, *Genome Bio.,* 2003, **4**, 219.

Figure 8 The biofilm life cycle leading to the generation of mature biofilms.[148]

The exo-cellular polysaccharide matrix, produced by the attached and growing bacterial colonies, protects biofilms against antibiotics and from the host body's intrinsic defense system.[148]

Bacterial biofilms on biomedical device surfaces are much more difficult to eradicate by antibiotics than circulating bacteria: as a result surgical removal of a substantial proportion of infected implants may be carried out in order to remove them. However, it is widely accepted that the most effective way to prevent biofilm formation is *a priori* suppression of bacterial adhesion, rather than *a posteriori* chemical- or drug-based treatment. Hence, a promising approach for reducing the presence of biofilms is to prevent the initial attachment of bacteria to implant and device surfaces.

For this reason, great effort has been put into designing substrates that prevent the early stage of bacterial adhesion.

This has encouraged research efforts on the development of thin coatings that can be applied to biomedical devices and are able to confer resistance to bacterial colonization.

Obviously, such antibacterial coatings should not affect other properties of biomedical device and implants, like the visual clarity of contact lenses or the flexibility of vascular grafts. In addition, they should not have adverse effects on cells or fluids, blood or tear fluid, of the human host.

Because of the variety of devices and implants, with causative bacteria, one single strategy may not be generally successful, and antibacterial strategies may need to be tailored to specific product needs.

Polymeric materials present great flexibility for the design of biomedical devices. Nonetheless, most polymers can be colonized by bacteria readily. A few polymers are capable to kill bacteria[151] or avoid bacteria from attaching,[152] but those polymers are often not appropriate as bulk materials for the fabrication of medical devices owing to other considerations, such as strength or flexibility. As a result, the emphasis has been on employment of bactericidal or attachment-resistant polymers as surface coatings applied onto existing devices.

If there is a relatively small number of antibacterial polymers, a significant number of low-molecular-weight molecules and some inorganic ions are known to exhibit antibacterial efficiency in solution. However, such antibiotics cannot be applied directly by solvent coating onto device surfaces, because their adhesion is weak and are displaced rapidly.

Generally, bacterial infections can be prevent using low-molecular-weight antibiotics through two ways, which are showed in **Figure 9**.
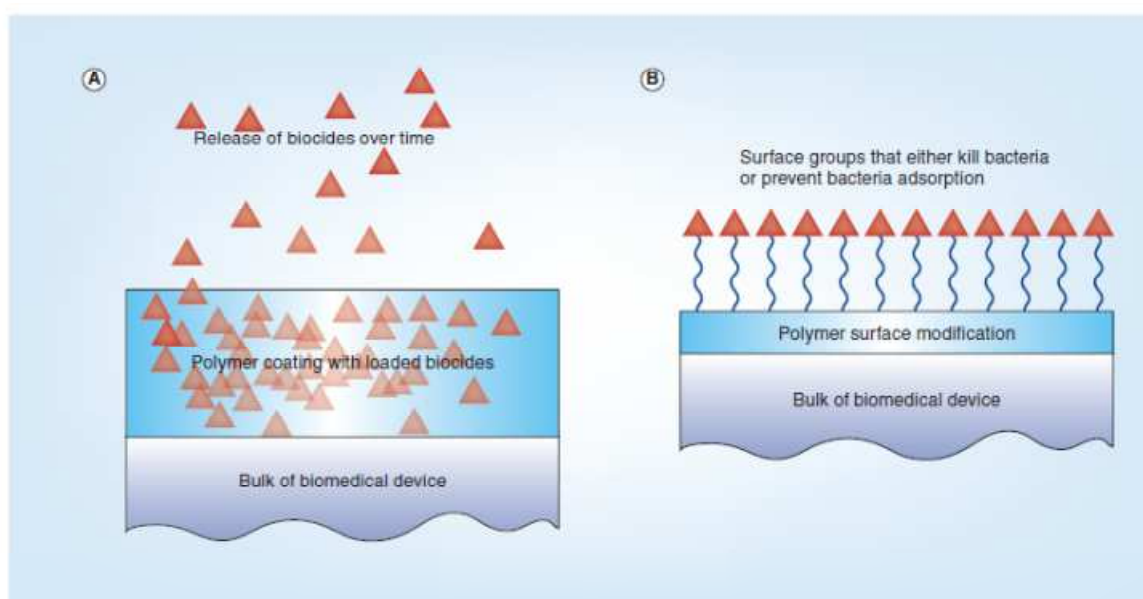
Figure 9 Strategies for antibacterial coatings**. (A)** Coating the surface of a device with a polymer film containing biocides that are released with time. **(B)** Attachment to the surface of a biomedical device of compounds that either kill bacteria or prevent bacterial adsorption.[153]

According to the first approach, a controlled release is exploited, in which the antibiotic is released from the biomedical device and intercepts bacteria in the environment. Even if this has been studied with some organic compounds, certainly the most common antibiotic used is silver and several silver-based approaches are well in progress. The development of antibiotic-releasing

[151] G. Cheng, H. Xite, Z. Zhang, S.F. Chen, S.Y. Jiang, *Angew. Chem. Int. Ed. Engl,* 2008, **47**, 8831.

[152] I. Fundeanu, H.C: van der Mei , A.J Schouten, H.J. Busscher, *Colloids Surf. B Biointerfaces*, 2008, **64**, 297.

[153] K. Vasilev, J. Cook, H.J. Griesser, *Expert Rev. Med. Devices.,* 2009, **6**, 553.

devices has been the subject of several reviews.[154] Various antimicrobial compounds have been loaded into polymers or polymer composite films, including organic antibiotics,[155] silver[156] and nitric oxide[157] for various intended biomedical applications. Furthermore, other metal ions have also been examined, though adverse effects on human tissue present a concern. The main disadvantage of the release strategy is that the duration and effectiveness of antibacterial action is limited by loading and release kinetics.

The purpose of the second approach is the application of a molecular surface layer of covalently immobilized, 'grafted', antibiotic molecules that are able to prevent bacterial attachment to materials surfaces. Besides to potentially much longer, perhaps indefinite, efficiency, this strategy is also encouraging when seeking regulatory authorization for new devices; if it can be established that the antibiotics are durably grafted hence to remain on the device surface, one can eliminate concerns regarding possible unfavorable effects because of accumulation of antibiotics in body tissues, like the brain, liver and spleen.

Often it may be gainful to fabricate a device firstly, and secondly apply a polymeric coating that can deliver or surface-graft an antibiotic. Therefore, for metallic and ceramic devices such as hip and knee implants, antibiotic molecules can usually be neither imbibed nor grafted onto the inorganic surface; though exceptional examples exist: the use of carbonated hydroxyapatite coatings that were precipitated onto titanium implants, which are appropriate for incorporation of antibiotics with carboxylic groups, such as cephalothin, carbenicillin and cefamandol;[158] an hydroxyapatite loaded with gentamycin for cementless joint prostheses;[156] and also post-traumatic osteomyelitis.[159] Mostly, a thin polymeric coating serves as an essential vehicle.

In general, the literature about antibacterial surfaces for implants and biomedical devices gives a great attention on polymeric coatings of various design variants.

For several decades, significant consideration has been given to the use of silver as an antibacterial agent. Silver, silver compounds and silver nanoparticles, AgNPs, have enjoyed a great deal of attention in recent years.[160] Wound dressing, bandages for burns and chronic wounds, silver and AgNPs coated catheters are an example of commercial products which have emerged recently. However, research works have focused not only on the efficiency of the coatings, but also on

[154] E.M. Hetrick, M.H. Schoenfisch, *Chem. Soc. Rev.,* 2006, **35**, 780.

[155] V. Alt, A. Bitschnau, J. Osterling,. *Biomaterials*, 2006, **27**, 4627.

[156] N. Shanmugasundaram, J. Sundaraseelan, S. Uma, D. Selvaraj, M. Babu, *J. Biomed. Mater. Res. Part B*, 2006, **77**, 378.

[157] B.J. Nablo, A.R. Rothrock, M.H. Schoenfisch, *Biomaterials,* 2005, **26**, 917.

[158] M. Stigter, J. Bezemer, K. de Groot, P. Layrolle, *J. Control. Release*, 2004, **99**, 127.

[159] U. Joosten, A. Joist, T. Frebel, B. Brandt, S. Diederichs, C. von Eiff, *Biomaterials*, 2004, **25**, 4287.

[160] M. Rai, A. Yadav, A. Gade, *Biotechnol. Adv.*, 2009, **27**, 76.

clinical concerns which have come out. In fact, several factors, both from the coating and the environment, have a key role in determining the efficiency of silver-based coating. Generally, it was found that coatings based on metallic silver are less efficient because silver needs to be in its oxidized form, Ag^+, in order to exhibit antibacterial action. Silver ions can be complexed by chlorine ions to produce AgCl, which precipitates, and is disadvantageous for antibacterial efficiency.[104] Moreover, another significant problem is the release of the loaded silver from the coating, which is very quick in many cases, consequently limiting the time of protection.

## 1.2.4.2 Antimicrobial Coating using AgNPs

As a result, there have been considerable research efforts towards engineering coatings loaded with silver and AgNPs in order to obtain a more prolonged release. Even if there are many *in vitro* studies relating to the effectiveness of this kind of biomedical devices, there are few *in vivo* studies which have verified the efficiency of these new approaches. For biomedical devices it may be useful to use thin films containing AgNPs fully encapsulated within the polymer matrix, as opposed to the situation where larger silver particles partly protrude from the polymer film layer.

Among the many applicative studies that have been published, recently Pallavicini and coworkers have shown a simple strategy to gain antibacterial coatings on surface of medical devices exploiting the ''layer-by-layer'' (LbL) approach,[161] which has been applied to obtain surfaces on which thin films of AgNPs are deposited on a molecular self-assembled monolayer (SAM) capable of interaction with silver.[162] In particular, in this work an efficient strategy to prepare glass surfaces with a monolayer of AgNPs firmly grafted on a suitable molecular SAM has been found out. AgNPs are confined to the surface and are capable of exerting an efficient antibacterial activity thanks to Ag^+ release. This activity is noticeably promoted by the high surface/mass ratio typical of AgNPs. Additionally, for an applicative point of view, preparing a monolayer of AgNPs on a flat surface, instead of a film or a silver nanoparticles loaded nanoporous matrix, not only reduces the amount of an expensive material used, silver, but also reduces the quantity of potentially dimension-risky materials, nanoobjects, enclosed in the device.

The authors have adopted a two-step wet synthetic process characteristic of the LbL approach, which is pictorially represented in **Scheme 1**.

[161] L. Netzer, J. Savig, *J. Am. Chem. Soc.*,1983, **105**, 674.
[162] P. Pallavicini, A. Taglietti, G. Dacarro, Y.A.D. Fernandez, M. Galli, P. Grisoli, M. Patrini, G. Santucci De Magistris, R. Zanoni, *Journal of Colloid and Interface Science*, 2010, **350**, 110.
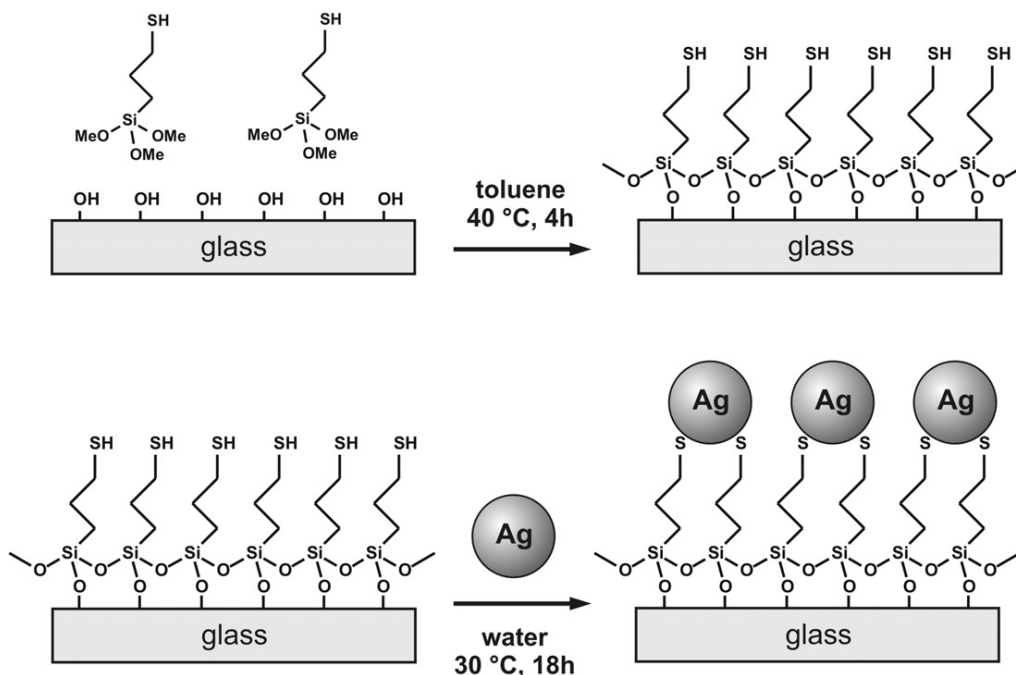
Scheme 1 Representation of the synthetic ''layer-by-layer'' approach used to prepare SAM of AgNPs on glass substrates.[162]

Firstly, a SAM of a mercaptosilane is formed on activated glass samples,[163] secondly the –SH terminated glass is immersed in a AgNPs colloidal solution. This leads to the self-assembly of a AgNPs monolayer covalently attached to the modified glass. Glass is an inexpensive material, totally non-toxic, resistant to agents chemical, transparent in a wide spectral region and easy to work for obtain forms or coatings of other materials; It is therefore an excellent substrate for SAM formation. It should also be remembered that any reaction carried on glass is in principle applicable to any substrate in silica, silicon oxidised or oxides of other elements.[163]

Thus, AgNPs monolayers were successfully immobilized obtaining a satisfactory coverage of the surface on glass ($3.57*10^{-7}$ g of Ag per cm^2, corresponding to ~1900 AgNPs/μ^2) and glass surfaces that are stable for weeks in dry conditions. While the AgNPs surface facing glass is hindered by thiol interaction, the remaining surface (ca. 66%) is exposed to the environment and interacts with it. The behavior of the modified glass surfaces has been studied when exposed to water and PBS, finding that only ~15% of the total quantity of silver loaded on the monolayer is released in solution, even after a 19 days period, probably by the oxidation of the medium-exposed part of the AgNPs surface. Moreover, no detachment of NP from the surface has been observed.

According to the authors, it is the formation or the thickening of a Ag$_2$O layer on the water-exposed surface of AgNPs the responsible of the observed time evolution of LSPR peaks, with the

---

[163] P. Pallavicini, G. Dacarro, M. Galli, M. Patrini, *J. Colloid Interface Sci.*, 2009, **332**, 432.

formation of an oxidized silver layer in the initial 3-days period, reaching a steady-state in which the slowly released Ag^+ ions are replaced by Ag oxidized from the bulk. To further investigate this, XPS experiments have been carried out on quartz slides modified with an AgNPs monolayer, after being aged in air and in water for 1 week. Assignment to Ag and Ag oxides of the XPS lines was performed by taking into account both the direct photoemission line Ag 3d and the auger line MNN. For the sample aged in water the only detected silver signal corresponds to Ag_2O, while in the case of the air-exposed sample both elemental Ag and Ag_2O are detected. Significantly, as a value of 1.3 nm was reported for the inelastic mean free path of Ag 3d photoelectrons excited by Mg Ka photons[164], the overall oxide layer should not exceed that value for the sample aged in air, while it is significantly thicker in the case of water-aged sample.

The antibacterial activity of the prepared glasses was investigated against *Staphilococcus aureus*, Gram-positive bacteria, and *Escherichia coli*, Gram-negative bacteria; as commonly considered representative strains for the evaluation of antibacterial activity of drugs;[165] finding an efficient antibacterial activity, stated by the parameter Microbicidal Effect (ME), that is calculated using the formula:

$$ME = \log NC - \log NE$$

(**NC** being the number of CFU/mL developed on the unmodified control glasses, and **NE** being the number of CFU/mL counted after exposure to modified glasses. For a more detailed description of the experiment, see **Paragraph 1.2.5.5**.

The values of ME are showed in **Table 1**.

Sample	*S. aureus* ATCC 6538	*E.coli* ATCC 10356
SURF-SH AgNPs (5h)	1.37	4.93
SURF-SH AgNPs (24h)	5.54	5.90

Table 1 Microbicidal Effect (ME) of AgNPs-modified glass after 5 and 24 h of contact. Reported data are the average of three experiments.

[164] A. Jablonski, S. Tougaard, *J. Vac. Sci. Technol*., 1990, **A8**, 106.
[165] S. Pal, Y.K. Tak, J.M. Song, *Appl. Environ. Microbio*l., 2007, **73**, 1712.

Considering the small amount of silver released from functionalized glass surfaces, antibacterial activity could not be evaluated through classical methods, such as the measure of inhibition halos on agar plates or the determination of the minimum inhibitory concentration (MIC) in nutrient broth. Thus, the authors have developed a practical test that simulates real-life conditions of use for our modified glasses and allows the evaluation of the bactericidal effect in a thin liquid film in contact with the surface. ME is remarkable after 24 h of contact on both the bacterial strains used. In particular *S. aureus* seems to be less sensitive after 5 h of contact and this result is in agreement with the observed lowered efficiency of AgNPs on Gram-positive strain.[165] Remarkably, in the tests proposed by EN 13697[166] the microbicidal activity of a disinfectant is considered acceptable when the decimal-log reduction rate (i.e. ME), is at least equal to 4 after 5 min of contact. In this case ME of the modified glass is superior to 4 even after 5 h of contact for *E. coli*, while for *S. aureus* ME overcomes 4 after 24 h. The results clearly indicate an efficient and long-lasting local microbicidal effect exerted by the NP-modified glass surfaces. Furthermore, as surface characterization of the AgNPs-covered slides has evidenced a non-compact monolayer of AgNPs, with the presence of some unreacted–SH groups, control experiments were also carried out on glasses modified with the only MPTS monolayer, i.e. with no grafted AgNPs. In this case the ME was completely absent.

As a result, thanks to this approach, materials displaying an intrinsic antibacterial effect, with negligible toxicity connected to Ag^+ release and with drastically reduced risk as regards in vivo contamination with objects of nanometric scale may be produced. Although these materials would be of poor use in flow-through or large volume systems (due to the small amount of released Ag^+), medical devices requiring a short, local action against the development of infections on their surface (e.g. catheters, artificial prosthetics and subcutaneous implants) could advantageously profit of this kind of coating.

In another work, which was published by the same research team, Dacarro and coworkers[167] have showed how a polyethylenimine (PEI) self-assembled monolayer (SAM) is capable of anchoring AgNPs which exert antibacterial activity against *E. coli* and *S. aureus*. In fact, surfaces coated with firmly grafted AgNPs could be obtained not only with a thiol-terminated SAM formed on the bulk surface,[162] but also by using amine–silver bonds or electrostatic interactions. Regarding the latter, amine–AgNPs interactions have been widely studied and amino groups proved to be efficient

---

[166] CEN (CEN European Committee for Standardization) EN 13697 Chemical Disinfectants and Antiseptics – Quantitative Non porous Surface Test for the valuation of Bactericidal and/or Fungicidal Activity of Chemical Disinfectants used in Food, Industrial, Domestic and Institutional Areas – Test Method and Requirements (Phase 2, Step 2), Brussells: CEN, 2002.
[167] G. Dacarro, L. Cucca, P. Grisoli, P. Pallavicini, M. Patrini, Angelo Taglietti, *Dalton Trans*., 2012, **41**, 2456.

coating and stabilizing agents for gold and silver nanoclusters.[168] Amines can bind to the metal cluster surface through an electrostatic interaction[168] or a stronger charge-neutral amine/metal interaction, described as a weak covalent bond.[169] For these reasons, the same type of interactions, amine terminated SAM have been used to anchor metal AgNPs on surfaces.[170]

Amino propyl-silanes[170] are a common choice for the preparation of amine-terminated monolayers, particularly on surfaces of SiO_2 type (glass, quartz, silica gel). Considering the enormously developed coordination chemistry of amino ligands, amines are to be considered a versatile moiety, since they can bind efficiently both NP and metal cations.

In this work, authors have used polyethylenimines (PEI), which are linear and branched polymers obtained by cationic polymerization of aziridine. Commercial branched PEI typically have an amino group ratio primary : secondary : tertiary = 1 : 1 : 1.[171] In order to obtain a covalently bound SAM of PEI on glass-like to graft a layer of AgNPs, the authors have employed a silane-derivatized PEI, which is an ideal candidate for the preparation of organic monolayers on Si–OH terminated surfaces (glass, quartz, etc) to obtain multipurpose materials, as depicted in **Scheme 2.** Using this strategy the polyaminic layer is covalently bound to the surface and is very stable as regards time and pH range.

[168] S. Tan, M. Erol, A. Attygalle, H. Du, S. Sukhishvili, *Langmuir*, 2007, **23**, 9836.
[169] D.V. Leff, L. Brandt, J.R. Heath, *Langmuir*, 1996, **12**, 4723.
[170] N. Nath, A. Chilkoti, *Anal. Chem*., 2004, **76**, 5370.
[171] A. von Harpe, H. Petersen, Y. Li, T. Kissel, *J. Controlled Release*, 2000, **69**, 309.
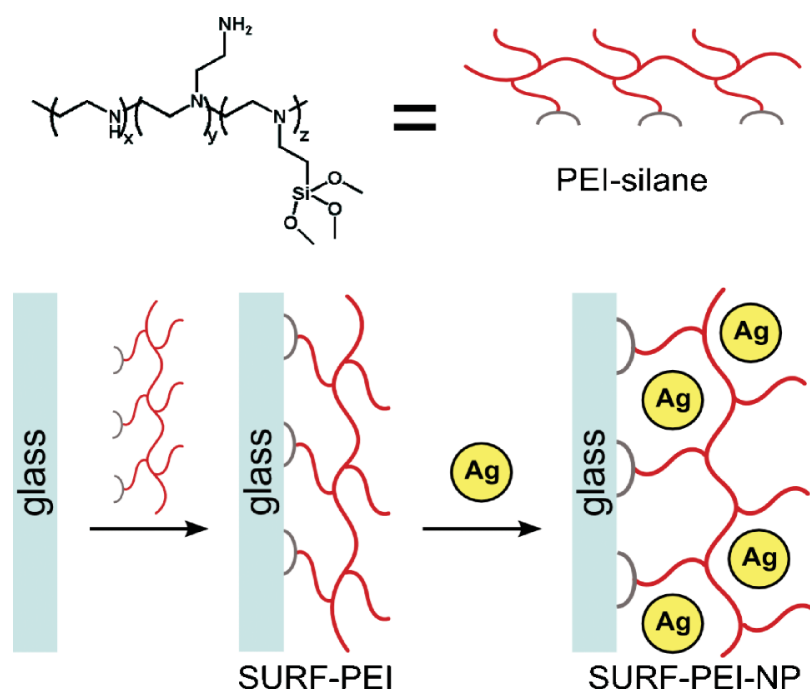
Scheme 2 Schematic representation of PEI-silane structure and two step synthesis of a AgNPs monolayer grafted on PEI SAM.[167]

The authors have demonstrated that trialkoxy-silane PEI is suitable for surface modification and firmly grafting of AgNPs, with the obtained materials able to exert antibacterial action.

Sample	*S. aureus* ATCC 6538	*E.coli* 10356
SURF-PEI AgNPs (5h)	0.03	2.57
SURF-PEI AgNPs (24h)	0.86	6.16

Table 2 Microbicidal effect (ME) of AgNPs-modified glass after 5 and 24 h of contact. Reported data are the average of three experiments.

Table 2 shows the results of the evaluation of the Microbicidal effect (ME) on functionalized glass slides. AgNPs-coated slides showed an efficient and long-lasting effect against *E. coli*. On the other hand, activity against *S. aureus* is poor. We recall that with the AgNPs monolayer prepared on MPTS, exerted ME effect was similar for *E. coli* (ME = 4.93 at 5 h and 5.90 at 24 h) but consistently stronger for *S. aureus* (ME = 1.37 at 5 h and 5.54 at 24 h).[162] In both cases AgNPs are firmly grafted

to the adhesive MPTS or PEI layer, and the microbicidal effect is due to slow Ag^+ release from the NP surface. Comparing Ag^+ release in pure water, measured by inductively coupled plasma optical emission spectrometry (ICP-OES), discloses similar values, with a slightly larger release in the present study. This strongly suggests also that the nature of the AgNPs surface offered to the interaction of bacteria has an important role in their antibacterial effect, at least for Gram-positive *S. aureus*. Although at an early stage of this research, authors have hypothesized an explanation which can be stated in this way: for an efficient antibacterial action *S. aureus* has to interact with a naked Ag–NP surface, even for high quantities of released Ag^+. This situation seems fully verified in the first example (grafting *via* MPTS), while only partially obtained in the second (grafting via PEI-silane), as some of grafted AgNPs seem fully embedded into the polymeric layer.

Recently, Taglietti and coworkers focused on another designed glass surface modified with AgNPs and on its antibiofilm properties.[172] Also in this case, a very simple, quick and cost-effective technique link of a self-assembled monolayer of AgNPs to glass was obtained through preliminary amino-silanization of the glass, using (3-aminopropyl)triethoxysilane (APTES), followed by immersion in an AgNPs colloidal suspension, as reported in **Scheme 3**.
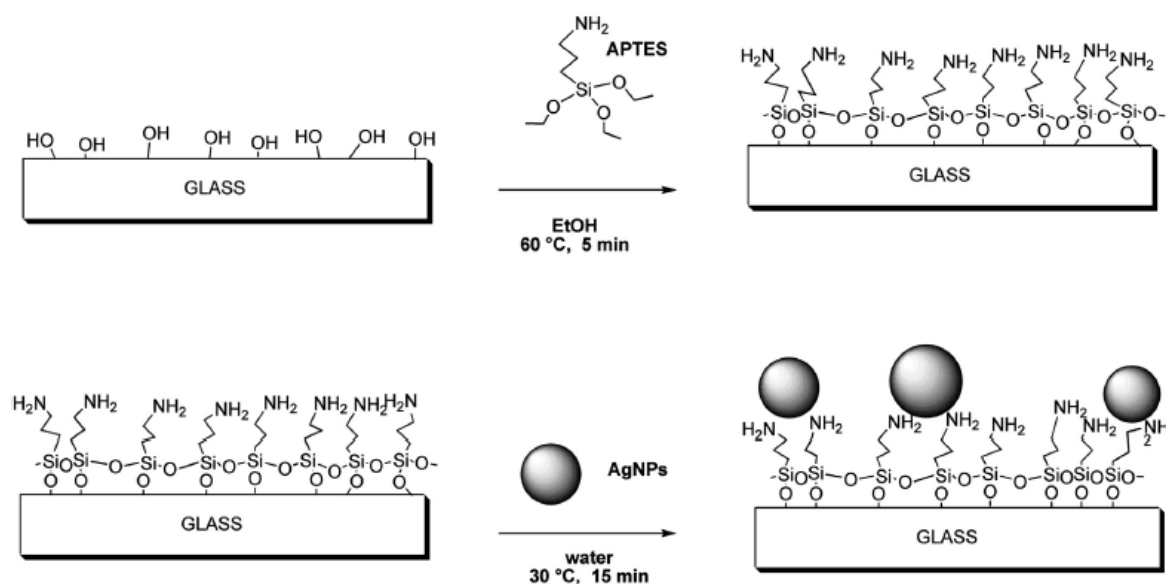
Scheme 3 Schematic representation of the silanization of glass surfaces with APTES and the subsequent grafting of a SAM of AgNPs.[172]

AgNPs-modified glass slides were stable in air, i.e. their spectra did not change significantly in a 3-week period. In addition, there were not any changes both in morphologies and dimension of

[172] A. Taglietti, C. Renata Arciola, A. D'Agostino, G. Dacarro, L. Montanaro, D. Campoccia, L. Cucca, M. Vercellino, A. Poggi, P. Pallavicini, L. Visai, *Biomaterials*, 2014, **35**,1779.

AgNPs grafted on glass kept in bidistilled water after twenty days as showed by Atomic Force Microscopy (AFM) images.

Furthermore, the study about Ag^+ release had revealed that: i) silver ions are progressively released in water as a function of immersion time, reaching a stationary concentration after approximately 3 days; ii) 80% of dissolved silver ions are released in the first day of immersion; iii) the maximum amount of silver ions released in these conditions is about 16% ($1.2*10^{-7}$ g/cm^2) of the total quantity of silver initially bound on the surface ($7.3*10^{-7}$ g/cm^2) as determined by quantitative oxidation and ICP analysis. According to authors, this behavior can be explained once again with the formation, in the initial 3-day period, of an Ag_2O layer on the water-exposed part of the surface of AgNPs linked to glass and placed in an aqueous environment, reaching a steady-state in which the slowly released Ag^+ ions are replaced by Ag oxidized from the bulk. Antibiofilm activity of control materials and of AgNPs-glass specimens was assayed with *S. epidermids* RP62A, a strain capable of producing a PIA-dependent biofilm. As clearly reported in **Figure 10**, significantly lower value of cell survivability was obtained from the AgNPs-glasses when compared with the control glasses: cell survival on the AgNPs-glasses was 10^5 times lower than that on the control glasses, as reported in **Figure 10A**. This finding corresponds to the results of ICP analysis, showing that AgNPs coatings are readily available to react with water and to release the Ag^+ ions. Therefore, authors deduced that Ag^+ interactions either with DNA or with the proteins of the bacterial cell-wall[173] led to cell death, as emerged from cell viability assay. To confirm the effect of AgNPs on bacterial viability, *Staphylococcal* biofilms of both controls and Ag-modified materials were studied by CLSM. The robust *Staphilococcus epidermidis* biofilms grown on the control materials presented a green fluorescence[172] and appeared organized as multilayered aggregates, as reported in **Figure 10B**. On the other side, presence of AgNPs caused the death of biofilm cells and biofilm disgregation, as can be seen from red coloration[172] reported in **Figure 10C**.

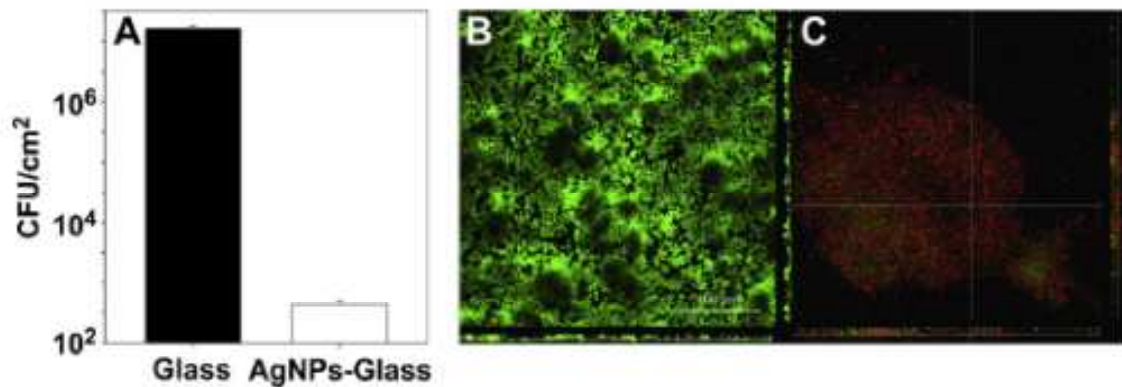[173]C. Damm, H. Münstedt, A. Rösch, *Mater Chem Phys*, 2008, **108**, 61.

Figure 10 Antibiofilm activity of AgNPs-modified glass specimens. Panel A: *S. epidermidis* RP62A biofilm was grown for 24 h at 37°C on unmodified glass or Ag-glass specimens. Data are representative of three experiments. Error bars indicate standard errors of the means. Panel B and C: CLSM images of *S. epidermidis* RP62A biofilm grown on plain glasses (B), and Ag-glass specimens (C). Biofilms were stained with BacLight Live/Dead Kit. Sagittal sections of the biofilms are shown below and to the right of each panel. Scale bar ¼ 100 mm.[172]

At CLSM analysis, the staphylococcal cells close to the surface of the AgNPs-modified glass appeared dead, and the poor biofilm-like substance in the proximity to Ag-glass exhibited only a scattered, extremely rarefied, and vanishing appearance, well different from the thick and dense biofilm clung to the unmodified glass.

In the presented experimental study, density and thickness of the biofilm observed under CLSM on the unmodified glass after 24-h confirmed that this culture period is suitable for the development of a mature biofilm by *S. epidermidis* RP62A and thus appropriate for the assessment of the modified glass anti-biofilm activity. Obviously in this context the ascertained anti-biofilm activity has to be intended as the ability to prevent biofilm establishment, and not as the ability to interfere with specific pathogenic mechanisms implicated in the biofilm production.[174] The powerful and, for some aspects, unprecedented antibiofilm activity observed on AgNPs-modified glass surfaces indicates that the new approach to achieve anti-infective surfaces has considerable potential.

It is important to stress the fact that, in all the three examples presented above, AgNPs are strongly anchored to the material surface, and cytotoxic effects on peri- and para-prosthesis cells and tissues can be expected to be negligible, or nearly absent for the tissues non in direct contact/distant from the surface of the biomaterial. With respect to the feared event of cytotoxic effects by free AgNPs, these studies show, by both physical and microscopic analyses, the stability

---

[174] D. Campoccia, L. Montanaro, C.R Arciola, *Biomaterials*, 2013, **34**, 8533.

of the AgNPs monolayers, seen in the lack of detachment of AgNPs from their anchor glass, as well as in the absence of variations in shape or size of the AgNPs.

Another important finding common to all reported works is the following: from the modified glass surfaces exposed to water, a controlled part of the total amount of silver loaded on the monolayer is always released in solution as Ag^+ ions, and Ag^+ release persists for several days, covering the period corresponding to the one in which bacterial adhesion and biofilm onset could more probably intervene after an implantation. This is the period more suitable to face the bacteria attempts at colonizing the material surfaces, when deep prostheses are going to integrate in the host tissues, and catheters, or other medical devices destined to be removed, perform and then complete their task. Obviously the higher the anti-infective action the lower will be the risk of an infection. Thus, by timely thwarting bacterial adhesion/colonization, the cause of the implant septic mobilization and failure could be removed, as well as catheters are prevented from becoming the source of a haematogenous spreading of bacteria deriving from biofilm leading to septicemia.[175]

Furthermore, Taglietti and coworkers have studied the mechanism of antibacterial activity of glutathione (gsh) coated silver nanoparticles AgNPs on model Gram-negative and Gram-positive bacterial strains.[116] Interference in bacterial cell replication have been observed for both cellular strains when exposed to gsh coated AgNPs in solution, and microbicidal activity was studied both when gsh coated AgNPs are dispersed in colloidal suspensions or grafted on thiol functionalized glass surfaces, exploiting the well-known layer-by-layer (LBL) approach, as depicted in **Scheme 4.**
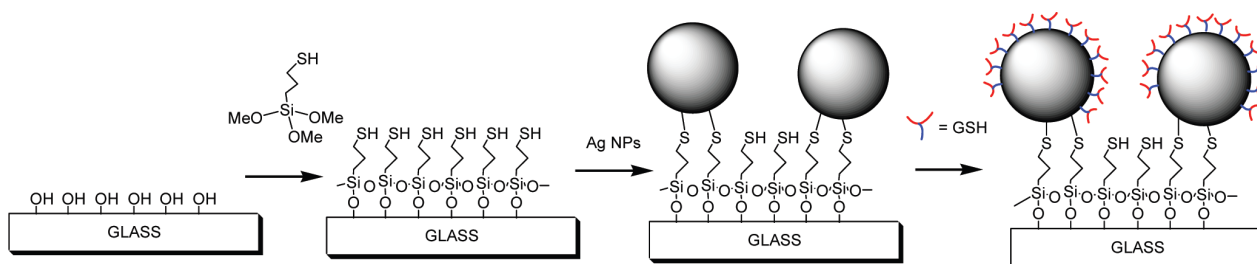
Scheme4 LbL approach for the preparation of glass samples functionalized with gsh coated AgNPs.[116]

The choice of the tripeptide glutathione (gsh) was done because it is an ideal candidate for this purpose, since this biomolecule displays a thiolic function, capable of being anchored to silver

---

[175] M. Lepainteur, M. Desroches, A.S. Bourrel, S. Aberrane, V. Fihman, F. L'hériteau, *Pediatr Infect Dis J*, 2013; **32**, 622.

surfaces,[176] and three pH-dependent, charged functional groups, carboxylates and amine, that promote water solubility and interactions toward more complex biostructures.[177]

Through TEM investigation, authors have observed that in some contrasted images the AgNPs coated with gsh, when used dispersed in colloidal suspensions containing bacterial cells, are visibly attached to the cellular wall of *S. aureus*, surrounded by lighter materials, presumably of biological origin, as can be seen in **Figure 11a** and **Figure 11b**. Massive aggregates of AgNPs surrounded by biological material are present in some TEM images of *S. aureus*, see **Figure 11c**, and less frequently in *E. coli* samples, see **Figure 11d**.
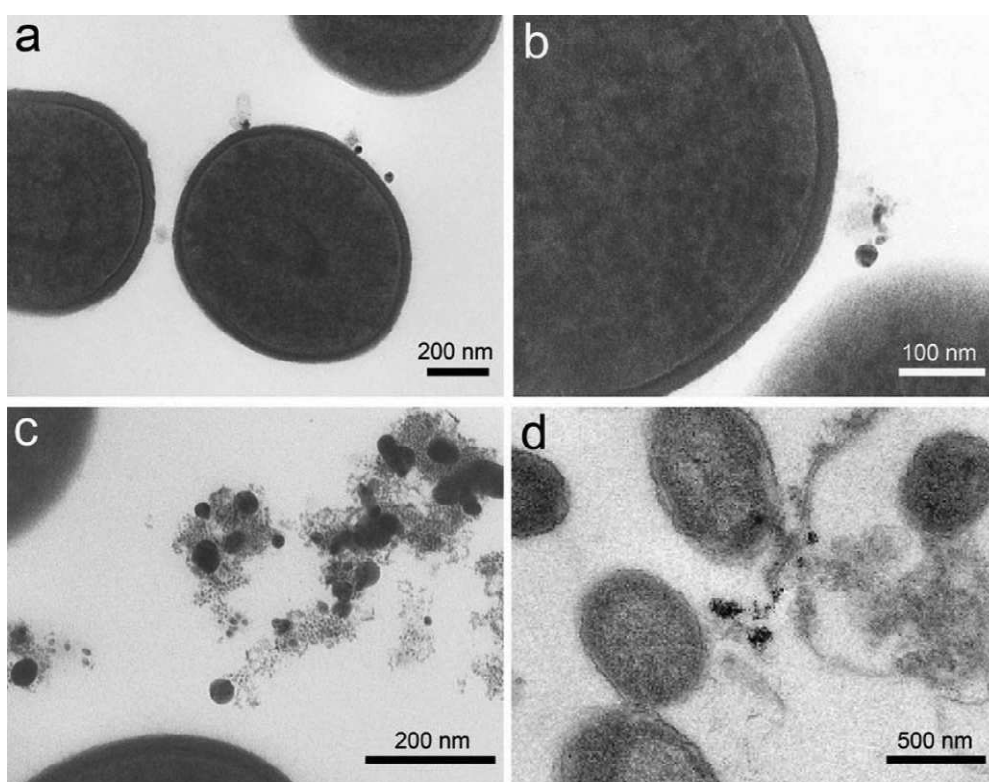

Figure 11 Interaction of gsh coated AgNPs with biological material from bacteria: (**a,b**) *S. aureus*, AgNPs attached to the cellular wall, surrounded by a lighter material presumably generated by the cells; massive aggregates composed by AgNPs and biological material observed outside the cells of (**c**) *S. aureus*, (**d**) *E. coli*.[116]

The results obtained from TEM imaging confirm that the effect of dispersed gsh capped AgNPs on *E. coli* is more intense because it can be associated with the penetration of the colloid into the cytoplasm, with the subsequent local interaction of silver with cell components causing damages to the cells. Conversely, for *S. aureus*, since the thick peptidoglycan layer of the cell wall prevents

[176] F. Frederix, J.M. Friedt, K.H. Choi, W. Laureyn, A. Campitelli, D. Mondelaers, G. Maes, G. Borghs, *Anal. Chem,* 2003, **75**, 6894.
[177] Q. Wu, H. Cao, Q. Luan, J. Zhang, Z. Wang, J.H. Warner, A.A.R. Watt, *Inorg. Chem*, 2008, **47**, 5882.

the penetration of the AgNPs inside the cytoplasm, the antimicrobial effect is limited and seems related to the interaction with the bacterial surfaces. In the case of *E. coli*, large zones of cellular damage associated to the NPs showed a local effect, once the NPs have been incorporated into the cytoplasm. The cellular material seemed to collapse around the included NP, and the cellular membrane was evidently disrupted to a large extent.

On the other hand, the antimicrobial activity of gsh AgNPs monolayers grafted on glass samples (by means of glass functionalization with MPTS as described at the beginning of this paragraph) against *E. coli* and *S. aureus* was investigated through the evaluation of the Microbicidal Effect (ME): data are reported in **Table 3.**

Sample	*S. aureus* ATCC 6538	*E.coli* 10356
gsh-AgNPs (5h)	0.24	0.42
gsh-AgNPs (24h)	0.96	1.38

Table 3 Microbicidal Effect (ME) of gsh AgNPs-modified glass after 5 and 24 h of contact. Reported data are the average of three experiments.

When the results of the ME on glass slides functionalized with gsh coated AgNPs are compared with the ME data for glass slides bearing the AgNPs monolayer as prepared (those reported in **Table 1**), it becomes evident that the coating with gsh of the exposed silver surface strongly reduces the antibacterial proprieties of this material. The dramatic decrease of ME is to be ascribed to the gsh coating itself, since the total amount of silver and the shape and dimensions of the NPs did not change after coating. It was also found that gsh-coated AgNPs grafted on glass released 12% (standard deviation 4%) of the total amount of silver in the monolayer, while glasses functionalized with bare NPs (i.e., in absence of gsh coating) reached a release of 14% (standard deviation 1%).[162] This evidence suggests that the antibacterial activity of grafted AgNPs is not necessarily related only to silver ion release, and that AgNPs surface coating plays a crucial role in the interaction with bacteria coming in close contact. In other words, if Ag^+ release was the only thing responsible for the ME, the value of ME should be the same in both cases (i.e., for glass samples coated with bare Ag NPs and with gsh coated AgNPs).

It is reasonable to conclude that, in the case of AgNPs grafted on glass, authors have observed two different processes that may concur with the overall microbicidal effects: the "long-distance" release of silver ions from the AgNPs and the "short-distance" nanomechanical action, involving interaction with membranes, which as expected is more intense toward Gram-negative bacteria. The overall mechanism of action of both grafted and dispersed AgNPs should be analyzed as a combination of these two processes.

In order to further investigate the action of the AgNPs grafted on the surface, authors have performed AFM characterization of the interaction of *E. coli* with functionalized glass surfaces. They decided to concentrate their efforts on *E. coli*, since this microorganism shows the greater sensibility to grafted AgNPs[168], and TEM data analysis revealed that internalization of AgNPs played an important role in their antibacterial activity against *E. coli*.

Figures 12 g-i report AFM imaging of *E. coli* after 5 h in contact with glass, functionalized with bare AgNPs, showing that cell membranes are completely disrupted, with evidence of cellular damage. The intracellular material has leaked and just a few cells still showed the rod-like characteristic morphology of *E. coli*, very distorted and characterized by irregular membrane surfaces. The volume of cells was considerably depressed, with respect to the control samples which are reported in **Figures 12a-c**. On the other hand, **Figures 12d-f** show AFM imaging of *E. coli* after 5 h in contact with glass samples functionalized with gsh coated AgNPs: in this case a less pronounced damaging is observed, in good agreement with the data obtained from ME experiments.
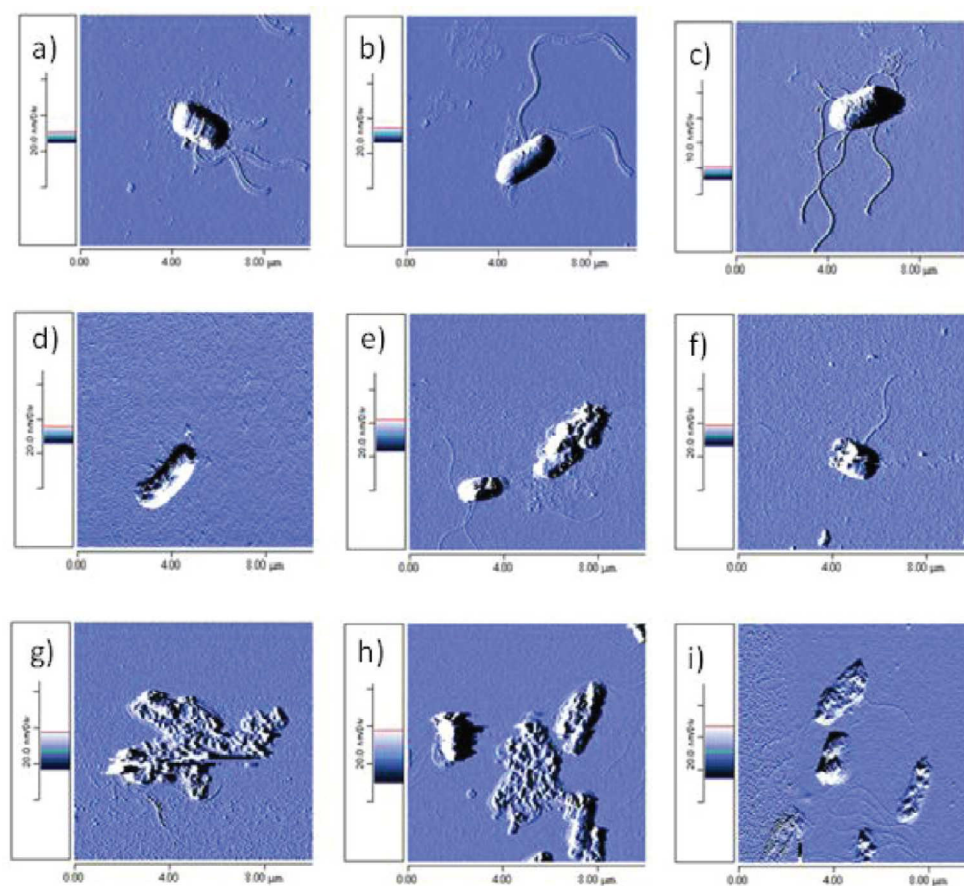
Figure 12 Representative AFM images of *E. coli* bacteria after contact for 5 h with (**a,b,c**) reference clean glass slides; (**d,e,f**) glass slides functionalized with gsh-coated AgNPs; (**g,h,i**) glass slides functionalized with bare AgNPs.[116]

These results can be interpreted again by considering the two mechanism of action discussed previously. When bacteria are exposed to glass functionalized with bare AgNPs, the Ag$^+$ release mechanism and the direct nanoscale contact with silver surface are both present. The synergy of these two processes leads to generalized cell damage and causes a very strong microbicidal effect. On the other hand, when *E. coli* cells are exposed to gsh-coated AgNPs grafted to glass surface, Ag$^+$ is released, but the gsh coating presumably prevents the direct contact of cell membrane structures with Ag surfaces; therefore, cellular damage is less evident, corresponding to less intense antibacterial activity. It is not surprising that the "nano-mechanical" contact effect produces the most dramatic damage to the cells, considering that cellular membranes contains thiol bearing proteins and phospholipids that present high affinity for silver surfaces.[178]

---

[178] W. Li, X. Xie, Q. Shi, H. Zeng, Y. OU-Yang, Y. Chen, *Appl. Microbiol. Biotechnol.*, 2010, **85**, 1115.

1.2.5 Characterizations of AgNPs

AgNPs are widely used in many applications consequently it is important to synthesize high-quality materials. In certain applications it is also important to prepare colloids with high concentrations. The size and size distribution become extremely significant when quantum-sized effects are used to control material properties. Therefore, the control and complete analysis of the average particle size and narrow size distribution is essential to use AgNPs in many applications.[179]

There are a number of methods for nanoparticles size characterization, for example, scanning/transmission electron microscopy (SEM/TEM), atomic force microscopy (AFM), dynamic light scattering (DLS). It is also possible to calculate particles size with the use of X-ray diffraction (XRD) patterns as well as with the shift of the band gap absorption in the UV-Vis spectrum. In case of the above-mentioned method, the particle size distribution is measured in dispersion or after drying the sample. Of course, also the morphology of the nano-objects is of enormous importance, as it is related to spectroscopic features as already stated. Another property of extreme interest is the surface charge of the nano-objects, as it can influence both their stability and interactions with living systems.

Some of the techniques of nanoparticles characterization the most commonly used are described below.

1.2.5.1 UV-Vis Spectroscopy

In case of UV-Vis spectroscopy, the intensity of light that is passing through the sample is measured. Nanoparticles have optical properties that are very sensitive on size, shape, agglomeration, and concentration changes. The unique optical properties of metal nanoparticles are a consequence of the collective oscillations of conduction electrons, which excited by electromagnetic radiation are called surface plasmon resonances (SPR).[74] Those changes have an influence on the refractive index next to the nanoparticles surface; thus it is possible to characterize nanomaterials using UV-Vis spectroscopy. UV-Vis spectroscopy is fast and easy to operate techniques for particles characterization, especially for colloidal suspensions. There are several advantages UV-Vis techniques: simplicity, sensitivity and selectivity to AgNPs, short time of measurement, and what is more, the calibration is not required.

---

[179] O.V. Salata, *J. Nanobiotech.,* 2004, **2**, 3.

Ultraviolet/Visible/Infrared (UV/Vis/IR) spectroscopy is a technique used to quantify the light that is absorbed and scattered by a sample (a quantity known as the extinction, which is defined as the sum of absorbed and scattered light). In its simplest form, a sample is placed between a light source and a photodetector, and the intensity of a beam of light is measured before and after passing through the sample. These measurements are compared at each wavelength to quantify the sample's wavelength dependent extinction spectrum. The data is typically plotted as extinction as a function of wavelength. Each spectrum is background corrected using a "blank" – a cuvette filled with only the dispersing medium to guarantee that spectral features from the solvent are not included in the sample extinction spectrum.

The transmittance of a sample (T) is defined as the fraction of photons that pass through the sample over the incident number of photons, i.e., $T = I/I_0$. In a typical UV-Vis spectroscopy measurement, we are measuring those photons that are not absorbed or scattered by the sample. It is common to report the absorbance (A) of the sample, which is related to the transmittance by $A = -\log_{10}(T)$.

Most samples have contributions from both scattering and absorption. In some cases, it is possible to calculate the contribution of each effect using Mie theory.[77] The calculated absorption spectrum for 40 nm AgNPs is shown in **Figure 4** (**Paragraph 1.2.2**) along with the expected contributions from scattering and absorption.

Scattering from a sample is typically very sensitive to the aggregation state of the sample, with the scattering contribution increasing as the particles aggregate to a greater extent. For example, the optical properties of silver nanoparticles change when particles aggregate and the conduction electrons near each particle surface become delocalized and are shared amongst neighboring particles. When this occurs, the surface plasmon resonance shifts to lower energies, causing the absorption and scattering peaks to red-shift to longer wavelengths. UV-Visible spectroscopy can be used as a simple and reliable method for monitoring the stability of nanoparticle solutions. As the particles destabilize, the original extinction peak will decrease in intensity, due to the depletion of stable nanoparticles, and often the peak will broaden or a secondary peak will form at longer wavelengths, because of the formation of aggregates. In the **Figure 13**, the extinction spectrum of 50 nm AgNPs is monitored as sodium carbonate is added to the solution (20 mM salt concentration).The rapid and irreversible change in the extinction spectrum clearly demonstrates that the nanoparticles are agglomerating. UV-Vis spectroscopy can be used as a characterization

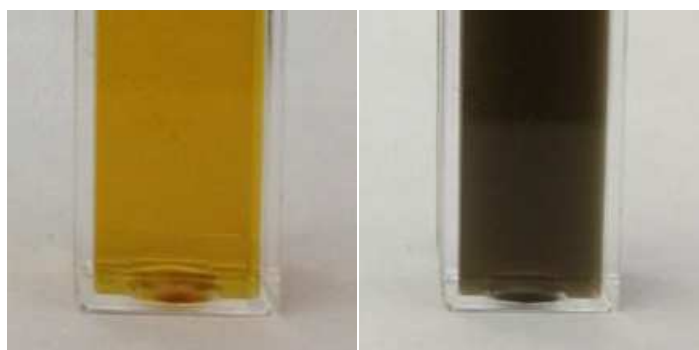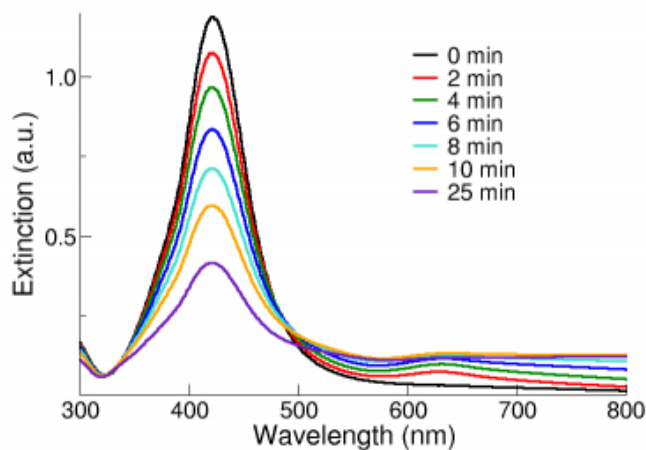technique that provides information on whether the nanoparticle solution has destabilized over time.

Figure 13 Absorption spectrum (upper) of silver nanoparticles changes as the particles transition from a well-dispersed state to an aggregated state following the addition of a concentrated salt solution; as aggregation proceeds, the plasmon peak at 420 nm decreases, a secondary peak at 620 emerges, and the baseline elevates due to scattering by aggregates. The final aggregated state is readily seen by eye, as the original dispersed particles form a yellow solution (lower, left) and the aggregated particles become grey (lower, right).[179]

1.2.5.2 Dynamic Light Scattering

Dynamic Light scattering, DLS, measures the light scattered from the laser that passes through a colloid. Next, the modulation of the scattered light intensity as a function of time is analyzed, and the hydrodynamic size of particles can be determined.[180] DLS, which is also known as photon correlation spectroscopy (PCS) or quasi- elastic light scattering (QLS), is a spectroscopy method used in the fields of chemistry, biochemistry, and physics to determine the size distribution of particles (polymers, proteins, colloids, etc.) in solution or suspension. In the DLS experiment,

---

[180] B.J. Berne, R. Pecora, *Dynamic Light Scattering: With Applications to Chemistry, Biology, and Physics*, (Dover,New York, 2000).

normally a laser provides the monochromatic incident light, which impinges onto a solution with small particles in Brownian motion. And then through the Rayleigh scattering process, particles whose sizes are sufficiently small compared to the wavelength of the incident light will diffract the incident light in all direction with different wavelengths and intensities as a function of time. Since the scattering pattern of the light is highly correlated to the size distribution of the analyzed particles, the size-related information of the sample could be then acquired by mathematically processing the spectral characteristics of the scattered light.

As a result of the Brownian motion, the distance between particles is constantly changing and this results in a Doppler shift between the frequency of the incident light and the frequency of the scattered light. Since the distance between particles also affects the phase overlap/interfering of the diffracted light, the brightness and darkness of the spots in the speckle pattern will in turn fluctuate in intensity as a function of time when the particles change position with respect to each other. Then, as the rate of these intensity fluctuations depends on how fast the particles are moving (smaller particles diffuse faster), information about the size distribution of particles in the solution could be acquired by processing the fluctuations of the intensity of scattered light.

In a typical DLS experiment, light from a laser passes through a polarizer to define the polarization of the incident beam and then shines on the scattering medium. When the sizes of the analyzed particles are sufficiently small compared to the wavelength of the incident light, the incident light will scatter in all directions: this is known as Rayleigh scattering. The scattered light then passes through an analyzer, which selects a given polarization and finally enters a detector, where the position of the detector defines the scattering angle. In addition, the intersection of the incident beam and the beam intercepted by the detector defines a scattering region of volume V. As for the detector used in these experiments, a phototube is normally used whose dc output is proportional to the intensity of the scattered light beam.

1.2.5.3 Zeta Potential

All materials will spontaneously acquire a surface electrical charge when brought into contact with a polar medium (i.e., water).[181] Generally an interface in deionized water is negatively charged, but there are materials that can be positively charged.[182] Among the various charging mechanisms awe can cite: electron affinity differences of two phases ionization of surface groups, differential

---

[181] Lyklema J, Fundamentals of Interface and Colloid Science. Amsterdam, The Netherlands: Elsevier Publishing Company (1991).
[182] Hunter RJ, Zeta Potential in Colloid Science. London, England: Academic Press (1981)

ion adsorption from electrolyte solution; differential ion dissolution from a crystal lattice, surface anisotropy isomorphous substitution.

When a particle dispersed in a liquid is solvated, the extent of the solvated layer is influenced by the solution conditions such as composition (i.e., pH, ionic strength), temperature and pressure.[183] The boundary between the edge of this solvated layer and bulk liquid is named shear plane.

A "structure", called the electric double-layer (EDL) will be developed such that the particle surface charge is neutralized by an adjacent layer in solution containing an excess of ions of opposite charge to that of the surface, i.e., counter-ions; ions of the same charge as the surface are termed co-ions.[184] Briefly, the EDL can be regarded as consisting of two regions or layers, hence the term electric double-layer.

Figure 14 schematically shows a region closest to the surface (the Stern layer) that is considered immobile (and it may include adsorbed ions) and an outer region (the diffuse layer) that allows diffusion of ions that are distributed according to the influence of electrical forces and random thermal motion.
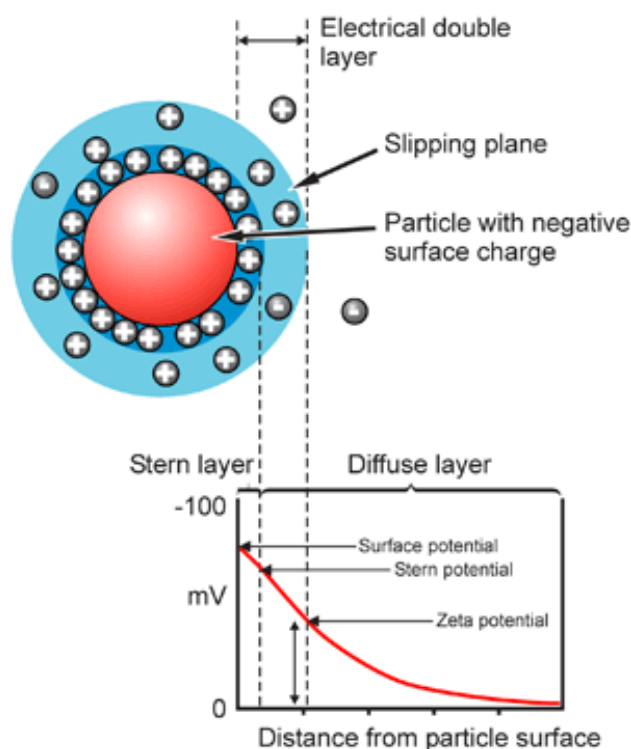

Figure 14 Schematic representation of the electrical double layer [181]

---

[183] Hunter RJ, *Foundations of Colloid Science, 2nd Edition*, (England: Oxford University Press 2001).
[184] R.J. Parsons, *Electroan. Interf. Electr.*, 1981, **118**, 3.

The electric potential decreases linearly from surface potential (the actual thermodynamic surface potential) to the Stern potential, in correspondence with the Stern layer, and then it decays exponentially to zero in the diffuse layer. The decay of electric potential with the distance from the particle surface depends on the ionic composition of the medium.

Unfortunately, the fundamental interfacial property, the surface potential, is inaccessible. What can be derived (and measured) is an electrokinetic potential termed the zeta potential P_z. This quantity, defined as the potential at the shear (or slipping) plane, has become a very useful experimental parameter to monitor electrokinetic behavior of suspensions, especially changes in such behavior.[183] Briefly, the shear plane can be considered as the boundary of a zone in which solvent molecules and ions "move togheter" with the particle: in other words one can consider that they act as if they are attached to the particle. Generally, nanoparticles with high zeta potential (negative or positive) are stabilized by strong electrostatic repulsions, while nanoparticles with low zeta potentials tend to coagulate or flocculate.

Zeta potential was measured with a Zetasizer Nano ZS90 Malvern instrument, equipped with dedicated cuvettes in which 1 mL of sample is placed. The values of P_z are expressed in mV.

1.2.5.4 Contact Angle

Wettability studies of surfaces usually have received tremendous interest from both fundamental and applied points of view. Wettability plays an important role in many industrial processes, such as oil recovery, lubrication, liquid coating, printing, and spray quenching.[185] In recent years, there has been an increasing interest in the study of superhydrophobic surfaces, due to their potential applications in, for example, self-cleaning, nanofluidics, and electrowetting.[186] Studies usually involve the measurement of contact angles as the primary data, which indicates the degree of wetting when a solid and liquid interact. Small contact angles (<90°) correspond to high wettability, while large contact angles (>90°) correspond to low wettability.

Consider a liquid drop resting on a flat, horizontal solid surface. The contact angle is defined as the angle formed by the intersection of the liquid-solid interface and the liquid-vapor interface (geometrically acquired by applying a tangent line from the contact point along the liquid-vapor interface in the droplet profile). The interface where solid, liquid, and vapor co-exist is referred to as the "three phase contact line". **Figure 15** shows that a small contact angle is observed when the

---

[185] J. Perelaer, C.E. Hendriks, A.W.M. de Laat, U.S. Schubert, *Nanotechnolog*, 2009, **20**, 165303.
[186] M. Rauscher, S. Dietrich, *Annu. Rev. Mater. Sci.*, 2008, **38**, 143.

liquid spreads on the surface, while a large contact angle is observed when the liquid beads on the surface. More specifically, a contact angle less than 90° indicates that wetting of the surface is favorable, and the fluid will spread over a large area on the surface; while contact angles greater than 90° generally means that wetting of the surface is unfavorable so the fluid will minimize its contact with the surface and form a compact liquid droplet. For example, complete wetting occurs when the contact angle is 0°, as the droplet turns into a flat puddle. For superhydrophobic surfaces, water contact angles are usually greater than 150°, showing almost no contact between the liquid drop and the surface, which can rationalize the "lotus effect".[187].
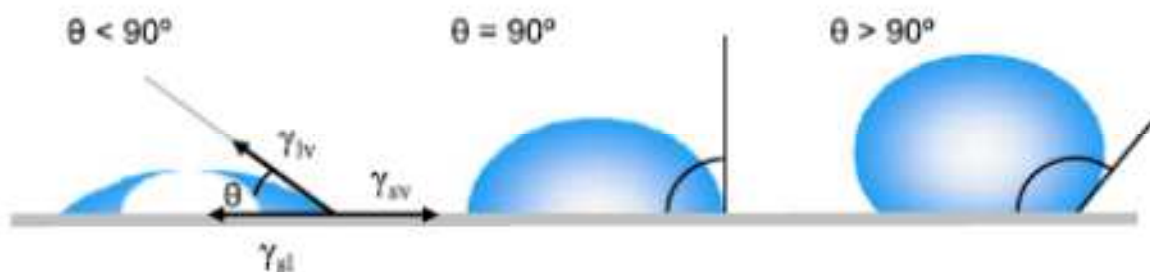

Figure 15 Illustration of contact angles formed by sessile liquid drops on a smooth homogeneous solid surface.[185]

Furthermore, contact angles are not limited to the liquid vapor interface on a solid; they are also applicable to the liquid-liquid interface on a solid. Theoretically, the contact angle is expected to be characteristic for a given solid-liquid system in a specific environment.[188]

As first described by Thomas Young in 1805[189], the contact angle of a liquid drop on an ideal solid surface is defined by the mechanical equilibrium of the drop under the action of three interfacial tensions, as shown in **Figure 15**.

$$\gamma_{lv} \cos \vartheta_Y = \gamma_{sv} - \gamma_{sl}$$

where γ_{lv}, γ_{sv}, and γ_{sl} represent the liquid-vapor, solid-vapor, and solid-liquid interfacial tensions, respectively, and ϑ_Y is the contact angle. It is usually referred to as Young's equation, and ϑ_Y is Young's contact angle.

Generally, contact angle was measured by an equipment that consists of a horizontal stage to mount a solid or liquid sample, a micrometer pipette to form a liquid drop, an illumination source,

[187] A. Lafuma, D. Quere, *Nat. Mater.*, 2003, **2**, 457.
[188] J.H. Snoeijer, B. Andreotti, *Phys. Fluids*, 2008, **20**, 057101.
[189] T. Young, *Philos. Trans. R. Soc. Lond.*, 1805, **95**, 65.

and a telescope equipped with a protractor eyepiece. The measurement was achieved by simply aligning the tangent of the sessile drop profile at the contact point with the surface and reading the protractor through the eyepiece. Over the years, modifications of the equipment have been made to improve the accuracy and precision. A camera can be integrated to take photographs of the drop profile so as to measure the contact angle at leisure. The use of relatively high magnifications enables a detailed examination of the intersection profile.

1.2.5.5 Microbicidal Effect

The evaluation of antimicrobial activity of AgNPs grafted on different kind of SAM (-SH[162], -NH$_2$[172], -PEI[167]) described so far and which has been used in this thesis, is effectuated through an *in vitro* procedure developed by Professor Pietro Grisoli at Drug Science Department of University of Pavia.

In the proposed procedure, the antibacterial activity of functionalized surfaces is typically investigated against *S. aureus* ATCC 6538, Gram-positive strain and *E. coli* ATCC 10356, Gram-negative strain. First of all, the microorganisms are grown overnight in Tryptone Soya Broth (Oxoid; Basingstoke, Hampshire, England) at 37 °C. Washed cells are re-suspended in Dulbecco's PBS and optical density (OD) was adjusted to 0.2 at 650 nm wavelength, corresponding approximately to 1x10^8 Colony Forming Units (CFU)/mL. Then, 10 µL of bacterial suspension are deposited on a standard glass slide (76x26 mm), as in **Figure 15a**, and after that the microbial suspension is covered with a functionalized cover glass slide (21x26 mm), forming a thin film between the slides that facilitates direct contact of the microorganisms with the active surface, as in **Figure 15b**. The two assembled glasses were introduced in a Falcon test-tube (50 mL) containing 1 mL of PBS to maintain a damp environment, see **Figure 15c**.

a)

b)

c)
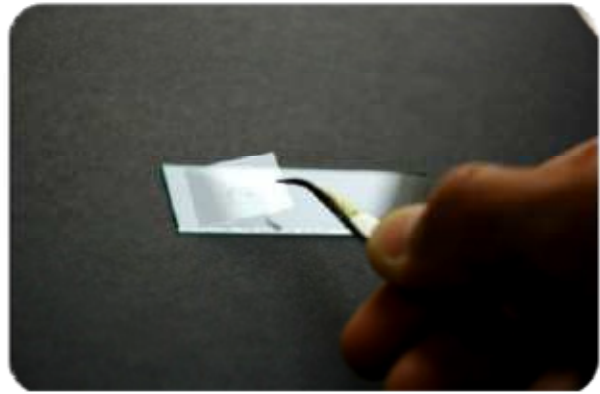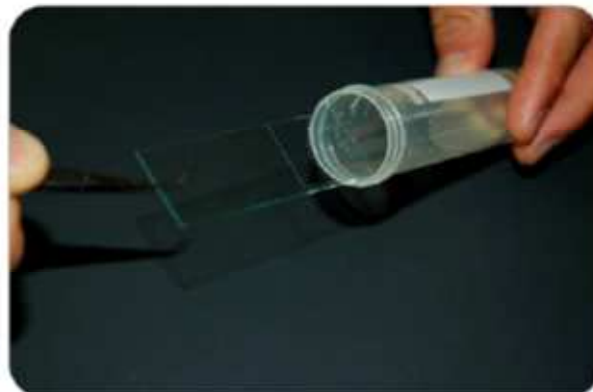
Figure 15 a) 10 µL of bacterial suspension was deposited on a standard glass slide (76x26 mm); **b)** a thin film between the slides that facilitates direct contact of the microorganisms with the active surface is formed; **c)** the two assembled glasses were introduced in a Falcon test-tube.

In this test microbes are incubated in non-nutritive suspensions that do not give the microorganisms the potential to grow during the test. For each bacterial strain more equivalent modified glasses are prepared; the slides are maintained in contact with the liquid films containing bacteria at room temperature for given times, usually reaching a long contact time of at least 24 hours; for each time of contact an unmodified glass slide is treated in the same way as control sample. After the times of contact, 9 mL of PBS are introduced in each Falcon test tube under a gentle shaking to detach the assembled glass slides. Bacterial suspensions are then cultured on Tryptone Soya Agar (Oxoid; Basingstoke, Hampshire, England) to count viable cells. The decimal-log reduction rate, *i.e.* the Microbicidal Effect (ME), can now be calculated using the formula:

$$ME = \log NC - \log NE$$

(**NC** being the number of CFU/mL developed on the unmodified control glasses, and **NE** being the number of CFU/mL counted after exposure to modified glasses).

The results expressed as ME represent the average of three equivalent determinations. This method can be considered as a version of the Japanese Industrial Standard JIS Z 2811 developed to measure the antibacterial activity of plastic surfaces.

The higher the value of ME, higher is antimicrobial activity of fuctionalized glass. It is necessary to underline that as the CFU counted in the control measures reach at least a value of 10^5, although varying every time as consequence of difference of the experimental conditions, when no CFU can be found in the samples coming from fuctionalized we assign to ME a value of 5, to indicate that at least 99.999% of bacteria were eliminated during the test.

In this thesis, in addition to ME here described, also another similarly defined parameter will be used: the thermal Microbicidal Effect (ME_T), which will describe the antimicrobial action given by the photo-thermal effect obtained with proper Laser irradiation of properly prepared glass slides bearing peculiar silver nano-objects: it will be introduced and described in **Paragraph 2.2 and 2.3**.

1.3 Purpose of Thesis

The research work of this thesis was devoted on two main topics: (A) anisotropic silver nanoparticles for antibacterial application; (B) spherical silver nanoparticles for pharmaceutical application.

(A) Two surfactant free seed-mediated growth methods were designed in order to obtain anisotropic silver nano-objects, silver nano-plates, with the desired shape, dimensions and plasmonic features. The two method imagined were: (i) seed growth synthesis with a subsequent grafting on properly functionalized glass samples (pre grafting growth method) (ii) synthesis with the direct growth on seeds previously grafted on glass (post grafting growth method). The common idea was to impart a double antibacterial action: the well-known, long term antibacterial effect based on the release of Ag$^+$ and an "on demand" action which can be switched on by the use of photo-thermal properties of silver nano-objects. Moreover, we also wanted to test the ability of this kind of materials to act as SERS substrates.

(B) Having in mind the design of pharmaceutical and surgical preparations based on silver nanoparticles conveniently coated with biomolecules typically used in pharmaceutical preparations, we have projected a green synthesis of spherical silver nanoparticles with pectin, a classical biopolymer. The project involved at first the study of the optimization of the synthetic conditions, followed by a complete characterization including studies of antibacterial and wound-healing properties.

Following the same interest, during the visiting research at School of Pharmacy of Queen's University (UK), interactions of spherical AgNPs with antimicrobial peptide (AMP) were investigated, as well the antimicrobial activity of AgNPs mixed with AMP against Gram-positive and Gram-negative bacteria strains.

CHAPTER 2: ANISOTROPIC AgNPs FOR ANTIBACTERIAL ACTIVITY

2.1 Introduction

The antibacterial and antiviral actions of AgNPs have been thoroughly investigated over the past few decades. We have already presented the main factors which influence antimicrobial activity of AgNPs, giving great attention about the possible mechanisms.

However, does the antibacterial activity of AgNPs depend on the size and shape of the nanoparticle? While a huge amount of papers reports about antibacterial effects of spherical AgNPs, until a few years ago a limited number of studies investigating the antibacterial activity of anisotropic silver nano-objects has appeared. A first fundamental report[1] showed that truncated triangular nanoplates, with a [111] lattice plane as the basal plane, were more efficient compared with spherical AgNPs and rod shaped nanoparticles in killing *E. coli*, suggesting the existence of a shape-dependent interaction between AgNPs and Gram-negative bacteria. Recently the use of anisotropic silver nanoparticles started to gain some augmented interest, also driven by the fact that Localized Surface Plasmon Resonance (LSPR) properties of noble metal nano-objects are strongly dependant from size and shape, and that this feature can be exploited to obtain nano-objects having a wide range of colors exploitable in coating of textile fibers to obtain colorful antibacterial fabrics.[2,3] Recent studies discussed the antibacterial effects of triangular, truncated triangular and hexagonal plates, and some comparison with spherical AgNPs was tempted.[4] In a very recent example, the strong antibacterial activity of anisotropic nanoparticles toward *P. aeruginosa* cells was demonstrated when applied to corneal replacements. [5]

2.1.1 Synthesis of Anisotropic AgNPs

Synthetic strategies for the fabrication of plasmonic nanostructures with controlled shape, size, and composition have undergone a severe revolution over the last ten years. If nowadays it is possible to prepare almost any imaginable structure for gold,[6] regarding silver, the preparation of well defined structures has also been achieved either directly through physical or chemical routes

[1] S. Pal, Y.K. Tak, J.M. Song, *Applied and Environmental Microbiology*, 2007, **73**, 1712.

[2] B. Tang, J.L. Li, X. Hou, T. Afrin, L. Sun, X.G. Wang, *Industrial & Engineering Chemistry Research*, 2013, **52**, 4556.

[3] I. Vukoje, V. Lazic, V. Vodnik, M. Mitric, B. Jokic, S.P Ahrenkiel, J.M. Nedeljkovic, M. Radetic, *Journal of Materials Science*, 2014, **49**, 4453.

[4] M.J. Gao, L. Sun, Z.Q. Wang, Y.B. Zhao, *Materials for Biological Applications*, 2013, **33**, 397.

[5] E.I. Alarcon, B. Vulesevic, A. Argawal, A. Ross,P. Bejjani, J. Podrebarac, R. Ravichandran, J. Phopase, E.J Suuronen, M. Griffith, Nanoscale, 2016, **8**, 6484.

[6] C. Burda, X. Chen, R. Narayanan, M.A. El-Sayed, *Chem. Rev.*, 2005, **105**, 1025.

or after one or more purification steps, [7] although progress in the control of the possible sizes and geometries is not comparable to the one obtainable for gold. At present, a wealth of methods are available for generating Ag nanostructures with different sizes and shapes. **Table 1** shows an overview of the many structures that have been synthesized in the solution phase.
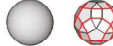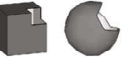
Shape	Illustration	LSPR[a]	Applications[b]	Method of Synthesis
Sphere and quasi-sphere		320 - 450	SERS; LSPR sensing; assembly	Polyol process (single-crystal); Citrate reduction (quasi-sphere)
Cube and truncated cube		400 - 480	SERS; LSPR sensing; assembly	Polyol process; Seed-mediated growth
Tetrahedron and truncated tetrahedron		350 - 450	SERS	Polyol process; Light-mediated Growth
Octahedron and truncated octahedron		400 - 500	Assembly	Polyol process; seed-mediated growth; light-mediated growth
Bar		350 - 900	SERS	Polyol process
Spheroid		350 - 900	SERS	Polyol process
Right bipyramid		500 - 700	-	Polyol process
Beam		-	Electron transport	Polyol process
Decahedron		350 - 450	-	Seed-mediated growth; light-mediated growth; citrate reduction
Wire and rod		380 - 460	Wave guiding; electronics; SERS; assembly	Seed-mediated growth
Polygonal plates and disc		350 - 1000	SERS; LSPR sensing	Light-mediated growth; polyol process
Branched structures		400 - 1100	SERS	Seed-mediated growth
Hollow structures		380 - 800	SERS; LSPR sensing	Template-directed growth

Table 1 Summary of the shapes, LSPR Absorption Peaks, applications, and methods for synthesis of silver nanoparticles.[8]

Among silver nanoparticles with different shape, a particularly interesting morphology has been shown to involve Ag nanoplates, also termed nanoprisms or nanodisks, in which the lateral dimensions are notably larger than their height, so that they possess an extreme degree of anisotropy.

---

[7] I. Pastoriza-Santos, L.M. Liz-Marzan, *J. Mater. Chem.,* 2008, **18**, 172.
[8] M. Rycenga, C.M. Cobley, J. Zeng, W. Li, C.H. Moran, Q. Zhang, D. Qin, Y. Xia, *Chem. Rev.*, 2011, **111**, 3669.

There are different approaches that have been reported for the synthesis of Ag triangular nanoplates with a significant yield, defined as the percentage of plate-like particles in the sample. Most of the methods included here are based on wet chemistry techniques.

Wet Chemical Reduction by Surfactant-Assisted Methods

In the midst of all available surfactants, cetyltrimethylammonium bromide, CTAB, has become one of the most extensively used capping agent in the synthesis of anisotropic Ag nanoparticles. This cationic surfactant has been applied for the preparation of a wide variety of geometries including spheres, rods, or nano- and microplates. In many cases CTAB plays an essential role in acting as shape-directing agent. Generally, these approaches for the preparation of nanoplates are based on the reduction of the metal salt with a mild reducing agent, usually ascorbic acid, in the presence of CTAB. Further investigation of the fundamental aspects of these experimental parameters, together with the use of other reducing agents[9] or temperature,[10] was carried out to properly understand and control the fabrication of silver anisotropic nanomaterials.

Moreover, another surfactant that is commonly used in the fabrication of nanoplates is bis(2-ethyl-hexyl)sulfosuccinate, AOT. Pileni et al.[11] used reverse micelles of AOT in isooctane to prepare Ag nanodisks by reduction of a silver salt with hydrazine. The size was controlled between 30 and 100 nm by the relative amount of hydrazine. However, the wide size distribution together with the important amount of Ag spheres ruined the interesting optical properties of the nanodisks. Nevertheless, using AOT as stabilizer, Jiang et al.[12] obtained Ag nanoplates and nanodisks with excellent optical properties in the visible-NIR range. They employed a self-seeding co-reduction method comprising a Ag seed suspension with traces of $NaBH_4$, subsequently grown by cooperative reduction with citric and ascorbic acid. Although the reaction products were triangular nanoplates, Ostwald ripening spontaneously promoted the evolution of the plates into disks at room temperature. The same authors discovered that particle evolution could be detained by attaching thiols onto the silver surface.[7]

[9] L. Zhang, C.Z. Huang, Y.F. Li, Q. Li, *Cryst. Growth Des.*, 2009, **9**, 3211.
[10] H.M. Chen, R.S. Liu, D.P. Tsai, *Cryst. Growth Des.*, 2009, **9**, 2079.
[11] M. Maillard, S. Giorgio, M.P. Pileni, *Adv. Mater.*, 2002, **14**, 1084.
[12] X. Jiang, Q. Zheng, A. Yu, *Nanotechnology*, 2006, **17**, 4929.

Wet Chemical Reduction by Polymer-Assisted Methods

Polyvinylpyrrolidone (PVP) is undoubtedly the most popular polymer in the chemical synthesis of a wide variety of metal nanocrystals since its introduction in the seventies.[13] Although the major role of PVP is to act as capping agent, it has been demonstrated that it may also act as a mild reducing agent.[14] Additionally, PVP has often been claimed to play a key role in determining the final particle morphology, through stronger adsorption onto certain crystalline facets.

The first application of PVP to stabilize silver nanoplates (truncated triangles, < 80 nm edge length), was devised by Pastoriza-Santos and Liz-Marzán by using *N*,*N*-dimethylformamide (DMF) as reducing agent and solvent.[15] The use of larger concentrations of both $AgNO_3$ and PVP proved a key factor to determine the final morphology. A mechanism was proposed involving the aggregation of small Ag nanoparticles, followed by recrystallization into single crystals, so that the edge size could be controlled through the reaction time.

A very similar approach was later used by Jiang et al.[16] who prepared silver nanoplates in DMF, also in the presence of PVP, but via an ultrasonic-assisted Ostwald ripening process. The authors invoked the role of PVP as a stabilizer and shape directing agent to induce triangular shapes through kinetic growth control of various faces through dynamic PVP adsorption and desorption processes. Similarly, a polyol-mediated synthesis was used by Xiong et al[17] by simply heating at 135 °C a solution of $AgNO_3$ in polyacrylamide (PAM). PAM was not only reported to serve as reducing and capping agent, but also to form complexes with Ag^+ ions through the amine groups. This coordination was supposed to slow the reduction process, so that in this case the particle shape was dictated by kinetics rather than by the capping agent effect.

Seed mediated growth

Seed-mediated growth represents a simple and robust route to nanocrystals with well-defined and controllable shapes or morphologies, and thus desired properties.[18] As a major advantage over conventional methods, introduction of preformed seeds into a synthesis allows growth to be

[13] H. Hirai, Y. Nakao, N. Toshima, *Chem. Lett.*, 1978, 545.
[14] I. Washio, Y. Xiong, Y. Yin, Y. Xia, *Adv. Mater.* 2006, **18**, 1745.
[15] I. Pastoriza-Santos, L.M. Liz-Marzán, *Nano Lett.*, 2002, **2**, 903.
[16] L.P. Jiang, S. Xu, J.M. Zhu, J.R. Zhang, J.J. Zhu, H.Y. Chen, *Inorg. Chem.,* 2004, **43**, 5877.
[17] Y. Xiong, A.R. Siekkinen, J. Wang, Y. Yin, M. J. Kim, Y. Xia, *J. Mater. Chem.*, 2007, **17**, 2600.
[18] R. Jin, Y.C. Cao, E. Hao, G S. Metraux, G.C. Schatz, C.A. Mirkin, *Nature,* 2003, **425**, 487.

disentangled from nucleation, thus making it easier to obtain a specific shape by only focusing on parameters that influence the growth. Unlike the methods discussed so far, the nucleation and growth steps are separated in this type of synthesis, allowing for a greater control over the final morphology.[19] In general, the outcome of a seed-mediated synthesis is determined by the following factors:[20] (i) the difference in lattice constant between the seed and the deposited metal; (ii) the internal structure of the seed, including twin defects, stacking faults, and grain boundaries; (iii) the facets expressed on the seed and the presence of capping agents such as surfactants, polymer stabilizers, ionic species, as well as unknown contaminants, that are capable of binding selectively to different types of facets; and (iv) the reduction or growth kinetics. When oxidative etching is involved, seeds that contain twin defects could be selectively oxidized and dissolved, even before the growth process is started.[21] As a result, the shape or morphology of the final product could be completely different from that of the seeds, depending on the experimental conditions.

Seed-mediated growth has been successfully applied to a number of noble metals such as Ag, Au, Pd, Pt, and Rh, including both mono- and bimetallic systems.[22] However, manipulation and control of the evolution of shape or morphology during seed growth remains a great challenge.

Recent studies have revealed that the growth rates of specific facets in Ag nanostructures depend on the capping agent.[23] In fact, the most popular theory at the early stages of research was the "face-blocking theory", in which a capping agent selectively adheres to a particular crystal facet of the growing nanocrystal and thus slows the growth rate of that facet relative to the others. In a reported example, introduction of citrate led to the formation of Ag plates, whereas addition of PVP led to the growth of plates and truncated plates: theoretical studies suggest that citrate binds more strongly to Ag {111} than Ag{100} facets at room temperature, which fits well with these experimental results.[24]

Because of the stronger binding of citrate, the {111} facets are expected to grow more slowly than the {100} facets during seed mediated growth when citrate ions are present. As a result, the {100} facets will disappear gradually while the {111} facets will become increasingly dominant on the surface.

[19] Y. Xia, Y. Xiong, B. Lim, S.E. Skrabalak, *Angew. Chem., Int. Ed.*, 2009, **48**, 60.

[20] X. Liu, Y. Zhang, D.K. Goswami, J.S. Okasinski, K. Salaita, M.J. Bedzyk, C.A. Mirkin, *Science* 2005, **307**, 1763.

[21] B.Wiley, T. Herricks, Y. Sun, Y. Xia, *Nano Lett.*, 2004, **4**, 1733.

[22] S.E. Habas, H. Lee, V. Radmilovic, G.A. Somorjai, P. Yang, *Nat. Mater.*, 2007, **6**, 692.

[23] J. Zeng, Y. Zheng, M. Rycenga, J. Tao, Z.Y. Li, Q. Zhang, Y. Zhu, Y.J. Xia, *Am. Chem. Soc.*, 2010, **132**, 8552.

[24] D.S. Kilin, O.V. Prezhdo, Y. Xia, *Chem. Phys. Lett.*, 2008, **458**, 113.

On the other hand, PVP binds more strongly to the {100} than {111} facets of Ag and can thereby reduce the growth rate along the [100] direction. This makes the {111} facets disappear more quickly than the {100} facets, resulting in the formation of truncated nanoprism capped by {100} facets. These results clearly demonstrate that one can control the shape of Ag nanostructures simply by adding a specific capping agent into a reaction system to take advantage of its different binding strengths with different facets. Adding a capping agent that has a stronger binding energy to a specific facet should result in a slower growth rate for this facet, and this facet will take up a larger proportion of the surface in the final product. However, the origin of the facet selectivity in this reaction is unclear and may be related to kinetic factors.[25]

Unfortunately, it can be hard to remove these capping molecules from the nanoparticles surfaces, and this often complicates the chemistry which is needed for further coatings.[26] Also, molecules like surfactants may have a toxic action on human cells, and this of course is a main issue when nano-objects, in colloidal suspension or grafted on a solid surface, are intended to be used in applications involving human health.[27] Even the presence of polymeric stabilizers, which can improve the growth as well the stability of anisotropic particles[28,29] can represent a problem, as it could affect the antibacterial activity, interfering with silver nanoparticles surface oxidation, a step which is needed for the further subsequent silver ion release[30], as well their grafting on surfaces, which can be strongly dependent from the nano-objects surface charge.

For these reasons, citrate may be considered as "magic" component critically required for the formation of silver nanoplates because: (i) produces and directs the anisotropic growth, preferentially binds to {111} facets of growing particles, slowing down the vertical expansion, and thus allowing to obtain anisotropic growth, producing nanoplates; (ii) it can be easily removed from the nanoparticles surface, (iii) it is not harmful, (iv) it ensures a negative surface charge which is crucial for grafting to bulk glass surfaces functionalized with amines (one of the goals pursued in this thesis, that will be described in **Paragraph 2.2**), which are protonated when used in water at neutral or slightly acidic conditions; (v) it does not affect the antibacterial activity of nano-object (the main interest of this part of the thesis) as it does not give interference with silver

[25] A.Tao, P. Sinsermsuksakul, P. Yang, *Angew. Chem., Int. Ed.*, 2006, **45**, 4597.

[26] Y.G. Sun, *Chemistry of Materials*, 2007, **19**, 5845.

[27] A.M. Alkilany, P.K. Nagaria, C.R. Hexel, T.J. Shaw, C.J. Murphy, M.D. Wyatt, *Small*, 2009, **5**, 701.

[28] D. Aherne, D.M. Ledwith, M. Gara, J.M. Kelly, *Advanced Functional Materials*, 2008, **18**, 2005.

[29] D.M. Ledwith, A.M. Whelan, J.M. Kelly, *Journal of Materials Chemistry*, 2007, **17**, 2459.

[30] P. Pallavicini, A. Taglietti, G. Dacarro, Y.A.D. Fernandez, M. Galli, P. Grisoli, M. Patrini, G. Santucci De Magistris, R. Zanoni, *Journal of Colloid and Interface Science*, 2010, **350**, 110.

nanoparticles surface oxidation, a step which is needed for the further subsequent silver ion release, as we have discussed in **Paragraph 1.2.4**.

2.1.2 Optical Properties of Anisotropic AgNPs

The optical properties of plasmonic nanoparticles are essentially determined by three factors: composition, size, and shape.[31] Non-spherical particles, anisotropic particles, can present various different LSPR modes as a result of the different possible oscillations that can arise from different orientations of the particle with respect to the electric field of the incident electromagnetic radiation.[32]

Mie theory[33] does an excellent job predicting the optical properties of spherical particles, spheroids, and infinite cylinders; however, complete solutions to Maxwell's equations are not available for more complex geometries. For anisotropic silver nanoparticles, the discrete dipole approximation (DDA) method is well known for producing good predictions for a variety of nonspherical shapes.[34]

DDA is a finite element-based method which was first introduced by Purcell and Pennypacker[35] and later improved by Draine and Flatau.[36] Using DDA, Maxwell's equations can be solved numerically, so that one can study scattering and absorption of electromagnetic radiation by particles with sizes of the order of the wavelength of the incident light or smaller.

Figure 1A shows the absorption, scattering, and extinction spectra calculated with Mie theory for a 40-nm silver sphere suspended in water. As the electromagnetic wave hits the particle, conduction electrons are pushed to one side of the sphere, leaving behind a positively charged region on the

opposite side of the particle to form a dipole. Coulombic attraction will draw the electrons back, but as the sign of the electric field changes, a dipole in the opposite direction will be induced. As a result, the conduction electrons are driven to oscillate at the same frequency as the incoming light, giving rise to a strong dipole resonance at ~410 nm. A small shoulder peak is also observed at ~370 nm, which is a quadrupole resonance (i.e., two dipoles in opposite directions) and is caused by non-uniform incident light across the sphere.[21]

[31] U. Kreibig, M. Vollmer, Optical properties of metal clusters, (Springer, Berlin, 1995).
[32] L.M. Liz-Marzan, *Langmuir*, 2006, **22**, 32.
[33] G. Mie, *Ann Phys*, 1908, **25**, 377.
[34] B.T. Draine , P.J. Flatau, *J Opt Soc Am A*, 1994, **11**, 1491.
[35] E.M. Purcell, C.R. Pennypacker, *Astrophys. J.*, 1973, **186**, 705.
[36] B. T. Draine and P.J. Flatau, Program DDSCAT, Scripps Institute of Oceanography, University of California, San Diego, CA.

The spectrum for a 40-nm silver cube suspended in water was calculated using the DDA method and is shown in **Figure 1B.** Though the cube is of the same size as the sphere, the peak is significantly red-shifted relative to the sphere. This difference can be attributed to the greater degree of charge separation available in particles with sharp corners. Recent calculations indicate that charges tend to concentrate at sharp corners, a phenomenon sometimes referred to as the "lightning rod effect".[37] This greater charge separation reduces the Coulombic restoring force, thus increasing the time needed for each oscillation and lowering the frequency, as compared to a spherical particle. Further examination of **Figure 1B** reveals that, in addition to the red-shifted resonance, a number of additional peaks are present in the spectra, as compared to **Figure 1A**. This difference can be attributed to the decreased symmetry of the cubic structure, with the number of peaks observed correlating with the number of ways in which the electron density can be polarized. In general, decreasing symmetry means more peaks in the LSPR spectrum. [21]

Taken together, these calculated spectra show the great degree of LSPR tuning that potentially can be achieved by the shape-controlled synthesis of silver nanoparticles. From these examples, it can be summarized that the number of resonant peaks displayed by a silver nanoparticle is mainly determined by the number of ways in which its electron density can be polarized and that the position of LSPR peaks can be tuned by shape anisotropy and corner sharpness. Excitingly, in recent years, it has become possible to target these nanoparticles of different shapes synthetically and systematically study their optical properties.

---

[37] L.J. Sherry, R. Jin, C.A. Mirkin, G.C. Schatz, R.P Van Duyne, *Nano Lett.*, 2006, **6**, 2060.
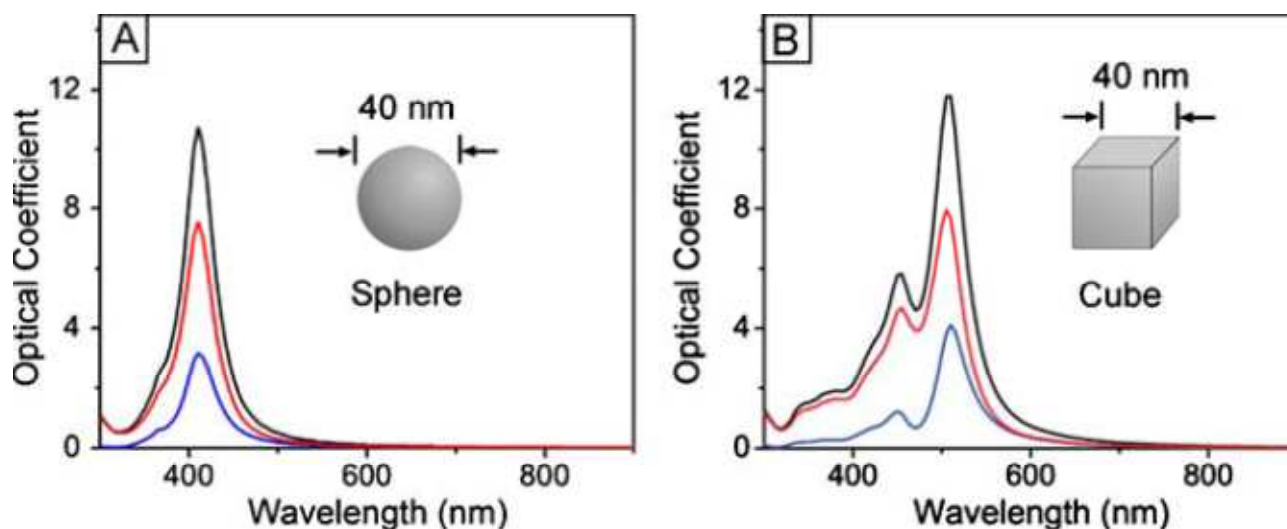
Figure 1 Mie theory (**a**) and the discrete dipole approximation (**b**). Absorption is shown in red, scattering in blue, and extinction in black. [38]

Schatz and co-workers[39] were the first to report theoretical calculations for Ag nanoplates using DDA, which were used to interpret experimental observations. Such calculations served to identify the plasmon bands measured from nanoplates dispersions and for the first time to distinguish two quadrupolar LSPR modes for a single metal particle. If the symmetry of silver particles is decreased further, by preparing triangular-shaped plates, charge separation will be even more pronounced, resulting in the primary SPR peak far into the red. For a triangular platelet with lateral dimensions of 100 mm and 16 nm thick, a spectrum was obtained where three bands were present, as depicted in **Figure 2B**.[28] The long wavelength peak at 770 nm was assigned to the in-plane dipole plasmon resonance, the weaker peak at 470 nm to the in-plane quadrupolar resonance, a small but sharp peak at 340 nm was identified as the out-of-plane quadrupole, while a weak shoulder around 410 nm was assigned to the out-of-plane dipolar resonance.

[38] C.M. Cobley, S.E. Skrabalak, D.J. Campbell, Y. Xia, *Plasmonics*, 2009, **4**, 171.
[39] R. Jin, Y.W. Cao, C. A. Mirkin, K.L. Kelly, G.C. Schatz, J.G. Zheng, *Science*, 2001, **294**, 1901.
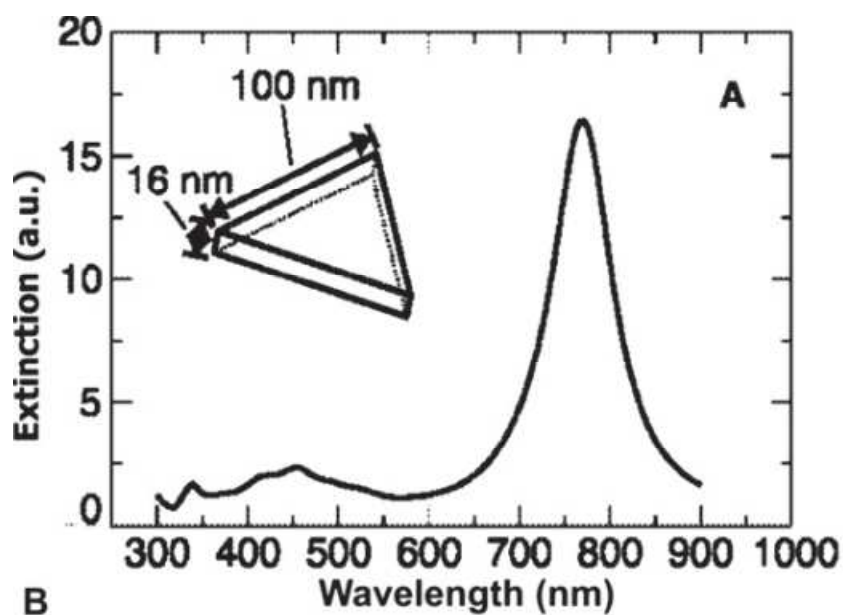
Figure 2B DDA simulations of the orientation averaged extinction efficiency spectra of a perfectly triangular nanoprism.[28]

The positions of plasmon resonances depend, among other parameters, on particle size, or more specifically on the ratio between lateral dimensions and thickness (aspect ratio). Theoretically it was also observed[40] that both the in-plane dipolar and quadrupolar modes red-shifted when the edge length increased as in **Figure 3A**. Since, experimentally, triangular nanoplates are often found to be truncated, the effect of snipping was also studied, with the general result that the bands are red shifted when the snip is decreased, as can be seen **Figure 3B**.[28] Other groups have studied the effect of snipping the corners off of triangular plates and found that a blue shift results.[38] Amazingly, as more area is snipped-off to produce a rounded structure, a larger blue shift was observed. In fact, a circular disc with similar dimensions has an LSPR peak blue-shifted by ~100 nm, as compared to the triangular. plate. This observation provides strong evidence for the role corner sharpness plays in determining the LSPR peak position.

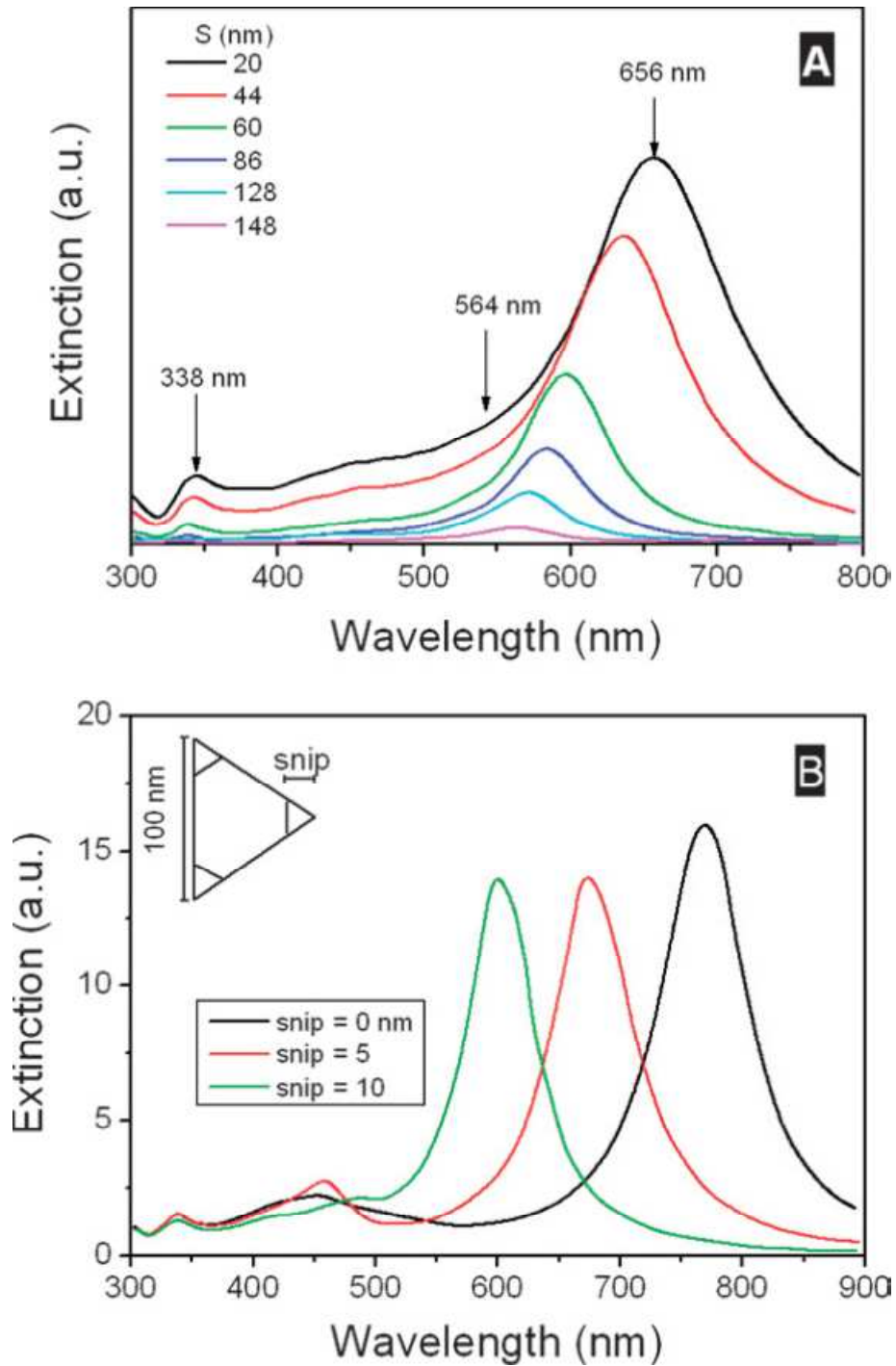[40] K.L. Kelly, E. Coronado, L.L. Zhao, G.C. Schatz, *J. Phys. Chem. B*, 2003, **107**, 668.

Figure 3 DDA simulations of the extinction efficiency of triangular nanoprisms. **(A)** Varying sizes (S, maximum length of the nanoplate base) as indicated, with constant aspect ratio (AR ¼ 4). **(B)** Snipped nanoprisms: from left to right, the snips are 0, 10 and 20 nm. The inset shows the shape and edge dimension of the snipped prism (16 nm thick).[28]

2.1.3 Photo-thermal Effect

One of the most appealing property of nanoparticles is the ability of plasmon oscillation to relax non-radiatively. Nanoparticles can absorb light at the frequency of their LSPR and return energy as heat. Thanks to ultrafast laser spectroscopic studies, it has been established that the photoexcitation of the metal nanoparticles free electrons is followed by their cooling back to equilibrium by energy exchange with lattice phonons at the rate of 1ps (in the case of gold) with a consequent heating of the nanoparticles.[41] Depending on the condition of energy deposition , like laser irradiation of nanoparticles, different phenomena can be obtained. At fast rate of energy deposition relative to lattice cooling, the photo-thermal heating can result in the desorption of surface-capping molecules,[42] useful for example in drug delivery, or it may melt and reshape the nanoparticles.[43] At slower rate the lattice cools via phonon-phonon processes leading to the heating of the medium surrounding the nanoparticle.

In these conditions nanoparticles can be considered "light activated nanoscopic heaters" and they can be used for example to reach selective, if proper capping of nanoparticles is used, laser photo-thermolysis of cancer cell or photo-thermal killing of bacteria and biofilm.

In medicine photo-thermal therapy (PPT) is not new. Usually organic dyes are used as absorbing light agents. When these dyes are laser-irradiated electronic transitions from the ground to the excited state occur. Then the system subsequently relaxes through non radiative decay channels resulting in the overheating of the local environment around the light absorbing species. The produced heat can be employed for local cell or tissue damage, as usually a ΔT≥5°C is sufficient to induce protein denaturation. In traditional photo-thermal therapy, the PPT agents can be natural chromophores already present in the tissue or externally added dye molecules.[44]

Plasmonic photo-thermal therapy (PPTT) foresee the use of plasmonic nanostructures instead of common organic dyes.

In addition, if the LSPRs of nanoparticle fall in the biologically transparent near-IR window (NIR, 750–1100 nm), a non-invasive photo-thermal laser treatment for antitumoral and antibiofilm use can be envisaged.

---

[41] S. Link, M.A. El-Sayed, *Annu. Rev. Phys. Chem.*, 2003, **54**, 331.

[42] P.K. Jain, W. Qian, M.A. El-Sayed, *J.Am Chem.Soc.*, 2006, **128**, 2426.

[43] S. Link, C. Burda, B. Nikoobakht, M.A. El-Sayed, *Chem. Phys. Lett.*, 1999, **315**, 12.

[44] W.R. Chen, R.L. Adams, E. Heaton, D.T. Dickey, K.E. Bartels, R.E. Nordquist, *Cancer Lett.*, 1995, **88**, 15.

For example, anisotropic gold nanostructure have been exploited for the hyperthermic therapy of deep tumors[45] also extended to other biological application, such as controlled denaturation of proteins, controlled release of drugs, destruction of viruses and bacteria[46] and eradication of biofilm.[47]

The ability to give an efficient photo-to-heat conversion is not only limited to gold nano-objects. In two recent and pioneering examples,[48,49] the photo-thermal effect given by silver nanoplates was smartly investigated for photo-thermal treatments of cancer cells when irradiated at 800 nm, a wavelength value where a plasmonic band can be easily placed by tuning morphology and dimensions of nanoplates themselves. Boca and coworkers have demonstrate the ability of chitosan-coated silver nanoplates (Chit-AgNTs) to operate as effective hyperthermia agents against a line of human non-small lung cancer cells (NCI-H460). They have adopted triangular nanoplates that exhibit a strong LSPR band for triggering hyperthermia in NIR. The fabrication of silver nanoparticles of triangular shape was essential for supporting plasmon resonances in NIR. Chitosan is a well-known biopolymer that offers distinctive advantages such as good biocompatibility, no cytotoxicity, remarkable affinity to proteins, and has already proved successful use in nanomedicine in delivering therapeutic drugs, proteins, and genes. The hyperthermia experiments were performed under continuous wave (CW) laser excitation at 800 nm wavelength and clearly demonstrated that Chit-AgNTs exhibit higher hyperthermia activity than already confirmed hyperthermia agents, thiolated poly(ethylene) glycol-capped gold nanorods (PEG-AuNRs).

Thus, anisotropic silver objects of different morphologies can be prepared in order to possess an LSPR band placed in the NIR and exert efficient photo-thermal action.[50] Silver flat nano-objects typically show an in-plane dipole plasmon resonance band, which position can be placed in the NIR region and tuned at a desired value, just by regulating the dimensions and the aspect ratio of the objects.[38] Few recent papers have been dedicated to bimetallic nanostructures in which the photo-thermal effects have been addressed to augment the release of silver, and then evaluating this increased release for microbicidal tasks.[51,52,53] Thus, it seems quite odd that no examples are

[45] X.Huang, P.K. Jain, I.H El-Sayed, M.A. El-Sayed, *Photochem. Photobiol.*, 2006, **82**, 412.

[46] V.P. Zharov, K.E. Mercer, E.N. Galtovskaya, M.S. Smeltzer, *Biophys. J.*, 2006, **90**, 619.

[47] P. Pallavicini, A. Donà, A. Taglietti, P. Minzioni, M. Patrini, G. Dacarro, G. Chirico, L. Sironi, N. Bloise, L. Visai, L. Scarabelli, *Chem. Commun.*, 2014, **50**, 1969.

[48] S.C. Boca, M. Potara, A.M. Gabudean, A. Juhem , P.L. Baldeck , S. Astilean, *Cancer Letters*, 2011, **311**, 131.

[49] S. Boca-Farcau, M. Potara, T.A. Simon, P. Baldeck, S. Astilean, *Molecular Pharmaceutics*, 2014, **11**, 391.

[50] I. Pastoriza-Santos, L.M. Liz-Marzan, *Journal of Materials Chemistry,* 2008, **18**, 1724.

[51] S. Mo, X. Chen, M. Chen, C. He, Y. Lu, N. Zheng, *Journal of Materials Chemistry B*, 2015, **3**, 6255.

reported in literature on the use of the photo-thermal effects of pure anisotropic silver nanoplates for antimicrobial applications. This part of the thesis is devoted to fill this void.

2.1.4 Role of Anisotropy on SERS Effects

Surface enhanced Raman scattering efficiency considerably depend on nanoparticle morphology and degree of aggregation. Several well-established strategies exist for the synthesis of spherical metal nanoparticles;[54] which have thus been widely used as SERS substrates due to their stability and ease of fabrication. Higher SERS efficiency is typically obtained when spherical nanoparticles are partially aggregated, because of junctions between the nanoparticles function as SERS hot spots where large field enhancements occur, allowing detection down to the single molecule level.[55] However, techniques that allow fine control over aggregation are not yet perfect and thus the reproducibility of SERS signals remains a challenge. Hot spots are highly localized regions of intense local field enhancement caused by surface plasmon resonances, usually occurring within interstitial crevices in metal structures. Such hot spots have been claimed to lead to extraordinary enhancement of SERS signals, up to even 15 orders of magnitude.[56]. Anisotropy in metal nanoparticles has been widely studied, as an alternative way to generate hot spots. Actually, theoretical modeling shows that anisotropic metal nanoparticles can concentrate high electromagnetic fields at specific locations at their surface.[57] Such intrinsic hot spots provide anisotropic metal nanoparticles with a high potential to yield intense SERS signals with no need to induce their aggregation, which is particularly useful in liquid phase. The main features that render anisotropic plasmonic nanoparticles as excellent SERS substrates are: (i) adjusting the aspect ratio the plasmon band can be tuned in resonance with Raman laser excitation sources; (ii) symmetry breaking creates highly localized electromagnetic fields; (iii) anisotropic nanoparticles provide new opportunities for controlled assembly into functional architectures for SERS.[58]

[52] C. Fasciani, M. Jazmin Silvero, M. Alexandra Anghel, G.A. Argueello, M. Cecilia Becerra, J.C. Scaiano, *Journal of the American Chemical Society*, 2014, **136**, 17394.
[53] K.C.L. Black, T.S. Sileika, J. Yi, R. Zhang, J.G. Rivera, P.B. Messersmith, *Small*, 2014, **10**, 169.
[54] J. Turkevich, P.C. Stevenson, J. Hillier, *Discuss. Faraday Soc.*, 1951, 11, 55.
[55] K. Kneipp, Y. Wang, H. Kneipp, L.T. Perelman, I. Itzkan, R.R. Dasari, M.S. Feld, *Phys. Rev. Lett.*, 1997, **78**, 1667.
[56] R. Maher, *Raman Spectroscopy for Nanomaterials Characterization*, (Springer, Berlin).
[57] E. Hao, G. Schatz, J. Hupp, *J. Fluoresc.*, 2004, **14**, 331.
[58] S. Eustis, M.A. El-Sayed, *Chem. Soc. Rev.*, 2006, **35**, 209.

It is well known that AgNPs are known to exert higher SERS enhancement respect to Au nanoparticles;[59] thus anisotropic AgNPs possess great potential as even brighter SERS nanoprobes. For these reason, the triangular shape has also been proposed for SERS enhancement because hot spots with high electromagnetic field can be created at the tips, **Figure 4**.
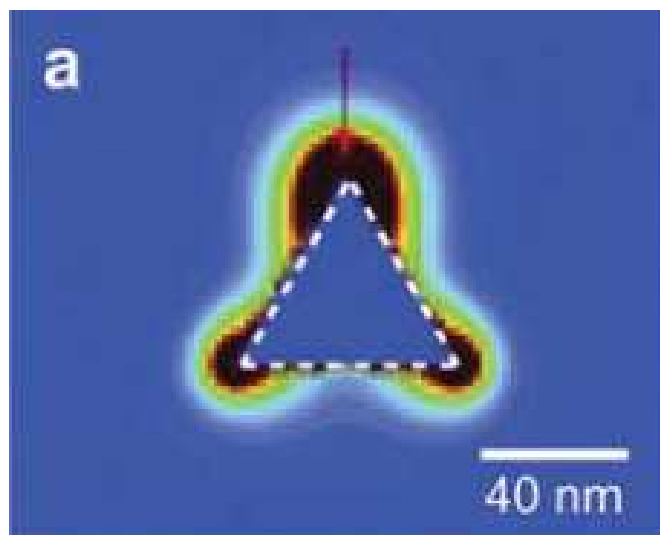

Figure 4 Calculated electric field intensities for silver nanoplates with hot spots at sharp asperities. Red color corresponds to highest intensity.[60]

In fact, although it has been demonstrated that triangles and plates provide higher signals in average SERS for the detection of various analytes including organic pollutants, inorganic anions, or biomolecules,[61] their complete optical performance is still hindered by several factors.

For example, one of the first reports[62] on silver nanoplates as SERS substrates demonstrated the comparable performance of these structures with conventional silver citrate reduced colloidal suspensions, the most common platforms for SERS. These seminal results were obtained in suspension by average SERS, that is, SERS from an ensemble of colloidal particles and aggregates, and characterized by a stable average spectrum with well-defined frequency and bandwidth. Obviously, reproducibility and uniformity are still major challenges in the fabrication of hot spots for SERS detection. Although the great potential of metal nanoparticles in solution for a number of SERS applications was demonstrated, many real-world applications require highly reproducible

[59] M. Rycenga, C.M. Cobley, J. Zeng, W. Li, C.H. Moran, Q. Zhang, D. Qin, Y. Xia, *Chem. Rev.*, 2011, **111**,3669.
[60] K.A. Stoerzinger, W. Hasan, J.Y. Lin, A. Robles , T. W. Odom, *J. Phys. Chem. Lett.*, 2010, **1**, 1046.
[61]Y. Sun, G.P. Wiederrecht, *Small*, 2007, **3**, 1964.
[62] I. Lee, S. W. Han, K. Kim, *J. Raman Spectrosc.*, 2001, **32**, 947.

enhancement factors and long term stability, which is easier to achieve with solid systems in which the metal nanoparticles are immobilized on a solid support.[63].

For chemically synthesized nanoparticles, self-assembly on surfaces is one of the most widely applied bottom-up approaches. The main advantage of the chemical assembly is the possibility to create macroscopic assemblies from precisely engineered nanoparticles, with low cost and in relatively short preparation times as compared to top-down approaches.

Four main factors can influence the result of the immobilization: (1) the functional group on the glass surface; (2) immersion time of the glass in the metal nanoparticle dispersion; (3) metal nanoparticle concentration; (4) surface chemistry of the metal nanoparticles. Therefore, control over these factors allows a wide range of the properties to be achieved for the substrates, which can in turn lead to various benefits for SERS measurements.[64]

[63] R.A. Alvarez-Puebla, L.M. Liz-Marzan, *Chem. Soc. Rev.*, 2012,**41**, 43.
[64] M. Fan, G.F.S. Andrade, A.G. Brolo , *Anal. Chim. Acta*, 2011, **693**, 67.

2.2 Bulk Surfaces coated with Silver Nanoplates

Our first purpose was to synthesize anisotropic silver nano objects, silver nanoplates, with the desired shape, dimensions and LSPR features, and subsequent grafting on properly functionalized glass samples, to impart a double antibacterial action: (i) the well-known, long term antibacterial effect based on the release of Ag^+, (ii) an "on demand" action which can be switched on by the use of photo-thermal properties of silver nano-objects. Irradiation of these samples with a Laser inside the so called "therapeutic window" in the Near InfraRed allows to reinforce, in the timescale of minutes, the classical antibacterial effect of silver nanoparticles.

The synthesis of anisotropic nanoparticles has been carried through a seed-mediated growth approach that involves the preparation of silver isotropic nanocrystals, the seeds. The seeds are added in controlled amounts to a growth solution containing all the reagents needed for the growth of anisotropic nano-objects: (i) a precursor salt containing Ag^+ ions ($AgNO_3$), (ii) citrate, playing the role of capping agent and reducing agent, but also performing a key role in the anisotropic growth, since it preferentially binds to {111} facets of the seed, thus preventing the growth in that direction and promoting the longitudinal growth of the plates, (iii) ascorbic acid that triggers the reduction mechanism of seeds. A long term systematic investigation on the synthetic conditions has been realized in order to obtain nanoplates with reproducible morphological and dimensional features, in order to produce LSPR absorption spectra with an intense band in the NIR, between 800 and 900 nm. Presence of LSPR absorptions at 800-900 nm is fundamental to use this approach in the biomedical field, for example to functionalize subcutaneous implants and medical devices, because tissue and blood are semitransparent to radiation in the near IR region (750-1100 nm).

After the development of a method that allows to obtain nano-objects that can produce absorption bands in the NIR at the desired wavelengths, we have performed the grafting of nanoplates on glass samples previously functionalized with a layer of PEI-silane, and taking advantage of the electrostatic interactions between the negative charge of the nanoplates and the positive charge of protonated amine groups of PEI at the pH of functionalization colloids. With SEM images we investigated the homogeneous grafting of objects on the PEI-silane SAM, to control that nano-objects are conserving size and morphological properties similar to those of the colloidal suspension, with the peak of the in-plane dipole plasmon resonance which can be easily positioned around to 800-840 nm.

Moreover, we have measured the localized hyperthermia produced by the photo-thermal effect of GLASS-PEI-TRI samples, through irradiation with Laser at 808 nm, achieving a local heating of more than 10 °C, in a time of few tens of seconds of irradiation with irradiance of 0.26 W/cm^2.

Measurements of antibacterial activity on the samples without Laser irradiation show that these materials exhibit a greater Microbicidal Effect (ME) against Gram-negative bacteria than for Gram-positive bacteria, an activity which depends on contact times with bacterial suspensions: it is almost completely absent in short times (15 min), becoming appreciable for longer contact times (5 hours). In 24 hours the PEI-plates surfaces can destroy more than 99% of the bacterial cells belonging to the investigated strains (*E. coli* and *S. aureus*), as already shown for similar systems[47,65,66]. Then, we have tested the antibacterial properties due to the photo-thermal effect of the GLASS-PEI-TRI samples under Laser irradiation. It was demonstrated that within 15 minutes of irradiation with an irradiance of 0.26 W/cm^2, a value which is below the maximum allowed for exposure of the skin, it is possible to obtain an important microbicidal effect against both *E. coli* (more than 99% of bacteria removed) and, to a lesser extent, of *S. aureus* (over the 97% of bacteria eliminated).
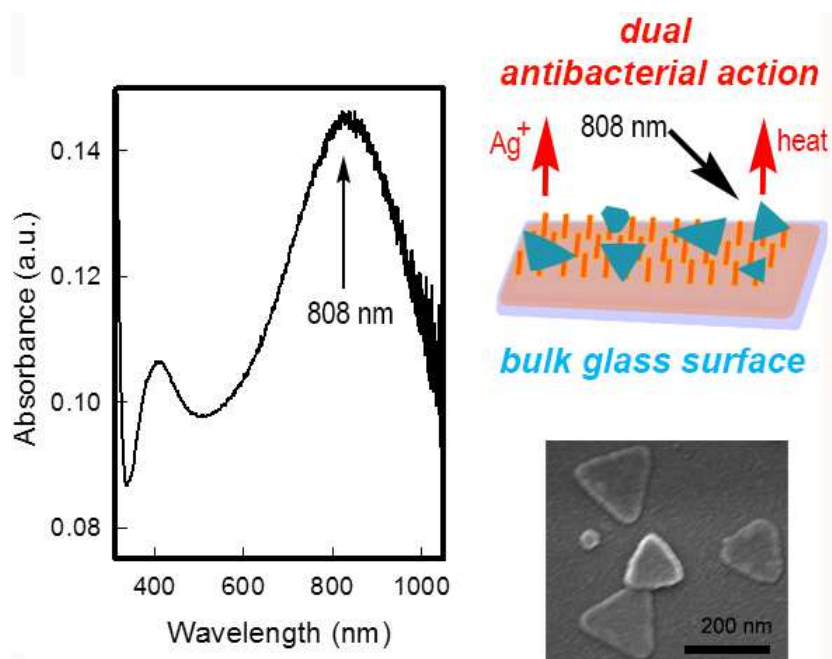
[65] G. Dacarro, L. Cucca, P. Grisoli, P. Pallavicini, M. Patrini, Angelo Taglietti, *Dalton Trans*., 2012, **41**, 2456.
[66] A. Taglietti, C. Renata Arciola, A. D'Agostino, G. Dacarro, L. Montanaro, D. Campoccia, L. Cucca, M. Vercellino, A. Poggi, P. Pallavicini, L. Visai, *Biomaterials*, 2014, **35**,1779.

2.2.1 Experimental Details: Synthesis and Characterization

2.2.1.1 Experimental Materials and Instrumentation

Materials

Silver nitrate (>99.8%), sodium borohydride (>99.0%), sodium citrate (TSC) (>99.0%), ascorbic acid ≥99% were purchased from Sigma Aldrich. Trimethoxysilylpropyl(polyethylenimine) (50% in isopropanol) was purchased from Gelest Inc. Reagents were used as received. Solvents were purchased from Sigma-Aldrich and used as supplied. Microscopy cover glass slides (21x26mm) were purchased from DelChimica. Water was deionized and then bidistilled.

Instrumentation and instrumental method

Absorbance spectra of colloidal supensions were taken with a Varian Cary 100 spectrophotometer in the 200–1100 nm range using glass cuvettes (optical path 1cm) and spectra of functionalized glasses were obtained placing the slides on the Varian Cary 100 spectrophotometer equipped with a dedicated Varian solid sample holder.

Zeta potential was measured with a Zetasizer Nano ZS90 Malvern instrument, equipped with dedicated cuvettes. Measurements were repeated three times using 1 mL of colloidal suspension for each one.

Centrifugation was carried out using the ultracentrifuge HermleZ366 with polypropylene 10mL tubes. Ultracentrifugation speed was 5000 rpm.

TEM images were obtained on colloidal solutions of silver nanoplates diluted five times with distilled water, deposited on Nickel grids (300 mesh) covered with a Parlodion membrane and observed with a Jeol JEM-1200 EX II instrument. Magnification is 100000.

SEM images were taken from Tescan Mira XMU variable pressure Field Emission Scanning Electron Microscope – FEG SEM (Tescan USA Inc., USA). Slides were mounted onto Aluminum stubs using double sided carbon adhesive tape and were then made electrically conductive by coating in

vacuum with a thin layer of Pt/Pd (2.5 nm). Observations were made in backscattered electrons mode (BSE) at 30 kV and with InBeam secondary electron detector for higher spatial resolution.

Static contact angle determinations were made with a KSV CAM200 instrument, with the water sessile drop method

X-ray powder diffraction measurements were performed by using a Bruker D5005 diffractometer with the CuKα radiation, graphite monochromator and scintillation detector. The patterns were collected with a step size of 0.03° and counting time of 2 s per step in the angular range 20–65°. XRD patterns of silver nanoplates were obtained of a sample centrifuged two times, concentrated, placed on a blank glass and dried as a powder.

Thermograms (Temperature vs time) were recorded on GLASS-PEI-TRI samples by means of a laser (multimode AlGaAs laser diode, L808P200, Thorlabs GmbH, emitting light at the wavelength of about 808 nm, power of radiation is 200 mW, irradiance is 0.26 W/cm^2). Temperature was recorded by means of a FLIR E40 thermocamera and FLIR Tools+ software.

The total Ag content of GLASS-PEI-TRI was determined by quantitatively oxidizing the silver plates grafted on a single slide by dipping it in 3 mL ultrapure concentrated HNO_3 diluted 1:5 with water (13% w/vas final concentration) in a becker, and keeping it overnight at RT on a Heidolph Promax 1020 reciprocating platform shaker. The Ag content in solution was then determined by inductively coupled plasma optical emission spectroscopy (ICP-OES) with an ICP-OES OPTIMA 3000 Perkin Elmer instrument. The measure was repeated on 8 glass samples coming from 4 different preparations.

Release of Ag^+ in water was measured on a set of 4 fuctionalized slides (21x26 mm coated on both sides, total coated surface 10.92 cm^2) prepared as described above. Each slide was then immersed in 3 mL of ultrapure water. Slides were taken off the water after 48 h. A UV-Vis spectra was measured on the water solution, and then the content of Ag^+ was determined by ICP-OES. Measures were repeated three times, and mean values are given. ICP data were collected with an ICP-OES OPTIMA 3000 Perkin Elmer instrument. UV-Vis spectra were collected on the glass samples after the immersion. One glass sample was then analyzed by SEM.

2.2.1.2 Glassware Pretreatment

The glassware used during experiments was always pretreated before use. It was washed in *aqua regia*, a mixture of nitric acid and hydrochloric acid, *f*or 30 min, then washed and filled with bidistilled water and ultrasonicated for 3 minutes before discarding water. The bidistilled water/ultrasound treatment was repeated 3 times.

2.2.1.3 Seeds Preparation

Seeds, spherical silver nanoparticles, were prepared according to a reported method.[67] To 20.0 mL of distilled water the following solutions were added in sequence under vigorous stirring: 0.100 mL of a solution of AgNO$_3$ 0.018 M, 0.100 mL of a solution of TSC 0.017 M, 0.600 mL of a solution of NaBH$_4$ 0.010 M. After the last addition, stirring was immediately stopped in order to avoid coagulation. The colloidal suspensions were stored in the preparation flask and maintained in the dark. Then this colloidal suspension of seeds were diluted with bidistilled water up to reach an absorbance value of 0.5 units in order to obtain a stock solution which was used for preparation of silver nanoplates.

2.2.1.4 Synthesis of Silver Nanoplates: Standard Preparation

Silver nanoplates were synthesized by a seeds mediated growth method. The approach used during the screening study performed to reach the optimal synthetic conditions, as well the details of a few of the several experiments carried for this task are described in the discussion section. The following procedure describes the standard preparation found and used. To obtain the desired nano-objects to be grafted on glass. Firstly, growth solution were prepared in a beaker with a stirrer adding 20.0 mL of a solution of TSC $8.5*10^{-3}$ M , 12 mL of a solution of AgNO$_3$ $5*10^{-4}$ M and 0.300 mL of ascorbic acid $1*10^{-2}$ M. Secondly, 0.300 mL of the stock solution of seeds were added and instantly magnetic stirring was stopped. A changing color of solution could be observed from pale yellow to dark pink and finally to blue/grey color, after a total of approximately 12 hours. Suspension colloidal of silver nanoplates were stored at 25°C and used without further treatments.

---

[67] .K. Sung, S.Y. Oh, C. Park,Y. Kim, *Langmuir*, 2013, **29**, 8978.

2.2.1.5 Preparation of PEI-silane Self-assembled Monolayers on Glass Surface (SURF-PEI glasses)

The samples were prepared according a reported method.[65] Briefly: glass substrates were cleaned for 30 min in freshly prepared Piranha solution (3:1 v/v H_2SO_4:H_2O_2 (30%). *Caution! Piranha solution is a strong oxidizing agent and should be handled with care.*), washed three times with ultrapure water in a sonic bath and oven-dried. The slides were then immersed for 6 min in a 4% (v/v) solution of PEI-silane in ethanol at room temperature. In a typical preparation, 8 glass slides were prepared at the same time, *i.e.* reacting in the same silane solution inside an 8-place holder (a microscope glass slides staining jar). After this, the slides were washed two times with ethanol and one time with ultrapure water in a sonic bath and blow-dried with nitrogen.

2.2.1.6 Preparation of GLASS-PEI-TRI

The silver nanoplates were grafted on SURF-PEI modified glass slides. In a typical preparation, 8 glass slides were covered with a colloidal suspension of silver nanoplates inside a 8-place holder (a microscope glass slides staining jar) for 14 hour at 25°C. Finally, functionalized glass slide were rinsed three times with distilled water and gently dried under nitrogen flux.

2.2.1.7 Antibacterial Activity Tests

The antibacterial activity of functionalized cover glasses was investigated against *Staphylococcus aureus* ATCC 6538 Gram-positive and *Escherichia coli* ATCC 10356 Gram-negative bacteria. The microorganisms were grown overnight in Tryptone Soya Broth (Oxoid; Basingstoke, Hampshire, England) at 37℃. Washed cells were resuspended in Dulbecco's PBS and optical density (OD) was adjusted to 0.2 at 650 nm wavelength, corresponding approximately to $1*10^8$ Colony Forming Units (CFU)/mL. 10 mL of bacterial suspension was deposited on a standard glass slide (76x26 mm), then the microbial suspension was covered with a functionalized cover glass slide (21x26 mm), forming a thin film between the slides that facilitates direct contact of the microorganisms with the active surface. The two assembled glasses were introduced in a Falcon test-tube (50 mL) containing 1 mL of PBS to maintain a damp environment. In this test microbes are incubated in non-nutritive suspensions that do not give the microorganisms the potential to grow during the test. For each bacterial strain three equivalent modified glasses were prepared; the slides were

maintained in contact with the liquid films containing bacteria at room temperature for 15 minutes, 5 and 24 h, respectively; for each time of contact an unmodified glass slide was treated in the same way as control sample. After the times of contact, 9 mL of PBS were introduced in each Falcon test-tube under a gentle shaking to detach the assembled glass slides. Bacterial suspensions were then grown in Tryptone Soya Agar (Oxoid; Basingstoke, Hampshire, England) to count viable cells. The decimal-log reduction rate, *i.e.* the Microbicidal Effect (ME), was calculated using the formula:

$ME = \log N_C - \log N_E$

(N_C being the number of CFU/mL developed on the unmodified control glasses, and N_E being the number of CFU/mL counted after exposure to modified glasses). The results expressed as ME represent the average of three equivalent determinations. This method can be considered as a version of the Japanese Industrial Standard JIS Z 2811 developed to measure the antibacterial activity of plastic surfaces.

2.2.1.8 Thermal Microbicidal Tests

Antibacterial activity due to photo-thermal effect of was investigated against *Staphylococcus aureus* ATCC 6538 Gram-positive and *Escherichia coli* ATCC 10356 Gram-negative. One functionalized slide was cut in 4 sections of 10x10 mm in order to be completely irradiated by Laser. A volume of 0.020 mL of bacterial suspension was deposited on 2 sections. For each pair of functionalised glasses, one was irradiated for 15 min whereas the other was not irradiated. After this time, the glass section covered with bacterial suspensions was suspended in 1 mL of sterile water, then it was taken away and water was used to make three dilution in 3 different tubes, in which 5 mL of sterile water was contained: 1:100, 1:10000, 1:100000. From each tube, 1 mL of suspension was taken and then grown in Tryptone Soya Agar (Oxoid; Basingstoke, Hampshire, England) to count viable cells. The decimal-log reduction rate, *i.e.* the "thermal microbicidal effect", ME_T was calculated with the following formula

$ME_T = \log N_C - \log N_T$

where N_C is the number of CFU/mL developed in contact with a not irradiated modified control glass sample, and N_T the number of CFU/mL counted after exposure to modified glass samples and irradiation. Each experiment was repeated three times.

2.2.2 Results and Discussion

2.2.2.1 Seeds Preparation

Seeds were prepared modifying a reported method[67] using $AgNO_3$ as precursor of silver ions Ag^+, that are reduced under stochiometric amount of $NaBH_4$, and then capped with citrate. This method yielded small spherical nanoparticles, seeds, of about 5 nm diameter, as confirmed by TEM images reported in **Figure 5**.
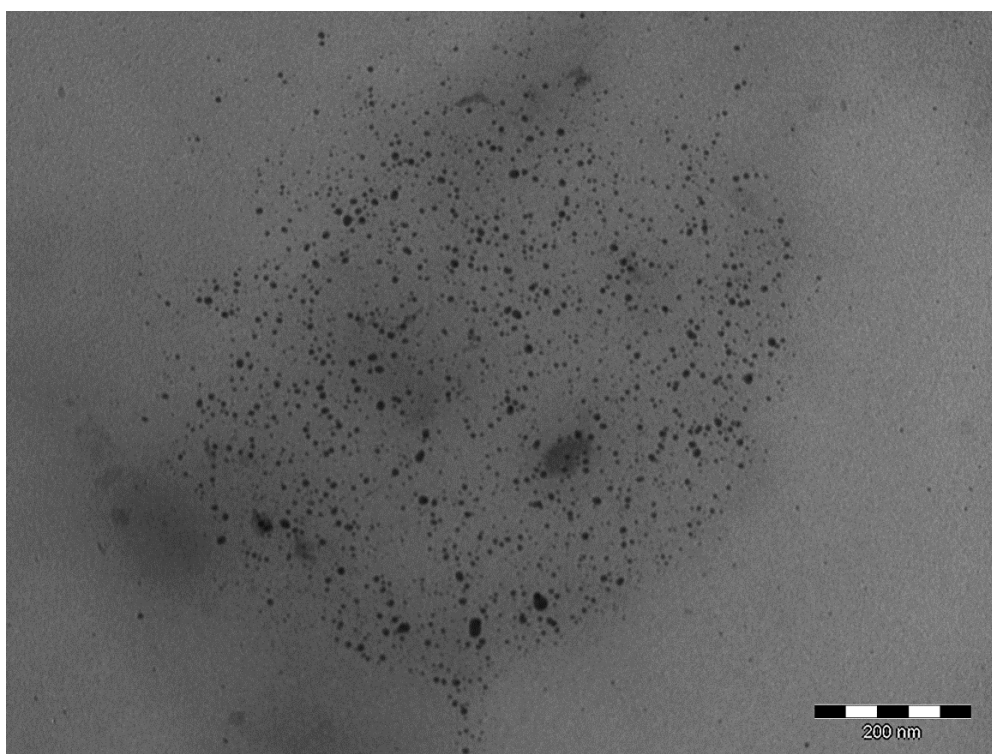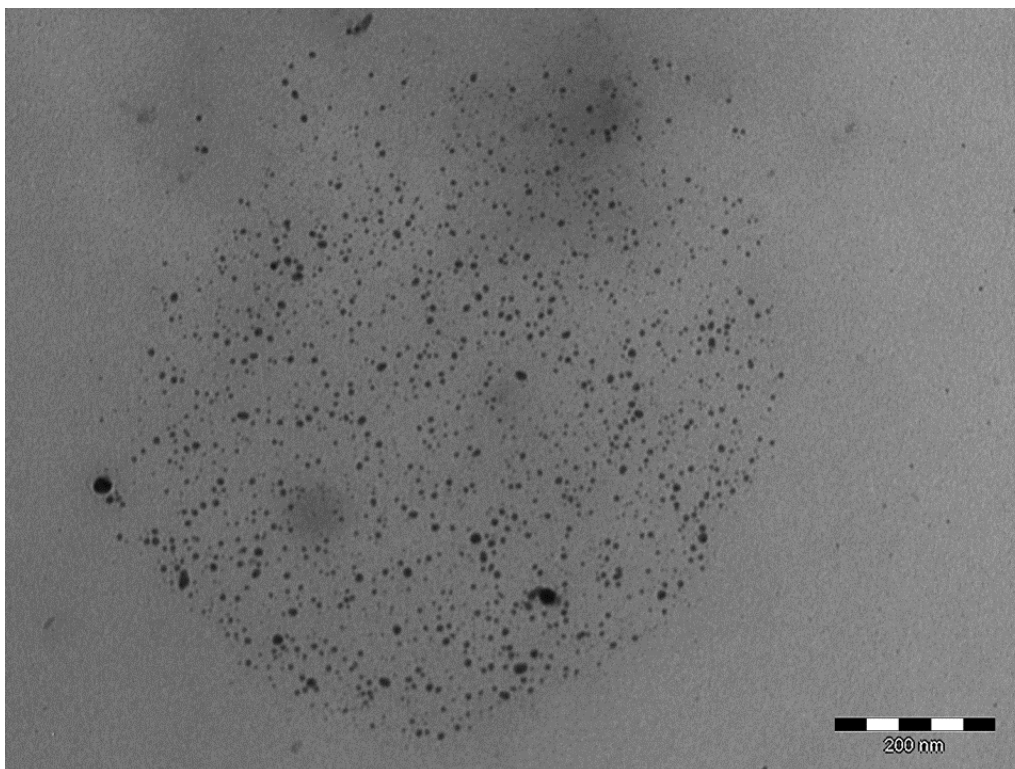
Figure 5 TEM images of two different preparations of seeds.

Colloidal suspensions of seeds show the typical yellow colour of spherical AgNPs, reported in **Figure 6**, with the expected narrow LSPR band centered at 394 (±2) nm, as can be seen in spectrum reported in **Figure 7**.

Figure 6 Photograph of a colloidal suspension of seeds.
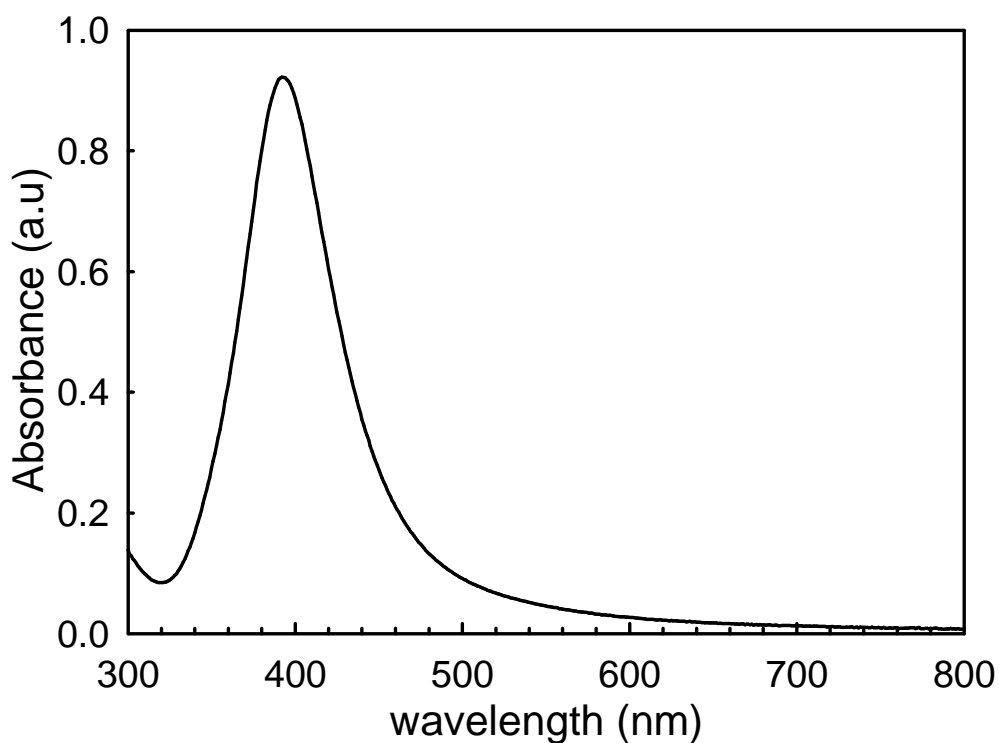
Figure 7 UV-Vis spectrum of a colloidal suspension of seeds.

The lack of reproducibility between different synthesis of seeds, though the same experimental conditions, reported in **Figure 8**, which probably depends on some poorly controllable variable in the synthetic setup (water purity, temperature, glassware cleaning) has brought us to the research of a standardization of the seeds preparation, in order to obtain colloidal solution with the same concentration of seeds. For these reasons, we have decided to dilute seeds in order to have a stock seeds solution with the LSPR band having an absorbance of 0.5 units.
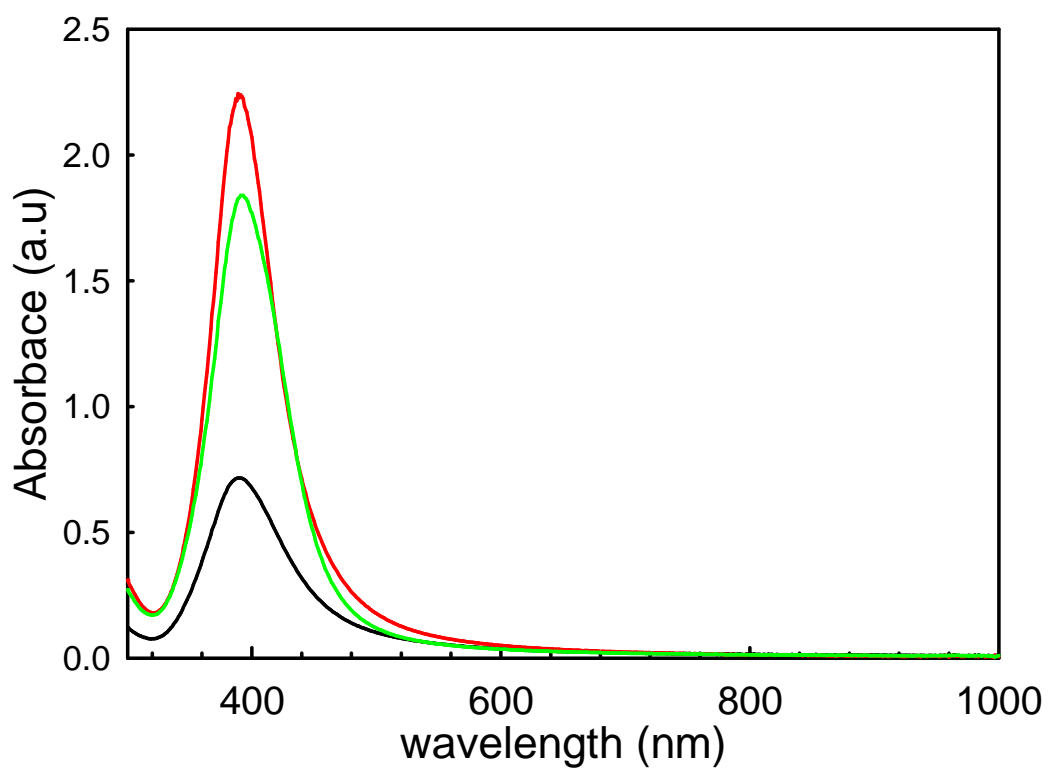
Figure 8 UV-Vis spectra of three identical preparations of seeds after one hour.
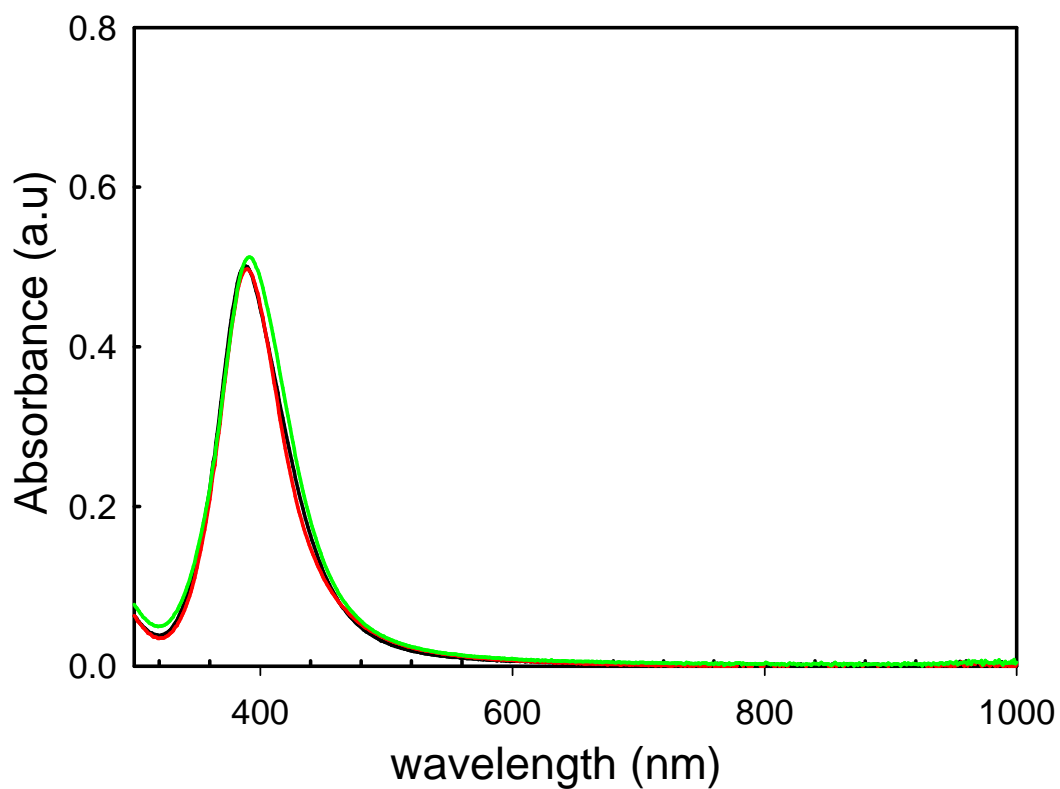
Figure 9 UV-Vis spectra of three stock solutions of seeds, after dilution to obtain an LSPR band having an absorbance of 0.5.

As can be clearly seen from **Figure 9**, once diluted to the same absorbance value, LSPR band are super-imposable, with the same wavelength and bandwidth, indicating that dimensions of the colloidal seed are almost the same, as also indicated from TEM images taken on different samples of seeds. Moreover we have established to use the same time interval of one hour between seeds preparation, stock dilution preparation and synthesis of silver nanoplates in order to obtain the higher degree of reproducibility possible in these conditions.

2.2.2.2 Synthesis of Silver Nanoplates

As already stated, we opted for a synthetic route based on a seed-growth method, but with the intention to avoid any surfactant or polymer, in the attempt to produce the nanoplates in absence of any potentially harmful reagent, as well with the aim to pursue an economic and "green" preparation and to obtain "safe" silver nano-objects with a potential antibacterial action.

The plates were prepared simply adding a precise volume of seeds at a proper volume of growth solution, which was composed only by the properly optimized amounts of ascorbic acid, sodium citrate and silver nitrate.

Preliminarily, we have widely investigated the synthetic conditions in order to obtain anisotropic AgNPs with triangular shape, characterized by: (i) LSPR absorption bands in the NIR; (ii) reproducibility among preparations with the same synthetic conditions; (iii) stability of colloidal suspensions to ultracentrifugation. At this stage we did not investigate shape and dimensions of objects with electronic microscopy, but just screened the conditions and searched for a synthetic setup able to yield a colloidal suspension of objects having the in-plane dipolar LSPR band placed at around 800 nm. In a typical experiment, an amount of 30 mL of the growth solution, made up of sodium citrate (TSC), silver nitrate ($AgNO_3$) and ascorbic acid (AA), with the concentrations indicated in **Table 2** was placed in a flask under stirring, and a fixed amount (600 μL) of seeds stock solution was added ("seeds last" column). In a second series of experiments seeds were added to the growth solution before addition of silver nitrate ("Silver Last" column). Or brevity, **Table 2** represents only a part of the screening of the synthetic conditions that we have investigated.

SYNTHESIS	GROWTH SOLUTION (M)	λ_{MAX} (nm) seeds last	Silver last
A	TSC $5*10^{-2}$ AgNO$_3$ $2*10^{-4}$ AA 10^{-4}	No plates	
B	TSC $5*10^{-3}$ AgNO$_3$ $2*10^{-4}$ AA 10^{-4}	No plates	
C	TSC $5*10^{-3}$ AgNO$_3$ $2*10^{-4}$ AA 10^{-3}	< 700	
D (std prep)	**TSC $5*10^{-3}$** **AgNO$_3$ $2*10^{-4}$** **AA 10^{-4}**	**750-800**	**<650**
E	TSC $1*10^{-3}$ AgNO$_3$ $2*10^{-5}$ AA 10^{-4}	< 650	<650
F	TSC $1*10^{-2}$ AgNO$_3$ $2*10^{-4}$ AA 10^{-4}	< 750	<750

Table 2 Some of the setup used in the screening of the synthetic conditions for the optimization of the preparation of silver nanoplates with the desired LSPR features.

Given the results which are summarized in table, we decide to focus on reaction conditions close to those of entry D.

At this stage, we have prepared four different growth solutions, using reaction condition of entry D, with the exclusion of one reactant TSC, AgNO$_3$, AA and seed respectively. UV-Vis spectra in **Figure 10, 11, 12, 13**, show behavior of growth solution under these condition of synthesis.

In absence of citrate, we can observe the existence of three different LSPR bands, which do not fall in the NIR region and are probably related to some anisotropical large object: absence of citrate and of its shape directing action rules out the formation of the desired flat and plate-like objects.

Absence of AgNO$_3$ (the precursor) or ascorbic acid (the reductant) obviously do not allow the growth of anisotropic AgNPs at all.

In absence of seeds we can observe the slow raise of a quite interesting LSPR spectra. An intense absorbance at 450 nm is probably ascribable to the formation of spheroidal AgNPs originating from reduction of the precursor which is present in growth solution, while another broad LSPR band centered at about 750 nm probably indicates the growing of anisotropic silver nano-objects of different shapes.
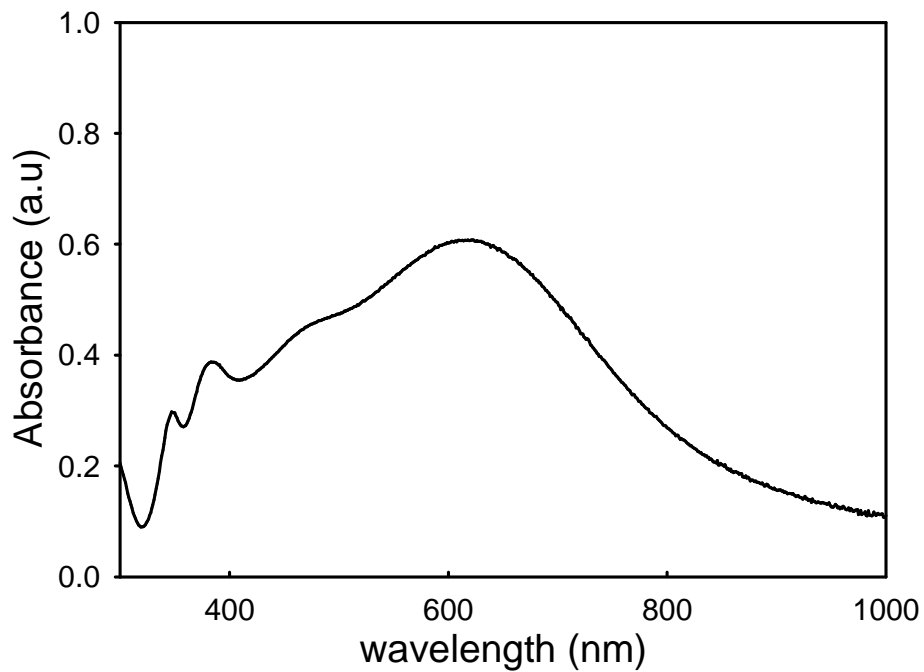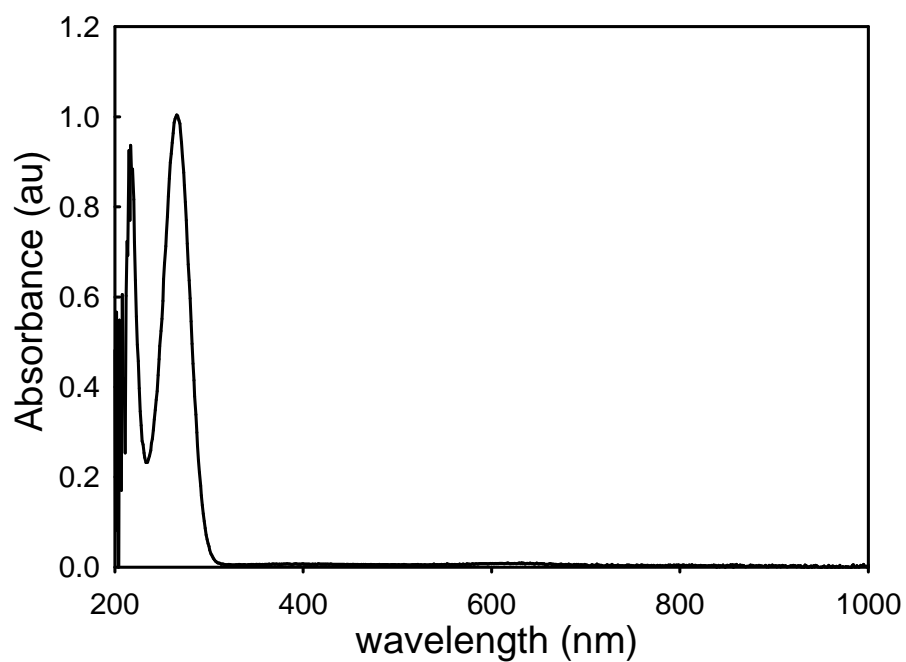

Figure 10 UV-Vis spectra of growth solution without sodium citrate (TSC).

Figure 11 UV-Vis spectra of growth solution without AgNO$_3$.
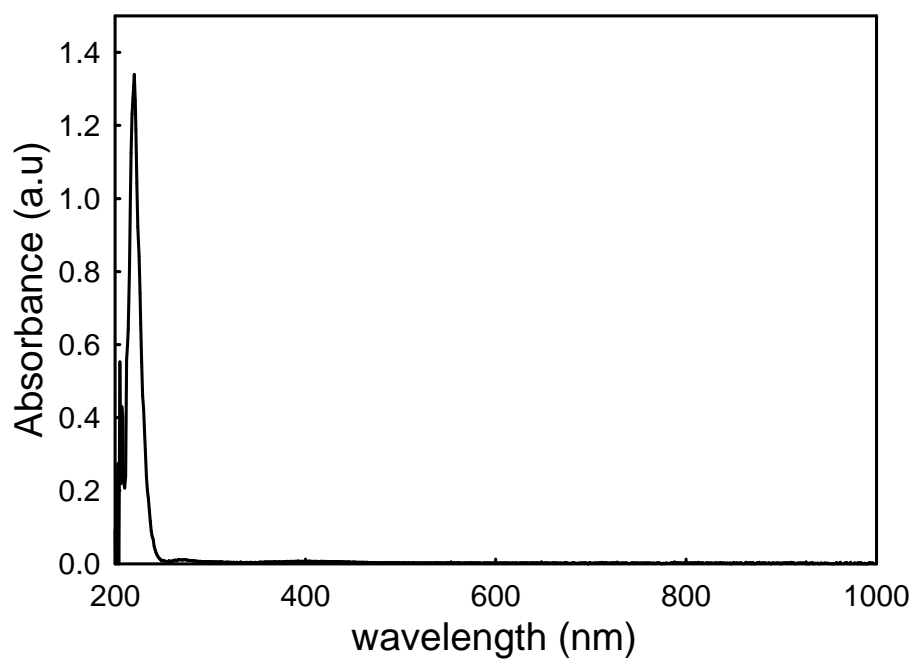
Figure 12 UV-Vis spectra of growth solution without ascorbic acid (AA).
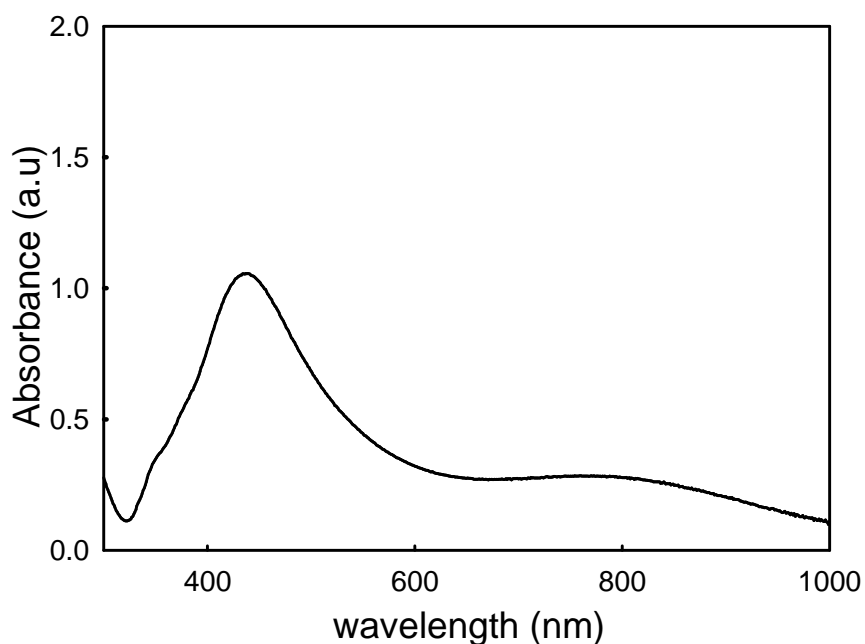
Figure 13 UV-Vis spectra of growth solution without seeds after one hour from silver nitrate addition.

2.2.2.3 Tuning of the in-plane dipolar LSPR Position with Different Amount of Seeds

At this point, we have decided to study the tuning of this absorption band as a function of different concentration of seeds.

Obviously, when the amount of silver ion precursor, $AgNO_3$, and other reactants, TSC and AA, are kept constant, the average size of silver nano-objects is going to depend from the amount of seeds added: smaller quantities of seeds will produce larger objects, having the in-plane dipole resonance moved to higher wavelengths, while the addition of an higher quantity of seeds will produce smaller objects having the in-plane dipole band shifted to lower wavelength. UV-Vis spectra of three different preparation, with different amount of seeds (200 μL, 400 μL, 600 μL) are showed in **Figure 14**.
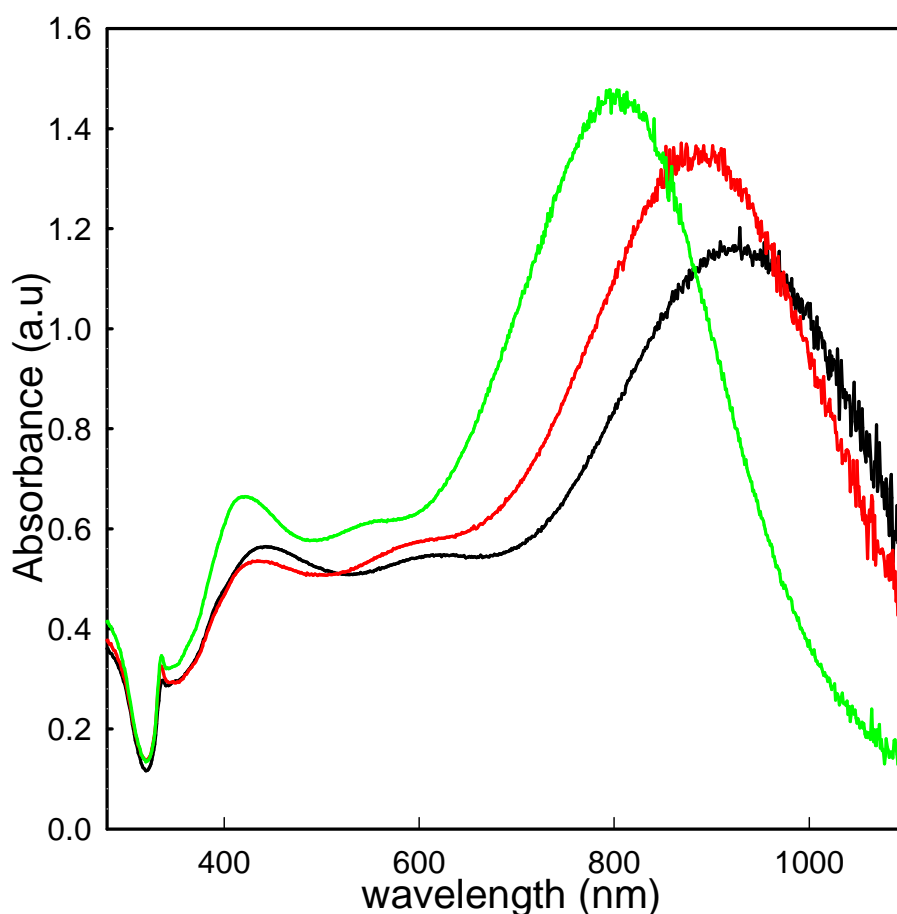
Figure 14 UV-Vis spectra of three different preparation of silver nanoplates with different amount of seeds: 200 µL (black line), 400 µL (red line), 600 µL (green line).

From **Figure 14** we can effectively notice a red shift of in-plane dipolar band with the decrease of the amount of seeds. So it is possible to tune this LSPR band, varying quantities of seeds and keeping constant concentration of growth solution, the same of the entry D in **Table 2**.

After this experiment, we have tried to evaluate the level of reproducibility and also the real control of this synthetic approach. With this purpose, we have set up four different preparation with 4 different amount of seed (200 µL, 300 µL ,400 µL, 600 µL) but with the same standard growth solution. Each preparation is repeated five times for a total of twenty.

In **Figure 15** we can observe the relation between the average of maximum of in-plane dipolar LSPR band (λ_{max}) and the amount of seeds add to growth solution.
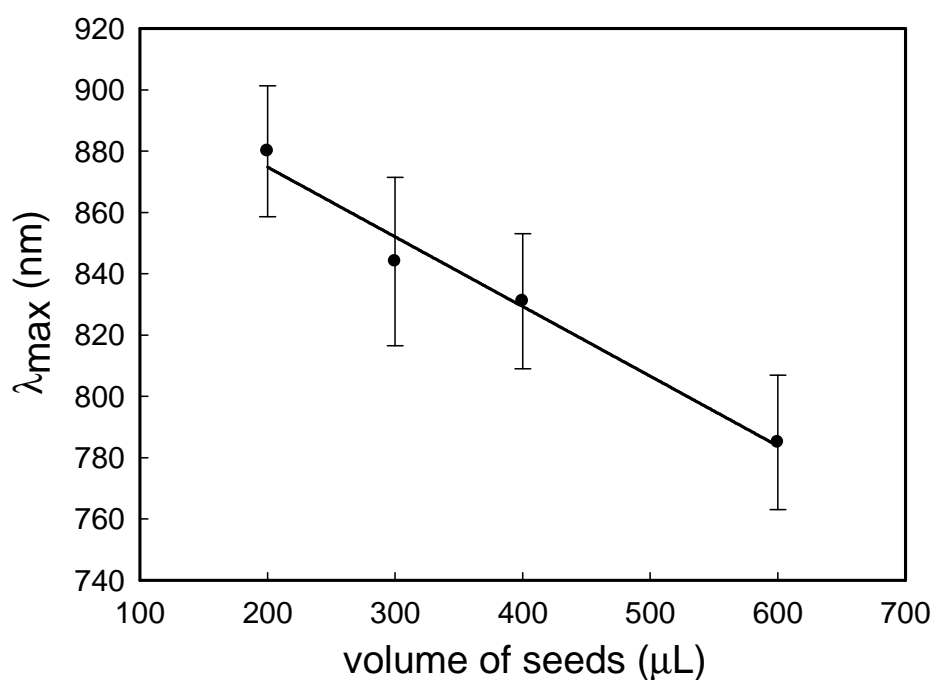
Figure 15 Relation between λ_{max} of in-plane dipolar band and amount of seeds added to a standard growth solution. λ_{max} is an average value of five preparation (R^2 = 0.9792).

The results show that LSPR band can be roughly adjusted by changing the quantity of seeds solution added: reducing of 33% the seed quantity results in a LSPR band moving toward 900 nm, while increasing the seed quantity added the growth solution to a double of the standard value shifts the final LSPR band close to 800 nm or less.

Though the synthesis are quite poorly reproducible, the preparation with an amount of 300 μL of seeds could be considered conform to our aim: the synthesis of silver nano-objects with LSPR band centered around 850 nm.

Consequently, for standard preparation of silver nanoplates we have used reaction conditions of entry D, **Table 2**, and 300 μL of seeds.

After the addition of the proper quantity of seeds, a slow change in the color of suspension was noted in almost all preparation, corresponding to growth of an intense LSPR band, which moves towards NIR with time while increasing its intensity. The phenomena arrives to completion in less than 12 hours, as can be seen from **Figure 16**, while no sensible further changes of LSPR features are observed in the time scale of one week, indicating the stability of the colloidal suspension obtained.
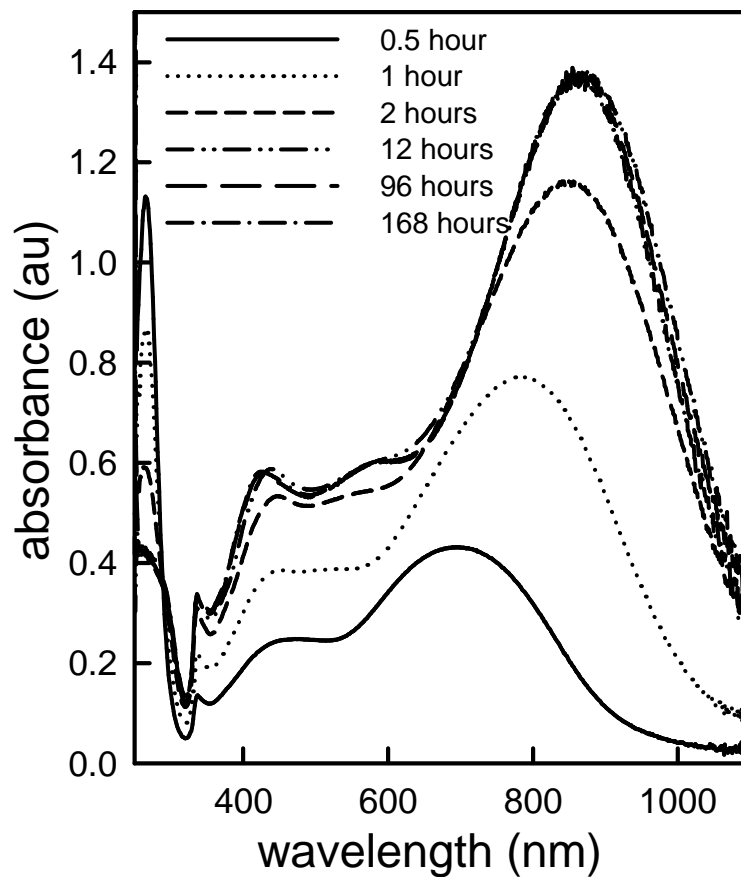
Figure 16 UV-Vis spectra showing the kinetic of evolution with time of the seed-growth preparation of silver nanoplates, with t=0 being the seed solution introduction into the growth solution.

Completion of nanoplates growth is also indicated by the complete disappearance of the UV absorption band of ascorbic acid, centered at 266 nm.

The synthesis made following the standard preparation allows to obtain colloidal suspensions with a blue-gray color, an image is reported **Figure 17**.
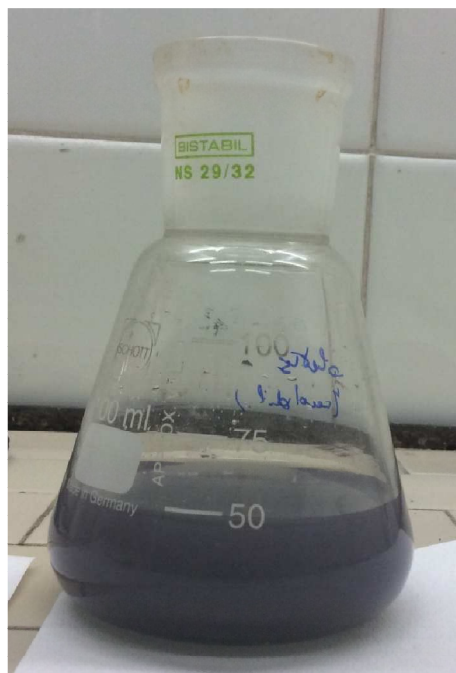
Figure 17 Photograph of colloidal suspension of silver nanoplates after 12 hours.

This colloidal suspension of nanoplates displays several bands, and at least three can be clearly recognized:[28] one band at 330 nm (which can be ascribed to the out-of-plane quadrupole resonance for triangular nanoplates), one at about 420-440 nm (the zone where usually is found the out-of-plane dipole resonance) and the more intense one, the in-plane dipole resonance, at about 845±30 nm, average value based on eight preparations. A typical spectrum obtained for a representative preparations is reported in **Figure 18**, while four spectra coming from four different preparations are reported in **Figure 19**, accounting for an acceptable degree of reproducibility.
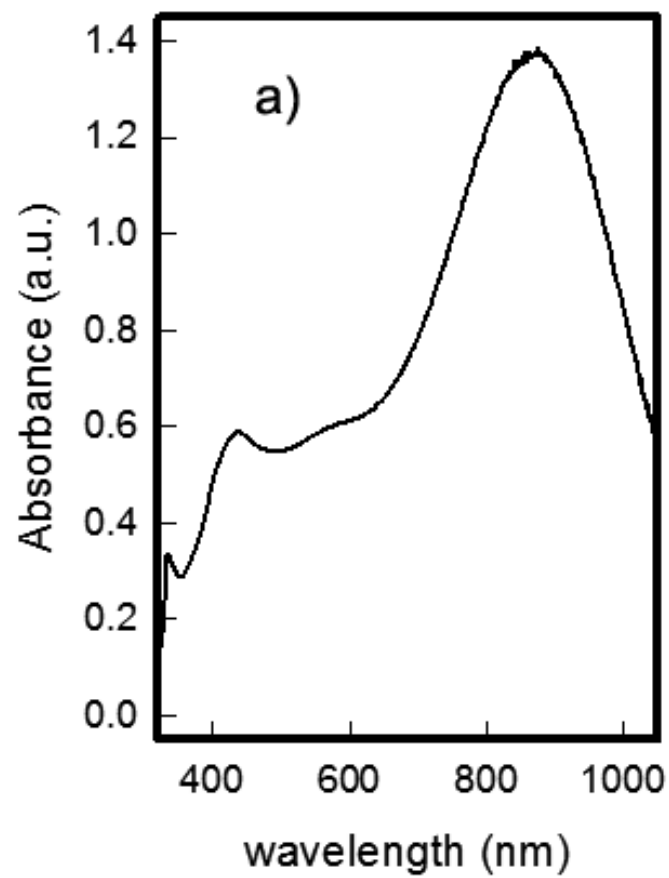
Figure 18 UV-Vis spectra of colloidal suspension of silver nanoplates obtained with the standard preparation.
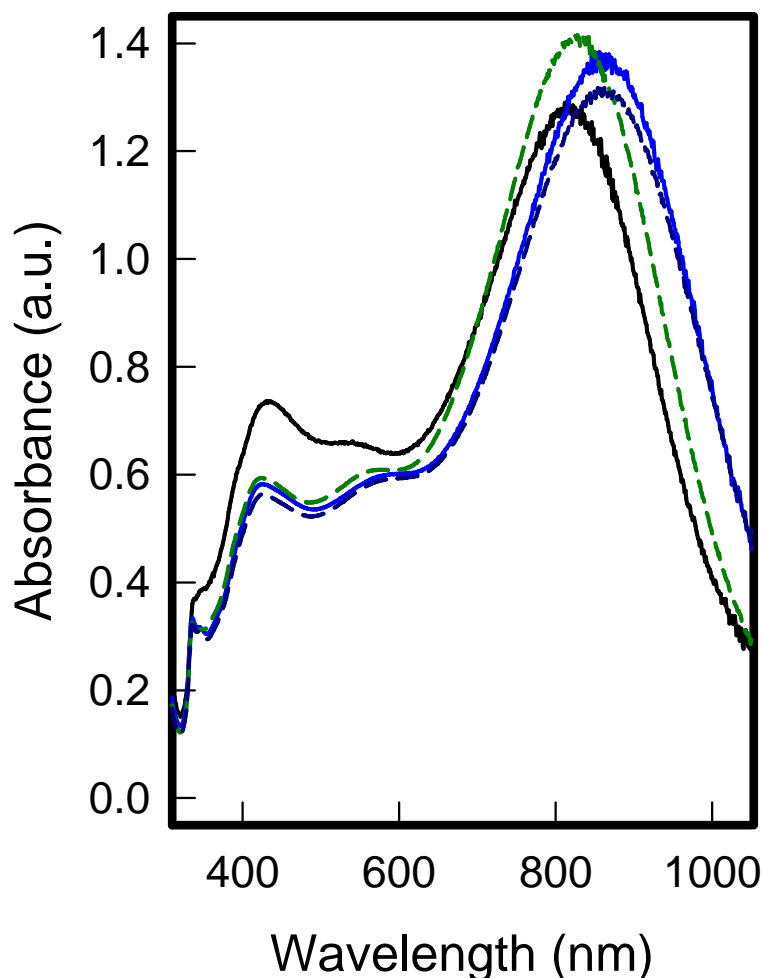
Figure 19 UV-Vis spectra of four different colloidal supensions of silver nanoplates obtained with the standard preparation.

The complexity of the spectra, as well the broad absorption in the range between 400 and 650 nm indicates the presence of several type of different objects.

TEM analysis of the suspensions obtained with the standard preparations yielding an in-plane dipolar LSPR placed at 845±30 nm confirms the presence of a majority of triangular plates, with various degrees of snipping of the corners: objects range from almost regular triangles with slightly rounded corners, to a few amount of almost hexagonal plates, as can be seen in **Figure 20**.
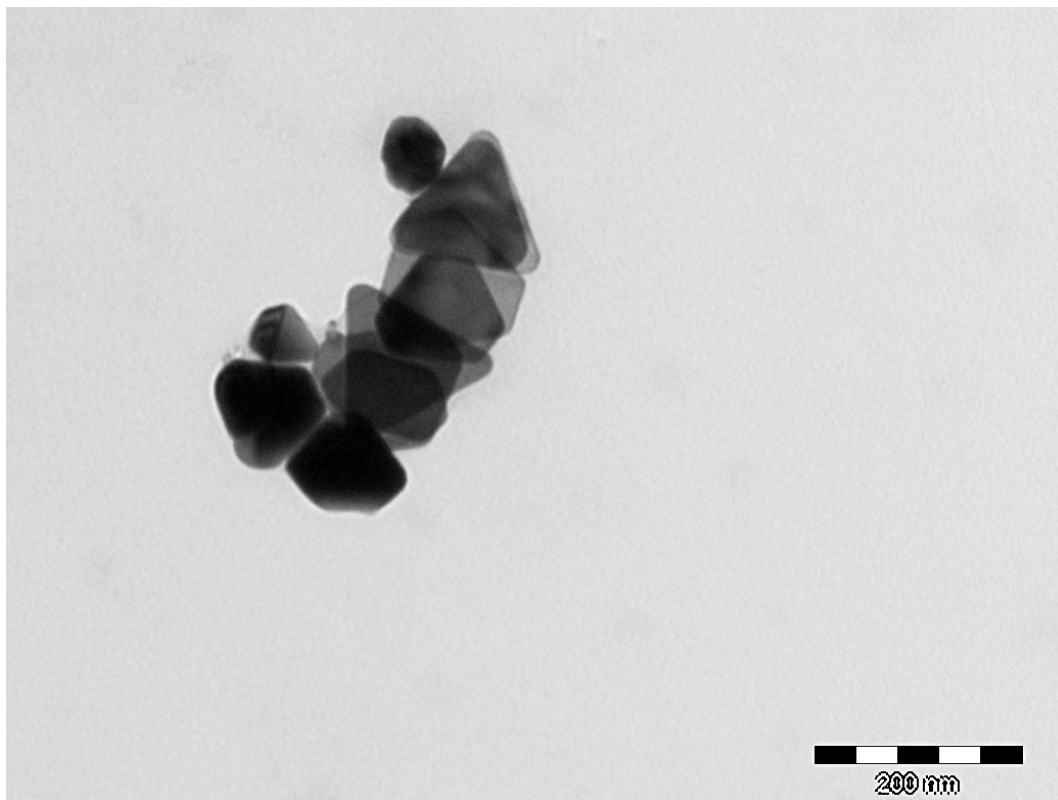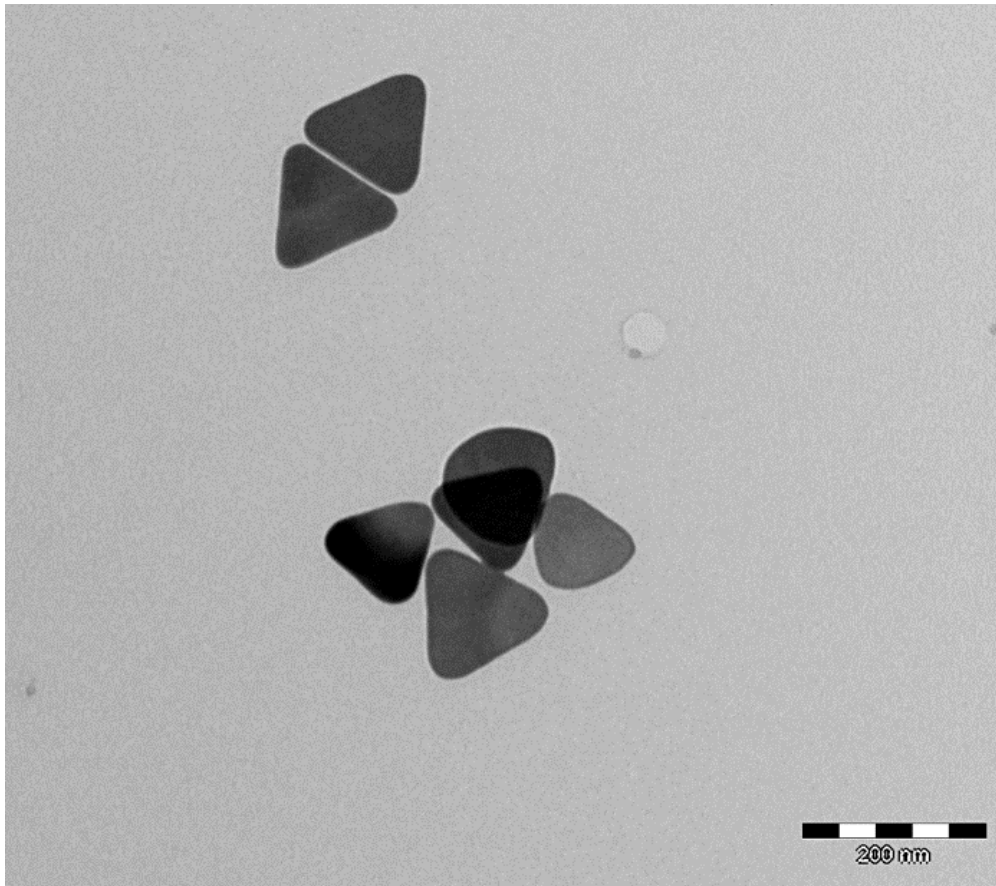
Figure 20 TEM images of silver nanoplates obtained with the standard preparation.

From a few number of objects which were placed vertically in agglomerates observed in TEM images, see **Figure 21**, we estimated an average thickness of about 20 nm.
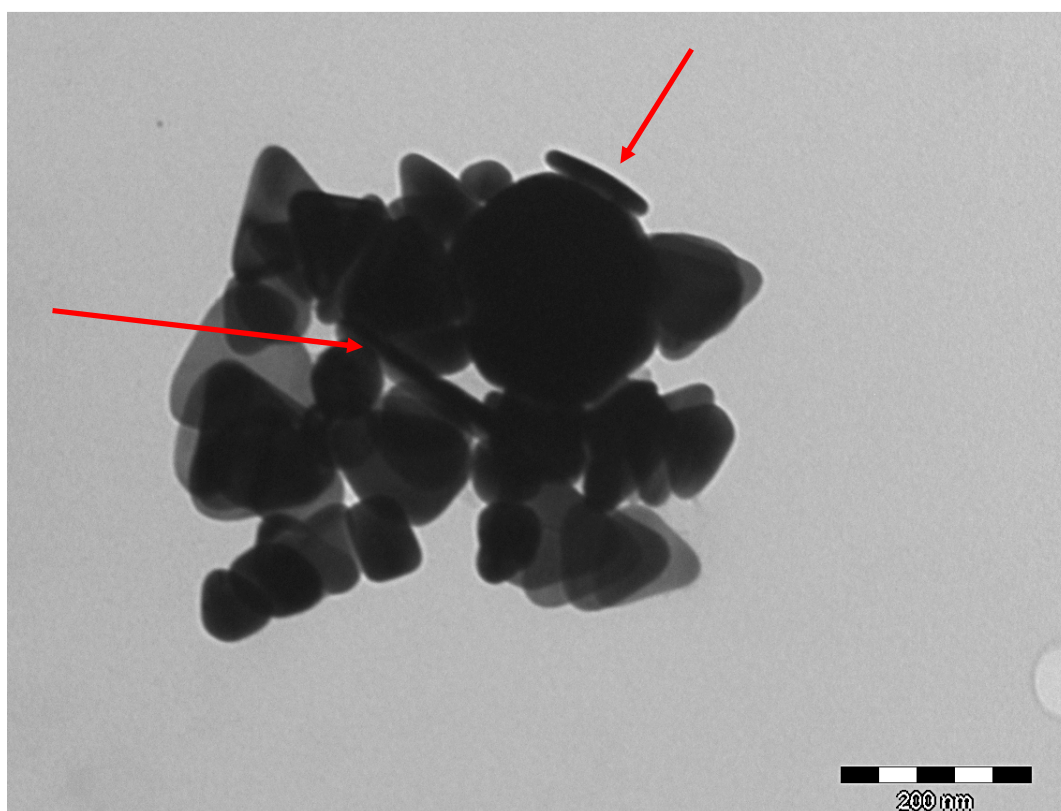

Figure 21 TEM image for a standard nanoplates preparation, showing the presence of a majority of triangular objects, with objects of various dimensions morphology, and of vertically placed objects (see arrows) with a thickness of about 20 nm.

The dimensions of regular triangles obtained with the standard preparations were measured, calculating, as a qualitative parameter, for each triangular plate, the three altitude values (defined as the distance between a vertex of a triangle and the opposite side at right angles) and obtaining an average value (coming from four preparations) of 120±25 nm.

In addition, a certain number of smaller, more rounded object, as well of objects of other shapes can be noticed in some TEM images, as can be observed from **Figure 22**.

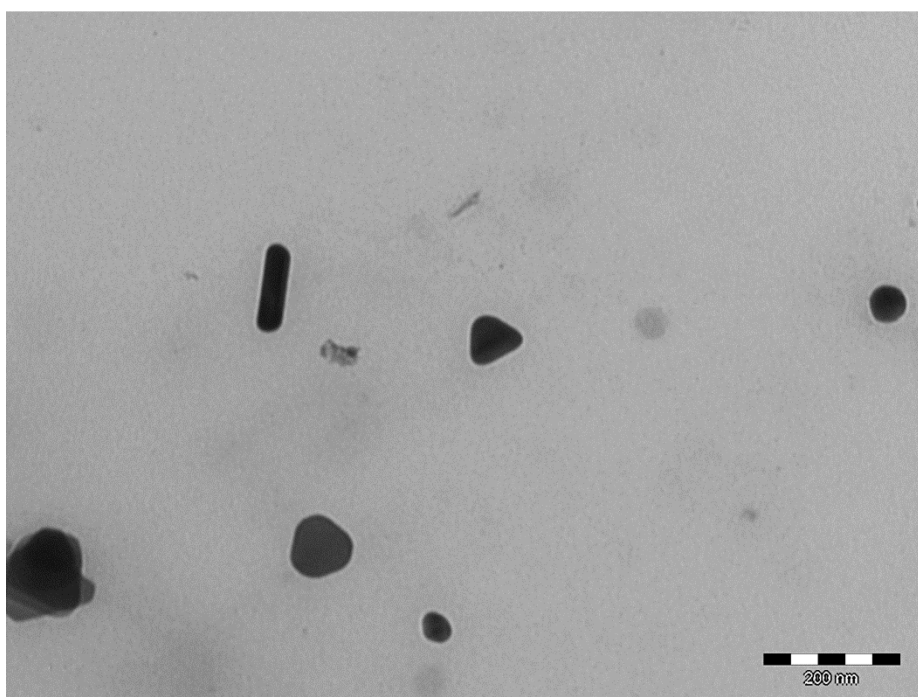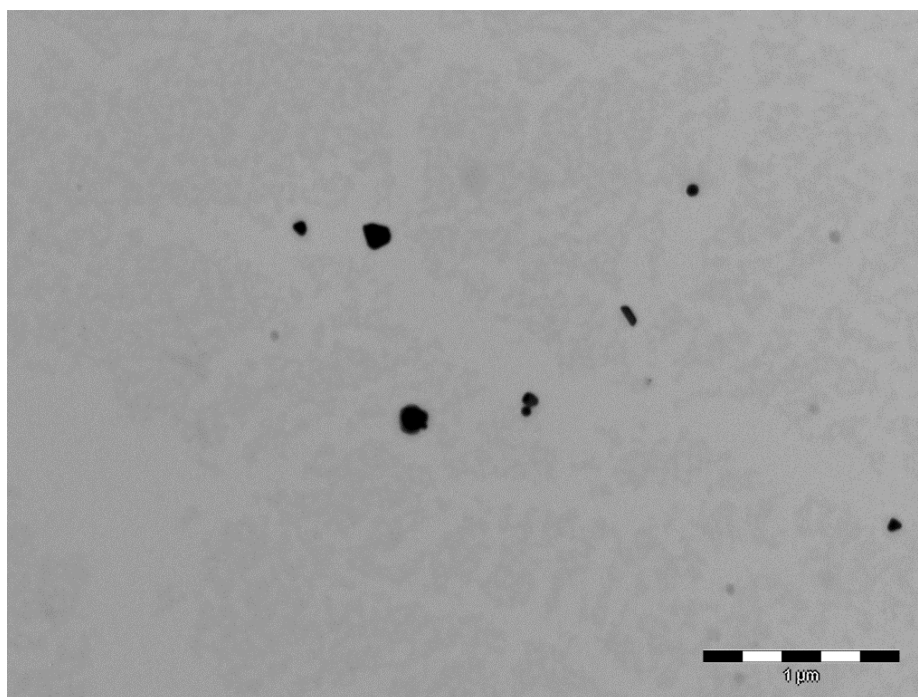**Figure 22** TEM images for a standard nanoplates preparation showing the existance of a few rod-like and almost spherical objects.

Presence of these objects is not straightforward to explain. One possibility is that they come from a competitive growth of objects which do not involve the added seed presence, as observed in the experiment described in **Figure 13**, where the growth of anisotropic objects was noted in the

growth solution in absence of seeds in hours timescales. In presence of the used amount of seeds, which are growing consuming silver nitrate, anyway, one can imagine that this competitive reaction is slowed and only marginally present, as confirmed by the relatively low population of undesired non-triangular objects.

On the other hand, we have also investigated morphology and size of silver nano-object obtained with different amount of seeds. Transmission Electron Microscopy in **Figure 23** refers to preparation with higher amount of seeds (600 μL) respect to standard preparation (300 μL). Also in this case, we can note the presence of AgNPs with triangular shape. However, the average value of altitude for each triangular plate (coming from four preparations) is 75±20 nm. This indicates that is possible a certain degree of control of nanoplates size by changing the amount of seeds while keeping constant other synthetic parameters: this is perfectly consistent with the observed blue shift of the in-plane dipole resonance under 800 nm for this kind of preparation as described above. Of course, reducing the amount of seeds produced larger objects (about 150-200 nm height, data not shown) with a red shift of the in-plane dipole resonance band.
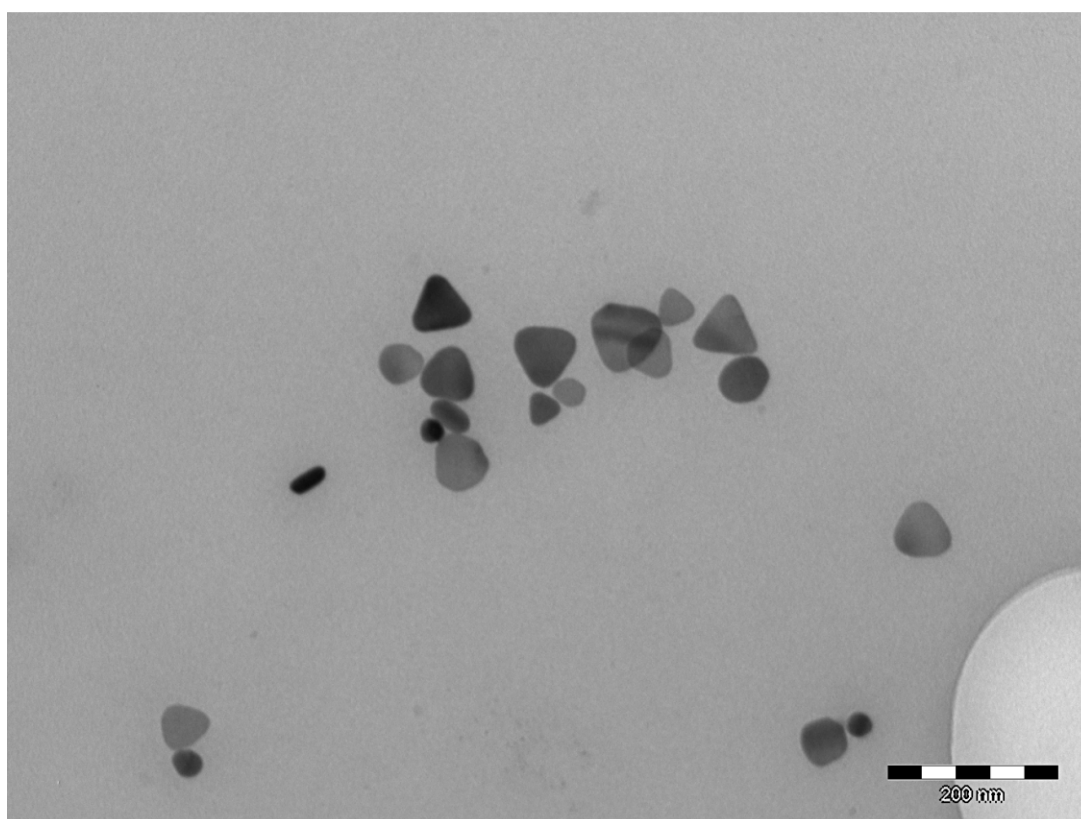

Figure 23 TEM image for nanoplates preparation with a higher amount of seeds respect to standard preparation, showing the presence of triangular objects, with the value of altitude is smaller than silver nanoplates obtained with standard preparation.

Dynamic Light Scattering (DLS) measurements of Z potential (P_z) of the standard nanoplates colloid gave a value of -40.6 ± 4.5 mV, suggesting quantitative coating of the objects with citrate and explaining the high stability of the suspensions, as citrate provide enough surface charge to stabilize particles against aggregation. Stability was also demonstrated by the fact that the nanoplates colloidal suspension can be centrifuged at 5000 rpm for 15 minutes and then re-dissolved in water without any visible change in their LSPR spectra, as showed in **Figure 24**.
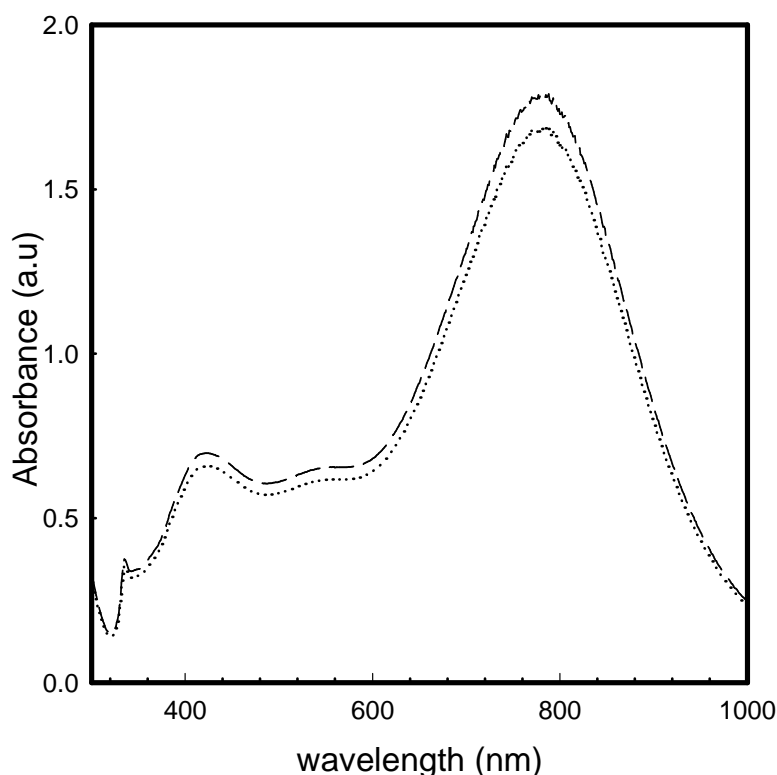
Figure 24 UV-Vis spectra of standard preparation of silver nanoplates (dashed line), the same after one cycle of ultracentrifugation and re-dissolution in water (solid line).

The role of citrate as stabilizing agent with a shape-directing action is well known: citrate anions preferentially bind to {111} facets of the crystals which are growing after the seed addition to the growth solution, slowing down the vertical expansion, and thus allowing to obtain anisotropic growth of the nanoplates.[68] This was also confirmed by XRD patterns (*vide infra*), obtained from a sample of nanoplates purified by centrifugation, concentrated and dried under vacuum. Only the

---

[68] I.Pastoriza-Santos, L.M. Liz-Marzan, *Journal of Materials Chemistry,* 2008, **18**, 1724.

[111] reflection of a FCC structure is observed, indicating that the basal lattice plane of nano-objects is (111), as expected from the growth-directing action of citrate.

It is important to stress once again the fact that a loose but, for our purposes, useful control on the plates morphology and dimensions was obtained using only ascorbate and citrate, and controlling the quantity of seeds. In absence of surfactant or polymeric stabilizers, we obtained a colloid with a LSPR spectra which fits our needs of an intense NIR absorption in the so called "therapeutic window". In addition, citrate ensures a high negative charge on nanoplates, which is crucial both for colloidal stability and for interaction with protonated amines (which will be brought on bulk glass surfaces as a grafting layer) in the same time allowing to avoid the use of harmful coating agents. Moreover, AgNPs prepared in presence of citrate usually show a very efficient antibacterial action[30,65,66,69,70], a fact which is not ensured in presence of coating agents which could interfere with silver ions release.

2.2.2.4 Grafting of Nanoplates: Preparation and Characterization of GLASS-PEI-TRI samples

In the last years, as largely described in **Paragraph 1.2.4**, it was shown how the antibacterial action of AgNPs can be easily brought on macroscopic scale. This can be done exploiting the Ag-S bond, after bringing a –SH layer on bulk glass (used as a model surface) by means of the formation of a first monolayer layer of mercaptopropyltriethoxy silane (MPTS).[30] Similar results are obtained using electrostatic interactions between ammonium groups and the negative charges on AgNPs surfaces. Recently we demonstrated that a monolayer of AgNPs, obtained through preliminary silanization of the glass with 3-aminopropyltriethoxysilane (APTES), can be conveniently used against the biofilm-producer *Staphylococcus epidermidis* RP62A.[66] The same can be done preparing a layer of polyethyleneimine (PEI) polymer on glass as an adhesive layer.[65] In all these cases, excellent stability in aqueous media, prolonged release of silver ions, controlled local concentration of Ag^+ without any detaching of AgNPs, and a strong antibacterial action with limited risks towards human health, were observed. Thus, we decided to use the same approach, and prepared a surface ready to graft silver nanoplates which will are negatively charged. The approach is reported in **Scheme 1**. We can prepare such a surface using PEI-silane, a polymer

[69] A. Taglietti, Y.A. Diaz-Fernandez, E. Amato, L. Cucca, G. Dacarro, P. Grisoli, V. Necchi, P. Pallavicini, L. Pasotti, M. Patrini, *Langmuir,* 2012**, 28**, 8140.

[70] E. Amato, Y.A. Diaz-Fernandez, A. Taglietti, P. Pallavicini, L. Pasotti, L. Cucca, C. Milanese, P. Grisoli, C. Dacarro, J.M. Fernandez-Hechavarria, V. Necchi, *Langmuir,* 2011, **27**, 9165.

composed of an average of 3.6 propyltrimethoxysilane groups and 56 ethylenimine monomers, i.e. 56 amine moieties (including primary, secondary and tertiary amines). Each polymer molecule has multiple alkoxysilane attaching points, so it is possible to produce monolayers by attaching polymer molecules on silica surfaces with an established method.
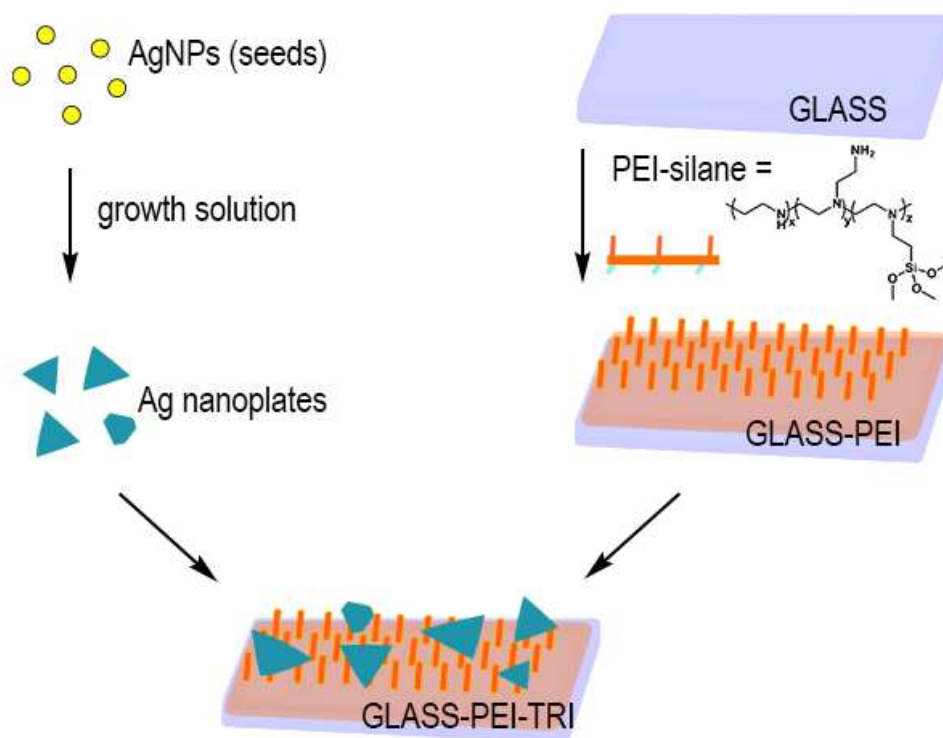
Scheme 1 A schematic representation of the synthetic route to GLASS-PEI-TRI samples: silver nanoplates are synthesized with a seed mediated growth approach and then are grafted on a GLASS-PEI sample.

In the standard procedure, 21x26 mm glass slides were cleaned and activated with piranha solution, producing an –OH rich, highly hydrophilic surface, having a contact angle <10° and ready to react quickly with PEI-silane in ethanolic solution, yielding PEI-functionalized surfaces (GLASS-PEI). A static contact angle (49±4°) was measured after functionalization, in good agreement with previous results.[54]

Grafting of nanoplates was obtained by dipping the GLASS-PEI glass slides for 14 hours in aqueous colloidal suspensions of citrate capped Ag nanoplates obtained from the standard preparation as described above. The typical UV-Vis-NIR spectra of glass samples obtained after this treatment (GLASS-PEI-TRI) reported in **Figure 25** clearly shows the grafting of the nanoplates.
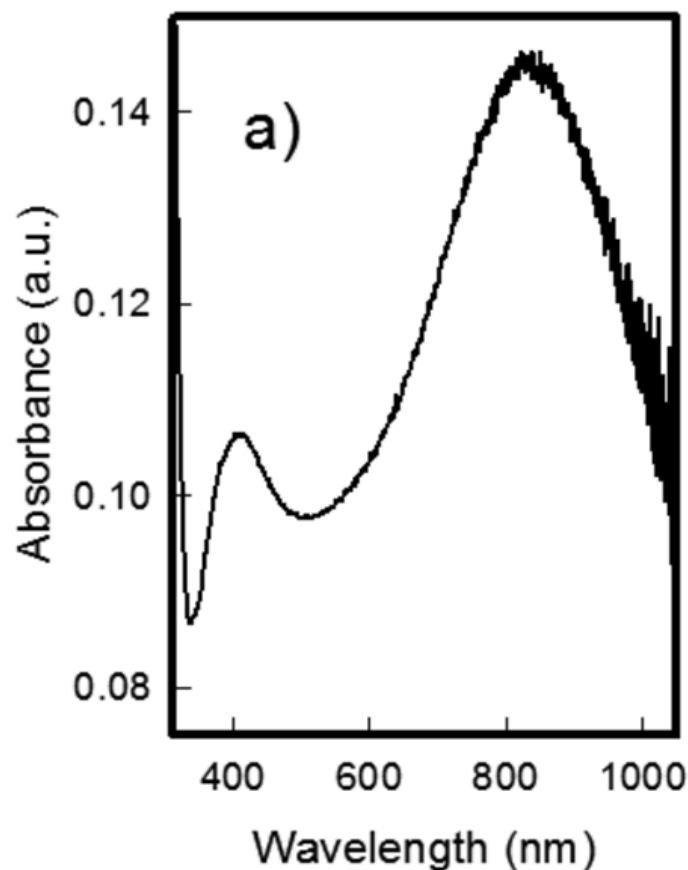
Figure 25 UV-Vis spectrum of GLASS-PEI-TRI.

The out-of-plane dipole band in the zone around 400-450 nm can be recognized. The in-plane dipolar band is centred in the 820 ± 30 nm range, with a 20-30 nm blue shift respect to the starting colloidal suspension. This shift is essentially due to the decrease of the local refractive index (n) on passing from water ($n_{water} = 1.3339$) to glass and air at the interface ($n_{air} = 1.0003$). The out-of-plane quadrupole resonance band observed at 330 cannot be found, probably as it is too weak and covered by the absorbance of glass itself in the UV region. Once again, broadening of the LSPR bands can be explained with the presence of objects with different morphologies and dimensions. **Figure 26** shows a couple of SEM images for GLASS-PEI-TRI samples at different magnifications.
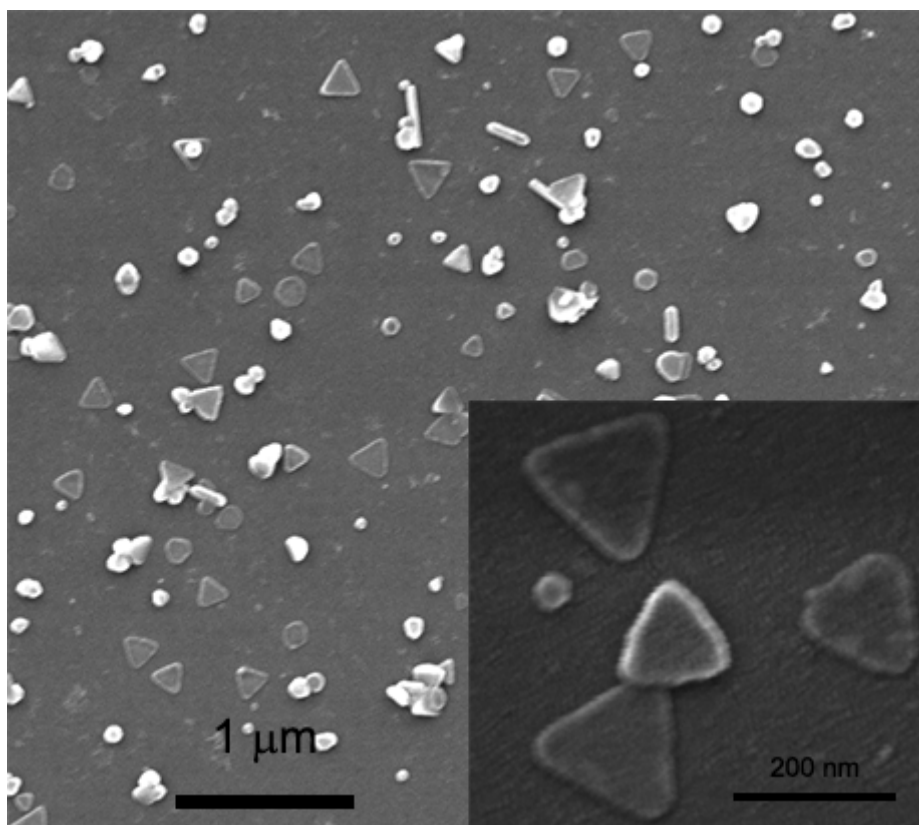
Figure 26 SEM images of a GLASS-PEI-TRI sample; inset: high magnification SEM image showing the presence of triangular nanoplates on a GLASS-PEI-TRI sample.

As can be seen in image reported in **Figure 26**, an homogeneous distribution of all the objects already observed in the TEM images was obtained, with the presence of some agglomerations of objects, which anyway retain dimension and morphology. This can be more precisely observed in the inset, where some regular triangles are shown. Measurements of dimensions of several regular triangles gave a value of 125 ± 25 nm for their altitude, in good agreement with the values derived from TEM.

The preparation of bulk glass samples coated with silver nanoplates is quite reproducible: in **Figure 27**, spectra of four samples coming from four different (i.e. obtained in four different reaction vessels), preparations obtained from the same standard colloidal suspension are reported, while **Figure 28** reports the spectra of seven samples obtained in a single preparation (i.e. in the same reaction vessel).
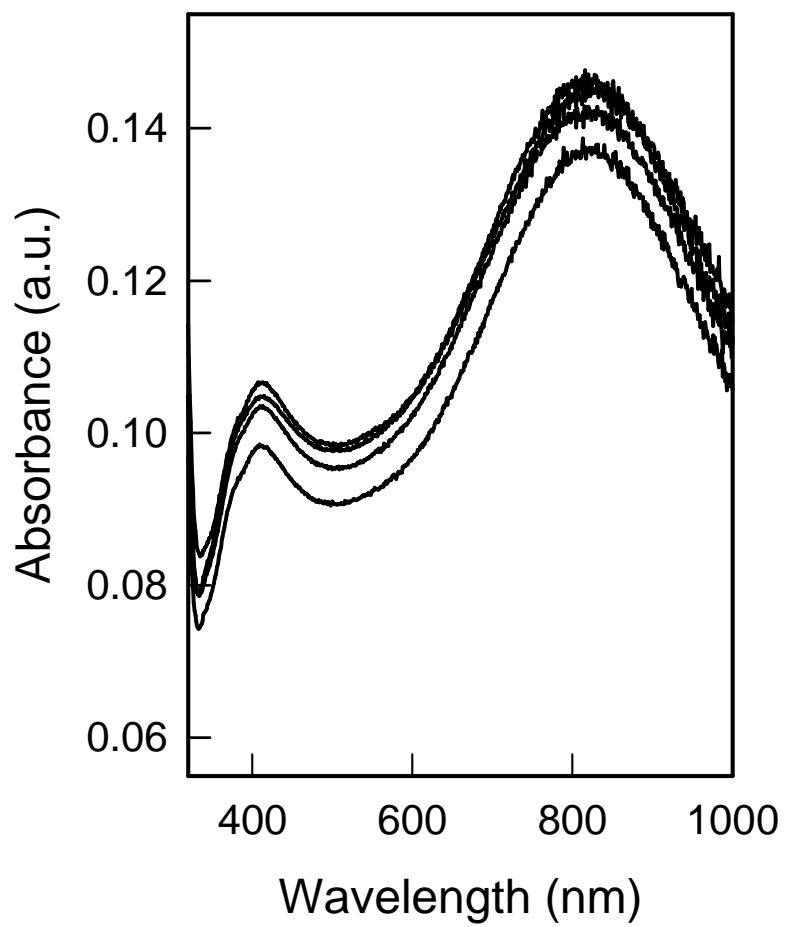
Figure 27 UV-Vis spectra of four GLASS-PEI-TRI samples obtained in four different vessels from four different preparations .
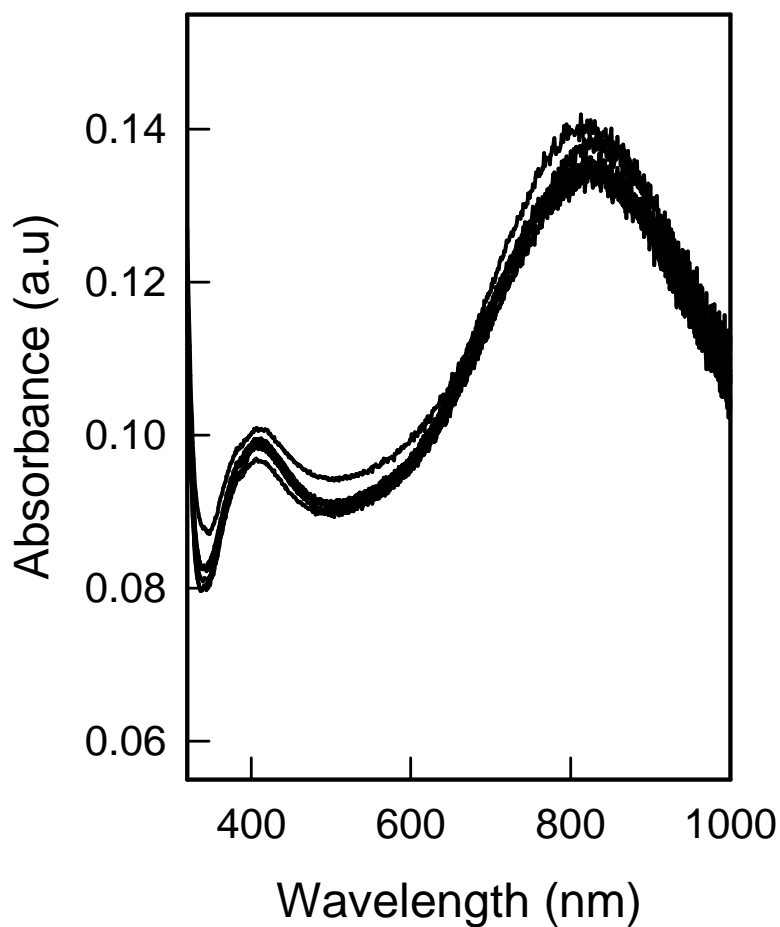
Figure 28 UV-Vis spectra of seven GLASS-PEI-TRI samples obtained, in the same vessel, from the same preparation.

Furthermore, PEI-TRI slides are very stable in air, i.e. their spectra did not change significantly for at least a 2-months period.

XRD patterns showed once again only the presence of (111) peak. In this case, a certain broadening is observed when the peak is compared to the one found in the case of the nanoplates powder, as reported in **Figure 29**. This broadening can be explained on the basis of the low surface concentration of plates in the GLASS-PEI-TRI samples.
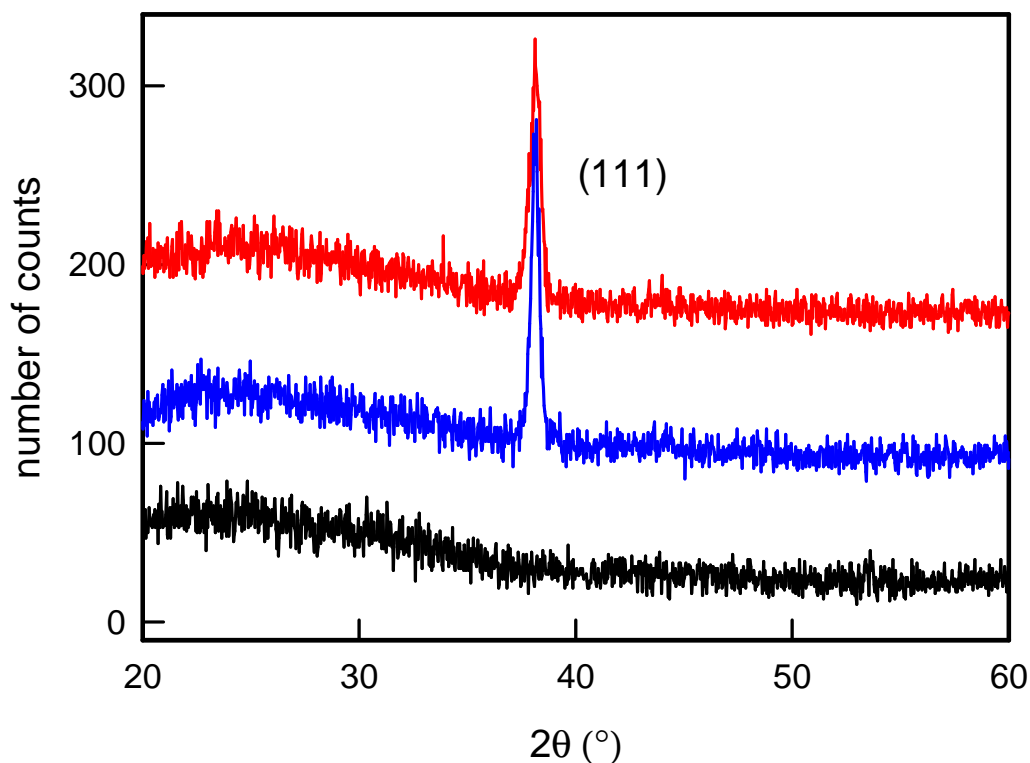
Figure 29 XRD patterns obtained for a blank glass (black line), for a sample of nanoplates centrifugated, concentrated, placed on a blank glass and dried as a powder (blue line), and for a GLASS-PEI TRI sample (red line), evidencing the presence of (111) diffraction peak.

We carried on the characterization of the PEI-TRI also with quantitative oxidation (using controlled amounts of strong acid) of the silver nanoparticles brought on the samples with the grafting procedure, and analysing the obtained solution by means of ICP. Data from eight different samples, coming from eight different preparations, gave an average of 1.87 (0.30) x 10^{-6} g/cm^2 of silver, a quantity which is higher than those usually found in samples in which a monolayer of small spherical AgNPs is grafted on a properly silanized,[30,65,66] but sensibly lower than in the case in which when a seed growth synthesis of flat silver objects is performed directly on glass.[71]

A feature which is of primary interest for the applications we have in mind is the ability to release a controlled quantity of silver when immersed in an aqueous environment without detachment of nano-objects in the environment. We investigated this aspect placing freshly prepared GLASS-PEI-TRI samples in ultrapure water for 48 hours, and after this measuring their UV-Vis-NIR spectra and

---

[71] A. D'Agostino, A. Taglietti, P. Grisoli, G. Dacarro, L.; Cucca, M. Patrini, P. Pallavicini, *RSC Adv.*, 2016,**6**, 70414.

their SEM images. We also measured the UV-Vis-NIR spectra of obtained solutions, which were subsequently analysed with ICP. Data from the solutions obtained after 48 h immersion in ultrapure water of GLASS-PEI-TRI samples showed the presence of 0.075 (0.030) x 10^{-6} g/cm^2 of silver. UV-Vis-NIR spectra on the same solutions did not show any presence of LSPR absorbance, thus ruling out the presence of plasmonic nano-objects and detachment of objects from the surfaces. Consequently, all the silver found in solution is ionic, and not belonging to detached metallic nano-objects. This was confirmed from SEM images on the samples extracted from the solutions after the immersion, which showed the same homogeneous distribution of the objects already observed in the freshly prepared samples, with objects conserving their average number, morphology and dimensions, as can be observed comparing **Figure 30** with **Figure 26**.
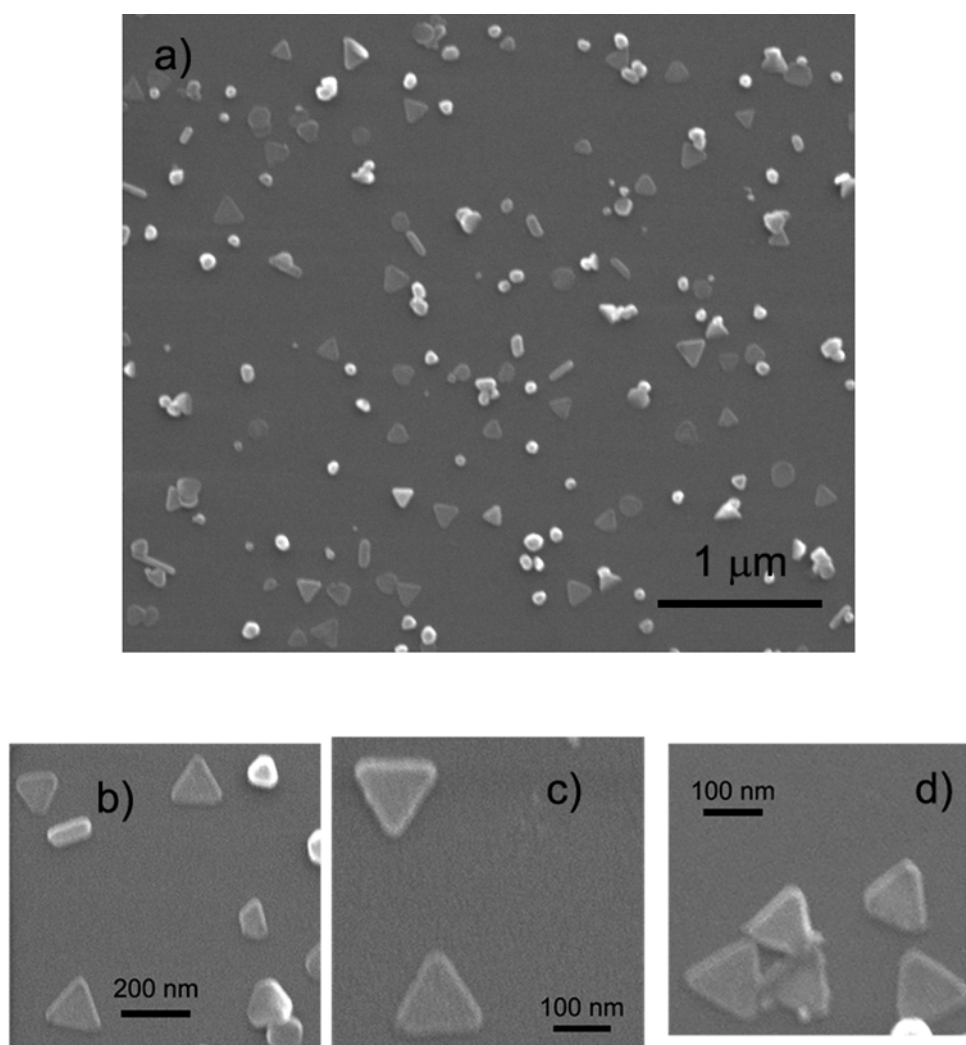
Figure 30 a) SEM image of a GLASS-PEI-TRI after 48 hours of immersion in water **b) c) d)** high magnification SEM images of the same sample showing images of triangular objects which retains morphology and dimension observed in the fresh samples.

Moreover, the UV-Vis-NIR spectra of the same GLASS-PEI-TRI samples are almost identical to the spectra registered before the immersion, as can be seen in **Figure 31**. Even if the situation in more complex media could be sensibly different, these experiments indicate that: i) the objects are stably grafted on the surfaces, ii) there is a limited release of silver ions from these objects, which compared to the total quantity of silver found on the samples means that only about 4 % of total grafted silver is released in 48 hours of immersion in water, iii) this release does not significantly change the shape and dimensions of the objects, as well their consequent LSPR features.

Figure 31 UV-Vis spectra of the same GLASS-PEI-TRI sample before (solid line) and after (dashed line) immersion in water for 48 hours.

2.2.2.5 Photo-thermal Effect of GLASS-PEI-TRI

At this stage, we wanted to check the photo-thermal features of the grafted nano-objects, i.e. their ability to produce localized hyperthermia when properly irradiated. To do this, GLASS-PEI-TRI sampl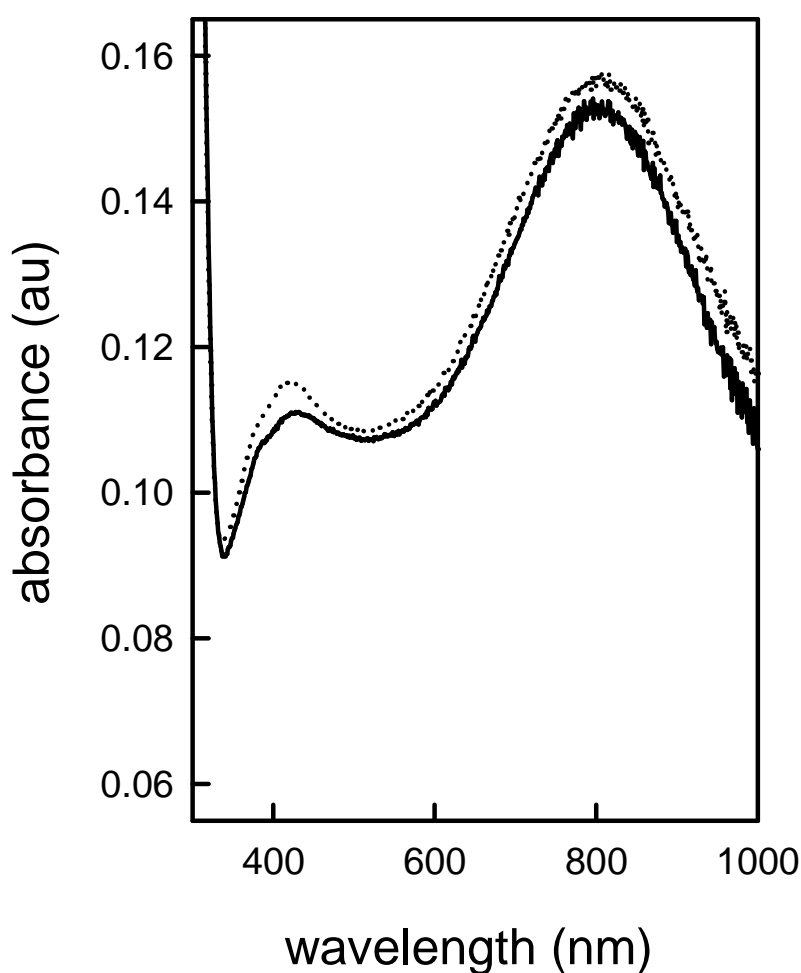es showing a LSPR maxima around 840 nm were irradiated with a Laser source at a 808 nm with a power of 200 mW, using a spot of 1.0 cm of diameter, corresponding to an irradiance of 0.26 W/cm^2. Using a thermocamera, the temperature in correspondence of the irradiated spot was measured and plotted against time of irradiation.
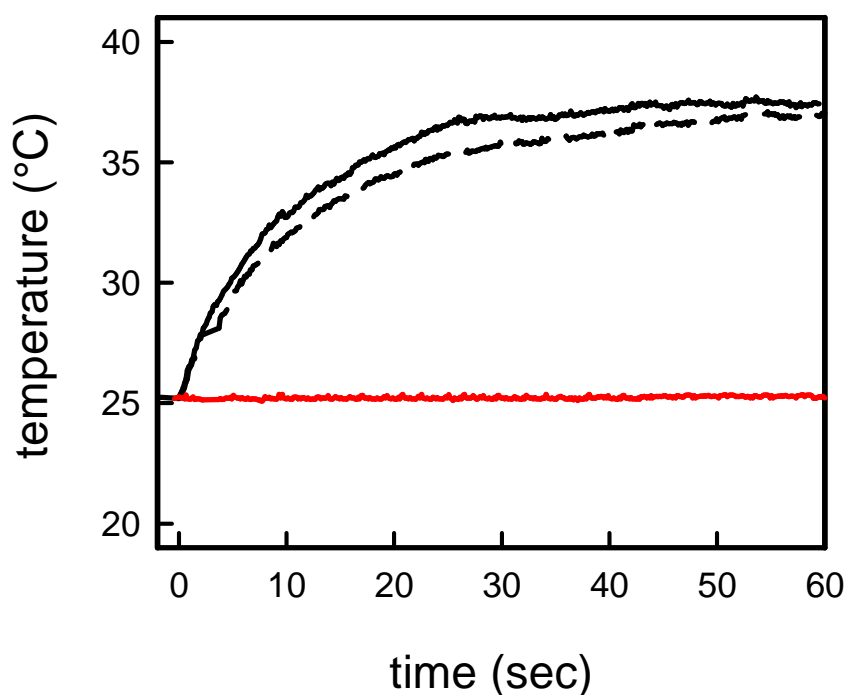
Figure 32 Temperature increase as a function of irradiation time, measured under NIR Laser irradiation (808 nm, 0.26 W/cm^2) for a freshly prepared GLASS-PEI-TRI sample (black solid line) and for a GLASS-PEI-TRI sample after an immersion of 48 hours water (black dashed line). The red solid line represents the thermogram obtained for an uncoated glass in the same conditions.

As can be clearly seen in **Figure 32**, irradiation causes a temperature increase in correspondence of the spot of about 11-12 degrees in a few seconds. The same behaviour is observed when the measure is repeated on a sample after 48 hours of immersion in water, demonstrating once again that a prolonged immersion in water does not produce any change of plasmonic features of the nanoplates layer. As predictable, irradiation of uncoated glass samples in the same conditions does not produce any measurable hyperthermia.

2.2.2.6 Antibacterial Tests of GLASS-PEI-TRI

As a first step to evaluate the antibacterial features, the Microbicidal Effect (ME) of GLASS-PEI-TRI samples against and *S. aureus and E.coli* , which are respectively representative strains of Gram-positive and Gram-negative bacteria, was investigated. As it was described in **Paragraph 1.2.5.5**, evaluation of the antibacterial features of a properly coated surface in contact with a thin liquid film containing bacteria can be done using the following formula:

$$ME = \log N_C - \log N_E,$$

where N_C is the number of CFU/mL developed on the unmodified control glasses, and N_E the number of CFU/mL counted after exposure to modified glasses (CFU = colony forming unit).

Contact time	S. aureus	E.coli
15'	< 0.3	< 0.3
5 h	0.9 (0.3)	3.2 (0.3)
24 h	2.5 (0.3)	3.6 (0.3)

Table 3 ME values of GLASS-PEI-TRI obtained as the average of three measurements.

We choose three contact times of 15 minutes, 5 and 24 hours and evaluated the ME after these intervals, which are reported in **Table 3**. Results show that GLASS-PEI-TRI glass slides exert a significant bactericidal effect increasing with the contact time. For what concerns *E. coli*, a contact time of 5 hours is enough to exert a eliminate at least 99.9% of bacteria cells. After 24 hours, more than 99 % of *S. aureus* are killed too. The effect on *S. aureus* seems a little less intense with 5 hours of contact, while no microbicidal effect towards both strains is present within the short (15 minutes) contact times. This is consistent with precedent studies on AgNPs coated antibacterial surfaces: as it is reported for similar systems,[30,65,66] one should expect a very limited release of silver ions for short (less than 1 hour) contact times, and this explains low ME observed in these timescale. Mechanisms by which AgNPs give their antibacterial effect is still debated, anyway it

was recently showed[72] that silver nano-objects are devoid of antibacterial action when used under anaerobic conditions which exclude oxidation to silver(I), thus preventing its release. This is consistent with the proposal[30] of the formation of an oxidized silver layer on the surface of citrate-coated grafted nano-objects, reaching a steady-state in which Ag^+ ions are slowly released, continuously being replaced by Ag oxidized from the bulk of the nano-objects. As we have already told, in the tests proposed by CEN (European Committee for Standardization) in -EN 13697 the microbicidal activity of a disinfectant is considered acceptable when the decimal-log reduction rate (which is strictly related to our ME), is at least equal to 4 after 5 min of contact. In our case the ME of the modified glass is very close to 4 after 24 h of contact for *E. coli*, showing a long term action which seems well suited to build antibacterial surfaces for medical devices.

This antibacterial effect, anyway, is not a surprise: it was largely expected and substantially confirms the behaviour obtained with spherical nanoparticles.[30,65,66] We were much more interested in the new features which are introduced by the anisotropic shape on nanoplates, i.e. the possibility to efficiently absorb a NIR laser radiation, to dissipate it as heat and to exploit this hyperthermia to kill bacteria cells.

In literature no precise information is present concerning the temperature values needed to eliminate bacteria with hyperthermia caused by a photo-thermal effect. Recently, it was described how a NIR Laser irradiation of a monolayer of GNSs on a glass bulk surface for 30 minutes causes a few degrees hyperthermia, which is enough to almost completely destroy a bacteria colony in a *S. aureus* biofilm layer. [47] Moreover, it is reported that the heating of *E. coli* cells at temperatures of 52° for a time longer than 5 minutes causes the destruction of the permeability barrier of bacteria cells. It is also reported that Laser irradiation of a cluster of gold nanorods for 5 minutes allows to reach a temperature of about 60°, thus destroying most bacterial cells in a biofilm of *E.coli*.[73] In any case, we must stress the fact that "macroscopic" effects described by thermograms registered with a thermocamera only show temperature changes of relatively large areas (in the range of 1 cm^2) of bulk glass samples, changes which are of course function of several experimental parameters.[74] So, information on the temperatures which are reached in the close surroundings of the nano-objects surfaces are completely missed, even if one can reasonably state that these temperatures will be considerably higher than those measured by thermograms.

[72] Z.M Xiu, Q.B Zhang, H.L Puppala, V.L Colvin, P.J.J. Alvarez, *Nano Letters*, 2012, **12**, 4271.

[73] W.Jo, M.J.Kim, *Nanotechnology*, 2013, **24**, 19.

[74] S.A. Khan, A.K. Singh, D. Senapati, Z. Fan, P.C. Ray, *Journal of Materials Chemistry*, 2011, **21**, 17705.

Thus, we moved toward the investigation of the antibacterial action given by Laser induced photo-thermal effects causing localized hyperthermia. GLASS-PEI-TRI samples, reduced in proper dimensions in order to be completely covered by the Laser spot, were irradiated for 15 min with a 808 nm Laser source, while in contact with the described bacteria suspensions, using an irradiance of 0.26 W/cm^2. In this case the "thermal microbicidal effect", ME_T, was calculated with the following formula:

$$ME_T = \log N_C - \log N_T$$

where N_C is the number of CFU/mL developed after the 15 min contact with GLASS-PEI-TRI samples in absence of irradiation, taken as control, and N_T the number of CFU/mL counted after 15 min of contact with GLASS-PEI-TRI samples in presence of NIR Laser irradiation. It is important to stress that in these conditions ME_T must be ascribed only to the photo-thermal effect, as any possible influence from the (limited) silver release occurring in absence of irradiation is already considered in the control count. Moreover, we have the evidence that no silver related ME is observed during the first 15 min of contact, as already reported in **Table 4**. It is also important to stress that when the experiment is repeated using non-functionalized glass samples the ME_T is absent (<0.3). This clearly states that Laser irradiation alone, in absence of plasmonic objects exerting photo thermal features, does not cause any harm to bacteria. The same set of experiments were replicated on a set of samples after their immersion in water for 24 hours, showing the same ME_T values, a fact that confirms stability of the sample property after long immersions in water.

	S. aureus	*E.coli*
GLASS-PEI-*TRI* 15 min	1.5 (0.3)	2.5 (0.3)
GLASS-PEI-TRI 15 min (after 24 h in water)	1.5 (0.3)	2.4 (0.3)

Table 4 ME_T values of GLASS-PEI-TRI obtained as the average of three measurements.

The ME$_T$ test results show that the laser treatment kills more than 99.7 % of *E. Coli* and about 97% of *S. aureus* cells in 15 minutes of irradiation at 0.26 W/cm^2, a value which is below the maximum allowed for exposure of the skin[75], and using a wavelength which is suitable for *in-vivo* use. As reported in **Table 4**, in the case of ME$_T$ we observe a higher activity against *E. coli* than against *S. aureus*, which was somewhat already observed in the values of ME due only to silver release. This may be due to the fact that Gram-positive bacteria present a relatively thick (20-80 nm) and continuous cell wall consisting mainly of peptidoglycane, while Gram-negative bacteria feature a thinner peptidoglycane layer (5-10 nm) surrounded by an outer phospholipidic membrane, which is expected to be less solid and resistant.[30,65,66] In this case hyperthermia caused by the photo-thermal effect seems particularly efficient in killing Gram-negative bacteria. As immersion in water for 24 hours does not change the shape and dimensions of objects and their LSPR features, as well their photo-thermal behaviour, it obviously has no effect on hyperthermia and subsequently induced antibacterial activity, which in fact is conserved. This behaviour allows to imagine the use of the Laser switched, hyperthermia related thermal ME after the surface has already exerted its silver-release related microbicidal action (described by ME reported in **Table 3**), in all the cases in which an "extra" action is needed.

2.2.3 Conclusions

The GLASS-PEI-TRI samples we have presented here exert an antibacterial action, which seems particularly active for Gram-negative bacteria like *E. coli*, exploiting two separate mechanisms. One is the long term action given by the "classical" silver ion release, which can be used for prevent the formation and adhesion of colonies over a long period of time, while the other is the Laser-switchable photo-thermal action, which can be activated on need (for example in the case of infections not sufficiently prevented by the first mechanism) and obtained using the peculiar spectral features of the objects grafted on the surface, objects which can be tailored in order to have their LSPR spectra matching with the wavelength of Laser source suitable for in vivo treatments.

The Laser switched antibacterial activity is obtained by irradiation of bulk surfaces in the NIR (which could be used *in vivo*) using a radiation intensity which does not damage the tissues. LSPR absorption was placed close to the laser wavelength at 808 nm, using a simple synthesis which

---

[75] ANSI, American National Standard for Safe Use of Lasers, Laser Institute of America, Orlando, FL, 2000

avoids reactants which can be dangerous to human health. Absorption can be tuned at any desired wavelength, depending on the needs, just tuning (or changing) the nanoplates synthesis. The typical antibacterial features usually observed in surfaces coated with silver nano-objects, which are due essentially to the controlled release of Ag^+ ions and which is ensured by the good stability of the grafted nano-objects layers, is conserved. As glass-like SiO_2 films can be easily deposited on a large spectrum of materials by gelification of a siloxane sol, the procedures here described can be applied also to cover a wide range of materials and used for several applications. These results could be thus be useful for a wide medical use: on prosthetic and subcutaneous devices, on surgical sutures, on wound dressings, to name a few examples. All these kind of bulk materials surely need a long term antibacterial surface protection, here ensured by the ability of silver nano-objects to release small and controlled amounts of silver ions for long contact times (some days), but also will profit of a switchable, very quick (a few minutes) Laser treatment to ensure elimination of bacteria cells.

2.3 Seed Mediated Growth of Silver Nanoplates on Glass

In the previous chapter, we have described how to prepare a bulk glass materials bearing silver nanoplates, tailored to have an high absorption in the NIR region and having strong photo-thermal features, in order to study their potential as model antibacterial surfaces. The long-term goal is the possibility of fabricating medical devices with coatings which could be active on long timescales as a result of the "classical" antibacterial effect due to silver ions release,[30,65,66] but with a further, additional antibacterial action which could be "switched on" on need by a NIR laser irradiation, producing localized hyperthermia, and to evaluate the possible synergy between these two kind of actions. In order to minimize the use of possibly toxic chemicals and avoid the use of classical surfactants, we have introduced the use of a simple seed-growth method using only citrate to obtain a proper growth of the desired object and then grafting them on glass (pre grafting growth method). In this chapter, we introduce another surfactant free seed-growth method to be applied directly on surfaces, involving once again the use of citrate as a shape directing agent on seeds which were already placed on the desired surface (post grafting growth method). The two routes are summarized in the **Scheme 2**.
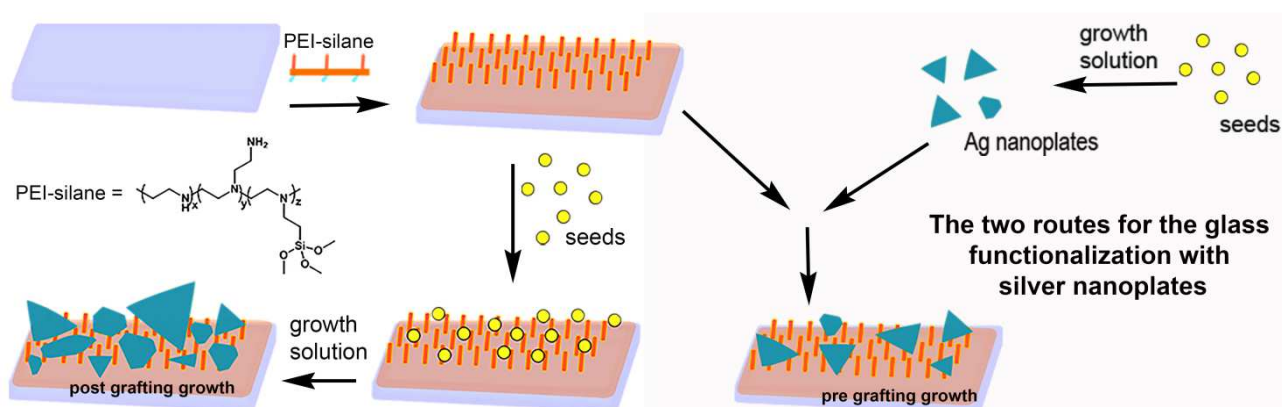
Scheme 2 Two routes for the glass functionalizaion with silver nanoplates.

The idea was to tune the geometric features of the nano-objects in single growing step maintaining an easy synthetic setup and just controlling the growth time. In this way an easy control the LSPR features of the samples is obtained, and an intense absorption in the NIR region can be gained and exploited for efficient laser induced photo-thermal effect.
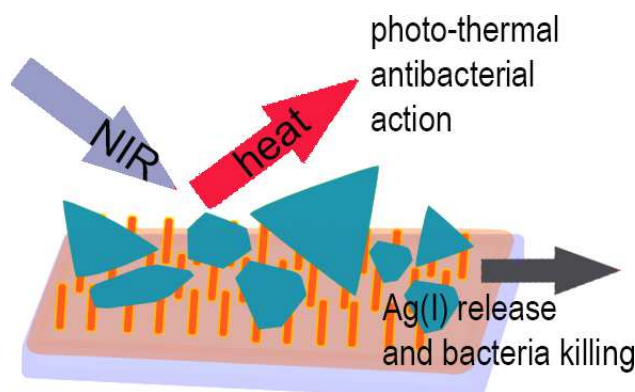
2.3.1 Experimental Details: Synthesis and Characterization

2.3.1.1 Experimental materials and Instrumentation

Materials

Silver nitrate (>99.8%), sodium borohydride (>99.0%), sodium citrate (>99.0%), ascorbic acid (>99%) were purchased from Sigma Aldrich. Trimethoxysilylpropyl(polyethylenimine) (50% in isopropanol) was purchased from Gelest Inc. Reagents were used as received. Solvents were purchased from Sigma-Aldrich and used as supplied. Microscopy cover glass slides (21x26 mm) were purchased from DelChimica. Water was deionized and then bidistilled. Tryptone Soya Broth (TSB) and Tryptone Soya Agar (TSA) for bacteria culture were purchased from Oxoid, England. *S. aureus* ATCC 6538 (LGC standards) and *E. coli* ATCC 10536 (LGC standards) bacterial strains were used.

Instrumentation and instrumental method

Absorbance spectra of colloidal suspensions were taken with a Varian Cary 100 spectrophotometer in the 200–900 nm range and spectra of functionalized glasses were obtained placing the slides on the Varian Cary 100 spectrophotometer equipped with a dedicated Varian solid sample holder.

SEM images and EDX analysis were taken from Tescan Mira XMU variable pressure Field Emission Scanning Electron Microscope – FEG SEM (Tescan USA Inc., USA) located at the Arvedi Laboratory, CISRiC, Pavia. Slides were mounted onto aluminum stubs using double sided carbon adhesive tape and were then made electrically conductive by coating in vacuum with a thin layer of Pt/ Pd (3–5

nm). Observations were made in backscattered electrons mode (BSE) at 30 kV and with InBeam secondary electron detector for higher spatial resolution. Textural observations, together with major element compositions, were performed by means of a Tescan FE-SEM (Mira 3XMU-series), equipped with an EDAX energy-dispersive spectrometer. The operating conditions were: 20 kV accelerating voltage, around 40 mA beam current, 15.8mmworking distance, counts of 100 s per analysis. The measurements were processed using the EDAX Genesis software and semiquantitative data obtained using the ZAF correction.

Thermograms (temperature vs. time) were recorded on SURF-PEI-PLATES samples by means of a laser (multimode AlGaAs laser diode, L808P200, Thorlabs GmbH, emitting light at the wavelength of about 808 nm, power of radiation is 200 mW, irradiance is 0.26 W/cm^2). Temperature was recorded by means of a FLIR E40 thermocamera and FLIR Tools+ software.

X-ray powder diffraction measurements were performed by using a Bruker D5005 diffractometer with the CuKa radiation, graphite monochromator and scintillation detector. The patterns were collected with a step size of 0.03° and counting time of 2 s per step in the angular range 20–65°.

The total Ag content of SURF-PEI-PLATES was determined by quantitatively oxidizing the silver plates grafted on a single slide by dipping it in 3 mL ultrapure concentrated HNO_3 diluted 1 : 5 with water in a becker, and keeping it overnight at RT on a Heidolph Promax 1020 reciprocating platform shaker. The Ag content in solution was then determined by inductively coupled plasma optical emission spectroscopy (ICP-OES) with an ICP-OES OPTIMA 3300 DV Perkin Elmer instrument. The measure was repeated on 8 glass samples coming from 8 different preparations.

Release of Ag^+ versus time was followed on a set of 10 SURF-PEI- PLATES slides (21x26 mm coated on both sides, total coated surface 10.92 cm^2) prepared as described above. Each slide was then immersed in 3 mL of ultrapure water. Slides were taken off the water after 20 minutes, 1 h, 3 h, 5 h, 24 h, 48 h, 96 h, 130 h, 168 h and 240 h. A UV-Vis spectra was measured on the water solution, and then the content of Ag^+ was determined by ICP-OES. Measures were repeated three times, and mean values are given. ICP data were collected with an ICP-OES OPTIMA 3300 DV Perkin Elmer instrument.

Release of Ag$^+$ of SURF-PEI-PLATES after laser excitation of 20 minutes was determined in the following mode. A 21x26 mm sample was cut in 4 sections of approximately 10x10 mm, with a surface which could be almost completely covered by the 1 cm^2 laser spot. The four samples were placed in four wells and covered with 0.75 mL of bidistilled water and each one was irradiated for 20 min with a 808 nm laser source. After irradiation time the water fractions were reunited obtaining 3 mL of water. A UV-Vis spectrum was measured and then the content of Ag$^+$ was determined by ICP-OES.

2.3.1.2 Glassware Pretreatment

The glassware used during experiments was always pretreated before use. It was washed in *aqua regia*, a mixture of nitric acid and hydrochloric acid, *fo*r 30 min, then washed and filled with bidistilled water and ultrasonicated for 3 minutes before discarding water. The bidistilled water/ultrasound treatment was repeated 3 times.

2.3.1.3 Preparation of PEI-silane Self-assembled Monolayers on Glass Surface (SURF-PEI glasses)

The samples were prepared according a reported method. [65]Briefly: glass substrates were cleaned for 30 min in freshly prepared Piranha solution (3 : 1 v/v H$_2$SO$_4$: H$_2$O$_2$ (30%)). (**Caution!** Piranha solution is a strong oxidizing agent and should be handled with care.), washed three times with ultrapure water in a sonic bath and oven-dried. The slides were then immersed for 6 min in a 4% (v/v) solution of PEI-silane in ethanol at room temperature. In a typical preparation, 8 glass slides were prepared at the same time, i.e. reacting in the same silane solution inside an 8-place holder (a microscope glass slides staining Jar). After this, the slides were washed two times with ethanol and one time with ultrapure water in a sonic bath and blow-dried with nitrogen.

2.3.1.4 Seeds Preparation

Seeds, spherical silver nanoparticles, were prepared according to a reported method.[65] Briefly, to 100 mL of ice cooled water the following solutions were added in sequence under vigorous stirring 1 mL of 1%(w/v) AgNO$_3$ solution, after a minute 1 mL of 1% (w/v) sodium citrate and, after a further minute, 0.500 mL of an ice-cooled solution 0.075% (w/v) in NaBH$_4$ and 1% (w/v) in sodium

citrate. After the last addition, stirring was immediately stopped, in order to avoid coagulation. The colloidal suspensions were stored in the preparation flask, maintained in the dark and used within 2 days from preparation.

2.3.1.5 Preparation of SURF-PEI-SEEDS Samples

The samples were prepared according a reported method.[65] PEI glasses were immersed in the colloidal suspension of seeds at room temperature for 15 min. In a typical preparation, 8 glass slides were prepared at the same time, i.e. they were made to react in the same seeds suspension (30 mL), inside a glass holder (Hellendhal staining Jars were used) where the slides were kept in vertical position. After this the obtained glass samples, showing a yellow colour, were placed in water and sonicated for 5 min. This procedure was repeated twice and then the glasses were blow dried with a nitrogen stream.

2.3.1.6 Growth Solution Preparation

Growth solution was prepared in a flask: to 30 mL of sodium citrate $8.5*10^{-3}$ M were added, under vigorous stirring, 18 mL of $AgNO_3$ $5*10^{-4}$ M and 0.450 mL of ascorbic acid $1*10^{-2}$ M. After the last addition, stirring was immediately stopped.

2.3.1.7 Preparation of SURF-PEI-PLATES Samples

In a typical preparation, up to 8 SURF-PEI-SEEDS samples were immersed in the proper amount of growth solution for the desired time in a Hellendhal staining Jar. Changing in colour of sample was observed from yellow, characteristic color of SURFPEI-SEEDS glass, to orange, red and dark blue on increasing dipping times. After this, the slides were washed with bidistilled water two times and dried under nitrogen flux.

2.3.1.8 Antibacterial Activity Tests

The antibacterial activity of functionalized cover glasses was investigated against *Staphylococcus aureus* ATCC 6538 Gram-positive bacteria and *Escherichia coli* ATCC 10356 Gram-negative bacteria. The microorganisms were grown overnight in Tryptone Soya Broth (Oxoid; Basingstoke, Hampshire, England) at 37°C. Washed cells were resuspended in Dulbecco's PBS and optical

density (OD) was adjusted to 0.2 at 650 nm wavelength, corresponding approximately to $1*10^8$ (CFU) per mL. 10 mL of bacterial suspension was deposited on a standard glass slide (76x26 mm), then the microbial suspension was covered with a functionalized cover glass slide (21x26 mm), forming a thin film between the slides that facilitates direct contact of the microorganisms with the active surface. The two assembled glasses were introduced in a Falcon test-tube (50 mL) containing 1 mL of PBS to maintain a damp environment. In this test microbes are incubated in non-nutritive suspensions that do not give the microorganisms the potential to grow during the test. For each bacterial strain three equivalent modified glasses were prepared; the slides were maintained in contact with the liquid films containing bacteria at room temperature for 20 minutes, 5 and 24 h, respectively; for each time of contact an unmodified glass slide was treated in the same way as control sample. After the times of contact, 9 mL of PBS were introduced in each Falcon test-tube under a gentle shaking to detach the assembled glass slides. Bacterial suspensions were then cultured on Tryptone Soya Agar (Oxoid; Basingstoke, Hampshire, England) to count viable cells. The decimal-log reduction rate, i.e. the Microbicidal Effect (ME), was calculated using the formula:

$ME = \log N_C - \log N_E$

(N_C being the number of CFU/mL developed on the unmodified control glasses, and N_E being the number of CFU/mL counted after exposure to modified glasses). The results expressed as ME represent the average of three equivalent determinations. This method can be considered as a version of the Japanese Industrial Standard JIS Z 2811 developed to measure the antibacterial activity of plastic surfaces.

2.3.1.9 Thermal Microbicidal Tests

Antibacterial activity due to photo-thermal effect of SURF-PEI-PLATES was investigated against *Staphylococcus aureus* ATCC 6538 Gram-positive bacteria and *Escherichia coli* ATCC 10356 Gram- bacteria. One functionalized slide was cut in 4 sections of 10x10 mm in order to be completely irradiated by laser. A volume of 0.02 mL of bacterial suspension was deposited on 2 sections. For each pair of functionalized glasses, one was irradiated for 20 min whereas the other was not irradiated. After this time, the glass section covered with bacterial suspensions was suspended in 1 mL of sterile water, gently shaken and then water was suitable diluted in 3 different tubes: 1 : 100, 1 : 10 000, 1 : 100 000. From each tube, 1 mL of suspension was taken and then cultured on Tryptone Soya Agar (Oxoid; Basingstoke, Hampshire, England) to count viable cells. The decimal-

log reduction rate, i.e. the "thermal microbicidal effect", ME_T was calculated with the following formula:

$ME_T = \log N_C - \log N_T$

where N_C is the number of CFU/mL developed in contact with a not irradiated modified control glass sample, and N_T the number of CFU/mL counted after exposure to modified glass samples and irradiation.

2.3.2 Results and Discussion

2.3.2.1 Seeds Preparation

For the post grafting growth method, the first step was the preparation of the seeds. We opted for a classical preparation used in our laboratory[65] based on silver nitrate, $NaBH_4$ and citrate, yielding a suspension of spherical citrate-stabilized AgNPs with a yellow-brown color, see **Figure 33**, which corresponds to a LSPR peak centered at 394 nm in aqueous solution, as reported in **Figure 34**.
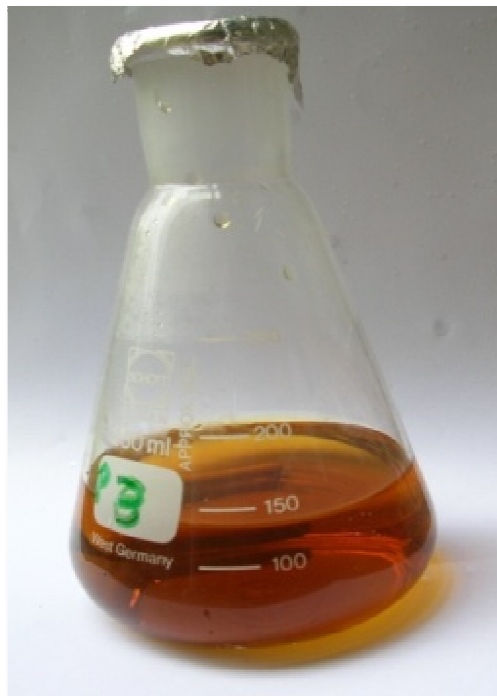

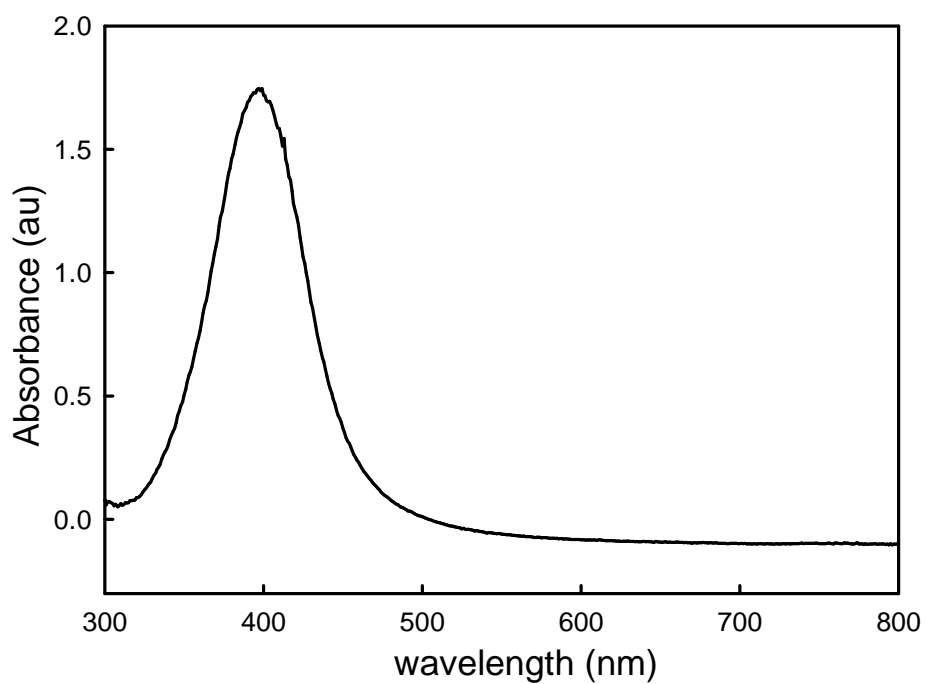**Figure 33** Colloidal suspension of seeds in a flask.

Figure 34 UV-Vis absorbance spectrum of colloidal suspensions of seeds.

The synthetic procedure chosen yields spherical AgNPs with a large size distribution of 7±4 nm diameter, as determined by TEM. One of the representative TEM images is reported in **Figure 35**.
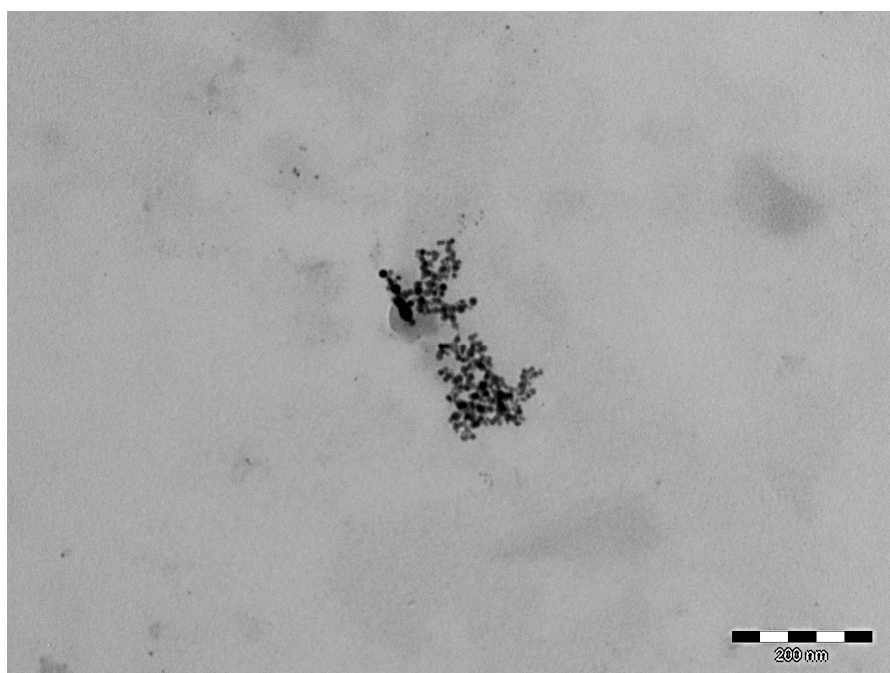

Figure 35 Representative TEM image of a colloidal suspensions of seeds used in the post grafting growth approach.

2.3.2.2 Seed Growth Synthesis on SURF-PEI-GLASS

After this step, we prepared a surface ready to graft the seeds for the growth of anisotropic silver objects. We can prepare such a surface using PEI-silane, **Scheme 4**, a polymer composed of an average of 3.6 propyltrimethoxysilane groups and 56 ethylenimine monomers,[65] i.e. 56 amine moieties (including primary, secondary and tertiary amines).

In the standard procedure, glass slides were cleaned and activated with a strong acidic and oxidizing solution, producing a completely hydrophilic surface (contact angle <10°) which reacts in a few minutes with an ethanolic solution of PEI-silane.
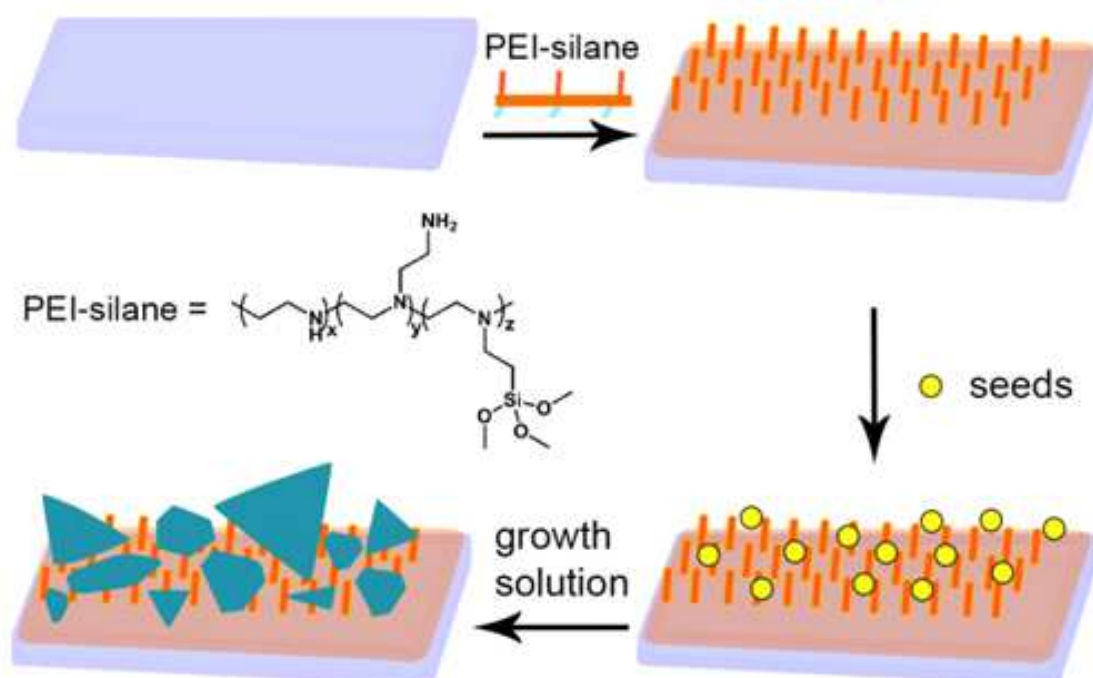
Scheme 4 Seed mediated growth of Ag nanoplates on PEI functionalized glass substrates.

After this step, PEI-functionalized surfaces showed a static contact angle of 41±5° on glass, in good agreement with previous results, see **Chapter 2.2.** Grafting of AgNPs was obtained by dipping the glass slides bearing SURF-PEI for 15 minutes in aqueous colloidal suspensions of seeds. Dipping time was kept to 15 minutes to avoid uncontrollable growth observed for longer immersion times, probably due to aggregation on surface. The typical spectra of a SURF-PEI-SEEDS sample shows the presence of a LSPR band centered at about 403 nm, clearly indicating the presence of small AgNPs grafted on glass, see **Figure 36**.
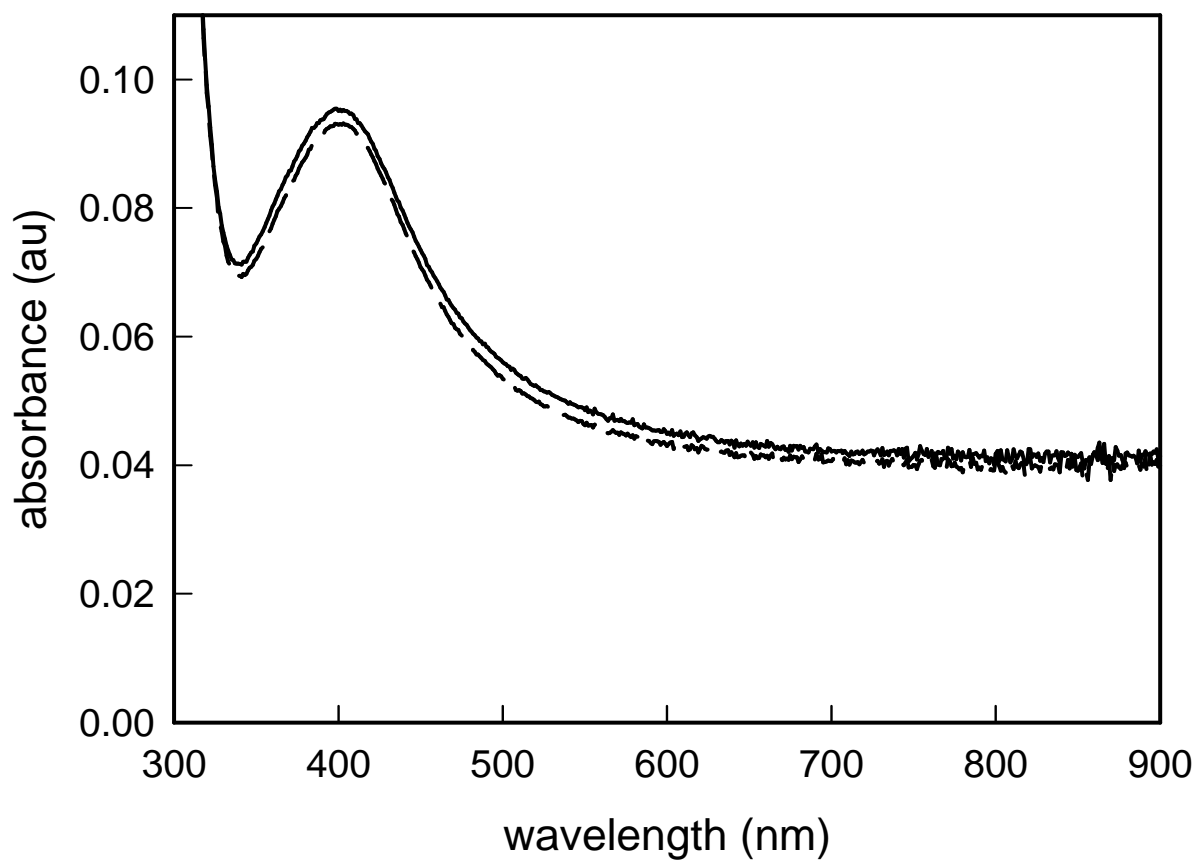
Figure 36 Representative UV-Vis Spectra of two SURF-PEI-SEEDS samples.

As a control, total Ag quantity grafted on glasses was measured using of ICP-OES, after quantitative oxidation of NP on functionalized glasses and analyzing the obtained solutions, obtaining a concentration of $7.4(\pm1.3)10^{-7}$ g cm^{-2} of Ag as previously reported.[65] A SEM image of a SURF-PEI-SEEDS sample, indicating the homogeneous coating of the SURF-PEI glass samples with SEEDS, is reported in the **Figure 37**.

SEM HV: 30.0 kV	WD: 3.17 mm			MIRA3 TESCAN
SEM MAG: 300 kx	Det: InBeam	200 nm		
View field: 0.963 µm	Date(m/d/y): 02/17/16			

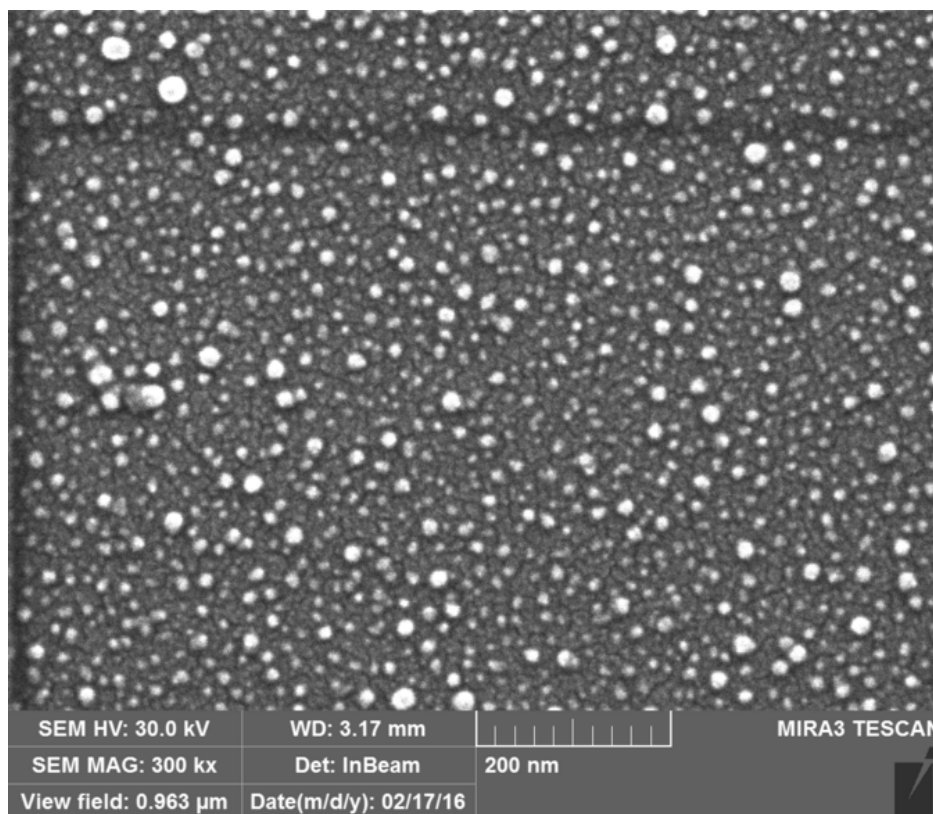**Figure 37** SEM image of SURF-PEI-SEEDS sample. Mean dimensions of the grafted silver spherical nanoparticles may appears slightly larger respect to the same colloid observed with TEM (7±4 nm) because of the thickness (2.5 nm) of Pd/Pt metallization performed on the sample to register the SEM image.

Growth of the seeds grafted on surface was obtained placing the SURF-PEI-SEEDS glass samples in a growth chamber containing the growth solution. The growth solution was prepared, taking inspiration from the results obtained in **Chapter 2.2**, adding to water $AgNO_3$ as silver source, ascorbic acid as reducing agent and citrate as shape-directing agent. As already mentioned, citrate anions preferentially bind to {111} facets of the crystals which are forming, slowing down the vertical expansion, and thus allowing to obtain anisotropic growth of the objects to give nanoplates. These flat nano-objects typically show an in-plane dipole Plasmon resonance band with a position which can be placed in the NIR region and tuned at a desired value just by regulating the aspect ratio of the objects. Our expectations were that it was possible to obtain increasing anisotropic growth on surface just increasing immersion time in presence of high citrate concentration, so that control of immersion times could allow tuning of the morphology and consequently the LSPR features of plasmonic objects brought on glass samples.

Figure 38 shows the UV-Vis-NIR spectra measured for samples extracted from the growth chamber at different interval times. The development of a broad, intense band which maximum, in about two hours, progressively shifts to NIR values, can be attributed to the growth of objects having different anisotropic shapes and increasing lateral dimensions.
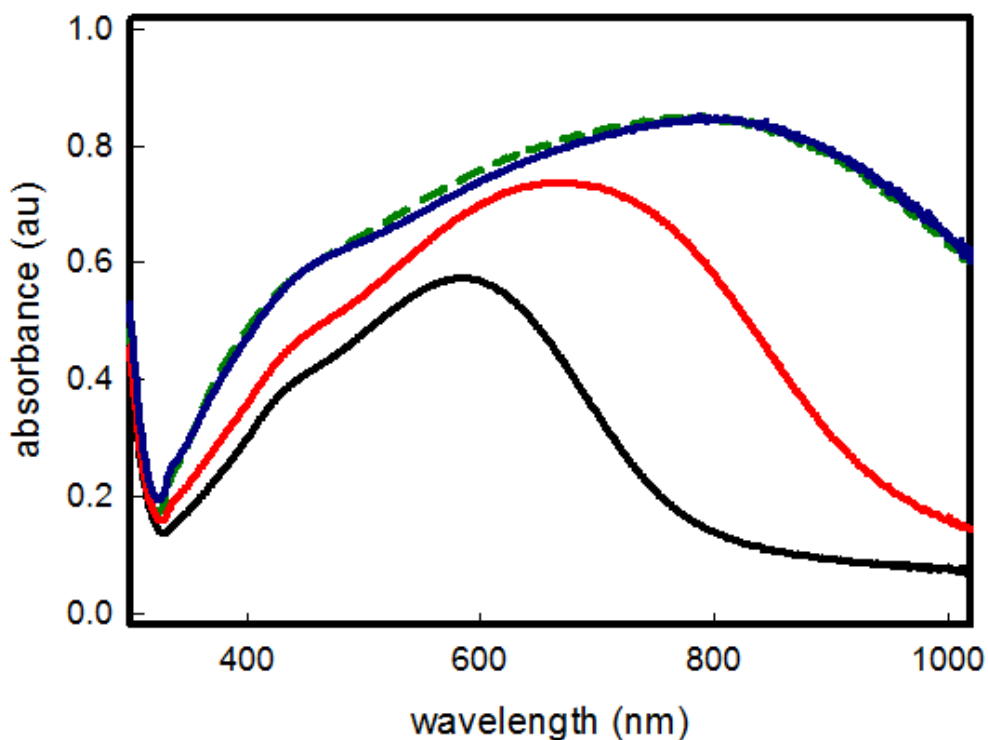

Figure 38 Uv-Vis-NIR spectra of samples after different times of seed mediated growth: 15 minutes (black line), 30 minutes (red line), 2 hours (blue line), 4 hours (green dashed line)

When the experiment was repeated, in the same growth solution, on simple SURF-PEI samples, i.e. in absence of grafted seeds, no objects formation and growth was observed, yielding transparent and uncoated glass samples.

It is important to stress one of the main results coming from this experiment: with this method the maximum of LSPR spectra of the obtained samples can be tuned to the desired value, in the range between 400 and 800 nm, just varying the immersion time of the seeds coated samples in the growth solution. Increase of immersion times longer than two hours does not produce any noticeable change in spectra, as can be clearly seen in **Figure 38**. (green dashed line spectrum) indicating that no further growth or shape changes are happening after this growing time.

From preliminary Atomic Force Microscopy imaging on final (two hours growth) samples, **Figure 39**, we observed the transformation of the small spherical SEEDS into a homogenous layer of disk-like bigger Ag nano-objects.
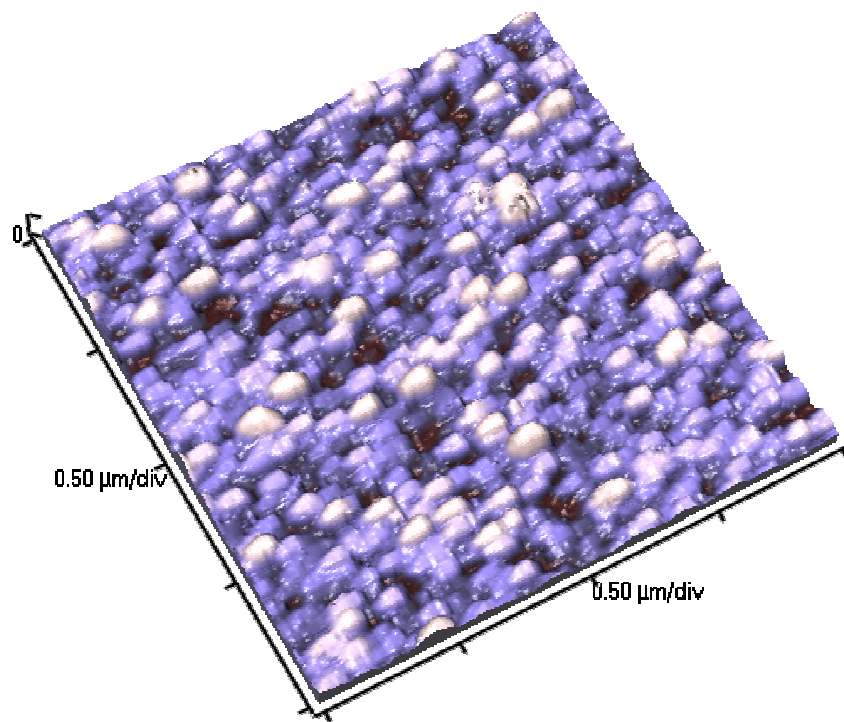

Figure 39 AFM image of a sample obtained after 2 hours in growth solution.

Further investigations to understand the shape of silver nanoparticles growth on glass samples with our post grafting growth method were performed using Scan Electron Microscopy.

In fact, SEM images were taken for the samples extracted after different immersion/growing times, and are reported in **Figure 40**.
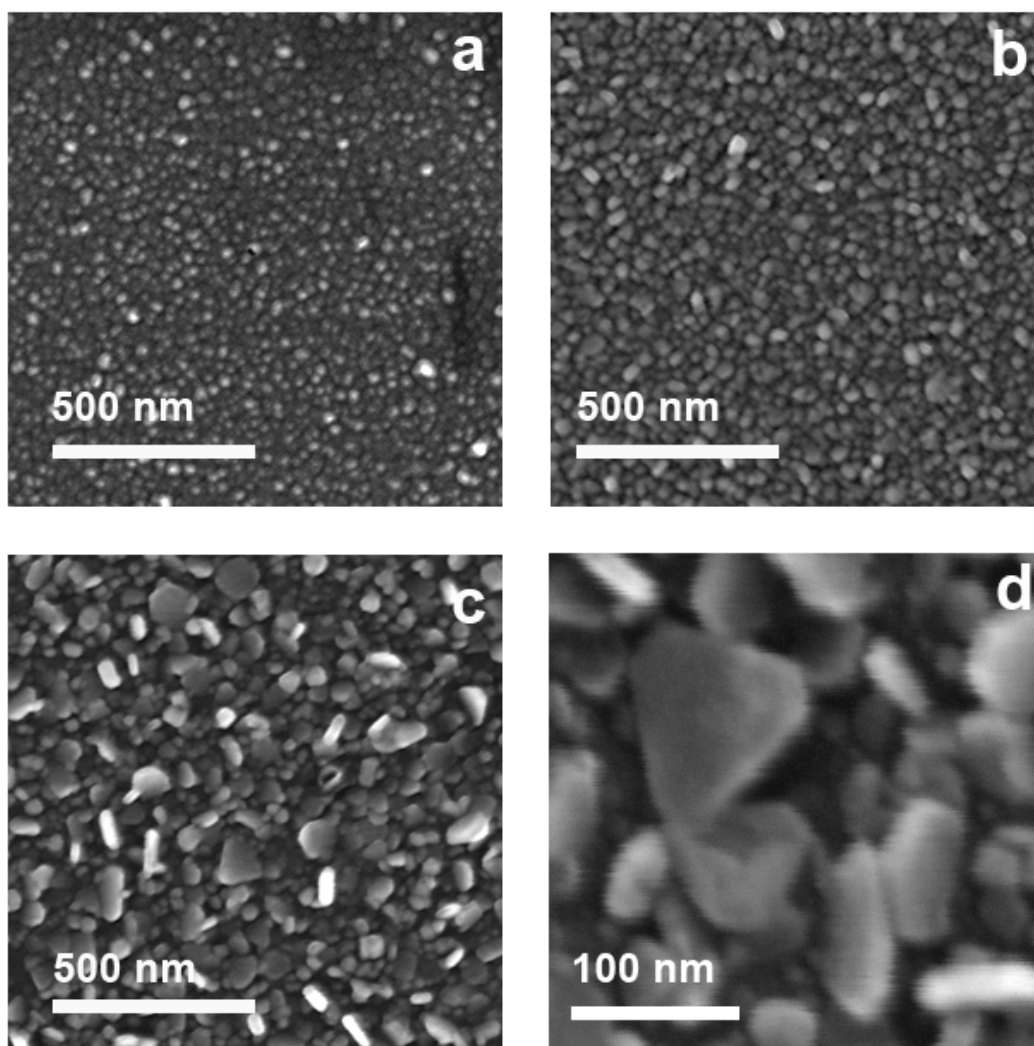
Figure 40 SEM images of samples after different times of seed mediated growth: a) 15 minutes, b) 30 minutes, c) 2 hours, d) 2 hours, higher magnification. SEM magnification of samples a), b), c): 145 kx; of sample d): 275 kx.

Growth of objects can be immediately perceived moving from **Figure 40a** (sample after 15 min immersion) to **Figure 40b** (30 min immersion) to **Figure 40c** (2 hours immersion). In **Figure 40d**, reporting a SEM image at an higher magnification, which is again relative to the two hours immersion time, the anisotropic growth of objects is evident: triangular and truncated triangular platelets, with longitudinal dimensions ranging between 40 and 120 nm can be observed, all having a thickness not exceeding a value of 20 nm. The extremely high degree of polydispersion explains the very broad LSPR spectra observed for increasing growth time. Nevertheless, the broad Vis-NIR absorption spectra is explainable with the presence of a distribution of objects having different longitudinal dimensions, and a subsequent broad range of dipolar in-plane resonance wavelength.[25-29] The glass samples have an homogeneous dark blue-grey color, which is consistent

with the poly-dispersed array of grafted silver nanoplates and the LSPR features described: a photograph of a representative slide after two hours growth is reported in **Figure 41**.
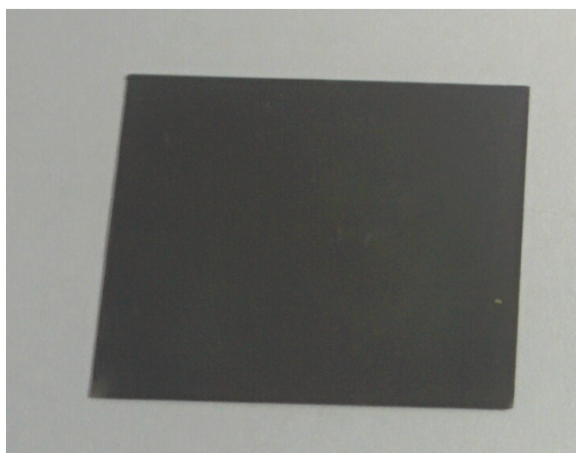
Figure 41 Photograph ofa freshly prepared SURF-PEI-PLATES sample after two hours growth.

As with two hours immersion the broad LSPR band was placed close to the desired wavelength value, we decided to use this growth time in the standard preparation for SURF-PEI-PLATES samples.

The preparation of SURF-PEI-PLATES is reproducible: spectra of several different samples are given and evidence that no sensible differences in intensity and position of the LSPR peak can be observed among the samples obtained simultaneously from the same preparation, as can be seen from spectra reported in **Figure 42**, or coming from different preparation batches , as can be seen from spectra reported in **Figure 43**.
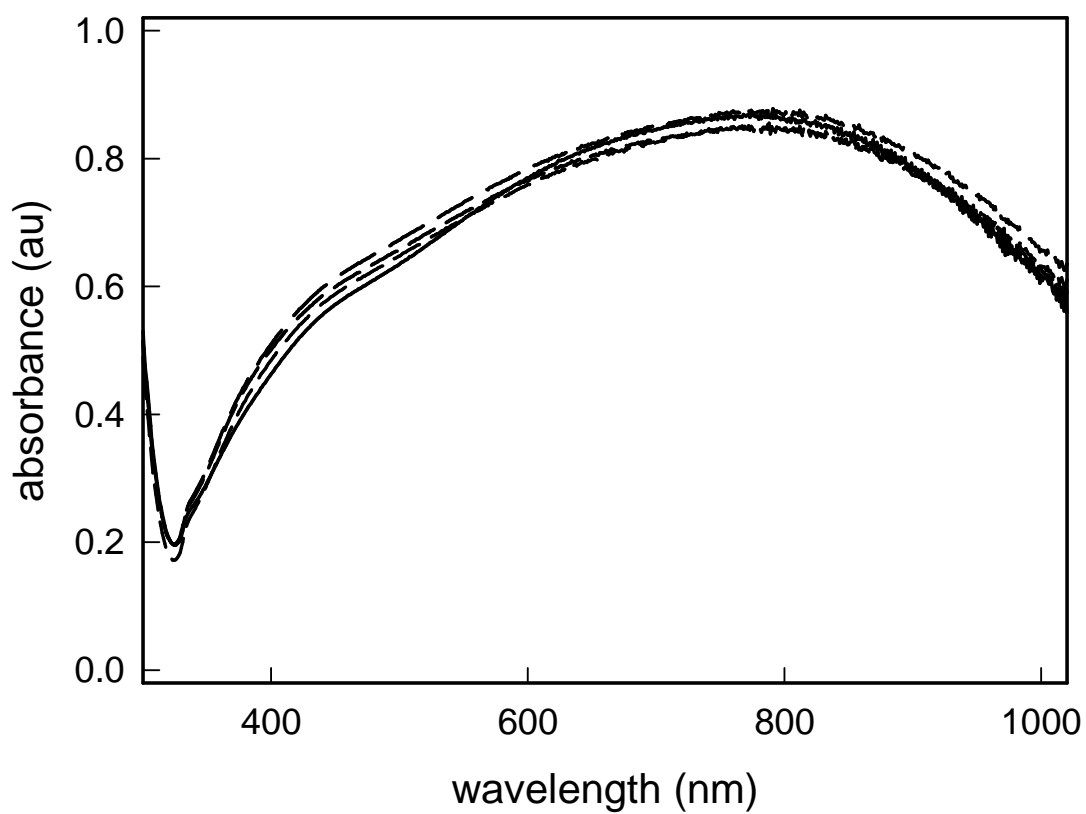
Figure 42 UV-Vis-NIR spectra of four SURF-PEI-PLATES samples obtained from the same growth vessel (2 hours immersion).
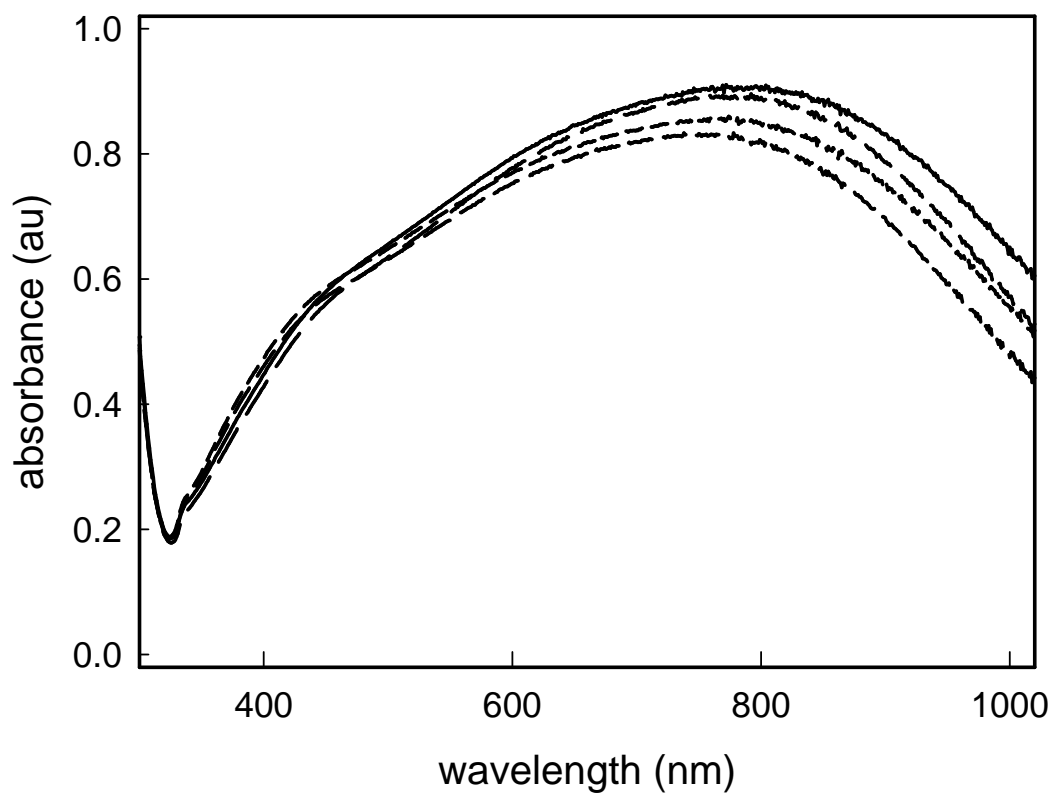
Figure 43 UV-Vis-NIR spectra of four SURF-PEI-PLATES samples obtained from four different growth vessels (2 hours immersion).

It also ensures a very homogeneous coating of the surface, as can be seen from the SEM images taken on large area, **Figure 44**.
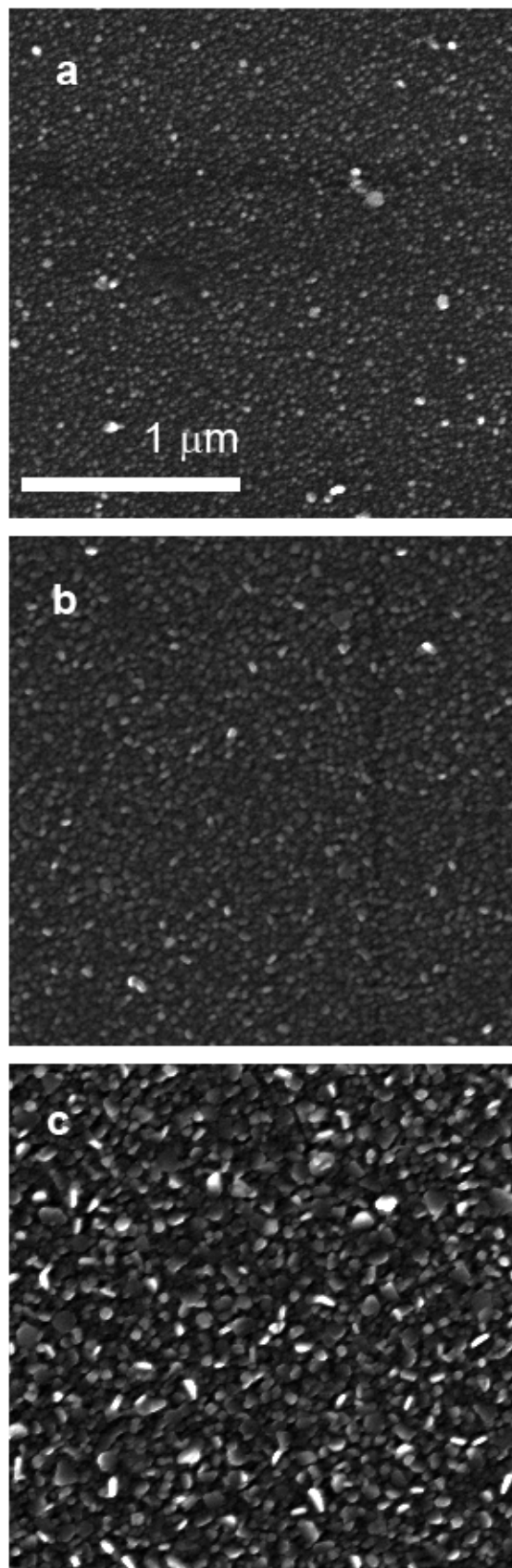
Figure 44 SEM images for samples obtained after different immersion times of SURF-PEi-SEEDS samples in the growth solution : a) 15 min; b) 30 min; c) 2 h (SURF-PEI-PLATES). SEM magnification: 35 kx.

SURF-PEI-PLATES slides are stable in air, i.e. their spectra did not change significantly for at least a 4-week period.

Energy Dispersive X-ray Analysis (EDX) were performed, and one example are reported in **Figure 45.** Beyond the glass substrate components, the evidence of Ag L spectral line is consistent with the preparation procedure. We notice that EDX analysis in different points of the sample surface shows chemical homogeneity of Ag films (within ±5%), the intensity of any spectral line in EDX analysis being proportional to element.

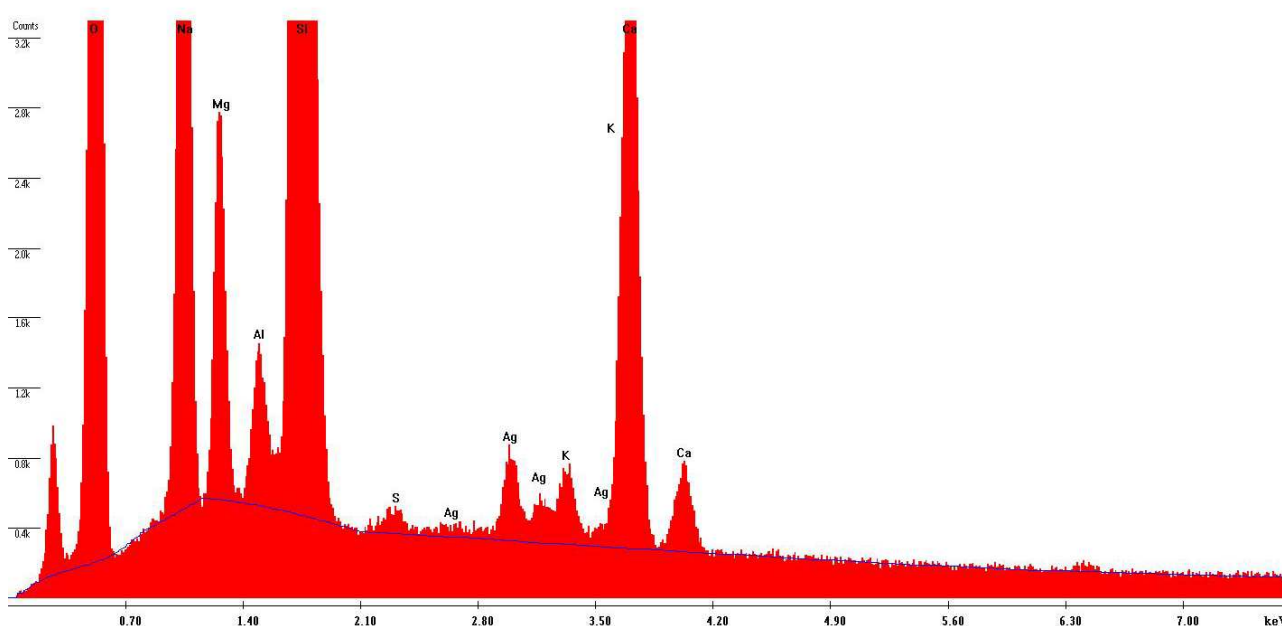| Element	Wt %	At %	K-Ratio	Z	A	F
O K	33.5400	47.5100	0.0877	1.0363	0.2520	1.0006
NaK	10.1200	9.9800	0.0466	0.9698	0.4725	1.0052
MgK	2.6600	2.4800	0.0142	0.9941	0.5322	1.0093
AlK	0.9900	0.8300	6.3000e-3	0.9649	0.6490	1.0172
SiK	41.9500	33.8500	0.3166	0.9930	0.7589	1.0013
S K	0.2500	0.1800	1.6000e-3	0.9793	0.6627	1.0032
AgL	2.1400	0.4500	0.0161	0.7927	0.9423	1.0057
K K	0.7300	0.4200	6.1000e-3	0.9426	0.8750	1.0098
CaK	7.6200	4.3100	0.0663	0.9648	0.9021	1.0000

Figure 45 EDX data obtained for a sample of SURF-PEI-PLATES. Beyond the glass substrate components, the evidence of Ag L spectral line is consistent with the preparation procedure. We notice that EDX analysis in different points of the sample surface shows chemical homogeneity of Ag films (within ± 5%), the intensity of any spectral line in EDX analysis being proportional to element abundance.

The presence of Ag plates is confirmed also from X-ray diffraction patterns, reported in **Figure 46**. Only the peak of 111 reflection of a FCC structure is clearly evident, suggesting that the basal lattice plane of nano-objects is (111), as expected from the shape-directing action of citrate, and also that exists a preferred orientation of plates on the glass surface. The peak broadening confirms the nanostructured nature of silver.
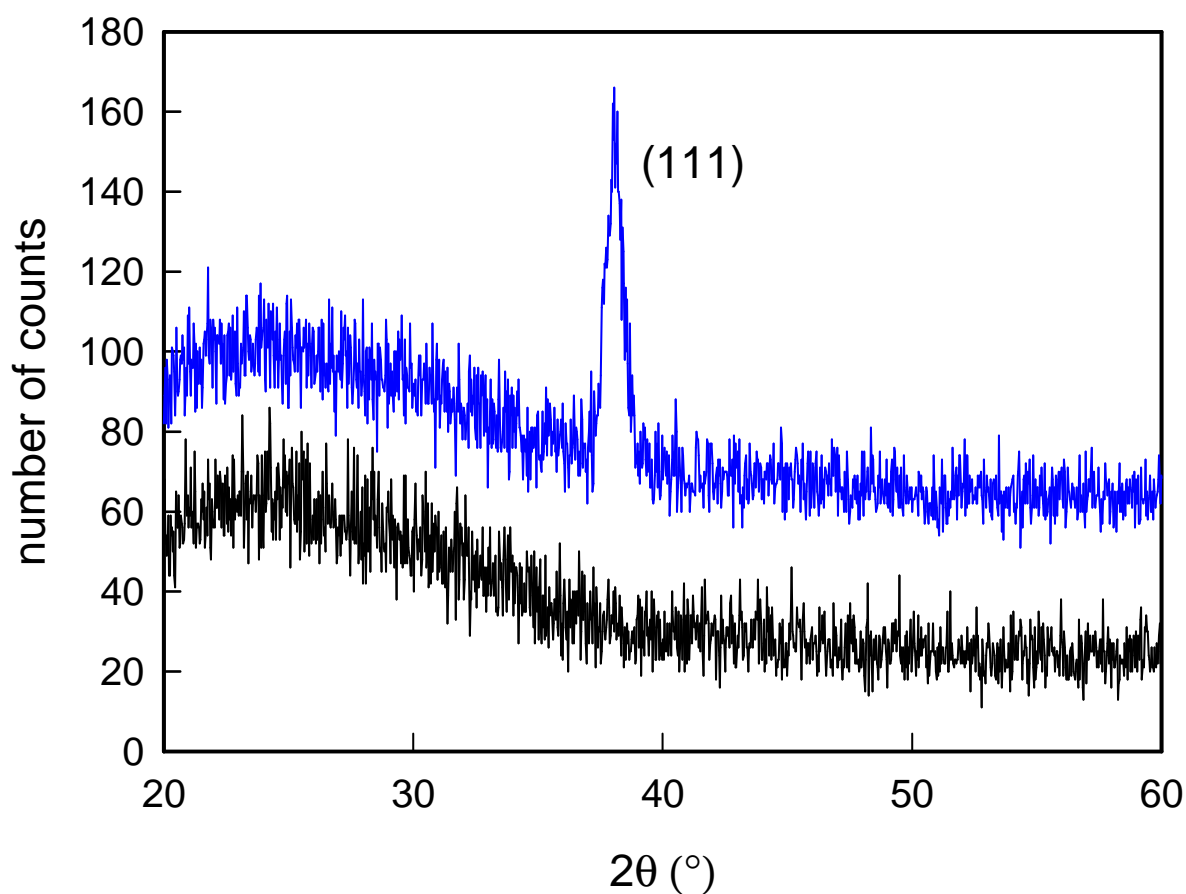
Figure 46 XRD patterns obtained for a blank glass (black line) and for a SURF-PEI PLATES sample (blue line), evidencing the presence of (111) diffraction peak.

We completed the characterization of the SURF-PEI-PLATES (i.e. the samples after 2 hours growth) by means of quantitative oxidation of the silver plates, and analysis of the obtained Ag^+ solution by means of ICP. Data from seven experiments, coming from seven different samples preparations, we found an average of 6.2 (0.6) x 10^{-6} g/cm^2 of silver, a quantity which is considerably high, when compared to samples obtained grafting a monolayer of spherical seeds on a silanized glass, as it was described in the recent past. [30,65,66]

2.3.2.3 Stability in Water and Silver Release

The stability in water, as well their ability to release silver ions in water as a function of time was determined by experiments on several SURF-PEI-PLATES samples. The 21 x 26 mm glass slides were immersed in 3 mL of ultrapure water for a given time interval, and then removed from the liquid. After registering their UV-Vis-NiR spectra, the solutions obtained after SURF-PEI-PLATES slides immersion in water were analyzed with ICP. The data of silver concentration found in these solutions were expressed as µg of released silver per cm^2 of exposed surface, as a function of time and reported in graph, reported in **Figure 47**, showing a well-defined trend. We must stress the fact that, in analogy with precedent investigations, these experiments were performed in ultrapure water.[30,65,66] Thus, the results cannot be of course simply transferred to more complex or biological environments, as silver ions can give poorly soluble salts or complexation with biomolecules when they are released in "real" media.

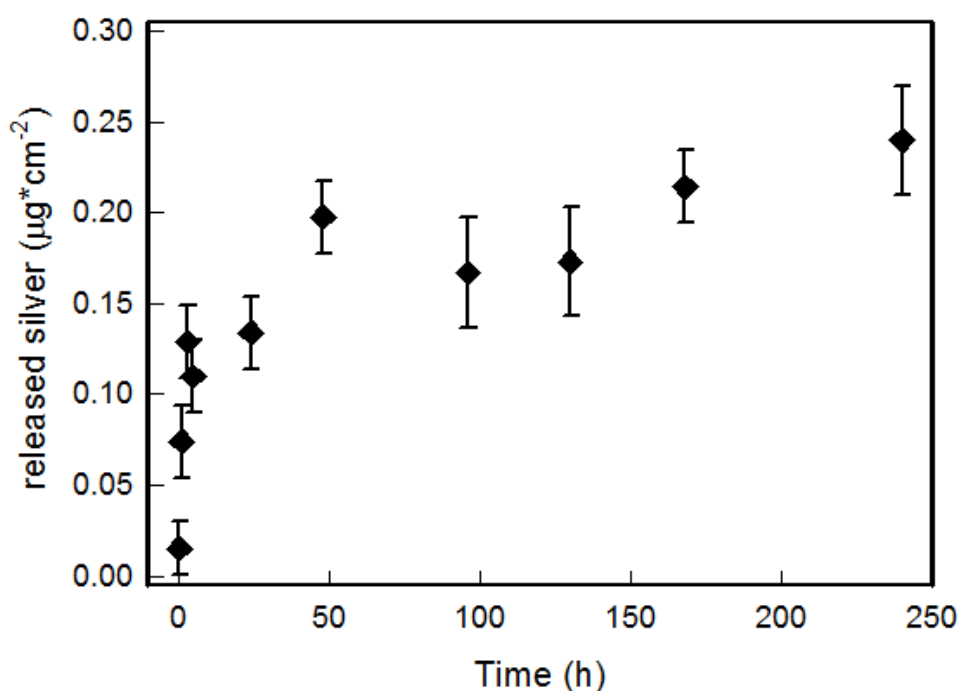**Figure 47** Silver ion released from SURF-PEI-PLATES (µg/cm^2 of exposed surface) versus time in 3 mL of water.

Nevertheless these experiments allow to state that (i) no silver nano-objects were released in water, as Uv-Vis-NIR spectra did not show the presence of any absorption which could be related

to presence of plasmonic objects detached from the surface; (ii) silver is released in water as a function of immersion time, reaching a stationary concentration after approximately 2-3 days; (iii) as already observed in similar systems, the most of dissolved silver is released in the first 24-48 hours of immersion. As it was already reported above, silver release should involve the formation or the thickening of a Ag_2O layer on the water-exposed surface of silver nano-objects, with the formation of an oxidized silver layer in the initial 1-2 days period, reaching a steady-state in which the slowly released Ag^+ ions are replaced by Ag oxidized from the bulk.[30] As in this case we start from a quite high surface concentration of silver, also the released amount is higher than the value which is usually released from monolayers made of small spherical silver nanoparticles grafted on glass.[30,65,66] As can be easily calculated, anyway, the amount of silver released in these conditions after 10 days is less than 5 % (about 2.5 x 10^{-7} g/cm^2) of the total concentration of silver present on the surface, in strict analogy with the case reported in **Chapter 2.2**. Once again, this allows to imagine surfaces retaining for a long time the possibility to release silver ions in an environment subjected to flow of aqueous media, a feature that is considered essential for fight bacterial proliferation leading to severe infection and/or biofilm formation: for example, recently it was demonstrated that biofilm growing on a biomaterial surface is a dynamic process able to reach a maximal thickness at 12-18 hours and maturation by 24 hours.[55]

SEM images and UV-Vis-NIR spectra were taken for selected samples after the immersion in water and silver ion release. **Figure 48** shows the SEM images taken for samples after immersions of 5 (**48b**), 24 (fig. **48c**) and 240 hours (**48d**), compared with the untreated, as-prepared sample (**48a**).
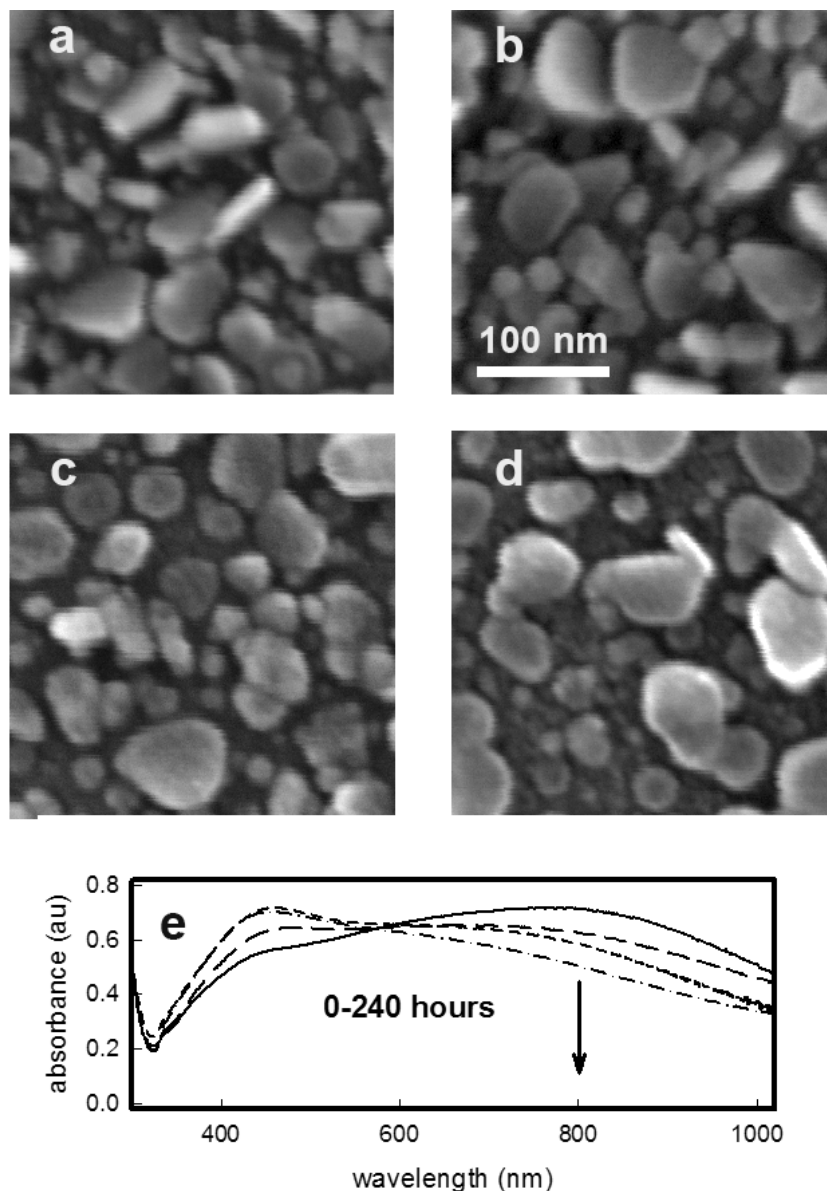
Figure 48 (a-d) SEM images of SURF-PEI-PLATES samples after increasing immersion times in pure water: **a)** 0 hours (as prepared), **b)** 5 hours immersion, **c)** 24 hours immersion, **d)** 240 hours immersion; **e)** UV-Vis-NIR spectra of the same samples. SEM magnification: 275 kx.

One can observe a progressive but limited consumption of the prismatic plates, causing a visible morphology change, from triangular like plates to more discoidal shapes. This of course modifies the UV-Vis-NIR spectra of the samples, causing a progressive depletion of the extinction at 800 nm, as reported in **Figure 48e**: the consumption of the plates results in a progressive flattening of the absorption in the NIR nm zone, as reduction of longitudinal dimensions as well the snipping of edges are expected to reduce the intensity and blue shift the dipolar in-plane resonance. On the other side, as can be clearly seen from large area SEM images reported in **Figure 49**, the overall homogeneity of the silver coating layer is preserved.
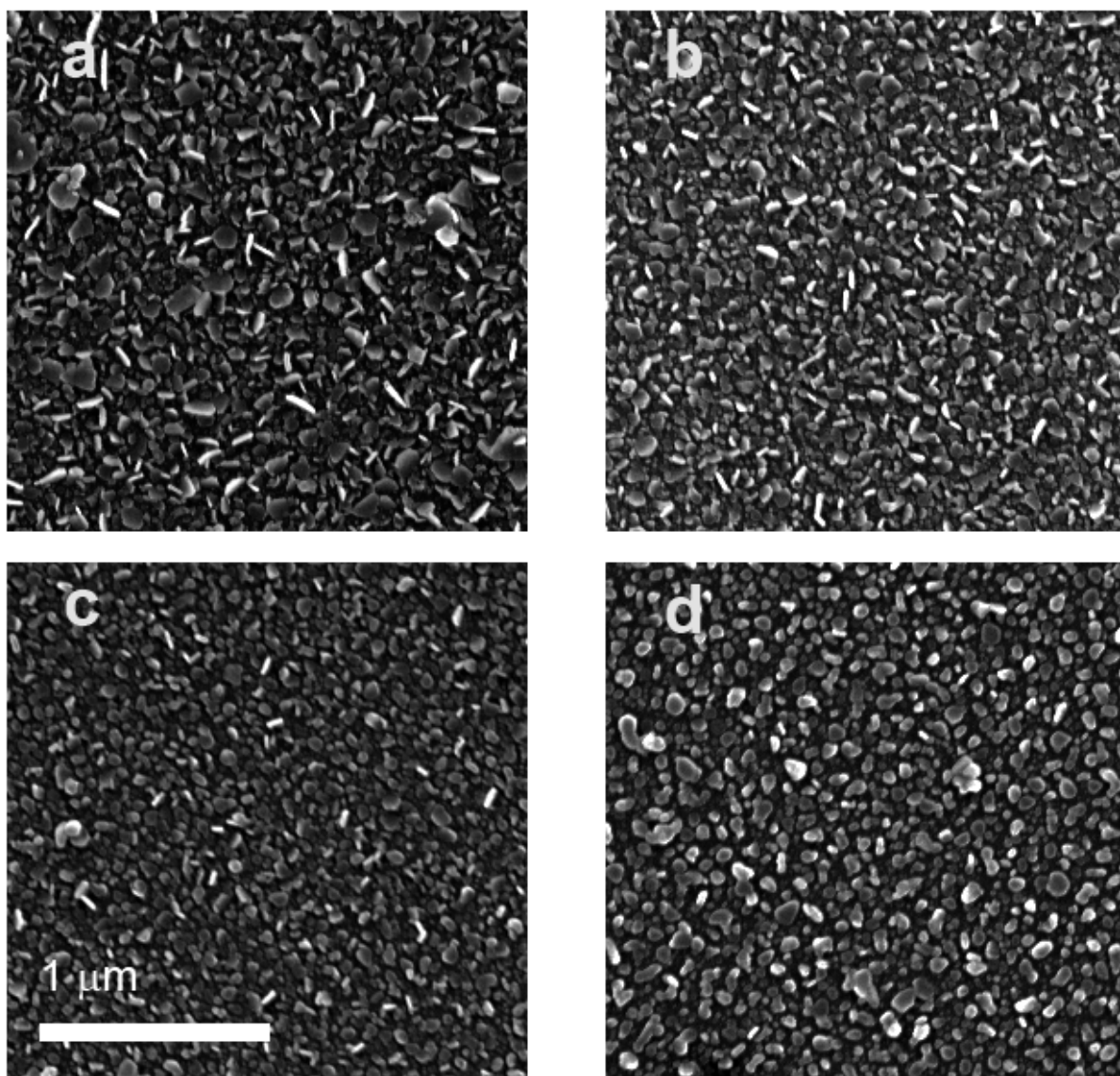
Figure 49 SEM images for SURF-PEI-PLATES samples **a)** as prepared ; **b)** after 5 hours of immersion in water; **c)** after 24 hours of immersion in water; **d)** after 240 hours of immersion in water. SEM magnification: 35 kx.

Visually, the dark blue color of the slides fades with prolonged immersion, as obvious consequence of the weakening of the broad band at 800 nm. In the same time a more yellowish aspect can be noticed, depending on the increase of the band in the 450-500 nm range, typical of discoidal and spheroidal silver nano-objects. A photograph of a glass slide after 240 hours of immersion is reported in the **Figure 50**: the dark blue color has faded and a yellow *nuance* can be seen. Morphological changes caused by long immersion times in water can thus be perceived by the naked eye. This feature could also be exploited to assess the material shelf life and usability: the

complete vanishing of the blue color indicates the disappearing of the broad absorption at 800 nm, and excludes the possibility of any exploiting of NIR Laser excitation.
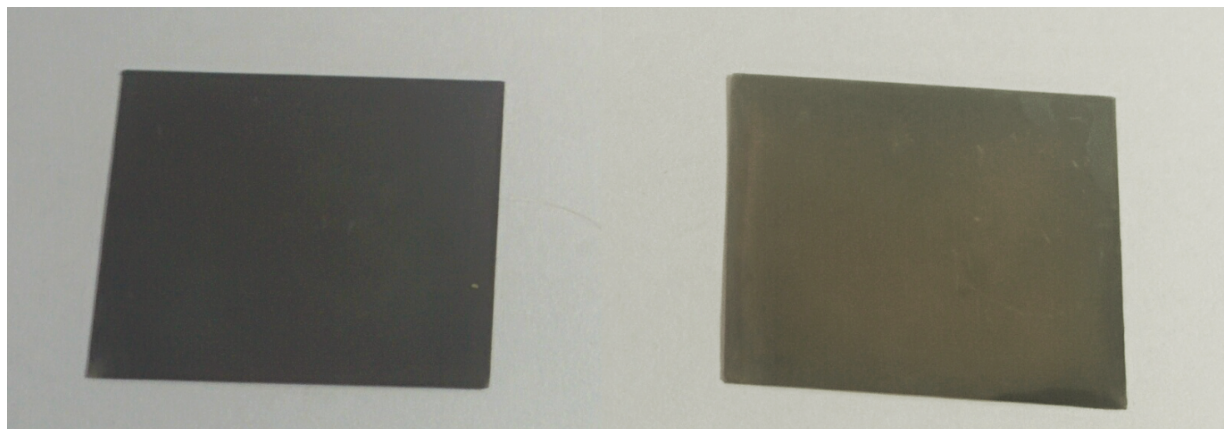
Figure 50 Photographs of: (left) a freshly prepared SURF-PEI-PLATES sample after two hours growth; (right) a SURF-PEI PLATES sample after 240 hours of immersion in water

2.3.2.4 Photo-thermal Studies

The photo-thermal behavior of the samples obtained with different growth time has been measured by irradiation with a 808 nm continuous Laser source (0.20 mW, spot diameter 1 cm, resulting irradiance 0.26 W/cm^2) on 10x10 cm glass slides, which were obtained by cutting the larger slides typically used in the samples preparation. Thermograms (Temperature vs time graphs) were recorded using a thermocamera to register the temperatures reached by the glass samples while irradiated, observing in all cases an increase-plateau profile, reaching a stationary temperature within 40 seconds, as reported in **Figure 51**.
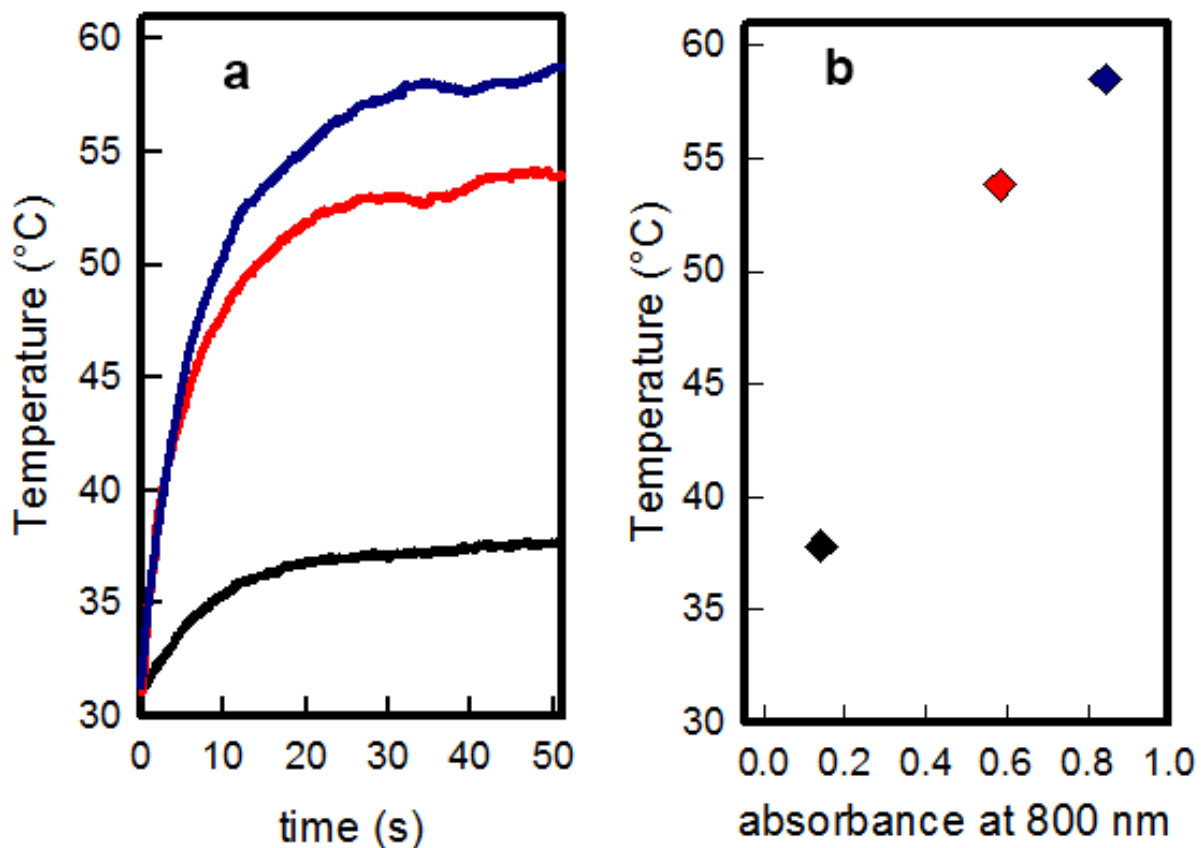
Figure 51 a) Temperature versus time thermograms obtained for samples under Laser irradiation at 808 nm, 0.26 W/cm^2: samples grown 15 minutes (black line), 30 minutes (red line) and two hours SURF-PEI-PLATES (blue line); **b)** maximum temperature reached by the sample vs its absorbance at 808 nm.

Temperature values recorded at plateau were of 37.8 (0.3), 53.8 (0.3) and 58.5 (0.3) degrees for the samples grown 15 minutes, 30 minutes and two hours, respectively. As can be seen from **Figure 51b**, the maximum temperature obtained increases with the absorbance value of the three samples at 808 nm, as measured from spectra reported in **Figure 38**: the higher LSPR absorption, the higher temperature is reached. UV-Vis-NIR spectra were recorded before and after irradiation for each sample, showing that the described treatment and relative produced hyperthermia did not change the LSPR features of the samples, an example is given in **Figure 52**.
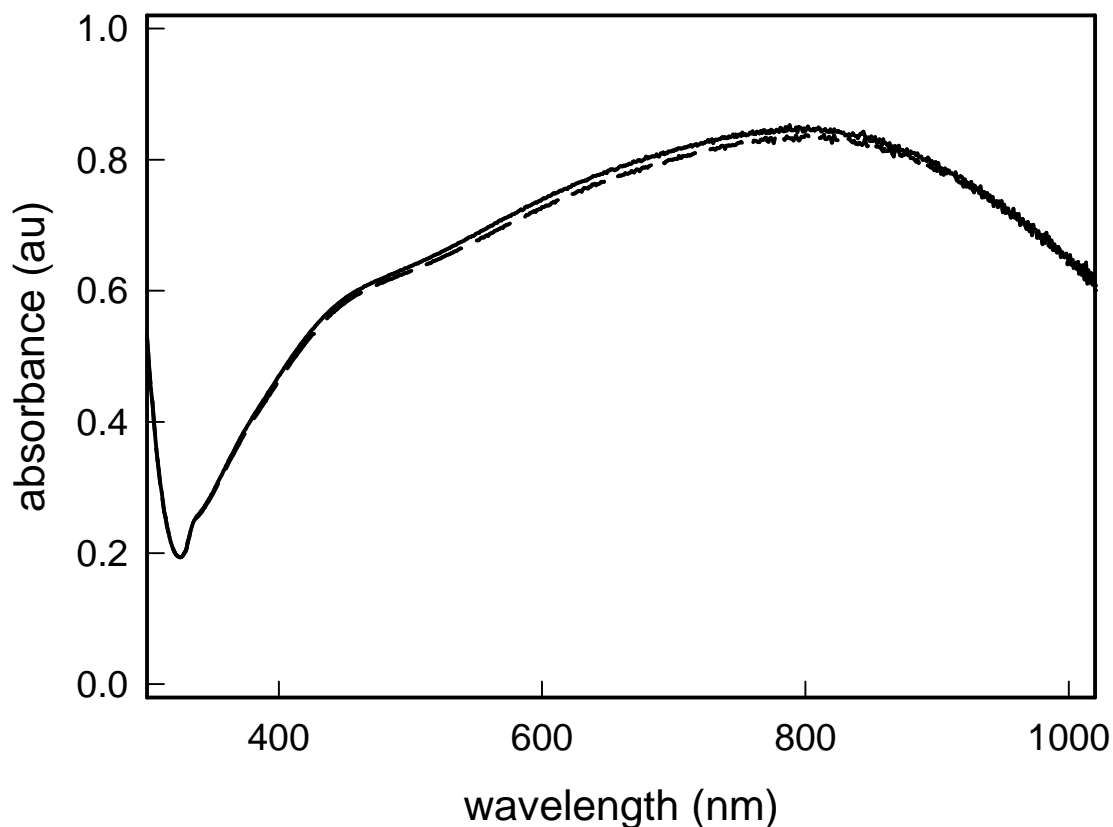
Figure 52 UV-Vis-NIR spectra of the same zone of the same SURF-PEI-PLATES sample before (full line) and after (dashed line) 20 min of Laser irradiation at 808 nm, irradiance 0.26 W/cm^2.

A similar set of experiments was repeated on a sample of SURF-PEI-PLATES (two hours growth) after 24 hours of immersion in water, to check if the silver release, producing the objects consumption and changes in LSPR features described in **Figure 48** and **Figure 49** could change drastically the photo-thermal effect. Only a slight decrease is observed in the value of temperature reached after irradiation of these samples about 55 °C, as showed by the thermogram in **Figure 53** for the thermogram, as it could be expected from the LSPR absorption at 808 nm, which decreases only marginally after 24 of immersion in water, as can be deduced from spectra reported in **Figure 48e**.
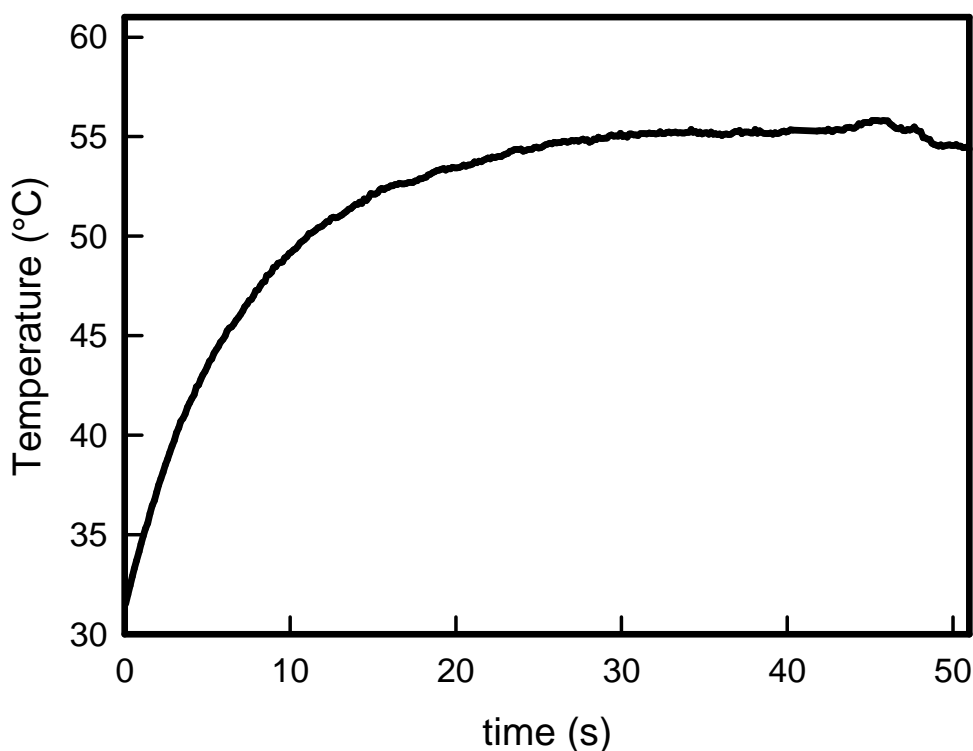
Figure 53 Temperature versus time thermograms obtained under Laser irradiation at 808 nm, 0.26 W/cm^2 for a SURF-PEI-PLATES sample after its immersion for 24 hours in water.

As already stated in **Paragraph 2.2.2**, to our knowledge, there are no precise data about the temperatures needed to eliminate bacteria with photo-thermal effects. We stress once again the fact that temperature values measured by thermograms in the shown experiments describe temperature changes on bulk samples, giving few or no information on the temperatures changes in the close surroundings of the nano-objects, which should reach considerably higher values. Anyway, it is known that heating of *E. coli* cells at temperatures of 52°C for more than 5 minutes results in the destruction of bacteria permeability barrier,[76] and it was reported that irradiating for 5 minutes with a Laser a cluster of gold nanorods it is possible to reach a temperature of about 60°C causing the death of most bacterial cells in a *E. coli* biofilm.[74] On the other side, it was demonstrated that a few degrees of hyperthermia, caused by low irradiance Laser excitation of a monolayer of GNS on a glass bulk surface for longer times (30 min), is sufficient to almost completely eliminate the bacteria cells of a *S. aureus* biofilm layer.[73]

---

[76] N. Katsui, T. Tsuchido, R. Hiramatsu, S.Fujikawa, M. Takano, I. Shibasaki, *J. Bacteriol.* 1982, **151**, 1523.

2.3.2.5 Antibacterial Tests

The antimicrobial activity of SURF-PEI-PLATES surfaces against *E coli* and *S. aureus* was investigated using the already described parameter ME, calculated with the formula:

$ME = \log N_C - \log N_E$,

where N_C is the number of CFU/mL developed on the unmodified control glasses, and N_E the number of CFU/mL counted after exposure to modified glasses (CFU = colony forming unit).[5]

Contact time	S. aureus	E.coli
20'	< 0.3	< 0.3
5 h	0.8 (0.3)	0.9 (0.3)
24 h	>5	>5

Table 5 ME values of SURF-PEI-PLATES obtained as the average of three measurements. A value higher than 5 indicates that no survived bacteria were found after the test.

Experimental results after contact times of 20 minutes, 5 and 24 h are reported in **Table 5**, and show that SURF-PEI-PLATES glass slides display a significant bactericidal effect after a long contact time. 24 hours contact times are able to exert a complete Microbicidal Effect, eliminating at least 99.999% of bacteria. The effect is much less intense with 5 hours of contact, while no Microbicidal Effect is present with very short contact times: it must be noted that silver release, which is considered as the main responsible of bacteria killing, is limited (0.015×10^{-6} g/cm^2, see **Figure 47**) after a 20 min time of contact with water. Mechanisms by which AgNPs exert their antibacterial effect are still hugely debated, anyway we stress once again the fact that Xiu et al. [77] showed that silver nano-objects are devoid of antibacterial action when used under anaerobic conditions which exclude oxidation to silver(I), thus preventing its release. SURF-PEI-PLATES samples action against *S. aureus* for long contact times seems much more intense than the one found for SURF-PEI-SEEDS samples bearing small spherical AgNPs,[65] and this should be due to the higher concentration of silver present on the former. Anyway, at this preliminary stage of investigation, one cannot

exclude that also the different morphology of objects on surfaces is playing a complex role. As already reported above, in the tests proposed by CEN (European Committee for Standardization) in -EN 13697,[§] the microbicidal activity of a disinfectant is considered acceptable when the decimal-log reduction rate (i.e. ME), is at least equal to 4 after 5 min of contact. In our case ME of the modified glass is superior to 4 after 24 h of contact for both strains, with a long term action which seems well suited to build antibacterial surfaces for medical devices.

Our main interest, anyway, was the investigation of the antibacterial effect given by local hyperthermia. SURF-PEI-PLATES samples, opportunely cut in order to be completely covered by the light spot, were irradiated for 20 min with a 808 nm Laser source, while in contact with the described bacteria suspensions, using an irradiance of 0.26 W/cm^2. In this case the "thermal microbicidal effect", ME_T was calculated with the following formula

$$ME_T= \log N_C - \log N_T$$

where N_C is the number of CFU/mL developed after the contact with SURF-PEI-PLATES samples in absence of irradiation, taken as control, and N_T the number of CFU/mL counted after exposure to SURF-PEI-PLATES sample in presence of irradiation.

It is important to stress that in these conditions ME_T has to be ascribed only to the photo-thermal effect, as any possible influence from the limited silver release in absence of irradiation is considered in the control count. Moreover, as very limited silver ion release is observed after 20 minutes (see **Figure 47**), reasonably no silver related ME is observed during this time (see **Table 5**). It is also important to stress that the ME_T values do not change when unmodified, blank glass samples (both irradiated and not irradiated) are used to obtain control CFU values instead of not irradiated, functionalized samples. This clearly states that Laser irradiation alone, in absence of plasmonic objects exerting photo thermal features, does not cause any harm to bacteria.

	S. aureus	*E.coli*
SURF-PEI-PLATES 20 min	3.7 (0.3)	>5
SURF-PEI-PLATES 20 min (after 24 h in water)	3.8 (0.3)	>5

Table 6. ME_T values of SURF-PEI-PLATES obtained as the average of three measurements. A value higher than 5 indicates that no survived bacteria were found after the test.

As reported in **Table 6**, once again in the case of ME_T we observe an higher activity against *E. coli* than against *S. aureus*. As already stated, this may be due to the fact that Gram-positive bacteria present a relatively thick cell wall consisting mainly of peptidoglycane, while Gram-negative bacteria feature a thinner wall which is expected to be less solid and resistant. The ME_T test result show that the laser treatment kills more than 99.999% of *E. coli* and about 99.95% of *S. aureus* cells in 20 minutes of irradiation at 0.26 W/cm^2, a value which is below the maximum allowed for exposure of the skin, and using a wavelength which is suitable for *in-vivo* use.

At this point, one question arising was whether antibacterial effect given by Laser irradiation was due only to hyperthermia or mediated by an augmented release of silver ions due the hyperthermia itself. Thus, we measured the quantity of silver released in a fixed volume (3 mL) of water after 20 minutes of irradiation in the same conditions used for the ME_T tests (laser spot 1 cm^2, Irradiance 0.26 W/cm^2). After irradiation, the solution was brought to ICP, revealing that the quantity of silver ion released from the surface after 20 minutes of Laser irradiation was identical, in the precision limits of the techniques used, to the one found after 20 minutes of immersion in water in absence of irradiation (0.015 x 10^{-6} g/cm^2). Thus, we can state that the Laser irradiation produces an antibacterial effect which apparently is only due to hyperthermia, and is not connected to an augmented silver release. SURF-PEI-PLATES samples can exert an antibacterial action exploiting two separate mechanisms: a long term action given by the "classical" silver ion release, which can be used for prevent the formation and adhesion of colonies for a long period of time, and a quick photo-thermal action, obtained using the peculiar spectral features of the

objects grown on the surface, tailored with their LSPR features to match with a Laser source suitable for in vivo treatments.

But what about the possibility to user the Laser irradiation on SURF-PEI-PLATES samples after their immersion in water, to simulate a situation in which, in addition to a microbicidal activity given by silver ions release, a reinforce of antibacterial action was desired, as it was described in the previuos part? (**Paragraph 2.2.2**) To answer this question, we repeated the ME_T tests on SURF-PEI-PLATES samples after their immersion in 3 mL of water for 24 hours. As we have already described, thermograms did not show dramatic decrease of photo-thermal activity after immersion in water for 24 hours, as UV-Vis-NIR spectra still show a intense absorption at 808 nm. As can be seen in **Table 6**, the ME_T in these conditions is completely conserved, suggesting once again that the antibacterial action obtained within the 20 minutes irradiation is caused by hyperthermia from the silver nano-objects: as long as they absorb sufficient radiation at the proper wavelength, hyperthermia is produced and antibacterial action takes place.

2.3.3 Conclusions

We demonstrated the coating of bulk surfaces with silver nanoplates which can exert an antibacterial action based on the photo-thermal effect, which can be switched on by a proper Laser excitation. This novel kind of antimicrobial action is added to the well-known microbicidal abilities typically showed by AgNPs containing surfaces. The goal, in this case, was reached by tuning the LSPR features of the nanoplates using a new seed growth synthesis, operated directly on bulk surfaces in absence of any surfactant or other harmful chemicals. We started by grafting small silver nanoparticles on bulk glass, previously treated with PEI-silane as grafting agent. This allowed to prepare stable (showing no release of nano-objects in the environment) and reproducible samples bearing an homogeneous layer of flat silver nano-objects of various dimensions and shapes, with an overall broad absorption spectra having a maximum centered around 800 nm. Under Laser irradiation at 808 nm and at safe irradiance values, in 20 minutes the almost complete elimination of bacteria *S. aureus* and *E. coli* is obtained in vitro through Laser-induced hyperthermia. Of course, a complete microbicidal action is observed also in longer timescales, as a result of the contact with the surface, an expected long-term antibacterial action which is explained with the slow and controlled release of silver ions from the nano-objects. Long time immersions in water produce morphological changes of the grafted object, reasonably

related to silver ions release, but a 24 hours immersion do not affect seriously the antibacterial action obtainable by Laser induced hyperthermia. We believe this new approach will have promising applications to several types of surfaces (prosthetic and subcutaneous devices, surgical sutures, wound dressings, to name a few examples), as it offers a long term antimicrobial protection which can be reinforced, on need, with the Laser induced action.

2.4 SUF-PEI-PLATES Sample for SERS chips

Generally, biochemical and genetic diagnostic tests not only need large numbers of samples to test, but also a large number of variables to screen and large sample populations. Furthermore, the reagents used in these assays can be very expensive and the sample itself may not be available in large quantities; therefore, smaller reaction volumes and parallel testing are essential.

Since the discovery of Surface-Enhanced Raman Scattering (SERS) in the 1970s, this non-destructive analytical method has been applied to a wide variety of analytical applications, including biochemistry and the life sciences.[77] SERS is based on vibrational spectroscopy and give a characteristic spectrum of specific molecules or bioagents and also offers a high degree of sensitivity wich strongly depends from the Enhancement Factor (EF) and the specific molecules features.

The SERS configurations commonly employed in biosensing are shown in **Figure 54**. Depending on the used strategy they can be divided in two main classes: (i) intrinsic detection and (ii) extrinsic detection.

In intrinsic detection (**Figure 54a**), the analyte is directly applied to the nanostructured surfaces and the inherent Raman spectrum of the biomolecule is directly measured to identify the specimen. Antibodies, aptamers, or related molecules can be immobilized onto nanostructured surfaces in order to detect a specific molecule, and the Raman spectral differences before and after capture of the analyte can be used to identify the species (**Figure 54b**).

In extrinsic detection, a Raman reporter molecule is used to produce a signal for detection. For example, a Raman reporter can be immobilized on a gold or silver nanoparticle, which may be used as the SERS-active substrate. In addition, by coating this structure with another layer of dielectrics such as SiO_2, TiO_2, or a polymer, a core-shell complex is formed in which the outer-shell may be decorated with capture molecules such as antibodies. Thus, specimens may be captured and detected via a sandwich structure. This extrinsic SERS detection method has been successfully used for in vivo SERS imaging of unique or rare cancer cells.

---

[77] P.R. Carey; *Biochemical Applications of Raman and Resonance Raman Spectroscopies, Academic Press*, New York, **1982**.
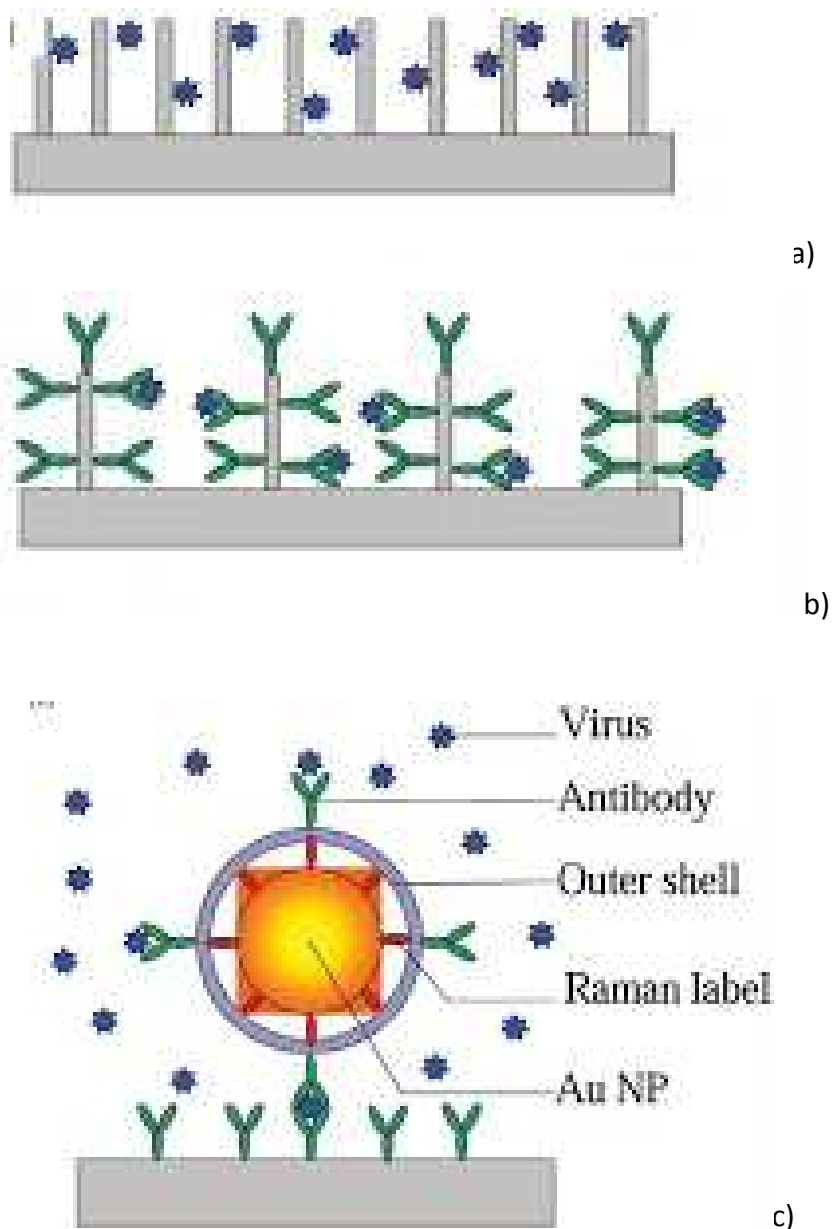
Figure 54: different SERS detection configurations: (a) direct intrinsic detection; (b) indirect intrinsic detection; and (c) extrinsic detection.[78]

Ag nanoplates have attracted much attention due to their highly anisotropic structure and high potential for practical application as SERS-based sensing platforms. The development of a high density array of Ag nanoplates on a solid substrate is also important to fabricate more robust SERS platforms because the SERS signal of Raman active molecules is expected to be more reproducible and highly enhanced on solid substrates coated with Ag nanostructures.[8] The applicability of the SURF-PEI-PLATES a SERS platform is here examined by using Rhodamine6G (R6G) as model

---

[78] A.R. Tripp; A.R. Dluhyb; Y. Zhaoc; *Nanotoday*, **2008**, 3,31.

compound. Furthermore, we have tested the possibility to use SURF-PEI-Plates to detect a biological fluid as blood, for a possible biomedical or forensic application.

2.4.1 Experimental Details: Synthesis and Characterization

2.4.1.1 Experimental Materials and Instrumentation

Materials

Silver nitrate (>99.8%), sodium borohydride (>99.0%), sodium citrate (TSC) (>99.0%), ascorbic acid ≥99%, rhodamine6G were purchased from Sigma Aldrich. Trimethoxysilylpropyl(polyethylenimine) (50% in isopropanol) was purchased from Gelest Inc. Reagents were used as received. Solvents were purchased from Sigma-Aldrich and used as supplied. Microscopy cover glass slides (21x26mm) were purchased from DelChimica. Water was deionized and then bidistilled.

Instrumentation and instrumental method.

SERS measurements. SERS measurement were carried out at room temperature by using a Labram Dilor spectrometer equipped with an Olympus microscope HS BX40.

2.4.1.2 Preparation of SURF-PEI-PLATES

For preparation of SURF-PEI-PLATES see **Paragraph 2.3.1.7**.

2.4.1.3 Preparation of SURF-PEI-PLATES for SERS Measurements with 6RG

The typical experimental setup for all samples investigated was performed placing on the SURF-PEI-PLATES functionalized glass sample a 20 μL drop of a water solution of R6G at the desired concentration. After this, a blank and clean 21x26 mm glass slide was placed to cover functionalized glass in order to spread completely the drop and to obtain an almost homogeneous film of R6G solution between the two glass slides. The so-assembled sample was then used quickly for Raman analysis.

2.4.1.4 Preparation of SURF-PEI-PLATES for SERS Measurements with Blood

For SERS measurements of blood, a drop of fresh blood was obtained from the operator with a small needle and immediately diluted in water to the desired concentration (1:50 and 1:2000 times). After a few seconds, the solution was placed on the SURF-PEI-PLATES and analyzed as explained in **2.4.1.3**.

2.4.2 Results and Discussion

2.4.2.1 SERS Measurements

In order to investigate the applicability of the prepared functionalized glass samples as SERS substrates, the Raman signal of R6G, a molecule widely used as a representative Raman reporter, was measured for SURF-PEI-PLATES. In **Figure 55**, the chemical structure of R6G is reported.
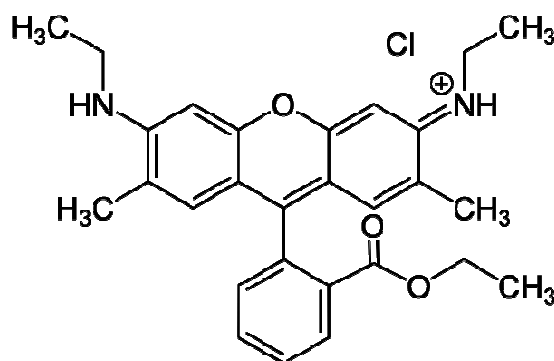

Figure 55 Chemical structure of R6G.

Typical Raman spectrum of R6G molecule is dominated by the modes inside the xanthene ring. The position of the main Raman modes (expressed in cm^{-1}) are listed in the following together with the vibrational assignement:[79]

---

[79] L. Jensen, G.C. Schatz, *J. Phys. Chem. A*, 2006, **110**,

610, 780 → in plane deformations of Xanthene ring;

1178 → in plane deformations of Xanthene ring and bending of C-H and N-H bonds;

1308 → breathing of xanthene ring and N-H bending and CH_2 wagging;

1358 → C-C stretching of xanthene and C-H bending;

1508 → stretching in-plane of C-C bond of xanthene, stretching of C-N and C-H and N-H bending;

1646 → stretching of xanthene and C-H bending.

As a preliminary experiment, evaluation of SURF-PEI-PLATES as SERS substrate was carried out on a solution of R6G 10^{-4} M. SERS chips were prepared as described in **Paragraph 2.4.1.3.** A Raman spectra of R6G at the same concentration was measured using the same solution on a blank glass slide. The results are shown in **Figure 56**, where the measured interval ranges between 1000-1900 cm^{-1}.
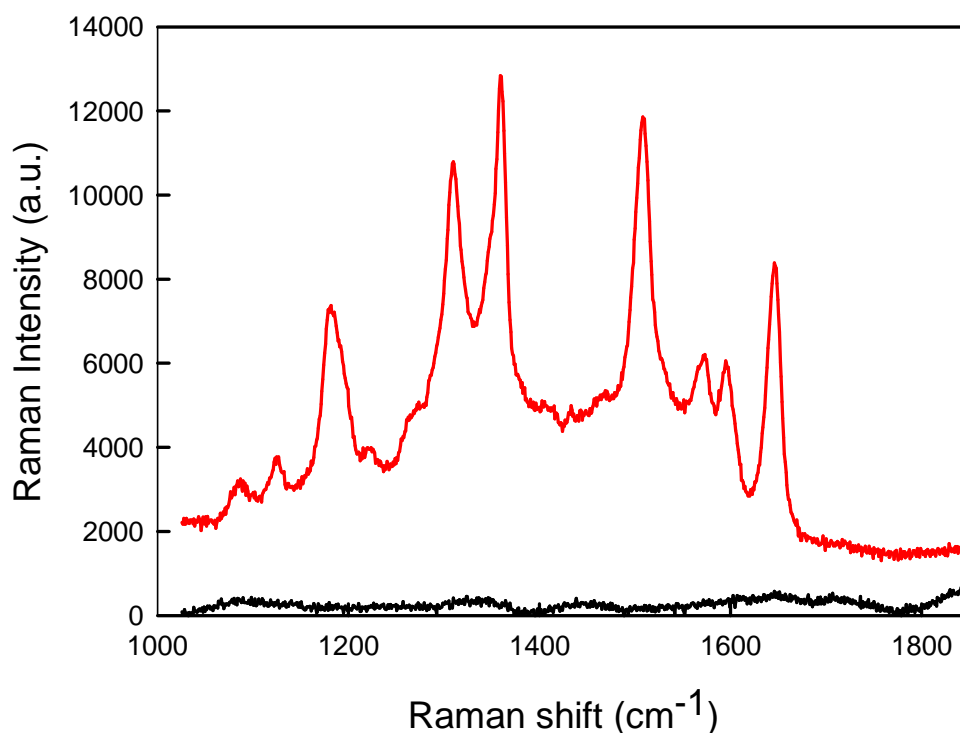

Figure 56 SERS spectrum of a 10^{-4} M solution of R6G on SURF-PEI-PLATES chip (red line), Raman spectrum of the same solution on a blank glass slide (black line).

There is a good match between expected and measured peak positions for SERS spectrum and this preliminary measurement demonstrated that SURF-PEI-PLATES acts as an effective SERS substrate, allowing to measure signal otherwise completely buried by the noise: as can be seen from Figure 56, in absence of enhancement given by the nano-objects, a normal Raman spectrum of the 10^{-4} M solution does not show any peak.

At this state, we have investigated the lowest concentration of R6G which is possible to detect with SURF-PEI-PLATES in the same experimental conditions and the results are reported in **Figure 57**.
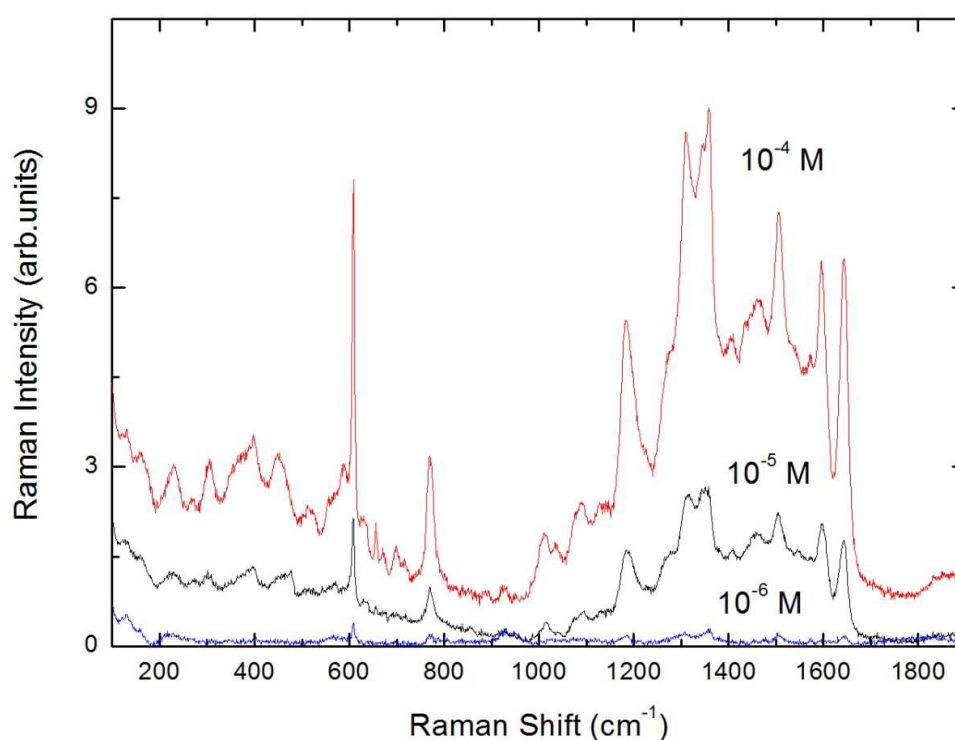
Figure 57 SERS spectra with solution of R6G on SURF-PEI-PLATES chip, 10^{-4} M (red line), 10^{-5} M (black line).

In this case the whole range 100-1900 cm^{-1} is reported, and also the inplane deformations of xanthene ring are visible at 610 and 780 cm^{-1} respectively. The spectra for all the concentrations investigated are in good agreement with the literature. In the measurement session reported, broad unresolved features appeared between 1000-1700 cm^{-1}, anyway they are completely negligible when one is interested in the evaluation of peak integrated intensities. One can

empirically estimate the enhancement factor by the comparison with other SERS substrates where the calculation of EF's has been carefully made.

In **Figure 58** the spectra obtained from SURF-pEI-PLATES (red line) and a similar SERS chip based on gold nanostars are reported. The data have been obtained using the same concentration of R6G (10^{-4} M), the same experimental setup and the same instrumental configuration. Thus the comparison of the signals allow to derive the EF for SURF-PEI-PLATES from the EF of the chip based on gold nanostars, which was calculated to be 9×10^5. A factor 3 can be deduced looking at the spectra, and this allow to calculate a value of EF for our SURF-PEI-PLATES SERS chips approximately equal to 3×10^6.
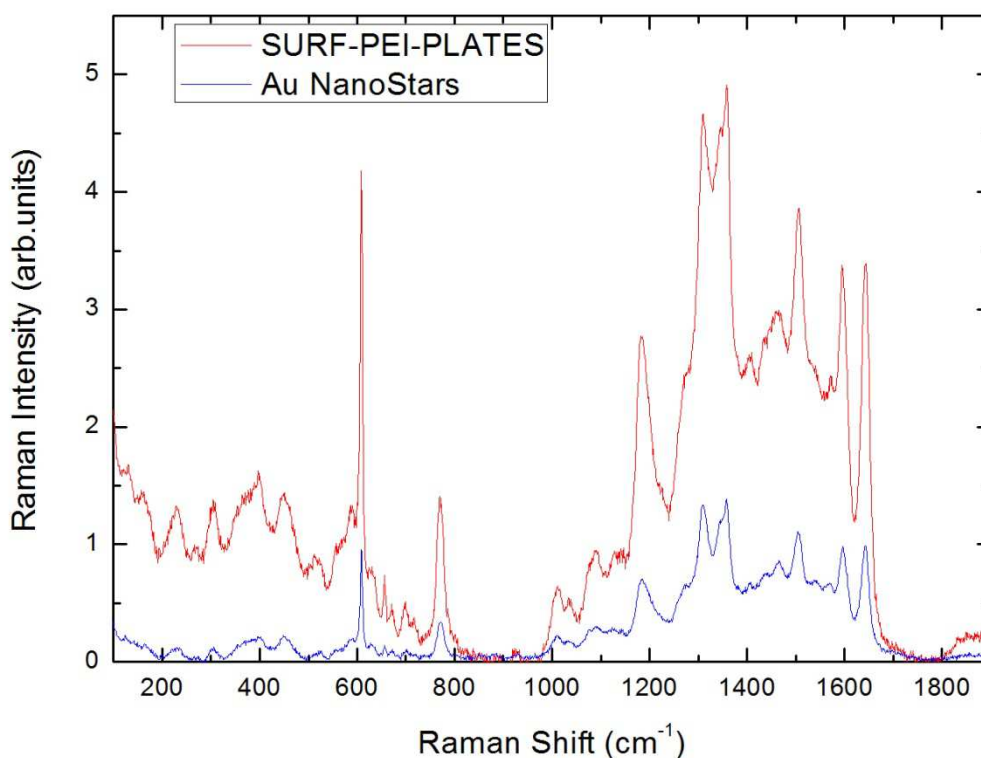
Figure 58 SERS spectra of a 10^{-4} M solution of R6G obtained from SURF-PEI-PLATES (red line) and from a similar SERS chip based on gold nanostars. The same experimental setup and the same instrumental configuration were used.

On this basis we have performed some preliminary measurements trying to work on blood without any preparation of the targeted material, as an example of biological fluid. The Raman

spectrum of dried blood is reported in **Figure 59**: it is characterized by a typical Raman fingerprint, with several Raman peaks: among these we can cite those at 1123 cm^{-1} , 1247 cm^{-1} and 1340 cm^{-1}. In addition, we can clearly notice two peaks which are attributed to the heme group at 1756 and 1620 cm^{-1}.
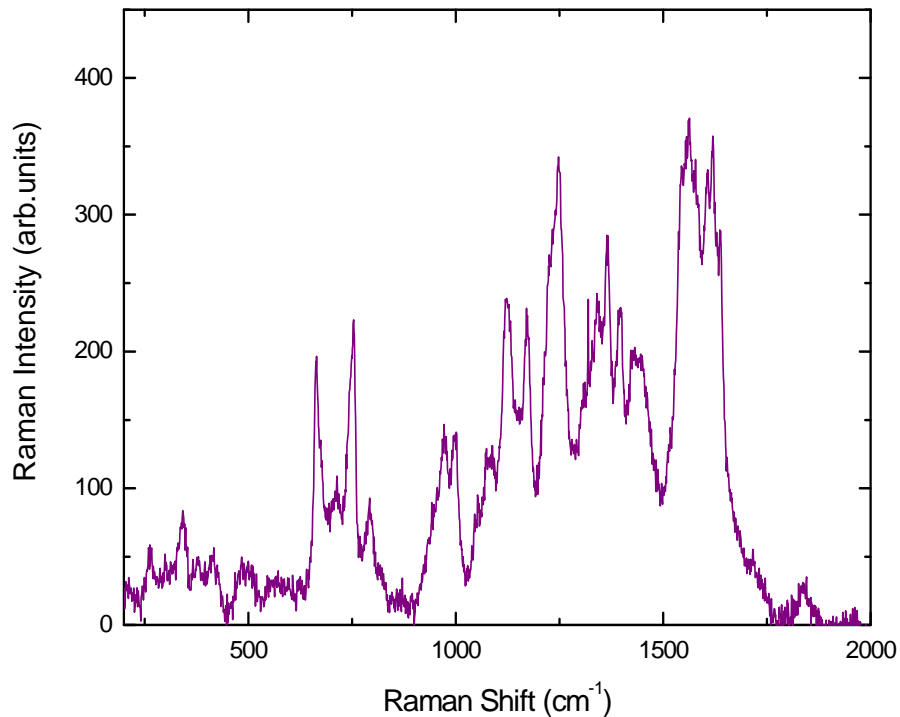
Figure 59 Raman spectra of a drop of blood dried on a blank glass.

A similar spectral fingerprint can be recognized in **Figure 60**, where two SERS spectra of blood with different dilution in bidistilled water are reported. Arrows evidence the presence of the cited peaks.

165
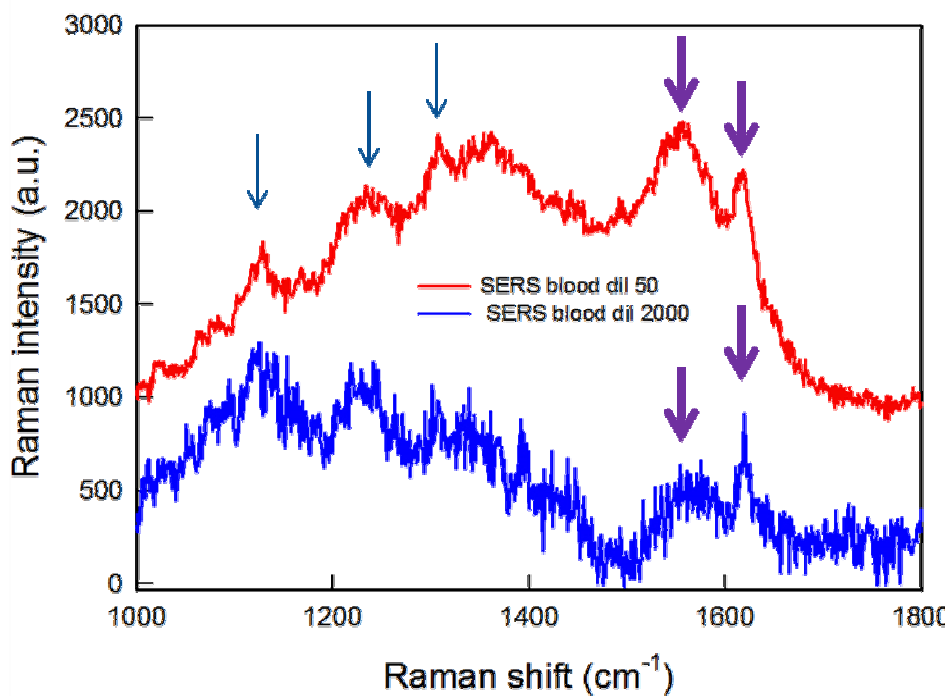
Figure 60 SERS spectra obtained with SURF-PEI-PLATES of hematic traces obtained with fresh blood dilution in water: arrows evidence the presence of signals typically associated to blood.

2.4.3 Conclusions

These preliminary results seem quite promising: demonstrated that using SURF-PEI-PLATES as SERS chips a test molecule can be detected at micromolar concentrations. Most importantly, also the presence of hidden traces of blood which hardly be revealed by eye or microscope was monitored with an easy experimental setup: the several potential applications for this kind of analysis using the described SERS chips are of obvious evidence, in the biomedical field or in forensic sciences, just to make two examples.

CHAPTER 3: AgNPs FOR PHARMACEUTICAL APPLICATION

3.1 Introduction

As we have told in **Chapter 1**, the research field involving AgNPs are growing at a high rate, and lots of products based on AgNPs has been highly commercialized. For example, clothing manufacturers have incorporated AgPNs into fabrics for socks and exploit the antibacterial activity for neutralization of odor-forming bacteria.[1] In addition, AgPNs has been integrated into various food contact materials, such as plastics used to fabricate food containers, refrigerator surfaces, storage bags and chopping boards, under the pretext of preserving foods longer by inhibiting microorganism growth.[2] The medical industry has been slow to exploit the potential of AgNPs in infection prophylaxis, but this field is now gaining momentum. Recent evidence suggests that AgNPs has a potent anti-inflammatory effect[3] and accelerates wound healing.[4] Silver is used clinically and AgNPs use is emerging as a valuable tool in the therapeutic armory, as summarized in **Figure 1**. Interest in silver and AgNPs has been motivated by the emergence of rampant antibiotic-resistant bacteria[5] and the increasing prevalence of hospital-acquired bacterial infections. Silver use has been severely limited by the toxicity of silver ions to humans; however, Nanotechnology has facilitated the production of smaller silver particles with increasingly large surface area-to-volume ratios, greater efficacy against bacteria and, most importantly, lower toxicity to humans.[6]

In this part of the thesis, the use of AgNPs in more pharmaceutically oriented approaches will be investigated, applied to wound healing and, once again, for antibacterial tasks.

---

[1] T.M. Benn, P. Westerhoff, *Environ. Sci. Technol.*, 2008, **42**, 4133.
[2] Q. Chaudhry, *Food Addit. Contam. A*, 2008, **25**,241.
[3] J. Tian, J.K.Y. Kenneth Wong, C.M. Ho, C.N. Lok, W.Y. Yu, C.M. Che, J.F. Chiu, P.K.H.Tam, *Chem. Med. Chem.*,2007, **2**, 129.
[4] J.B. Wright, K. Lam, A.G. Buret, M.E. Olson, R.E. Burrell, *Wound Repair Regen.*, 2002, **10**, 141.
[5] O. Choi, K.K. Deng, N.J. Kim, L.J. Ross, R.Y. Surampalli, Z.Hu, *Water Res.*, 2008, **42**, 3066.
[6] R. Foldbjerg, P. Olesen, M. Hougaard, D.A. Dang, H.J. Hoffmann,H. Autrup, *Toxicol. Lett.*, 2009, **190**, 156.
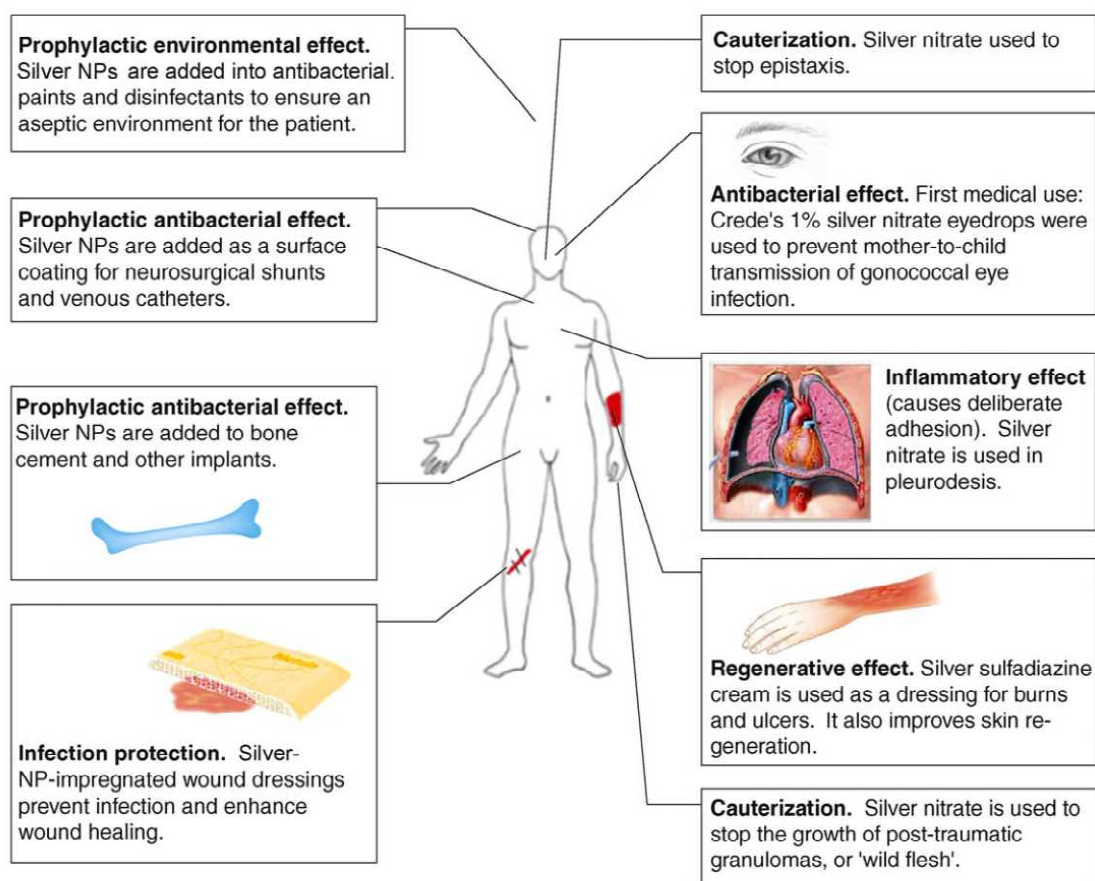
Figure 1 Uses of silver (right-hand side) and silver AgNPs (left-hand side) in medicine.[7]

3.1.1 Green Synthesis of AgNPs

The synthesis of silver nanoparticles (AgNPs) is a relatively easy process thanks to the noble metal nature of this element. A plethora of reductants is able to transform Ag^+ in $Ag(0)$, typically from $AgNO_3$. The borohydride ion, hydrazine, citrate, ethylene glycol are widely employed examples.[8] Anions (e.g. citrate), small neutral molecules (e.g. amines) or polymeric species[8,9] (e.g. polyols) may instead stabilize AgNPs by adhering to their crystal faces and preventing aggregation by electrostatic or steric repulsion. When reduction of Ag^+ is carried out in the presence of such agents, stable colloidal solutions of coated AgNPs are obtained instead of a macroscopic silver precipitate. If AgNPs are to be used for biomedical purposes, the oxidation products of the reductant, the reductant excess and the protecting agent must also be taken into consideration, as they may as well have detrimental effects on cell lines or on living organisms. In this perspective,

[7] K. Chaloupka, Y. Malam, A. M. Seifalian, *Biotechnology*, 2010, **28**, 580.
[8] T.M. Thabet, M. Tolaymat, A.M. El Badawy, A. Genaidy, K.G. Scheckel, T.P. Luxton, M. Suidan, *Sci. Total Environ.*, 2010, **408**, 999.
[9] B. Wiley, Y. Sun, Y. Xia, *Acc. Chem. Res.*, 2007, **40**, 1067.

several green syntheses of AgNPs have been recently published. These are based on natural, biocompatible products such as plant extracts,[10,11,12,13] that contain mixtures of molecular species capable of reducing Ag^+, like alkaloids, proteins, polysaccharides, enzymes, alcohols, aminoacids, quinones. Moreover, due to their rich composition, plant extracts may also contain molecular species acting as protecting agents, so that stable AgNPs colloidal solutions are obtained in one-step. However, the complexity of such extracts may lead to shape mixtures and to a large size-distribution of the obtained nanoparticles. In addition, reproducibility could be poor as it depends heavily on the origin, preparation and pre-treatment of the plant extract. On the other hand, beside the necessary biocompatibility of reductants, subproducts and coatings, a definite shape and a narrow dimensional distribution are prerequisites if a pharmaceutical use of AgNPs is to be imagined.

The primary requirement of green synthesis of AgNPs is silver metal ion solution and a reducing biological agent. In most of the cases reducing agents or other constituents present in the cells acts as stabilizing and capping agents, so there is no need of adding capping and stabilizing agents from outside. The Ag^+ ions are primary requirement for the synthesis of AgNPs which can be obtained from various water soluble salts of silver. However, the aqueous $AgNO_3$ solution with Ag^+ ion concentration range between 0.1 - 10mm (most commonly 1 mm) has been used by the majority of researchers. The reducing agents are widely distributed in the biological systems. The AgNPs have been synthesized using different organisms belonging to four kingdom out of five kingdom of living organisms. Green synthesis of AgNPs has been discussed under headings microorganisms, plants, and biopolymers.

The term biopolymer is generally understood as an organic polymer that is produced naturally by living organisms.[14] One major advantage of biopolymers is that they are also fully capable of biodegradation at accelerated rates, breaking down cleanly into simple molecules found in the environment, such as carbon dioxide, water or methane, under the enzymatic action of microorganisms, in a defined period of time. Polymeric materials derived from renewable resources can be biodegradable or compostable under specific environmental conditions. Among biopolymers, the mostly used are:

---

[10] N.V. Ivanova, N.N. Trofimova, V.A. Babkin, *Chem. Nat. Compd.*, 2014, **50**, 60.

[11] V. Kumar, S. Kumar Yadav, *J. Chem. Technol. Biotechnol.*, 2009, **84**, 151.

[12] S. Iravani, *Green Chem.*, 2011, **13**, 2638.

[13] V.K. Sharma, R.A. Yngard, Y. Lin, *Adv. Colloid Interface Sci.*, 2009, **145**, 83.

[14] I. Armentano, N. Bitinis, E.Fortunati, S. Mattioli, N. Rescignano, R. Verdejo, M.A. Lopez-Manchado, J.M. Kenny, *Progress in Polymer Science*, 2013, **38**, 1720.

Starch is a potentially interesting biodegradable material due to its availability, low cost and renewability. Moreover, the use of starch in the plastics industry can reduce dependence on synthetic polymers. Although its structure has not been fully elucidated, it was established that starch is a heterogeneous material consisting primarily of two types of polymers: amylose, reported in **Figure 2**, and amylopectin, in **Figure 3**.
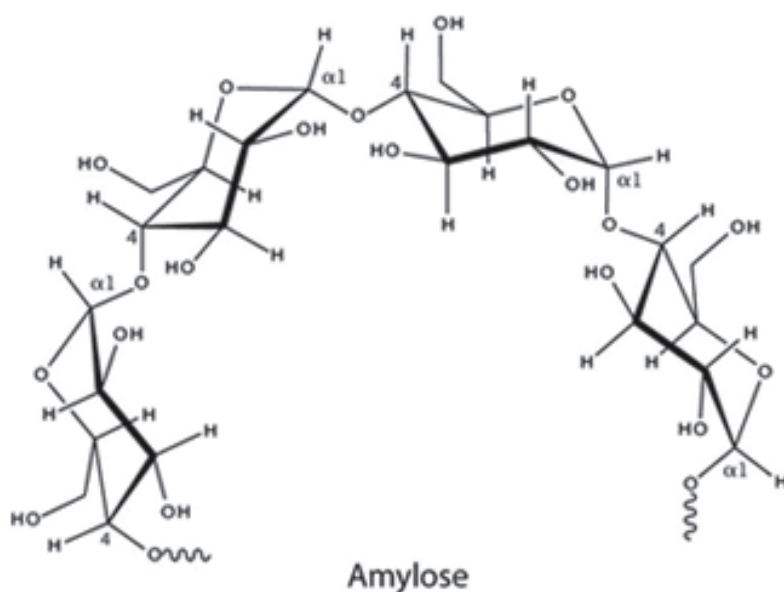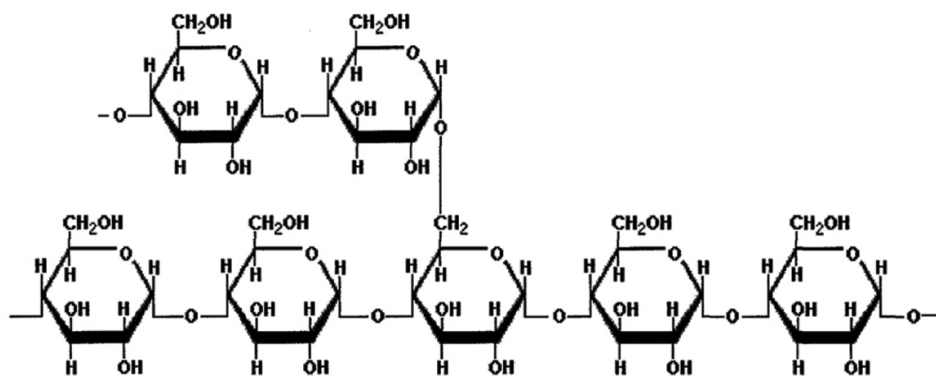

Figure 2 Structure of amylose.

Figure 3 Structure of amylopectine.

Starch is a widely used material for making biodegradable plastics, but pure starch based films possesses low mechanical properties.[15] Starch is the most important polysaccharide; it is the most abundant in nature and relatively inexpensive. Natural starch exists in granular form and, as such, it has been used as filler in polymers, but it can also be processed with classical plastic processing technologies such as extrusion, foaming and film blowing after thermoplasticization. The main limitation for starch is its hydrophilic nature, which limits its use in high moisture environments.[16]

Chitosan, as a unique positively charged polysaccharide, has been one of the most popular biopolymers for development of drug delivery systems for various applications, due to its promising properties, including high biocompatibility, excellent biodegradability, low toxicity, as well as abundant availability and low production cost.[17] Chitosan is a biopolymer derived by deacetylation of chitin, which is the second most abundant biopolymer in nature after cellulose. Chemical structure of chitin and chitosan is shown in **Figure 4**.
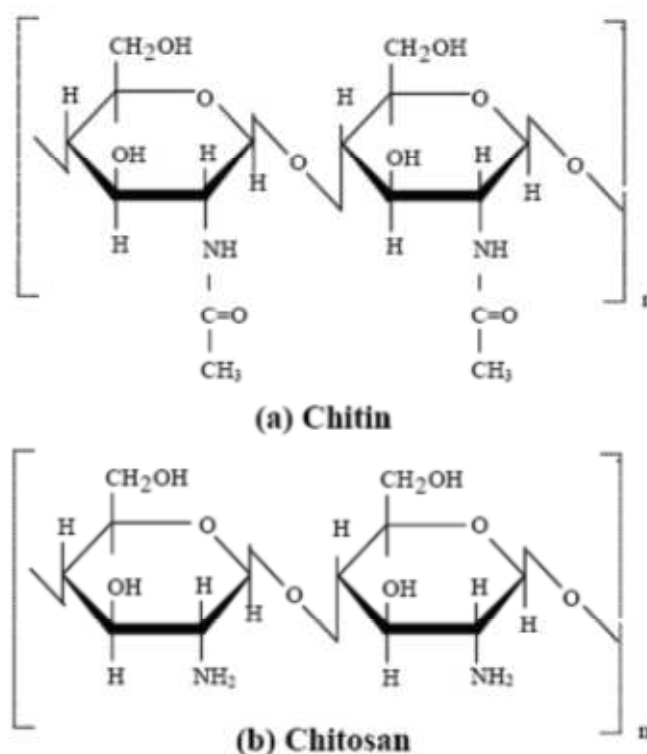
Figure 4 structure of chitin (**a**) and chitosan (**b**).

[15] N.Akter, R.A. Khan, S. Salmieri, N. Sharmin, D. Dussault, M. Lacroix, *Radiation Phisics and Chemistry*, 2012, **81**, 995.

[16] G. Mensitieri, E. Di Maio, G.G. Buonocore, I. Nedi, M. Oliviero, L. Sansone, S. Iannace, Trends in Food Science & Technology, 2011, **22**, 72.

[17] M. Bomou, Q. Aiwen, L. Xiang, Z. Xinzhen, H. Chunju, *International Journal of Biological Macromolecules*, 2014, **64**, 341.

Chitin is present in the exoskeleton of arthropods such as insects, crabs, shrimps, lobsters and certain fungal cell walls. The production of chitosan from crustacean shells, wastes of the seafood industry, is economically feasible. Chitosan has been reported as a potential material of food packaging, especially as edible films and coatings due to its film forming properties. However, one of the main drawbacks of chitosan based materials relates to its relatively weak mechanical strength. Because of reactive amino and hydroxyl functional groups, chitosan is frequently blended with other polymers or crosslinked to improve their functional properties by inducing inter- or intra-molecular crosslinking in the polymer matrix.[15] The antibacterial activity of chitosan is affected by molecular weight and degree of deacetylation. Low molecular weight chitosan has strong antibacterial properties and it is also harmless to human body. For the food packaging industry, food quality and safety to human health are the two major concerns as consumers prefer fresh and minimally processed products. Chitosan has proven a useful antimicrobial agent in food processing, particularly for improving the shelf life of food materials. [18]Chitosan and its derivatives have been receiving significant scientific interests and became one of the hottest topics in recent decades, especially for its food, medical and pharmaceutical applications, including drugdelivery and tissue engineering.[19] Chitosan membrane, an important form of chitosan, presents potential application in tissue engineering, food preservation, wastewater purification, environmental protection, fuel cell and separation technology.[17]

Pectin is a complex mixture of polysaccharides that makes up about one third of the cell wall dry substance of higher plants. Much smaller proportions of these substances are found in the cell walls of grasses. The highest concentrations of pectin are found in the middle lamella of cell wall, with a gradual decrease as one passes through the primary wall toward the plasma membrane.[20] Although pectin occurs commonly in most of the plant tissues, the number of sources that may be used for the commercial manufacture of pectin is very limited. Because the ability of pectins to form gel depends on the molecular size and degree of esterification (DE), the pectin from different sources does not have the same gelling ability due to variations in these parameters. Therefore, detection of a large quantity of pectin in a fruit alone is not in itself enough to qualify that fruit as a source of commercial pectin.[21] At present, commercial pectins are almost exclusively derived from citrus peel or apple pomace, both by-products from juice (or cider) manufacturing. Apple

[18] I.Bano, M.A. Ghauri, T. Yasin, Q. Huang, A. D'Souza Palaparthi, *International Journal of Biological Macromolecules*,2014, **65**, 81.
[19] M. Lavorgna, I. Attianese, G.G. Buonocore, A. Conte, M.A. Del Nobile, F. Tescione, E. Amendola, *Carbohydrate Polymers*, 2014, **102**, 385.
[20] Z.I. Kertesz, *The pectic substances*, (Interscience, New York, 1951)
[21] B.R. Thakur, *Food Science and Nutrition*, 1997, **37**, 47.

pomace contains 10-15% of pectin on a dry matter basis. Citrus peel contains of 20-30%.[22] From an application point of view, citrus and apple pectins are largely equivalent. Citrus pectins are light cream or light tan in color; apple pectins are often darker. Pectin is an essentially linear polysaccharide. Like most other plant polysaccharides, it is both polydisperse and polymolecular and its composition varies with the source and the conditions applied during isolation. In any sample of pectin, parameters such as the molecular weight or the content of particular subunits will differ from molecule to molecule. The structure of pectin is very difficult to determine because pectin can change during isolation from plants, storage, and processing of plant material.[23] At present, pectin is thought to consist mainly of D-galacturonic acid (GalA) units joined in chains by means of á-(1-4) glycosidic linkage. These uronic acids have carboxyl groups, some of which are naturally present as methyl esters and others which are commercially treated with ammonia to produce carboxamide groups. Structure of pectin is reported **Figure 5**.
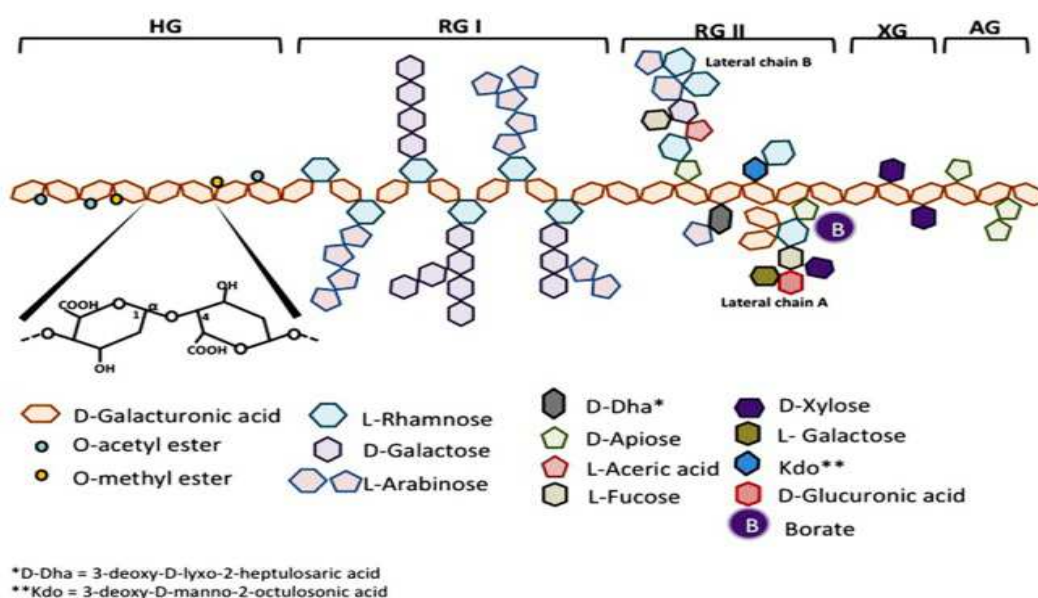
Figure 5 Structure of pectin.

Pectin contains from a few hundred to about 1000 saccharide units in a chain-like configuration; this corresponds to average molecular weights from about 50,000 to 150,000 Da. Large differences may exist between samples and between molecules within a sample, and estimates may differ between different methods of measurement. Pectins are soluble in pure water.

---

[22] C.D. May, *Carbohydrate Polymers*, 1990, **12**, 79.
[23] I.L. Novosel'skaya, *Chemistry of Natural Compounds*, 2000, **36**, 1.

Monovalent cation (alkali metal) salts of pectinic and pectin acids are usually soluble in water; di- and trivalent cations salts are weakly soluble or insoluble. Dry powdered pectin, when added to water, has a tendency to hydrate very rapidly, forming clumps.

Pectin has applications in the pharmaceutical industry. Pectin has a promising pharmaceutical uses and is presently considered as a carrier material in colon-specific drug delivery systems (for systemic action or a topical treatment of diseases such as ulcerative colitis, Crohn's disease, colon carcinomas), as indicated by the large number of studies published over the last few years. The potential of pectin or its salt as a carrier for colonic drug delivery was first demonstrated by two studies, i.e. Ashford[24] and Rubinstein et al.[25] The rationale for this is that pectin and calcium pectinate will be degraded by colonic pectinolytic enzymes, but will retard drug release in the upper gastrointestinal tract due to its insolubility and because it is not degraded by gastric or intestinal enzymes. Moreover, Rubinstein[26] demonstrated that pectin-degrading bacteria, *Klebsiella oxytoca*, could adhere to a film casted of low methoxylated pectin. The ability of the bacteria to adhere to the films, however, was not correlated with their ability to degrade pectin. When the dissolution of pectin matrix tablets was analysed with and without *K. oxytoca*, a significant retardation in the dissolution rate was observed in the presence of *K. oxytoca*, suggesting the formation of a biofilm on the matrix or sedimentation of insoluble pectin salts. Pectin is an interesting candidate for pharmaceutical use, e.g. as a carrier of a variety of drugs for controlled release applications. Many techniques have been used to manufacture the pectin-based delivery systems, especially ionotropic gelation and gel coating. These simple techniques, together with the very safe toxicity profile, make pectin an exciting and promising excipient for the pharmaceutical industry for present and future applications.

Recently, pectin which act as reducing and capping agents for nanoparticles synthesis, are more advantageous over other biological processes,[27] because they eliminate the elaborated process of culturing and maintaining of the cell, and can also be scaled up for large-scale nanoparticle synthesis. Moreover, pectin nanoparticles synthesis is preferred because it is cost-effective, environmentally friendly, a single-step method for biosynthesis process and safe for human therapeutic use.[28] Different kind of pectin from different type of fruit and fruit peels have been

---

[24] M. Ashford, *Journal of Controlled Release*, 1993, **26**,213.
[25] A. Rubinstein, R.Radai, M. Ezra, S. PathakJ, J.S. Rokem, *Pharmaceutical Research*, 1993, **10**, 258.
[26] A. Rubinstein, *Microbios*, 1992, **70**, 284.
[27] M.M.I.Haytham, *Journal of Radiation Research and Applied Sciences,* 2015, **8**, 265.
[28] K. Vineet, S. Kumar Yadav, *J. Chem. Technol. Biotechnol.*, 2009; **84**, 151.

studied so far for the synthesis of silver, gold, platinum and titanium nanoparticles in different sizes and shapes.

3.1.2 Wound Healing

A wound can be described as a defect or a break in the skin, resulting from physical or thermal damage or as a result of the presence of an underlying medical or physiological condition. According to the Wound Healing Society, a wound is the result of "disruption of normal anatomic structure and function".[29] Based on the nature of the repair process, wounds can be classified as acute or chronic wounds. Acute wounds are usually tissue injuries that heal completely, with minimal scarring, within the expected time frame, usually 8–12 weeks.[30] The primary causes of acute wounds include mechanical injuries due to external factors such as abrasions and tears which are caused by frictional contact between the skin and hard surfaces. Mechanical injuries also include penetrating wounds caused by knives and gun shots and surgical wounds caused by surgical incisions to for example remove tumors. Another category of acute wounds include burns and chemical injuries, which arise from a variety of sources such as radiation, electricity, corrosive chemicals and thermal sources. The temperature of the source and the exposure time influence the degree of a thermal burn. Burns will normally require specialist care because of the associated trauma. Chronic wounds on the other hand arise from tissue injuries that heal slowly, that is have not healed beyond weeks 8-12 and often reoccur. Such wounds fail to heal due to repeated tissue insults or underlying physiological conditions[31] such as diabetes and malignancies, persistent infections, poor primary treatment and other patient related factors. These result in a disruption of the orderly sequence of events during the wound healing process (see later). Chronic wounds include decubitus ulcers (bedsores or pressure sores) and leg ulcers (venous, ischemic or of traumatic origin). Wounds are also classified based on the number of skin layers and area of skin affected.[32] Injury that affects the epidermal skin surface alone is referred to as a superficial wound, whilst injury involving both the epidermis and the deeper dermal layers, including the blood vessels, sweat glands and hair follicles is referred to as partial thickness wound. Full thickness wounds occur when the underlying subcutaneous fat or deeper tissues are damaged in addition to the epidermis and dermal layers.

---

[29] G.S. Lazarus, D.M. Cooper, D.R. Knighton, D.J. Margolis, E.R. Percoraro, G. Rodeheaver, M.C. Robson, *Arch Dermatol*, 1994, **130**, 489.

[30] J.N.Percival, *Surgery*, 2002, **20**, 114.

[31] K. Moore K, R. McCallion, R.J. Searle, M.C. Stacey, K.G.Harding, *Int Wound J.*, 2006, **3**, 89.

[32] D. Krasner, K.L. Kennedy, B.S. Rolstad, A.W. Roma, *Wound Manag*, 1993, **66**, 68.

Ferreira et al.[33] have described wounds both acute and chronic that are difficult to heal as 'complex wounds' with unique characteristics. The properties of complex wounds from their review can be summarized as: (a) extensive loss of the integument which comprises skin, hair, and associated glands, (b) infection (e.g. Fournier's gangrene) which may result in tissue loss, (c) tissue death or signs of circulation impairment and (d) presence of pathology (bacteria commonly isolated from chronic wounds are aerobes like *Acinetobacter baumanii*, *Coliforms*, *Enterococcus faecalis*, *Pseudomonas aeruginosa*, *Staphylococcus aureus*, *Staphylococcus epidermidis* and anaerobes such as *Bacteroides* spp, *Fusobacterium* spp, *Peptostreptococcus* spp, *Porphyromonas* spp, *Prevotella* spp, *Veilonella* spp).[34]

Wound healing is a specific biological process related to the general phenomenon of growth and tissue regeneration. Wound healing progresses through a series of interdependent and overlapping stages in which a variety of cellular and matrix components act together to reestablish the integrity of damaged tissue and replacement of lost tissue.[35] The wound healing process has been reviewed and described by Schultz[36] and involves complex biochemical and cellular processes. These process are described **Figure 6**. Furthermore, Cooper[37] has argued for expanding the understanding of wounds beyond the cellular level to a molecular context as well. He emphasized the need to approach wound healing at multiple levels (cellular and molecular) to help improve wound treatment and management. Wound healing formulations (dressings) and novel technologies developed to date focus on one or more of these aspects of the natural healing process[38] that are summarised briefly below.

---

[33] M.C. Ferreira, P. Tum, V.F. Carvalho, F. Kamamoto, *Clinics*, 2006, **61**, 571.
[34] Association for the Advancement of Wound Care (AAWC). Advancing your practice: Understanding Wound Infection and the Role of Biofilms.Malvern, PA. 2008.
[35] P. Shakespeare, *Burns*, 2001, **27**, 517.
[36] G.S. Schultz GS, *Molecular regulation of wound healing*, (Bryant RA, editor, St. Louis, 1999)
[37] D.M. Cooper, *Nurs Pract Forum*, 1999, **10**, 74.
[38] J.B. Debra, O. Cheri, *Wound healing:Technological innovations and market overview,* 1998, **2**, 1.
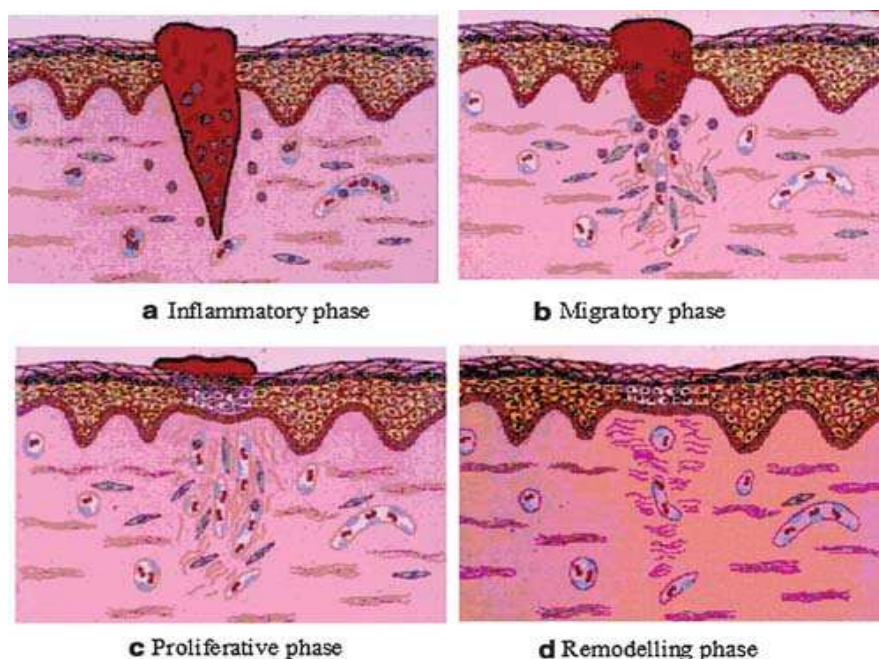
Figure 6 Schematic representation of these phases of wound healing: **a)** infiltration of neutrophils into the wound area, **b)** invasion of wound area by epithelial cells, **c)** epithelium completely covers the wound, **d)** many of the capillaries and fibroblast, formed at early stages have all disappeared. [35]

3.1.3 AgNPs and Wound Healing

Silver has been used for centuries to prevent and treat a variety of diseases including pleurodesis, cauterisation, and healing of skin wounds.[3] Its antibacterial effect may be due to blockage of the respiratory enzyme pathways and alteration of microbial DNA and the cell wall.[39] In addition to its recognized antibacterial properties, some authors have reported on the possible pro-healing properties of silver.[40] The use of silver in the past has been restrained by the need to produce silver as a compound, thereby increasing the potential side effects. Nanotechnology has provided a way of producing pure silver nanoparticles, AgNPs. This system also markedly increases the rate of silver ion release.[41]

The final aim of burn management and therapy is wound healing and epithelization as soon as possible in order to prevent infection and to reduce functional and aesthetic after effects.[42] The use of topical chemotherapy has been fundamental in that regard and has helped to improve the survival of patients with major burns and to minimize the incidence of burn wound sepsis, a

---

[39] S.M. Modak, C.L. Fox Jr., *Biochem. Pharmacol.*, 1973, **22**, 2391.

[40] J.B. Wright, K. Lam, A.G. Buret, M.E. Olson, R.E. Burrell, *Wound Repair Regen.*, 2002, **10**, 141.

[41] F.R. Fan, A.J. Bard, *Proc. Natl. Acad. Sci. USA*, 1999, **96**, 14222.

[42] L. Salas Campos, M. Fernandes Mansilla M, A.M. Martinez de la Chica, *Rev Enferm*, 2005, **28**, 67.

leading cause of mortality and morbidity in these patients.[43] One of the strategies that is gaining renewed attention for combating the threat of bacterial infection and preventing wound sepsis, is the use of noble metal antimicrobials the most prevalent of which is silver.[44]

Typically, the wound repair process involves steps that include inflammation around the site of injury, angiogenesis and the development of granulation tissue, repair of the connective tissue and epithelium, and ultimately remodeling that leads to a healed wound. However, the progression from an injured site to a healed wound is potentially slowed or arrested by a number of different events and conditions. One event that impedes wound healing is colonization of the wound bed by microorganisms.[44] In addition to the production of a variety of toxins and proteases, the presence of microorganisms in a wound bed may also lead to a prolonged inflammatory response. The host inflammatory response is remarkably effective at eliminating the invading microbial population, but that same process, over time, may also damage the surrounding tissues.[44]

The use of antimicrobial prophylaxis is important in reducing the wound's microbial load. Once a wound becomes infected, healing is delayed. Increased bacterial burden on the surface and in wounded tissue increases the metabolic requirements of the wound and of the host's response to that heavy bacterial load. Bacteria produce endotoxins, exotoxins, proteases, and local tissue injury. The presence of a bacterial burden in a wound stimulates a pro-inflammatory environment; the presence of bacteria induces also migration of monocytes, macrophages, and leukocytes, all of which initially act in an appropriate fashion but later produce a response that is exaggerated and deleterious. This is evidenced by the fact that wounds associated with a heavy bacterial burden often show healing failure.[45]

Bioburden may be defined as the metabolic load imposed by bacteria in the wound bed. Bacteria will compete with normal cells for available oxygen and nutrients. In addition, bacteria and bacterial products, such as endotoxins and metalloproteinases, can cause disturbances in all phases of wound healing [45] prolonging the debilitation of the patient by slowing wound healing and increasing health care costs for the patient. Increased bacterial burden in a wound also affects tissue oxygen availability. Leukocytes are needed in the wound bed to kill phagocytic bacteria-by mechanisms that involve an oxydated burst and the consumption of significant amounts of molecular oxygen. In severely under perfused wounds, increased oxygen consumption by inflammatory cells can act as a sump, ''stealing'' oxygen required for basic wound metabolism. In

[43] J.F. Fraser, L. Cuttle, M. Kempf, R.M. Kimble, *ANZ J Surg*, 2004, **74**, 139.
[44] J.B. Wright, D.L. Hansen, R.E. Burrell, *Wounds*, 1998, **10**, 179.
[45] R. Warriner, R. Burrell, *Adv Skin Wound Care*, 2005, **18**, 2.

addition, the white blood cells' inflammatory response needed to kill bacteria increases the release of damaging oxygen free radicals. The increased production of enzymes and the release of toxins can also facilitate an induced cellular failure.[45]

Studies support the concept of eradicating infection to help wound healing. From a pathophysiologic standpoint, treating an infection reduces the wound's bacterial burden, which has favorable effects on the dynamics of oxygen delivery and utilization within the wounds. This favorably impacts cellular metabolism. Treating infection also diminishes the chronic inflammatory response, which is primarily degradative. Finally, treating infection adjusts the tissue's capacity to respond to cell signaling and to develop sustained growth.[45] Silver-based wound dressings are often used to prepare the wound for healing and from that perspective silver products may have a definite positive effect on wound healing and may be used to maintain a microbe-free, moist wound healing environment.[45]

Besides its antimicrobial activity, silver was proven to have other beneficial effects on the wound bed.[45] However, only recently with the new concepts on wound healing and healing impairment, a mechanism of action can be presented. The major focus of wound healing has been on the relationship between tissue destruction by a group of collagenase enzymes known as metalloproteinases (MMP) and tissue synthesis which is stimulated by growth factors. It is well recognized that matrix metalloproteinases are needed to heal a wound, but excess levels degrade fibronectin and peptide growth factors. This effect is exacerbated further by diminished levels of tissue inhibitors of metalloproteinase (TIMPs).[45] Silver-based technologies in particular provide added benefits by down-regulating MMPs to levels that facilitate wound healing.[45] The results of several studies suggest that nanocrystalline silver specifically may play a role in altering or compressing the inflammatory events in wounds and facilitating the early phases of wound healing. These benefits are associated with reduced local matrix metalloproteinase levels and enhanced cellular apoptosis.[36]

The potent anti-inflammatory properties of silver ion on a wound have been recognized for centuries and have been demonstrated histologically. Most of the reports, however, are purely descriptive in nature identifying the decrease in erythema and increased healing. It must be stressed however that not all silver is anti-inflammatory. The anti-inflammatory properties depend on the delivery vehicle, the available concentration and species of silver, and the duration of release.[44,45] Increased inflammation observed with silver sulfadiazine is caused by the water soluble cream base itself. This surface inflammation increases neutrophil exudate and increases

protease activity on the wound surface, which may be useful to break down surface dead tissue but is deleterious to a viable healing wound bed. On the other hand, MMP levels in wounds treated with silver nitrate for example skyrocket, indicating an exaggerated inflammatory response.[45] Nanocrystalline silver dressing, on the other hand, modulates the inflammatory process at or above the level of TNF-[alpha] expression, thus generating an anti-inflammatory effect.[46] It also induces apoptosis, which is an anti-inflammatory process in the sense that it prevents cells from undergoing necrosis, which is a highly inflammatory.[36,45]

Despite its beneficial effects, some adverse effects of silver products on wound healing have also been described. Delayed wound healing is often observed clinically following the use of silver-containing topical antimicrobial agents.[40] Clinical trials undertaken to look at the effect of silver sulfadiazine on the rate of healing of burn wounds comparing silver sulfadiazine to vaselinated tulle gras indicated that there is a clear delay in the healing process of the silver sulfadiazine treated wounds.[40] Delay in eschar separation associated with silver sulfadiazine treatment of deep burns is due to the low bacterial load of the burn wounds. Necrotic tissues are not quickly sloughed because silver sulfadiazine delays or prevents colonization by microorganisms. Prolonged conservative treatment with silver sulfadiazine, especially in the early years even longer than three weeks, usually results in healing with hypertrophic or atrophic scars. Apart from the possibility that the sloughing of dead tissue in partial thickness burns is retarded, silver sulfadiazine ointment might also slow down the proper healing mechanisms of the wound. Numerous adverse reactions and side effects have also been reported together with increasing resistance to silver sulphadiazine.[45]

Bacterial colonization of wounds may delay wound healing.[34] Modern silver-containing dressings are antimicrobial, yet cellular toxicity is a serious side-effect.[47] Though it has been reported traditionally that silver has a low mammalian cell toxicity [35] silver ion does have direct cytotoxic effects on various mammalian cells. Cytotoxicity of cement loaded with silver salts made this kind of silver unsuitable for clinical use in the past.[35] Silver nitrate in vitro has been shown to have a negative impact on fibroblasts[48], hepatocytes[49] and lymphocytes. Studies on anodically generated silver ions, however, did not demonstrate any cytotoxic effect on mammalian cells in culture and no tissue toxicity could be determined by clinical evaluations.[50]

---

[46] H.N. Paddock, G.S. Schultz, K.J. Perrin, *Annual Meeting of the Wound Healing Society*, 2002.

[47] K. Ziegler, R. Gorl, J. Effing, J. Ellermann, M. Mappes, S. Otten, *Pharmacol Physiol*, 2006, **19**, 140.

[48] H. Liedberg, T. Lundeberg, *Urol Res*, 1989, **17**, 359.

[49] C. Baldi, C. Minoia, A. Di Nuici, E. Capodaglio, L. Manzo, *Toxico.Lett.*, 1988, **41**, 261.

[50] K. Bador, *PRS,* 1966, **37**, 550.

Even though it was claimed in earlier reports that nanosilver was free of in vitro cytotoxicity and showed high effectiveness against multi-resistant bacteria[51] it was later reported that high concentrations of nano-silver base inorganic antibacterial agents had cytotoxic effects on rat fibroblasts. Cytotoxicity was directly proportional to the silver concentration. Low silver ion release rate may prevent interference with wound-healing mechanisms.[49]

So, the potential benefits of AgNPs in all wounds could therefore be enormous. In fact, basic scientific research has been carried out to elucidate the mechanism underpinning the anti-inflammatory activity of AgNPs observed clinically. Anti-inflammatory properties of nanocrystalline silver were assessed by topically applying 1,2-dinitrochlorobenzene to induce contact dermatitis in swine.[52] Nanocrystalline silver outperformed saline- and silver nitrate-soaked wound dressings for treatment of the resulting contact dermatitis. Histopathology revealed near-normal pig epidermis at 72 h after treatment with nanocrystalline silver. Immunohistochemical staining revealed higher levels of the proinflammatory cytokines TGF-b and TNF-a in the saline and silver nitrate groups. The negative control and nanocrystalline silver groups showed similar levels of staining, leading to the conclusion that nanocrystalline silver has anti-inflammatory activity. Anti-inflammatory AgNPs activity might be mediated by reducing cytokine release[53], decreasing lymphocyte and mast cell infiltration[54] and inducing apoptosis in inflammatory cells. [54]

Matrix metalloproteinases (MMPs) contribute to tissue injury and inflammatory processes and their overexpression is associated with chronic ulcers rather than acute wounds, which suggests that MMPs might contribute to the non-healing nature of chronic ulcers. Nanocrystalline silver dressings significantly reduced MMP-9 levels in a porcine model and improved wound healing, although no mechanism was proposed.[55] In a human clinical study (n=15), nanocrystalline silver dressings promoted healing of stalled chronic leg ulcers.[56] This might have been achieved by reducing not only the number of bacteria in the wound, but also the inflammatory response, as evidenced by a decrease in neutrophil infiltration during biopsy.

[51] V. Alt, T. Bechert, P. Steinrucke, M. Wagener, P. Seidel, E. Dingeldein, *Biomaterials*, 2004, **25**, 4383.
[52] J.W. Richard III, B.A. Spencer, L.F. McCoy, *J Burns Surg Wound Care*, 2002, **1**,11.
[53] A.T. Hendry,I. Stewart, J Microbiol, 1979, **25**, 915.
[54] J.M. Hamilton-Miller, S. Shah, C. Smith,Chemotherapy, 1993, **39**, 405.
[55] S.M. Mirsattari, R.R. Hammond, M.D. Sharpe, F. Leung, G.B. Young, Neurology, 2004, **62**, 1408.
[56] A.D. Russell, W.B. Hugo, *Prog Med Chem*, 1994, **31**, 351.

3.2 Antibacterial Green-synthesized Silver Nanoparticles for Wound Healing

In this study we have used a commercial pectin (from citrus peel) with low ester content (methoxy groups ≥ 6-7 %, galacturonic acid ≥ 74%) and determined the optimal pH, T and concentration conditions to obtain a highly reproducible conversion of $AgNO_3$ into a pectin stabilized colloidal solution of spherical AgNPs (p-AgNPs) with a narrow dimensional distribution. Moreover, an analytical method was developed to determine the Ag^+-Ag(0) conversion yield, that in our case resulted ~ 100%. The stability of such pectin-embedded AgNPs and the Ag^+ release with time were also investigated using absorption spectroscopy, dialysis and quantitative analysis by ICP-OES (inductive coupled plasma optical emission spectroscopy). The MIC (minimum inhibitory concentration) of p-AgNPs for *Escherichia coli* PHL628 (*E. coli* PHL628, Gram-negative) and *Staphylococcus epidermidis* RP62A (*S. epidermidis* RP62A, Gram-positive) was determined and compared with that of Ag^+ (from $AgNO_3$). Since the two bacterial strains are biofilm producers, their viability in biofilm was tested, both with the bacteria plated in the presence of p-AgNPs in the medium (pre-biofilm formation) and with the biofilm produced in the absence of p-AgNPs, which were added in a second step (post-biofilm formation). Finally, as the capability of AgNPs to promote wound healing has been recently reported,[3,57] we also investigated the biocompatibility of p-AgNPs towards fibroblasts and the ability of p-AgNPs to improve human fibroblast proliferation.

[57] G. Nam, S. Rangasamy, B. Purushothaman, J.M. Song, *Nanomater. Nanotechnol.*, 2015, **5**, 23.
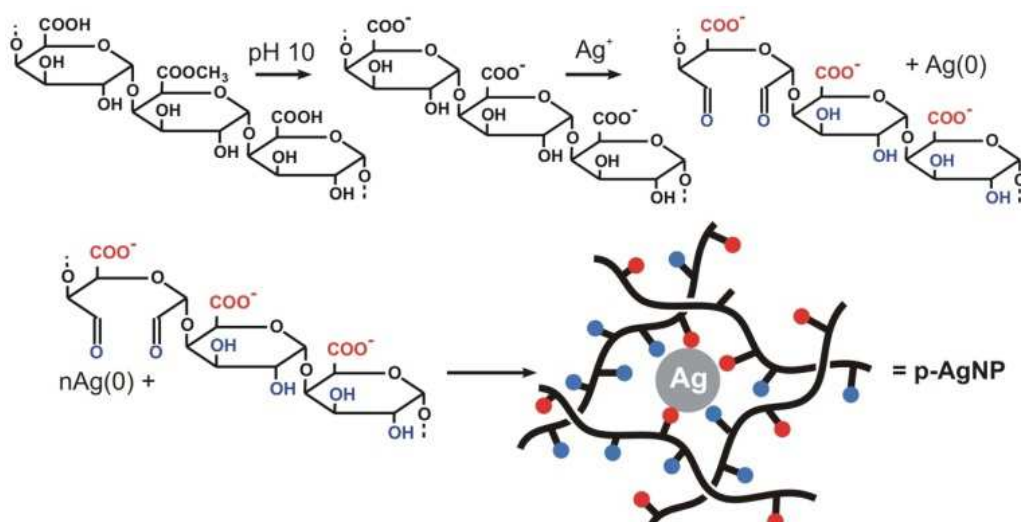
Figure 7 Working and reaction scheme for pectin/Ag$^+$ reaction at basic pH. The blue circles in the lower sketch represent alcoholic and aldehyde functions, red circles represent carboxilates.

3.2.1 Experimental Details: Synthesis and Characterization

3.2.1.1 Experimental materials and Instrumentation

Materials

Pectin from citrus peel, silver nitrate, sodium chloride, hydrochloric acid (37%), sodium citrate, sodium bromide, sulphuric acid (96%), sodium hydroxide, ethanol (95%) were all purchased from Sigma-Aldrich and used without further purification. Water was bidistilled from deionized water prior to use.

Instrumentation and instrumental method

Absorbance spectra of colloidal suspensions were taken with a Varian Cary 100 spectrophotometer in the 200–900 nm range and spectra of functionalized glasses were obtained placing the slides on the Varian Cary 100 spectrophotometer equipped with a dedicated Varian solid sample holder.

Determination of Ag^+ content in the p-AgNPs solutions.

The Ag^+ content in the p-AgNPs colloidal solutions was determined by potentiometric titration, using the standard addition method.[58] A combined silver electrode consisting of a silver bar (diameter 8 mm) and a Mercury/Mercurous Sulfate (Hg/Hg_2SO_4, saturated K_2SO_4) reference electrode were used (Radiometer Analytical, code MC6091Ag-9). Measures were performed with a Haita model 903 potentiometer, with a precision of ± 0.1 mV. Prior of the analysis, KNO_3 was added to the samples as a supporting electrolyte, so that the final solution was 0.1 M with respect to this salt. A calibration line was built by adding known amounts of silver nitrate (from 0.1 up to 200 mg/L) to 0,5%, 1% or 2% w/w pectin solution in 0.1M KNO_3, and plotting log $[Ag^+]$ vs E (mV). A straight line with a Nernstian slope (ca 60 mV for ten-fold change in concentration) was always obtained. The entire operation was carried out at 20°C in less than 20 min and in the absence of added base, to avoid reduction of silver by pectin.

Ag^+ release studies.

A 20 mL volume of p-AgNPs prepared from 1 mM Ag^+ in 1.0% w/w pectin was cooled at room temperature after 12h at 60°C and subsequently confined inside a dialysis membrane tube (Mires Emanuele – Milano, Molecular Weight Cut Off (MWCO) 12-14000 Dalton, 28.5 mm diameter), that was immersed in 20.0 mL bidistilled water (external liquid phase). At given times (0.5, 1, 3, 6, 24 h), 3.0 mL of the external liquid phase was collected, treated with 100 μL of 1.0 M HNO_3 and analysed with an ICP-OES Optima 3000 Perkin Elmer instrument. A volume of 3.0 mL bidistilled water was re-added after each sampling in the external liquid phase to maintain its starting volume.

Differential scanning calorimetry (DSC) and thermogravimetric analysis (TGA).

These measurements were run on dry p-AgNPs, prepared as described in **Paragraph 3.2.1.4**. A simultaneous thermogravimetric – calorimetric Q600 analyser by TA Instrument was used. 10 mg samples were dispersed in an open alumina crucible and heaten at 10 °C/min from room temperature to 1000°C under a nitrogen flux. Pure pectin was also analysed. Before analysis it was subjected to the same experimental conditions used for p-AgNPs synthesis (12 h at 60 °C in basic solution, dilution with ethanol, ultracentrifugation, drying). Thermogravimetric analysis was run

---

[58] R. Kataky , M.R. Bryce, B. Johnston, *Analyst*., 2000; **125**, 1447.

with a Q5000 TA Instrument thermobalance by heating 10 mg sample in a Pt crucible under inert atmosphere, from 25 °C to 1000 °C, at a 10 °C/min rate.

X-ray diffraction.
This measurement was run on dry p-AgNPs, using a Bruker D5005 instrument with Bragg-Brentano geometry. Powders were deposited on a silicon slide cut with an orientation avoiding diffraction in the used instrument geometry, and analysed from 10° to 80° with a 0.02° angular step and 10 seconds per step.

TEM imaging. TEM (transmission electron microscope) images were taken on a Jeol JEM-1200 EX II instrument on 10 μL samples, deposited on Nickel grids (300 mesh) covered with a Parlodion membrane. TEM magnification is 100 kx.

Dynamic Light Scattering (DLS) and Z-potential. DLS experiments were carried out on a Malvern Zetasizer NanoZS90 instrument. Z-potential was measured with the same instrument using a dedicated Malvern device.

3.2.1.2 Glassware pretreatment

The glassware used during experiments was always pretreated before use. It was washed in *aqua regia* for 30 min, then washed and filled with bidistilled water and ultrasonicated for 3 minutes before discarding water. The bidistilled water/ultrasound treatment was repeated 3 times.

3.2.1.3 Synthesis of AgNPs from Pectin solution (p-AgNPs)

Pectin from citrus peel was dissolved in 50 mL bidistilled water to form 0.5%, 1% and 2% (w/w) solutions. Complete dissolution was obtained by magnetic stirring at 60 °C for 20 minutes. The solution was then cooled at room temperature and the calculated volume of an $AgNO_3$ 0.1 M aqueous solution was added to obtain final Ag^+ concentration = 0.001M or 0.01 M. Then, standard 0.5 M NaOH solution was immediately added to obtain 0.025 M OH- (measured pH = 10.5-11.0). Such a mixture was kept under vigorous magnetic stirring for 12 hours either at 60 °C and for 24 h

at RT (20 °C). After 10-15 min a yellow brown color started to appear, that increased in intensity with time. After this, yellow-brown colloidal solutions of AgNPs (p-AgNPs) were obtained, that were kept in a stoppered flask at RT and used with no further treatment.

3.2.1.4 Preparation of Dry p-AgNPs

9.0 mL of 95% ethanol were added to 1.0 mL of p-AgNP solution observing a quick turbidity formation. The mixture was then ultracentrifuged at 13000 rpm (15870 g) for 60 minutes, obtaining a brown dense suspension at the bottom of the test-tube (1.5 mL volume) and a colorless supernatant. The latter was removed and the remaining suspension transferred in an Eppendorf vial (2.5 mL) and further ultracentrifuged at 13000 rpm (17760 g) for 20 + 20 minutes. After each time slot the supernatant was removed, ending with a wet brown precipitate of < 0.2 mL, that was dried first in a N_2 flux for 1h, then overnight in a vacuum desiccator.

3.2.1.5 Antibacterial and Antibiofilm Studies

3.2.1.5.1 Bacterial Strains and Culture Condition

The microorganisms used in this study, *Escherichia coli* PHL628 and *Staphylococcus epidermidis* RP62A, are biofilm-producing strains.[59,60] *E. coli* PHL628 was provided by Dr Roberta Migliavacca (University of Pavia, Italy) whereas *S. epidermidis* RP62A was a kind gift from Prof Timothy J. Foster (Department of Microbiology, Dublin University, Ireland). A starter culture of *E. coli* PHL628 or *S. epidermidis* RP62A was grown overnight, respectively in Luria Bertani Broth (LB) and in tryptic soy broth (TSB) (Difco Laboratories Inc., Detroit, MI, USA), under aerobic conditions at 37 °C using a shaker incubator (Certomat® BS-T, B.Braun Biotech International, Melsungen, Ger) at 200 rpm.

---

[59] D. Campoccia, L. Montanaro, C.R Arciola, *Biomaterials*, 2013, **34**, 8533.
[60] A. Taglietti, C. Renata Arciola, A. D'Agostino, G. Dacarro, L. Montanaro, D. Campoccia, L. Cucca, M. Vercellino, A. Poggi, P. Pallavicini, L. Visai, *Biomaterials*, 2014, **35**,1779.

3.2.1.5.2 Evaluation of Antimicrobial Activity of p-AgNPs and AgNO$_3$

Prior to any use, p-AgNPs were sterilized at 60°C for three hours and filtered through 0.45µm filter membrane to eliminate possible precipitated pectin. Instead, AgNO$_3$ was filter-sterilized (0.22 µm).

i) Planktonic bacterial culture conditions: to determine the Minimum Inhibitory Concentration (MIC) of the generated p-AgNPs suspensions and AgNO$_3$ in planktonic conditions, overnight starter cultures were diluted in appropriate fresh medium to 1 x 10^4 bacteria/mL by comparing the OD600 of the overnight culture with a standard curve correlating OD600 to bacteria number. Geometric dilution of p-AgNPs suspensions or AgNO$_3$ were performed starting from the initial concentration of 1 mM for successive ten 1:10 dilution in 100 µL. Then, 100 µL of the diluted bacterial suspension was added to the microtiter plate and incubated for the indicated times at 37°C in static conditions. Bacteria viability was estimated through the quantitative 3-[4,5-dimethylthiazol-2-yl]-2,5diphenyltetrazoliumbromide (MTT) (Sigma Aldrich, St.Louis, MO, USA) test. This colorimetric assay measures dehydrogenase activity as an indicator of the bacterial metabolic state. Briefly, 5 mg/mL of MTT solution, dissolved in PBS (0.134 M NaCl, 20mM Na$_2$HPO$_4$, 20 mM NaH$_2$PO$_4$), was used as stock solution and the working concentration was 0.5mg/mL. The test was performed at 37°C for 3 hours. Upon presence of viable bacteria, reduction of the MTT salt results in purple insoluble formazan granules that are dissolved in acidified 2-propanol (0,04 N HCl). The result was recorded through an iMark® Microplate Absorbance Reader (Bio-Rad, Hercules, CA, USA) at 562 nm with the reference wavelength set at 655nm. Cell survival was expressed as percentage of the number of bacteria treated with p-AgNPs or AgNO$_3$ to the number of bacteria grown in absence of any treatment.

ii) Bacterial biofilm culture conditions: bacterial viability in biofilm-forming conditions was evaluated as follows: the overnight starter culture was diluted in 0.25% glucose-containing medium to induce biofilm formation. *E. coli* PHL628 was diluted at a final ratio of 1: 100 and *S. epidermidis* RP62A at 1:200. Pre-biofilm conditions: geometric dilutions of p¬AgNPs suspensions or AgNO$_3$ in glucose-enriched medium were incubated with 100 µL of bacterial suspension for 24 hours as previously described.

iii) Post-biofilm conditions: biofilm was allowed to form for 24 hours at 37°C. The supernatant, containing planktonic bacteria, was carefully removed and p-AgNPs suspensions or AgNO$_3$ already diluted in the appropriate medium were added to the formed biofilm and incubated for further 24

hours. In both culture conditions, at the end of the incubation period, biofilm was vigorously suspended by pipetting and scratching. The viability was assessed through MTT assay as previously described. Experiments were performed in triplicate.

3.2.1.6 Confocal Laser Scanning Microscopy (CLSM) studies

For confocal studies, 1.5 mL of diluted bacterial suspensions were dispensed into 24-well microplates (Costar) containing on the bottom sterile glass coverslips. Coverslips containing bacterial suspensions were incubated for 24 h at 37° C to allow biofilm formation. After a delicate wash with PBS, either p-AgNPs or $AgNO_3$ (final concentration 500 µM) were added to formed biofilms. After 24 hours, the viability of bacteria within the biofilms after p-AgNPs or $AgNO_3$ treatment was estimated with the BacLight Live/Dead viability kit (Molecular Probes, Eugene, OR, USA). The kit includes two fluorescent nucleic acid stains: SYTO9 and propidium iodide. SYTO9 penetrates both viable and nonviable bacteria, while propidium iodide penetrates bacteria with damaged membranes and quenches SYTO9 fluorescence. Dead bacteria, which take up propidium iodide, fluoresce red, and bacteria fluorescing green are deemed viable. For assessing viability, 1 µL of the stock solution of each stain was added to 3 mL of PBS and, after being mixed, 500 µL of the solution was dispensed into 24-well microplates containing treated and untreated biofilms and incubated at 22° C for 15 min in the dark. Stained biofilms were examined under a Leica CLSM (model TCS SPII; Leica, Heidelberg, Germany) using a 40x oil immersion objective.

The excitation and emission wavelengths used for detecting SYTO9 were 488 and 525 nm, respectively. Propidium iodide was excited at 520 nm, and its emission was monitored at 620 nm. The optical sections of 0.9 µm were collected over the complete thickness of the biofilm, and for each sample, images from three randomly selected positions were acquired.

3.2.1.7 In vitro Cytotoxicity and Cell Proliferation Studies

Materials

Dimethyl sulfoxide, Dulbecco's Phosphate Buffer Solution, MTT (3-(4,5-dimethylthiazol-2-yl)-2,5-diphenyltetrazolium bromide), Antibiotic Antimycotic Solution (100×; stabilized with 10,000 units penicillin, 10 mg streptomycin and 25 µg amphotericin B per mL), trypan blue solution, trypsin–

EDTA solution, Hank's balance salt solution (HBSS), all purchased from Sigma-Aldrich, were used. Dulbecco's Modified Eagles Medium (DMEM) was purchased from Lonza BioWhittaker (Walkersville, USA), and inactivated foetal calf bovine serum from Euroclone (Milano, Italy).

3.2.1.7.1 NHDF Fibroblast Cell Culture

Normal Human Dermal Fibroblasts (NHDF) (Promocell GmbH, Heidelberg, Germany) from 6th to 16th passage were used. Cells were cultured in a polystyrene flask (Greiner bio-one, PBI International, Milan, Italy) with 13–15 mL of complete culture medium, consisting of Dulbecco's modified Eagles medium with 4.5 g/L glucose and l-glutamine supplemented with 1% Antibiotic Antimycotic Solution and 10% (v/v) inactivated foetal calf bovine serum. Cells were maintained in incubator (Shellab® Sheldon® Manufacturing Inc., Oregon, USA) at 37°C with 95% air and 5% CO_2 atmosphere. All the operations required for cell culture were carried out in a vertical laminar air flow hood (Ergosafe Space 2, PBI International, Milan, Italy). After the cells had reach 80–90% confluence in the flask (one week) a trypsinization was performed: at first, the monolayer was washed with Dulbecco's Phosphate Buffer Solution in order to remove bivalent cations that could inactivate trypsin, then 3 mL of 0.25% (w/v) trypsin-EDTA solution was left in contact with the monolayer for 5 min. After that time, the cell layer was harvested with 7 mL of the CM to stop the proteolytic activity of trypsin and to facilitate the detachment of cells. Afterwards, cell suspension was centrifuged (TC6, Sorvall Products, Newtown, USA) at 1500 rpm for 10 min. The supernatant was eliminated and then the cells were re-suspended in 6 mL of CM. The amount of cells in suspension was determined in a counting chamber (Hycor Biomedical, Garden Grove, California, USA), using 0.5% (w/v) trypan blue solution to visualize and count viable cells.

3.2.1.7.2 Assessment of Fibroblast Viability in presence of p-AgNPs suspension

The effects of p-AgNPs on the viability of human fibroblasts were investigated. Cells were seeded on 96-well plates (3.5 104 cells in 200 µL of complete medium/well) and left in incubator for 24 h in order to reach confluence. PEC aqueous solution (1% w/w) and p-AgNPs suspension were diluted (1:10, 1:20 1:40 v/v) in medium without fetal bovine serum (M (w/s)) and 200 µL of each sample was put in contact for 24 h with cells. Complete medium (CM) and medium without fetal

bovine serum (M (w/s)) were used as references. After incubation, samples were removed from the plate well and 50 µl of MTT (3-(4,5-dimethylthiazol-2-yl)-2,5-diphenyltetrazolium bromide) 7.5 µM in 100 µl of HBSS (pH 7.4) was added to each well and incubated for 3 h. Finally, 100 µL of a solubilization solution (dimethyl sulfoxide) was added to each well, and mixed with the cells to allow the complete dissolution of formazan crystals, obtained from the reduction of the dye MTT into cells by dehydrogenase enzyme. The solution absorbance was determined at a wavelength of 570 nm, with a 690 nm reference wavelength, by means of an IMark® Microplate reader (Bio-Rad Laboratories Srl, Segrate, Milan, Italy) after 60 s shaking. Results are expressed as % viability, normalizing absorbance measured after contact with samples with that measured after contact with M (w/s). Eight replicates were performed for each sample.

3.2.1.7.3 Assessment of Cell Proliferation Properties of p-AgNPs suspension

The capability of p-AgNPs to improve NHDF fibroblasts growth was also evaluated. Cells were seeded on 96-well plates ($2*10^4$ cells in 50 µl of M w/s / well) and immediately put in contact with p-AgNP suspension (200 µL) for 24 h. The sample was diluted 1:10, 1:20 and 1:40 v/v in M (w/s). M (w/s) was used as reference. At the end a MTT test was performed (as described in the previously paragraph).

3.2.1.7.4 Wound Healing Test

The in vitro wound-healing test is based on the employment of a Petri µ-dish (35 mm, Ibidi, Giardini, Milan, Italy) in which an insert is enclosed. The insert is constituted of two chambers with a growth area of 0.22 cm^2 divided by a septum, mimicking the lesion area, with a width of 500 µm ± 50 µm. Fibroblasts were seeded in each chamber at 10^5cells/cm^2 and growth at confluence in standard conditions as above mentioned. After 24 h, cells reached confluence and the insert was removed, displaying two areas of cell substrate divided by the prefixed gap. Cell substrates were put in contact with 400 mL of p-AgNPs diluted 1: 20 v/v with M(w/s). Wound healing test was also performed on M (w/s) and CM, used as references. At prefixed times (24, 48 and 72h) microphotographs were taken to evaluate the invasion and cell growth in the gap. At each time the maximum value of gap width was measured. Three replicates were performed for each sample.

Statistical analysis. Whenever possible, experimental values of the various type of measures were subjected to statistical analysis, carried out by means of the statistical package Statgraphics 5.0 (Statistical Graphics Corporation, Rockville, MD, USA). In particular, Anova one way- Multiple Range Test was used. The controls in the texts that have been executed are CM, as a medium of cell culture. It is defined as a basic medium (DMEM) supplemented with components necessary for cell growth (present in fetal bovine serum) and antibiotics, to prevent the growth of mold and bacteria. The second control is the Medium without serum (M w/s: serum-free and consists only of the middle base and antibiotic). The use of this second control is due to the fact that the samples were prepared in serum-free medium, hence the need to compare them with the same means. The control with CM is required because it is a positive control: growth of cells is 100%.

3.2.2 Results and Discussion

3.2.2.1 Synthesis of p-AgNPs

The synthesis of colloidal solutions of AgNPs stabilized by pectin (p-AgNPs) was carried out using 0.5, 1.0 and 2.0 % w/w pectin solutions in bidistilled water. $AgNO_3$ was added from a concentrated aqueous solution to obtain final Ag^+ concentrations of 0.001 M or 0.01 M. Reaction did not start until base was added to a concentration of NaOH of 0.025 M. The measured pH was 10.5-11.0, depending on pectin concentration. Temperature was kept at 20 °C or 60 °C, with vigorous stirring on a magnetic stirrer. Ag reduction to p-AgNPs started within 5 minutes after base addition and it was visually perceivable by the appearance of a yellow color, turning soon into the characteristic deep yellow-brown of AgNPs. The reaction was quantitatively followed by measuring the absorption spectra of the reaction mixture, in which the LSPR of AgNPs was observed. In the case of 0.001 M Ag^+ the LSPR band maximum was at 409-416 nm under all conditions, see **Table 1**.

% pectin	AgNP diameter (nm)[a]		LSPR band, λmax (nm)[b]	
	20 °C	60 °C	20°C	60 °C
0.5	5.8 (2.2)	8.0 (3.6)	411(68)	409(63)
1.0	8.8 (3.5)	8.0 (2.6)	412(69)	412(63)
2.0	8.4 (3.4)	8.0 (3.6)	411(63)	416(61)

Table 1 Dimensional and optical data for p-AgNPs prepared with 1 mM $AgNO_3$ ([a]standard deviation in parenthesis; [b]width at half height (nm) in parenthesis).

From **Table 1**, a narrow dimensional distribution was found (standard deviations are 2-3 nm) as confirmed also by the sharp shape of the LSPR bands, as reported in **Figure 8**. Also band widths at half height were small, i.e. in the 61-69 nm range (**Table 1**), and no shoulders were observed at > 450 nm, neither at 24h nor after several days after preparation evidencing that no aggregation or unsymmetrical NP.

The intensity of the LSPR absorption band increased during the first reaction hours, reaching a limiting value within 24 h at 20 °C and within 6 hours at 60 °C. **Figure 8** reports the series of absorption spectra recorded in the case of 0.001 M Ag^+ at 20 °C and 60 °C in 1% pectin.
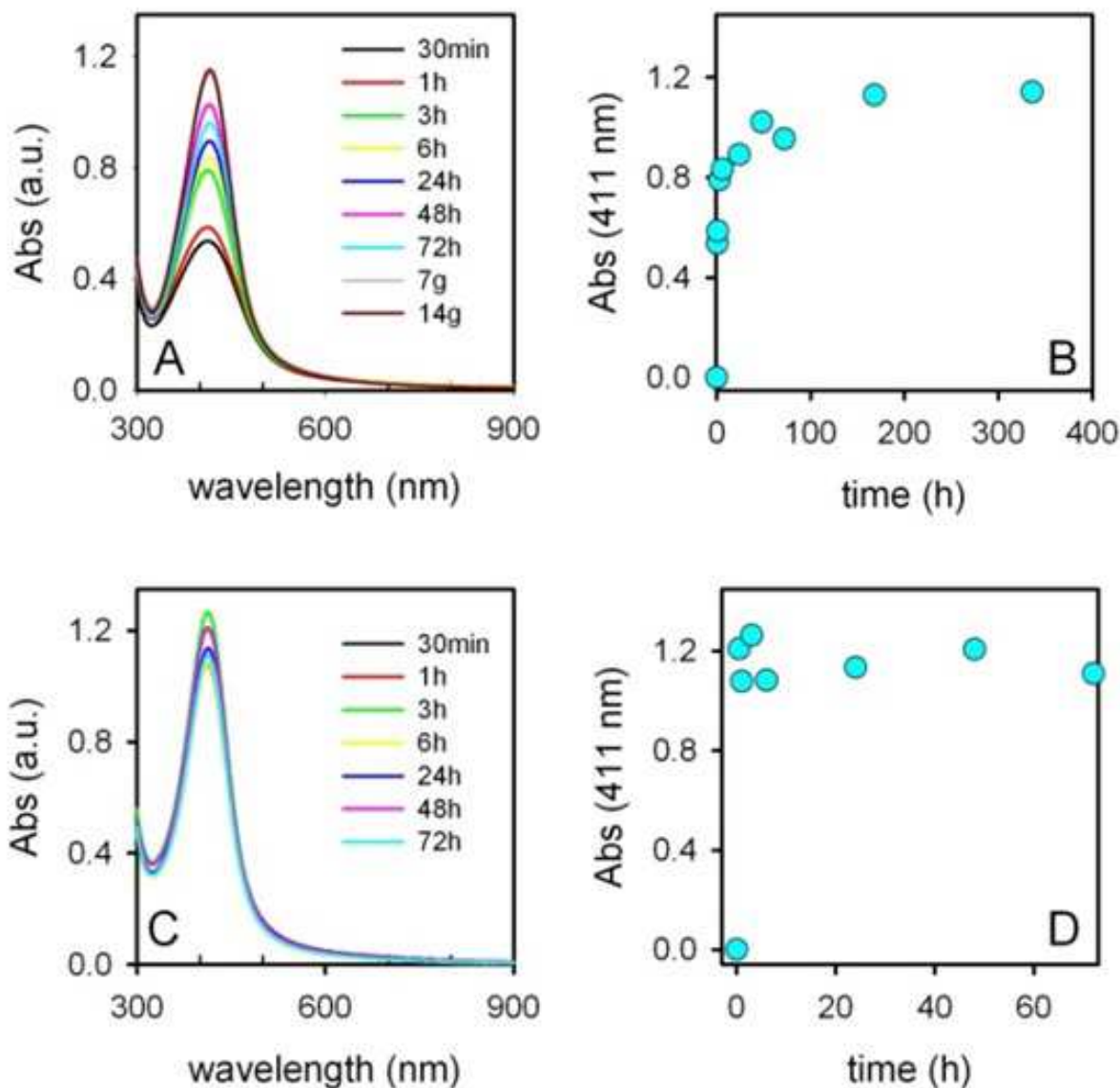
Figure 8 A and **C**: series of absorption spectra in a solution of pectin/Ag$^+$ at basic pH, at 20 °C (panel A) and at 60 °C (panel C); the time at which spectra were taken can be read by the color in the inset list. **B** and **D**: absorbance at the LSPR maximum (411 nm) vs time, obtained from the spectra of panel A and C, respectively.

Nanoparticles dimensional analysis was carried out on all preparations using Transmission Electron Miscroscopy. TEM measurements are shown in **Figure 9**, **Figure 11**, **Figure 13**. In addition, for each preparation, the dimensional count for the same images is reported, **Figure 10**, **Figure 12**, **Figure 14**.
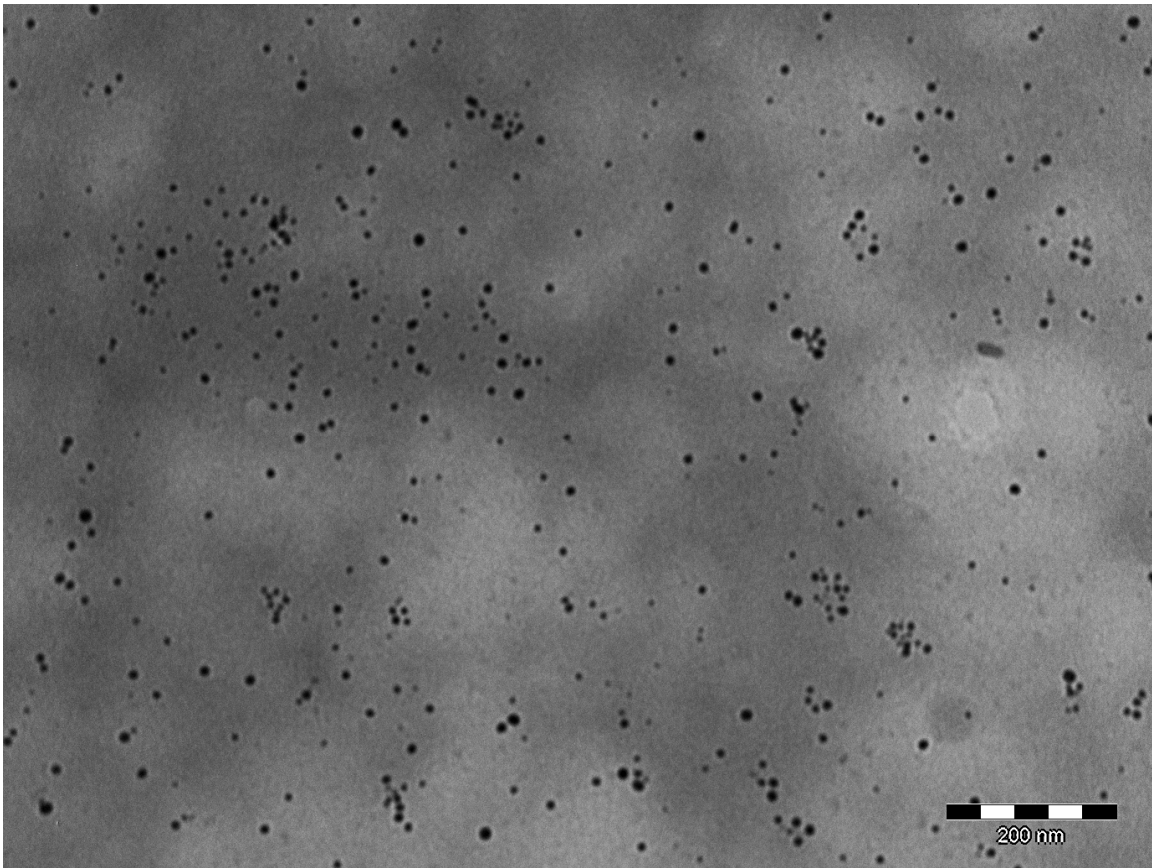
Figure 9 Example of TEM image for a 0.001M Ag$^+$, 1% pectin, 60 °C synthesis.

Count: 77	Min: 2.207
Mean: 8.348	Max: 16.405
StdDev: 2.999	Mode: 6 (10)
Bins: 100	Bin Width: 0.500
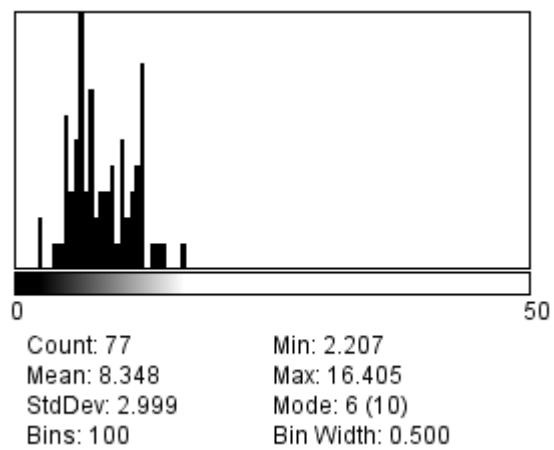
Figure 10 Dimensional counting from image in **Figure 9**.
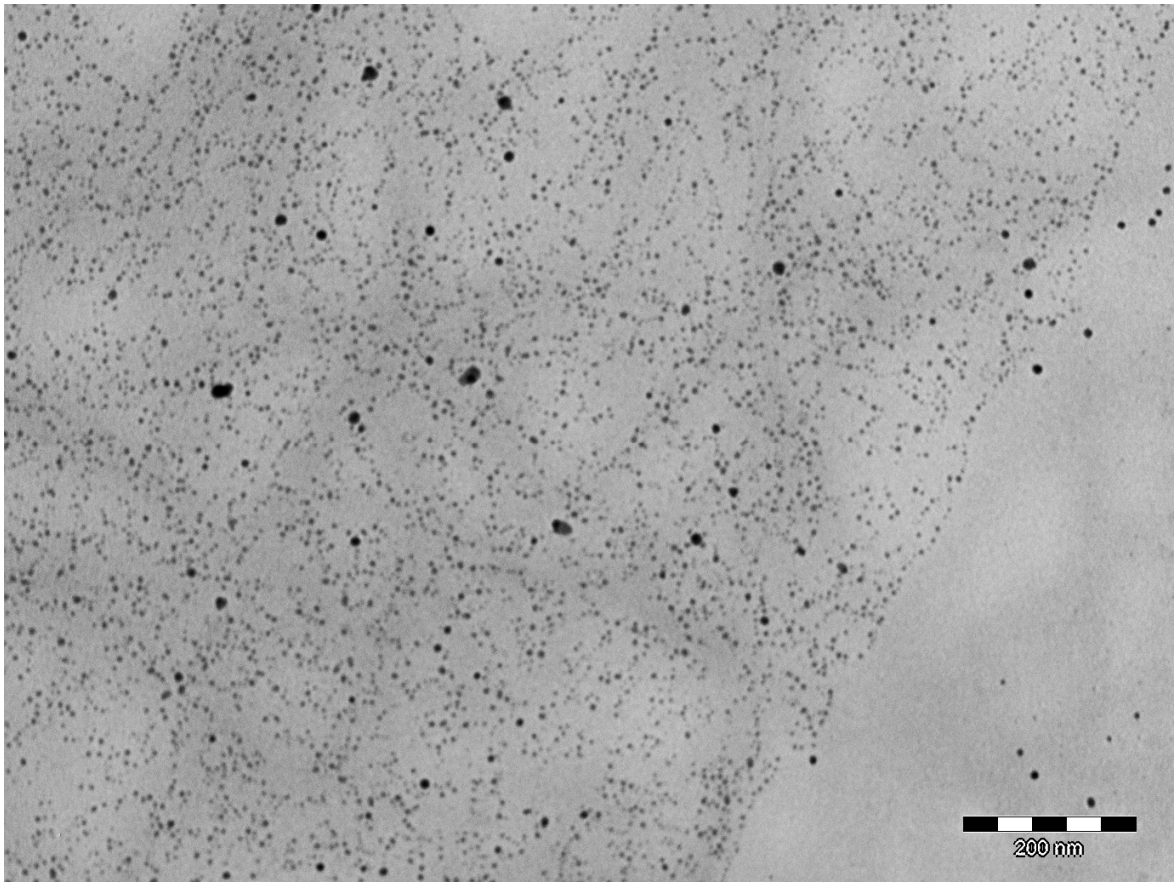
Figure 11 Example of TEM image for a 0.001M Ag$^+$, 0.5% pectin, 20 °C synthesis.
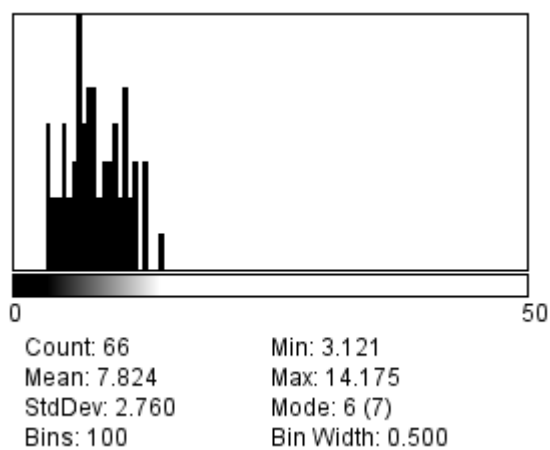

Count: 2970	Min: 2.207
Mean: 5.848	Max: 22.043
StdDev: 2.160	Mode: 5 (278)
Bins: 100	Bin Width: 0.500
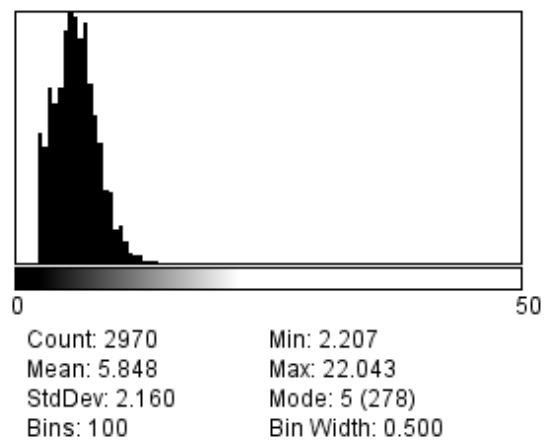
Figure 12 Dimensional counting from image in **Figure 11**.
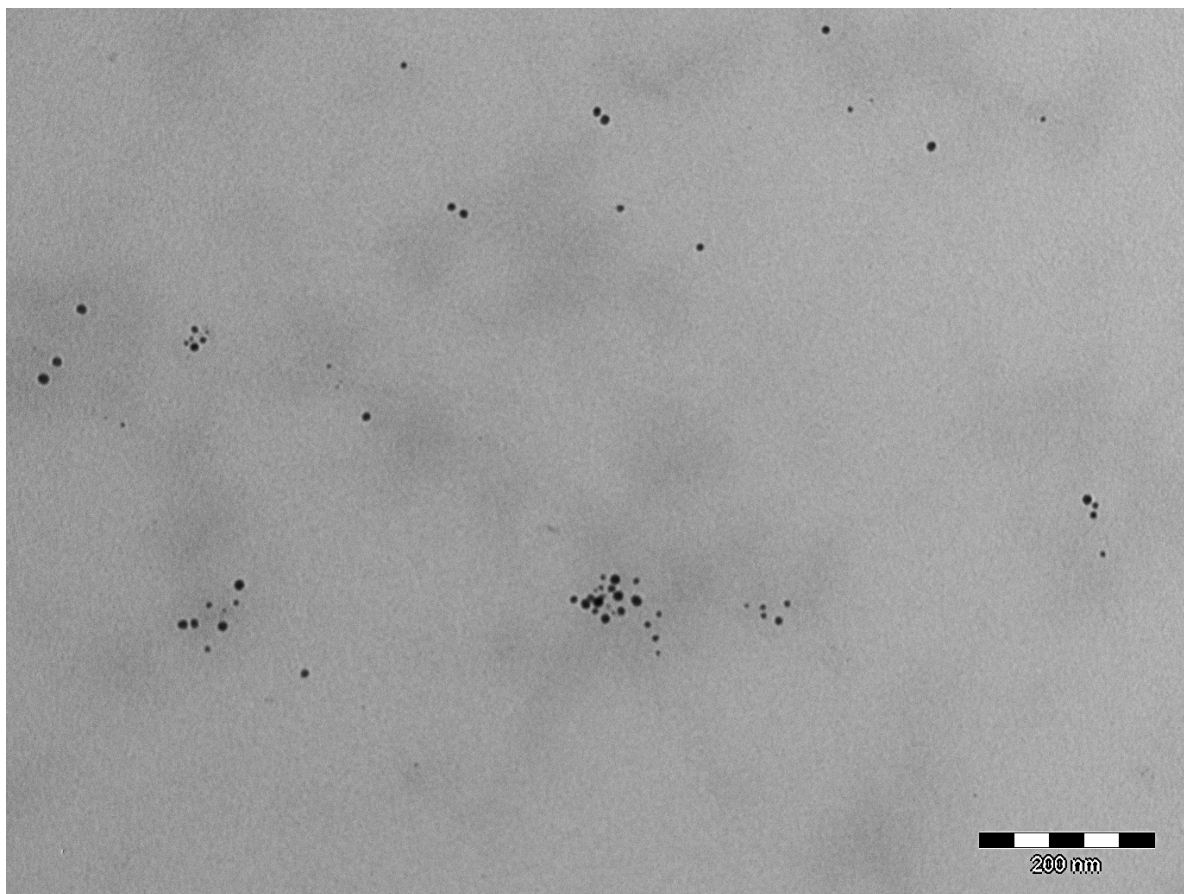
Figure 13 Example of TEM image for a 0.001M Ag$^+$, 2% pectin, 60 °C synthesis.

Count: 66   Min: 3.121
Mean: 7.824   Max: 14.175
StdDev: 2.760   Mode: 6 (7)
Bins: 100   Bin Width: 0.500

Figure 14 Dimensional counting from image in **Figure 13**.

With 0.001 M Ag$^+$ spherical AgNPs were observed with a ~ 8 nm average diameter, except for the case of 0.5% pectin and 20 °C, see growth took place.

Formation of AgNPs was efficient also at higher Ag^+ concentration, i.e. 0.01 M Ag^+, with slightly higher maximum absorption wavelength (415-420 nm) observed with preparations carried out with 0.5-2% pectin at 20 and 60 °C, as showed in **Figure 15.**
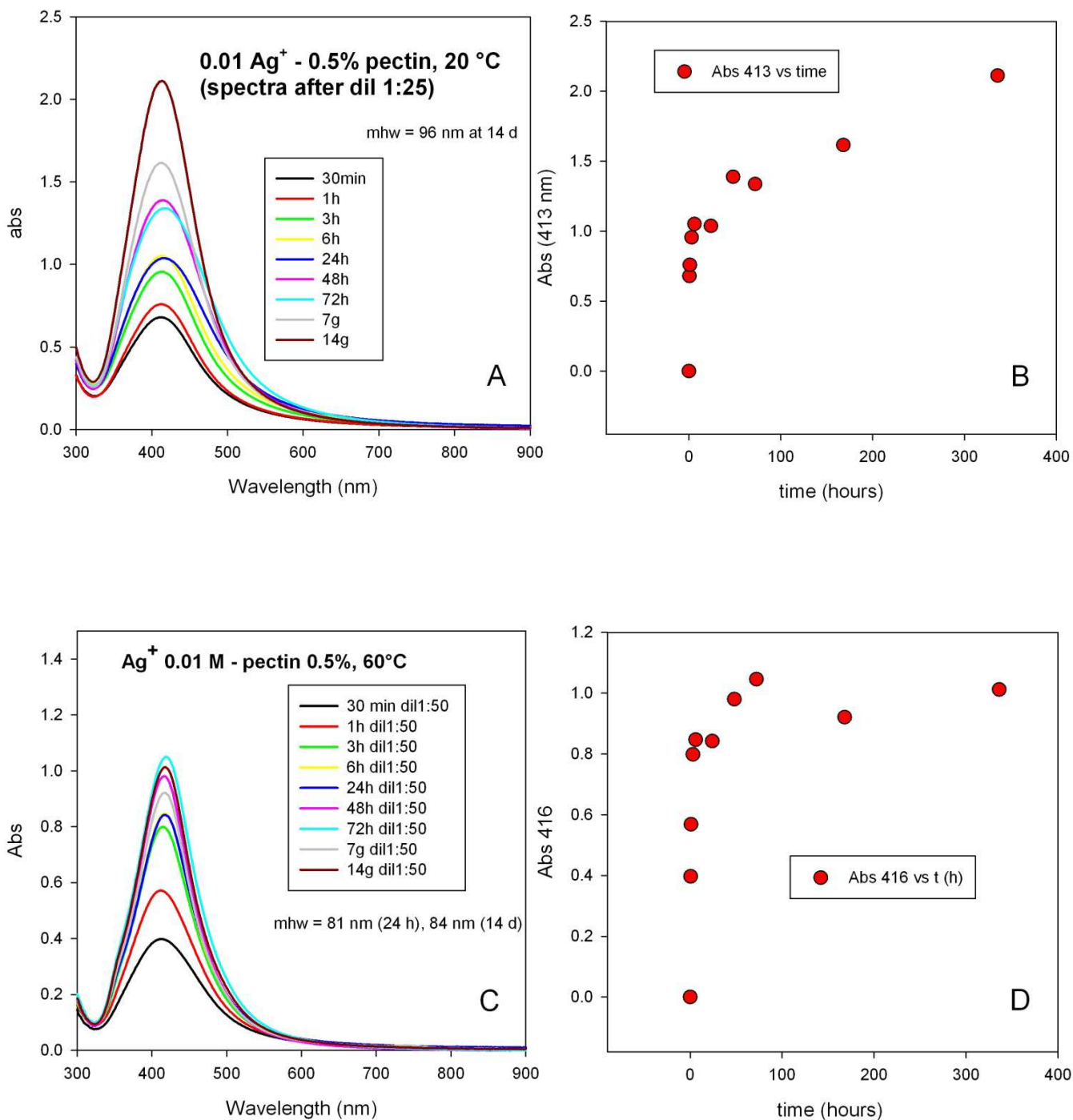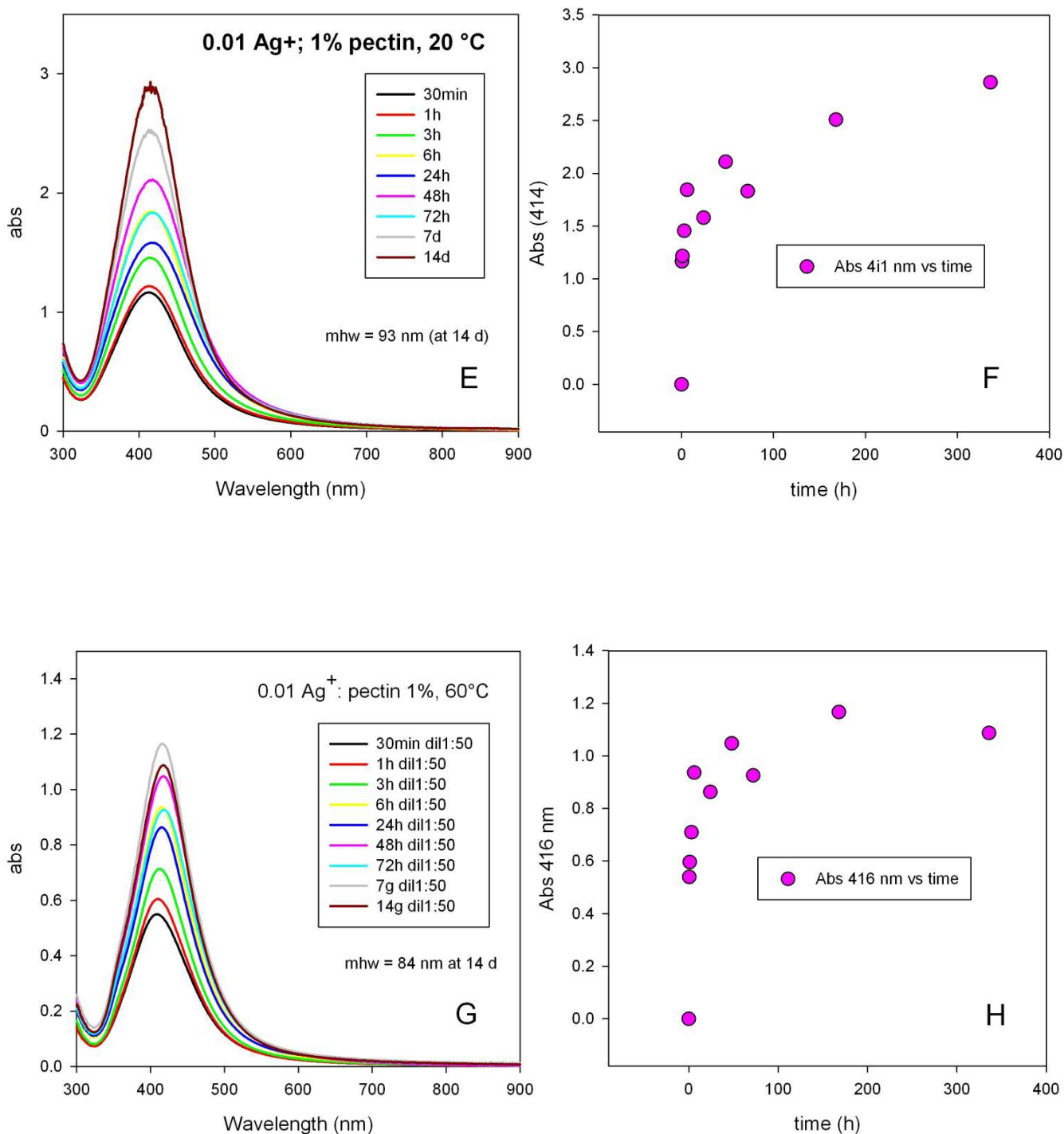
Figure 15 A, series of absorption spectra for 0.01 Ag+ in 0.5% pectin at 20 °C (from 30 min to 14 days). **B**, absorption at λmax (413 nm) vs time. **C**, series of absorption spectra for 0.01 Ag+ in 0.5% pectin at 60 °C (from 30 min to 14 days). **D**, absorption at λmax (416 nm) vs time. **E**, series of absorption spectra for 0.01Ag+ in 1% pectin at 20 °C (from 30 min to 14 days). **F**, absorption at λmax (414 nm) vs time.**G**, series of absorption spectra for 0.01Ag+ in 1% pectin at 60 °C (from 30 min to 14 days). **H**: absorption at λmax (416 nm) vs time.

Furthermore, also dimensional TEM characterizations of different preparations show a larger dimensional distribution, including the presence of large aggregates and non-spherical objects, as cen be observed in **Figure 16**, **Figure 18** and **Figure 20**. Even in this case, for each preparation, the dimensional count for the same images is reported, **Figure 17**, **Figure 19**, **Figure 21**.
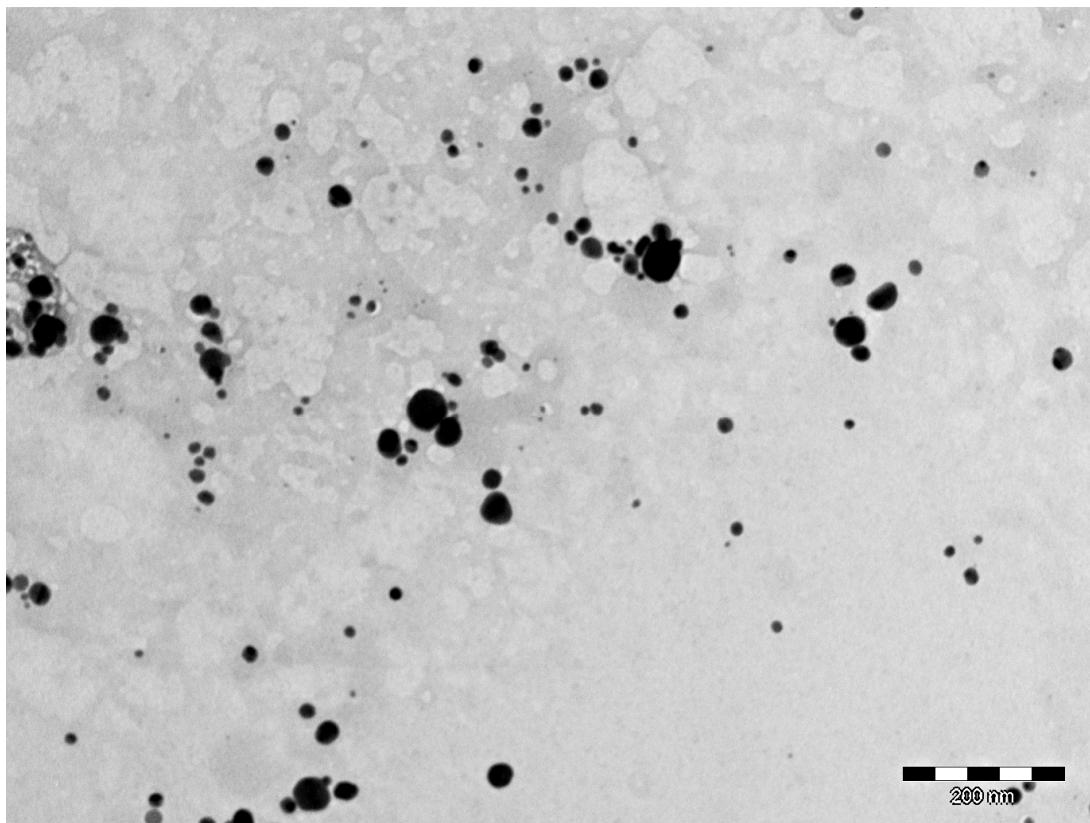

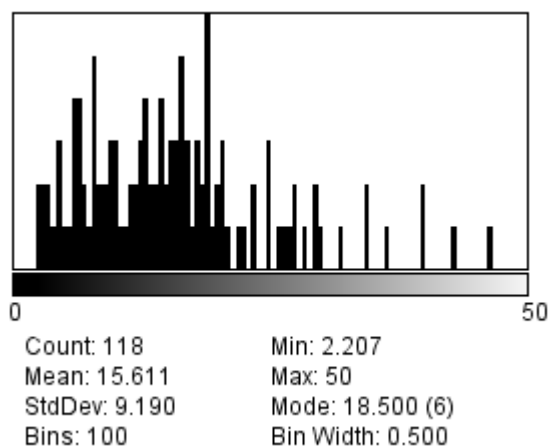**Figure 16** TEM image for synthesis with 0.01M Ag$^+$, 0.5% pectin, 60 °C.

Count: 118   Min: 2.207
Mean: 15.611   Max: 50
StdDev: 9.190   Mode: 18.500 (6)
Bins: 100   Bin Width: 0.500

Figure 17 Dimensional counting from from image in **Figure 16**.
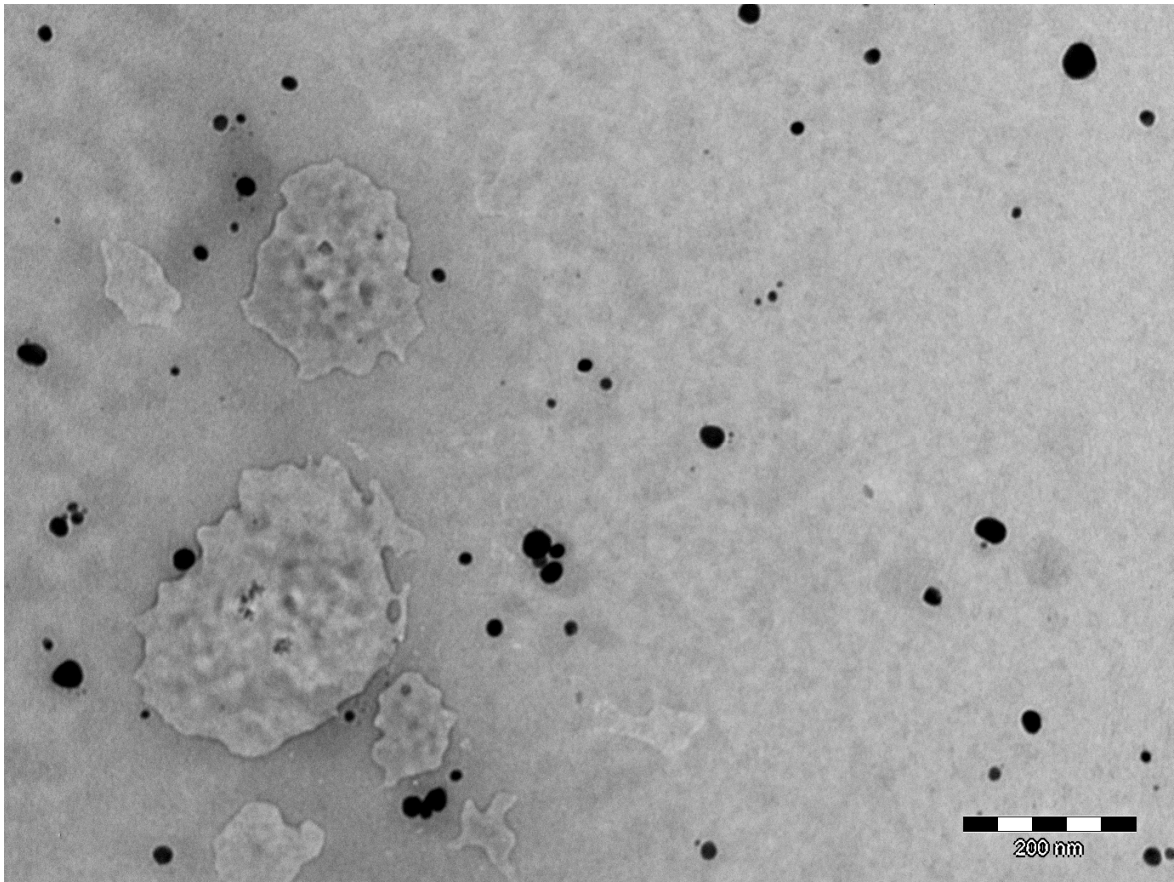
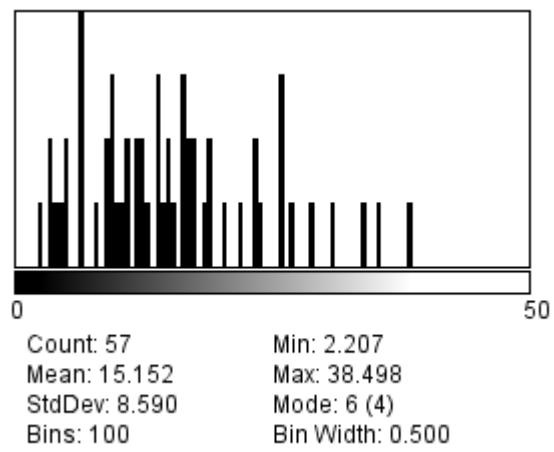**Figure 18** TEM image for synthesis with 0.01M Ag$^+$, 1.0% pectin, 60 °C.

Count: 57   Min: 2.207
Mean: 15.152   Max: 38.498
StdDev: 8.590   Mode: 6 (4)
Bins: 100   Bin Width: 0.500

Figure 19 Dimensional counting from from image in **Figure 18**.
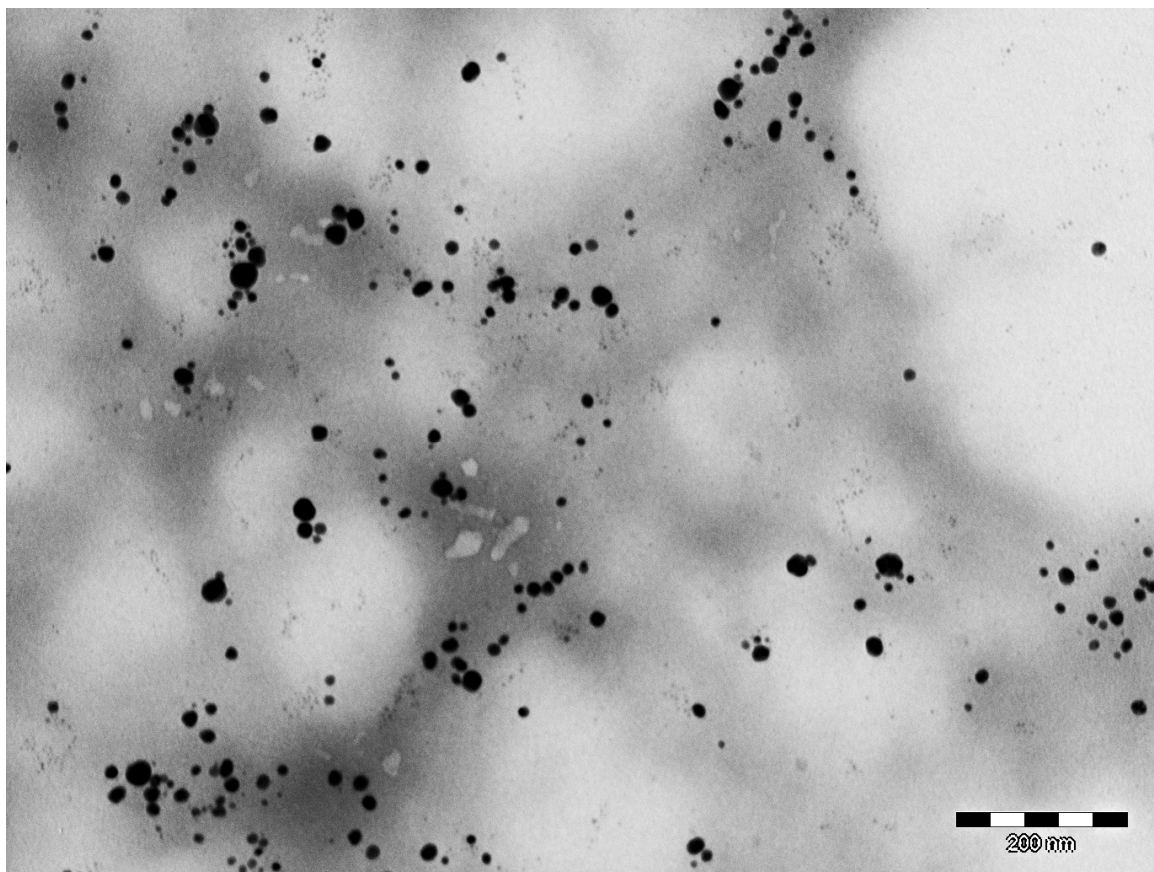
Figure 20 TEM image for synthesis with 0.01M Ag$^+$, 2.0% pectin, 60 °C.

Count: 215   Min: 2.468
Mean: 11.786   Max: 32.155
StdDev: 5.504   Mode: 6 (12)
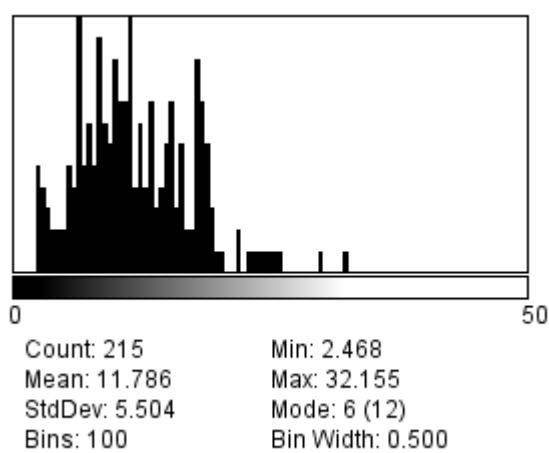Bins: 100   Bin Width: 0.500

Figure 21 Dimensional counting from image in **Figure 20**.

Since all the preparations with 0.001M Ag$^+$ seemed feasible for use in biomedical treatments, due to their reproducibility, narrow dimensional distribution and fast preparation time, we decided to

use the preparation with 1.0% pectin and 60 °C as our synthesis of choice, due to short completion time and best stability after preparation. In fact, as it is shown in **Figure 22**, the absorption spectra carried out after 1 day and after 14 days are perfectly superimposable, while preparations with 0.001 M and 0.5 or 2.0% pectin showed slight increases of the band width at half height after 14 days.
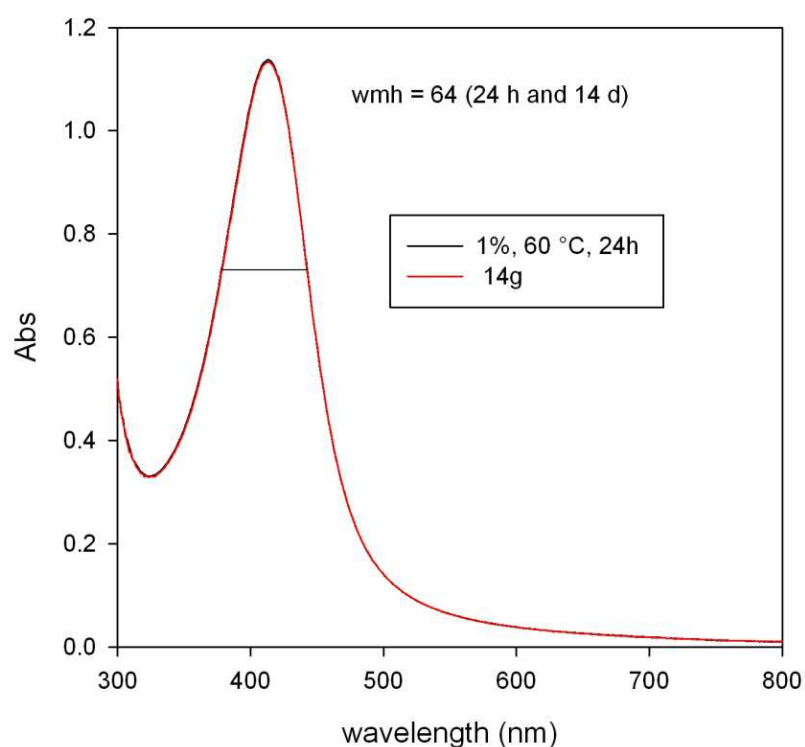

Figure 22 Absorption spectra for 1.0 % pectin, 0.001M Ag$^+$, 60°C 24h and 14 days.

Finally, the chosen synthetic conditions also assure high reproducibility, as it can be seen from the superimposition of absorption spectra from different preparations, as reported in **Figure 23**.
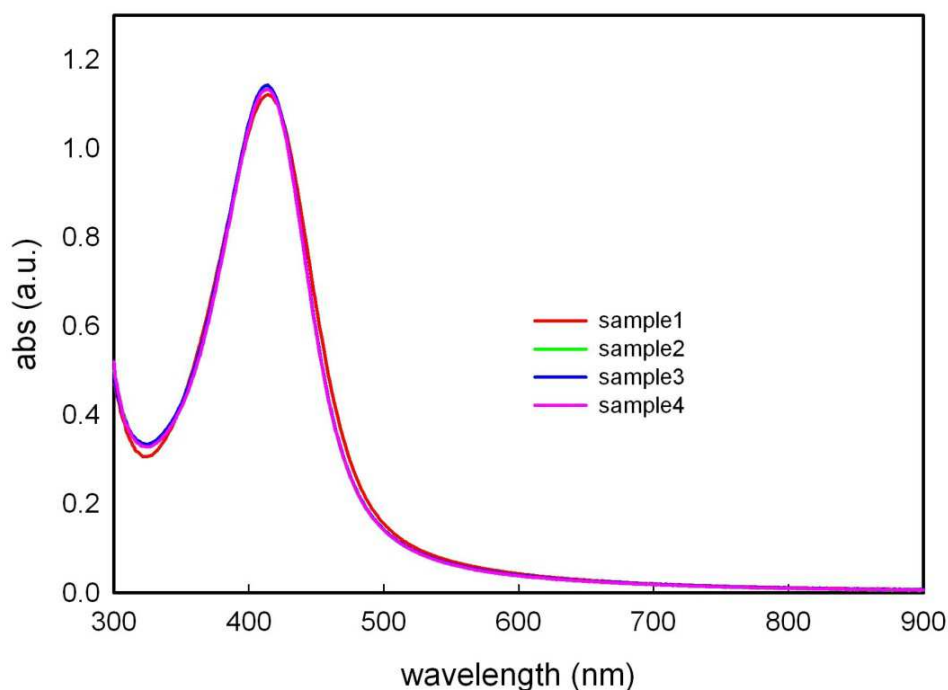
Figure 23 Absorption spectra from 4 different preparations with 0.001Ag$^+$, 1.0% pectin, 60 °C (24 h time).

The starting base concentration of 0.025 M NaOH was also used as a standard, as less basic conditions led to slower reaction or not complete Ag$^+$→ Ag(0) conversion.

We also controlled the p-AgNPs stability under three conditions on the 0.1% pectin 60 °C product: i) NaCl added as a solid at a 0.1 M concentration; ii) 0.1M HCl added until pH 7.4 was reached; iii) a 1:1 v/v mixture with PBS (phosphate saline buffer). In all cases no precipitation or turbidity was observed, with the shape of the LSPR band remaining unchanged under absorption spectra examination. Finally, as free Ag$^+$ may play a role in the antibacterial action of p-AgNPs or in its cytotoxicity, we examined the conversion yield of Ag$^+$ to Ag(0) in the preparations with 0.001 M Ag$^+$, 0.5-2.0% pectin and T = 20 °C and 60 °C.

Attempts to separate p-AgNPs from the solvent by ultracentrifugation were unsuccessful (with ultracentrifugation at 13000 rpm), and this prevented the use of the simpler technique of analysing free Ag$^+$ in the supernatant. We used instead an electrochemical method elaborated on purpose. The method allowed us to determine Ag(I) in pectin solutions, despite the presence of the polysaccharide. In fact, when known amounts of silver nitrate (from 0.1 up to 200 mg/L) were added to plain KNO$_3$ solution, 0,1%, 0,5%, 1% or 2% pectin solution, and a log [Ag$^+$] vs E (mV) plot

was performed, a straight line with Nernstian slope (ca 60 mV for tens time change in concentration) was observed in all cases,[61] both at <5 mg/L silver concentration and at >5 mg/L Ag^+ concentration, without changes in the slope of the curve.[62] A recovery >>95% of the silver added was observed in these condition by standard addition method. This prove that both the silver complexed by the macromolecule and the free ion are determined with this method.[63] In these conditions, a LOD of 0.1 mg/L was found. Briefly, potentiometric measurements of free Ag^+ were carried out with the standard additions technique. A calibration curve was calculated using the same pectin concentrations and adding measured Ag^+ quantities. In the case of the calibration curve, measurements were carried in few minutes (< 5) after additions and with no added base, to rule out p-AgNPs formation (no yellow color was noticed under these conditions).

When examining the free Ag^+ found in p-AgNPs preparation after 12 h reaction time, a concentration ≤ 1 ppm was found in all cases, corresponding to ≤ 1% of the overall starting Ag^+, i.e. a complete conversion (> 99%) for 0.001M Ag^+ in 0.5-2.0% pectin. In particular, in the preparation with 0.001 M Ag^+ and 1.0% pectin at 60 °C, 0.79 ppm ($7.38*10^{-6}$ mol/L) of free Ag^+ were found, corresponding to the 0.74% of the total Ag. **Table 2** shows % of free Ag^+ found after each preparation. Calibration curves and determination of free Ag^+ for each preparation are shown respectively in **Figure 24**, **Figure 25**, **Figure 26** and **Figure 27.**

%pectin	0.5		1.0		2.0	
T (°C)	20	60	20	60	20	60
% Ag^+	0.946	1.34	-[a]	0.198	<0.1	0.47

Table 2 % of free Ag^+ (total Ag = 0.001 M) [a]not determined.

[61] United States Dep of Commerce, NIST,Maurice H. Stans,Lewis N. Branscomb, Ion-Selective Electrodes, Maryland, 1969, p 59 and following; p 380 and following).
[62] T. W. Bresnahan, C.L. Grant, J.H. Weber, *Anal. Chem.*, 1978, **50**, 1675.
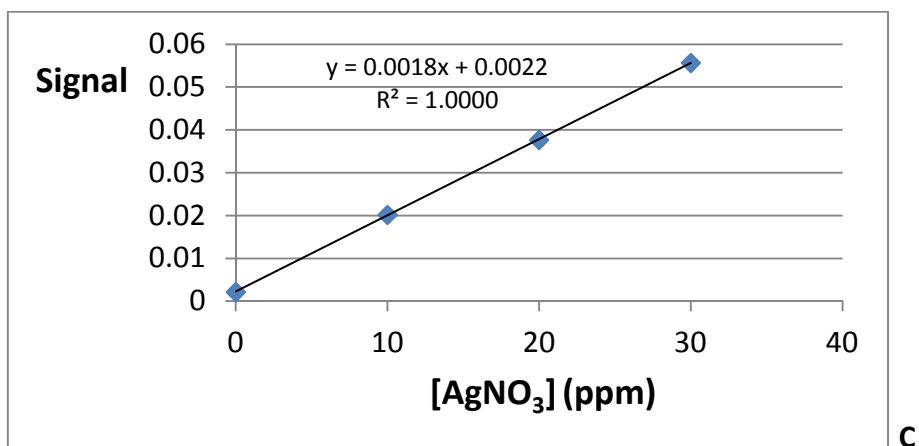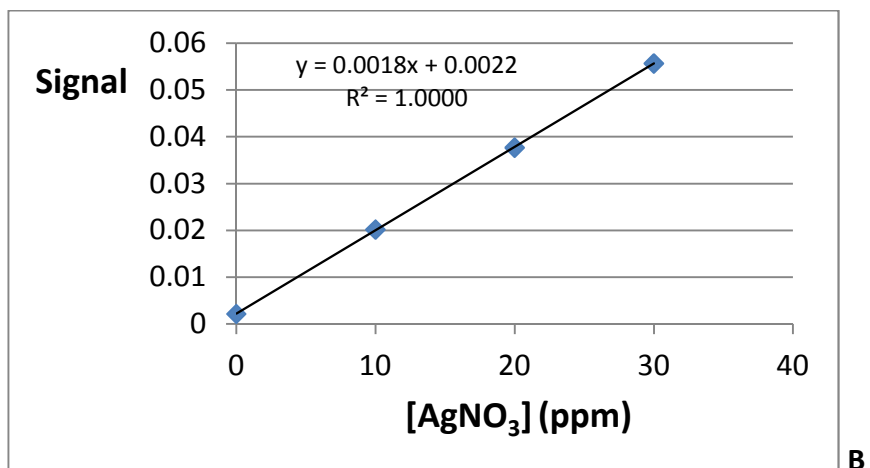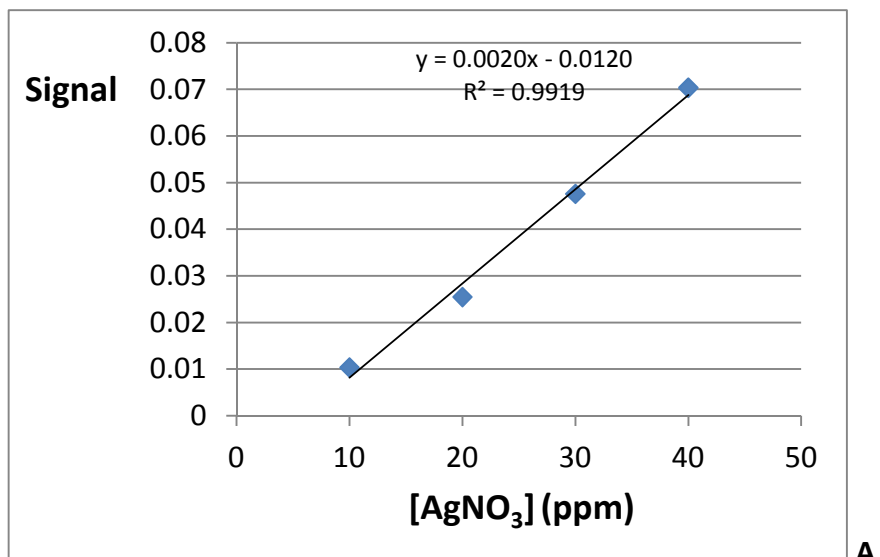[63] R. Kataky, M.R. Bryce, B. Johnston, *Analyst*, 2000, **125**, 1447.

Figure 24 Calibration curves in 0.5% (**A**), 1.0% (**B**), 2.0% (**C**) pectin, as DPV signal intensity vs added AgNO$_3$ (in ppm).

0.5% pectin, 10⁻³ M Ag⁺, 20°C

$y = 0.0005x + 0.0009$
$R^2 = 0.9798$

A

0.5% pectin, 10⁻³ M Ag⁺, 60°C

$y = 0.0003x + 0.0007$
$R^2 = 0.9929$

B

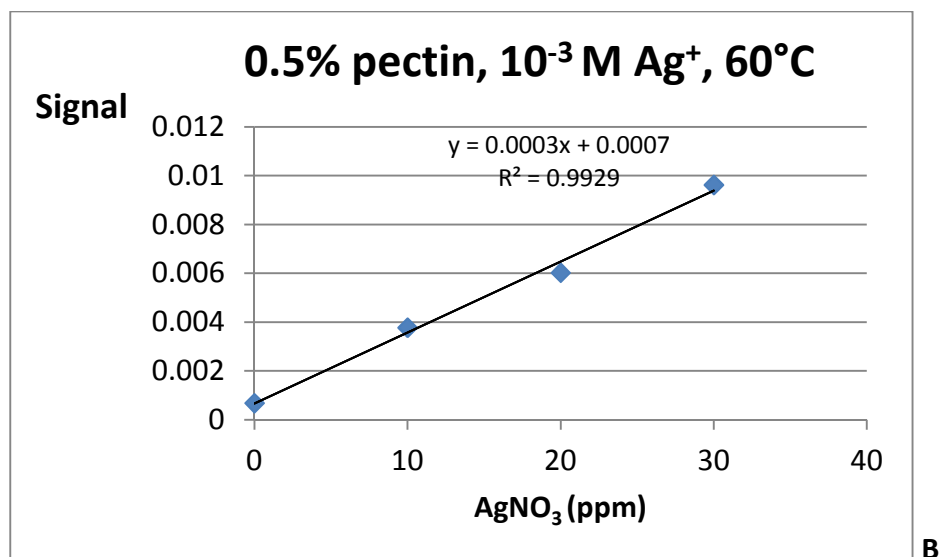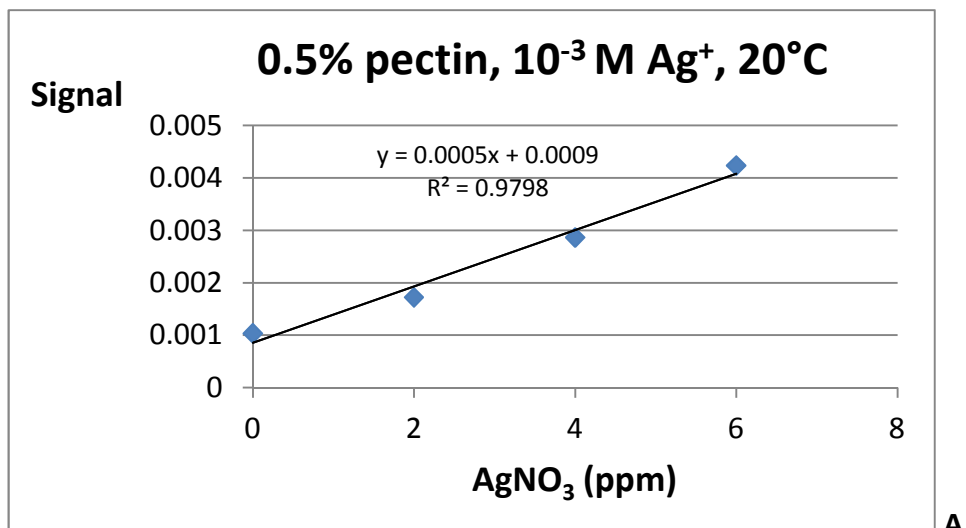**Figure 25** Determination of free Ag^+ in syntheses with 0.001M Ag^+, 0.5% pectin, carried at T = 20 °C (**A**) and 60 °C (**B**). DPV signal intensity vs added $AgNO_3$ (in ppm).
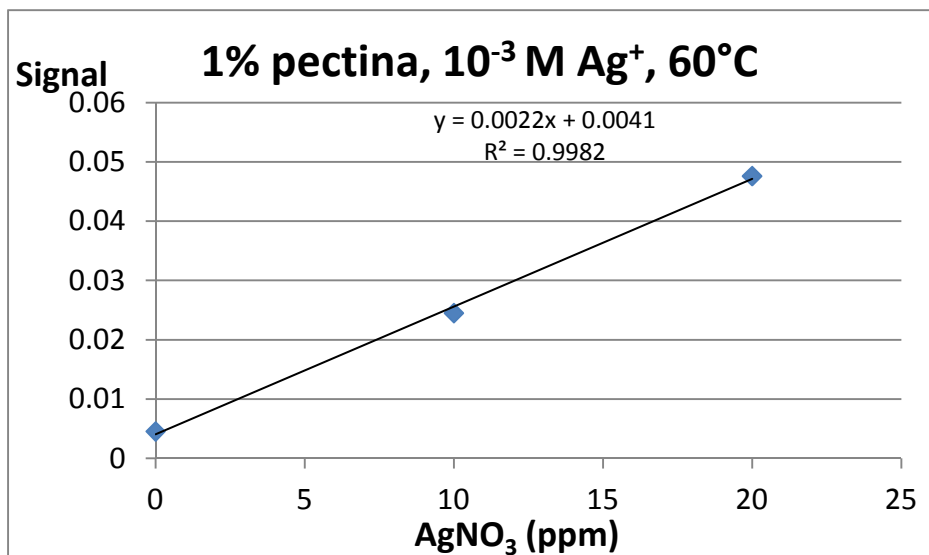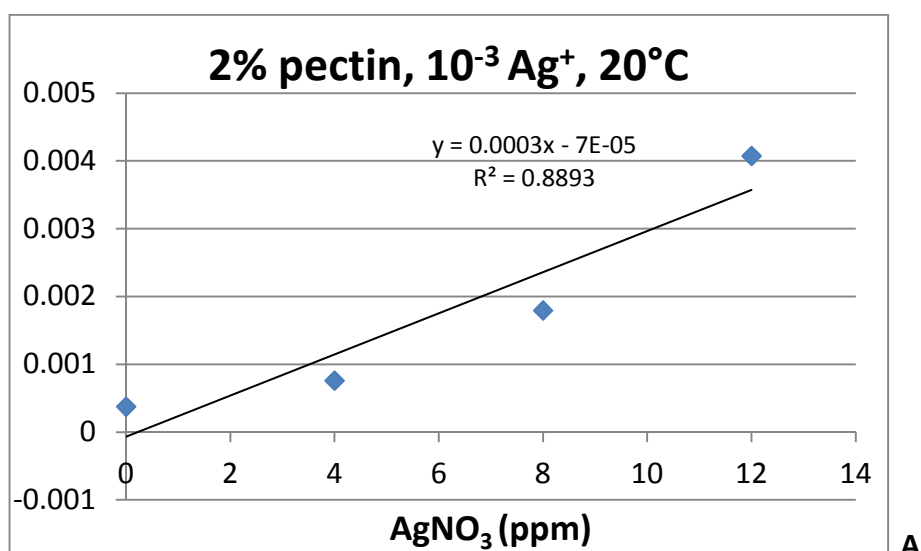
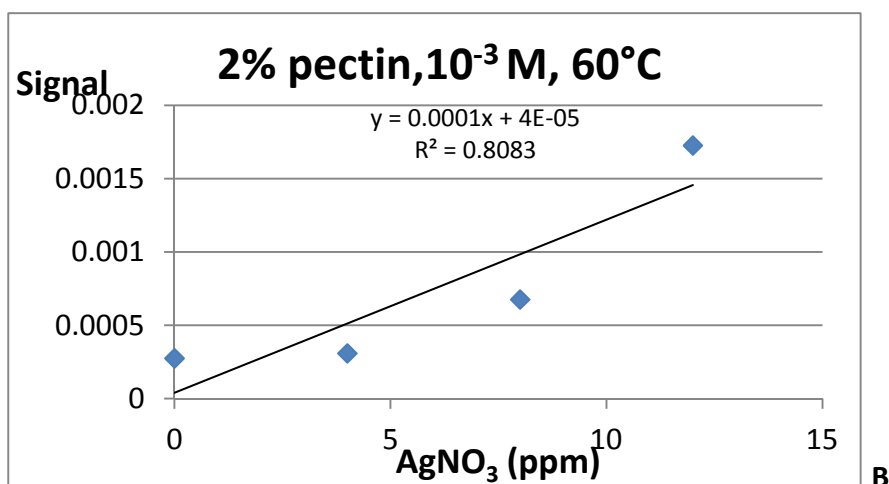**Figure 26** Determination of free Ag$^+$ in synthesis with 0.001M Ag$^+$ 1.0 % pectin, 60 °C.

A

Figure 27 Determination of free Ag^+ in synthesis with same, in 2.0 % pectin, synthesis carried out at 20 °C (**A**) and 60 °C (**B**).

3.2.2.2. Qualitative Reaction Mechanism and Product Characterization

The qualitative reaction mechanism of the synthesis was investigated by FT-IR spectroscopy,as showed in **Figure 28**. The spectrum of commercial pectin powder, black line, shows a carbonyl absorption band at ~ 1735 cm^{-1} that is due both to the carboxylic acid and to the ester groups of pectin. A less intense band at 1608 cm^{-1} can be attributed to the presence of some deprotonated carboxylic acid groups. Finally, a large absorption at > 3000 cm^{-1} is due to adsorbed water and to –OH stretching. Pure pectin (1% w/w) was treated with base (NaOH 0.025 M, pH 10.5-11.00) for 6 h at 60 °C, then isolated as described in the experimental (briefly: precipitation by 1:10 dilution in ethanol, followed by ultracentrifugation). In its FT-IR spectrum, red line, the band at 1735 cm^{-1} has disappeared, while the band at 1608 cm^{-1} is increased. Under these conditions all the –$COOCH_3$ ester groups are hydrolyzed to –COOH, and all –COOH groups are in their carboxylate form. The FT-IR spectrum of the p-AgNPs product, blue line, obtained with 0.001 M Ag^+, 1.0% pectin and T 60 °C (isolated af for hydrolyzed pectin) is very similar to that of the pure pectin treated under the same conditions but in the absence of Ag^+. This is not surprising, as in the used synthetic conditions it may be calculated that the added $5*10^{-5}$ mol Ag^+ has $2.35*10^{-3}$ mol of galacturonic acid available for reaction (considering, as an approximation, pectin composed only by the latter). If the secondary alcohol groups are responsible of the Ag^+ reduction, only 1/100 of the galacturonic acid units would react with Ag^+, this resulting in negligible spectral changes. To further investigate this point we run the Ag^+-pectin reaction at 60 °C also in 1:1 silver/galacturonic

acid conditions, i.e. 0.5 g pectin (2.35×10^{-3} mol of galacturonic acid) in 50 mL water, with 0.400 g (2.35×10^{-3} mol) $AgNO_3$, at pH 10.5. Also in this case abundant formation of p-AgNPs was observed, as an orange-brown slurry formed. Isolation and drying of the product with the same work up gave a powder whose FT-IR spectrum is displayed in **Figure 29**, green line. In this case, beside an increase of intensity of the carboxylate band and a decrease of the OH stretching band, a band at 1730 cm^{-1} is clearly present. This may be attributed to the oxidation of the diol moiety of the galacturonic acid units to dihaldehyde, reducing Ag^+ to Ag according to the scheme described in **Figure 7** and, in more detail, to Reaction (1)

$$\text{R-CH(OH)-CH(OH)-R} + 2Ag^+ \rightarrow 2\ \text{RCH=O} + 2Ag + 2H^+ \qquad (1)$$

The determination of pH before and after the synthesis completion also agrees with this kind of reaction (and of course with hydrolysis of ester groups and –COOH deprotonation). We found final pH values 8.40-8.80 in all preparations, starting from pH values 10.5-11.0. Attempts to prepare p-AgNPs without base addition resulted in no AgNPs formation.
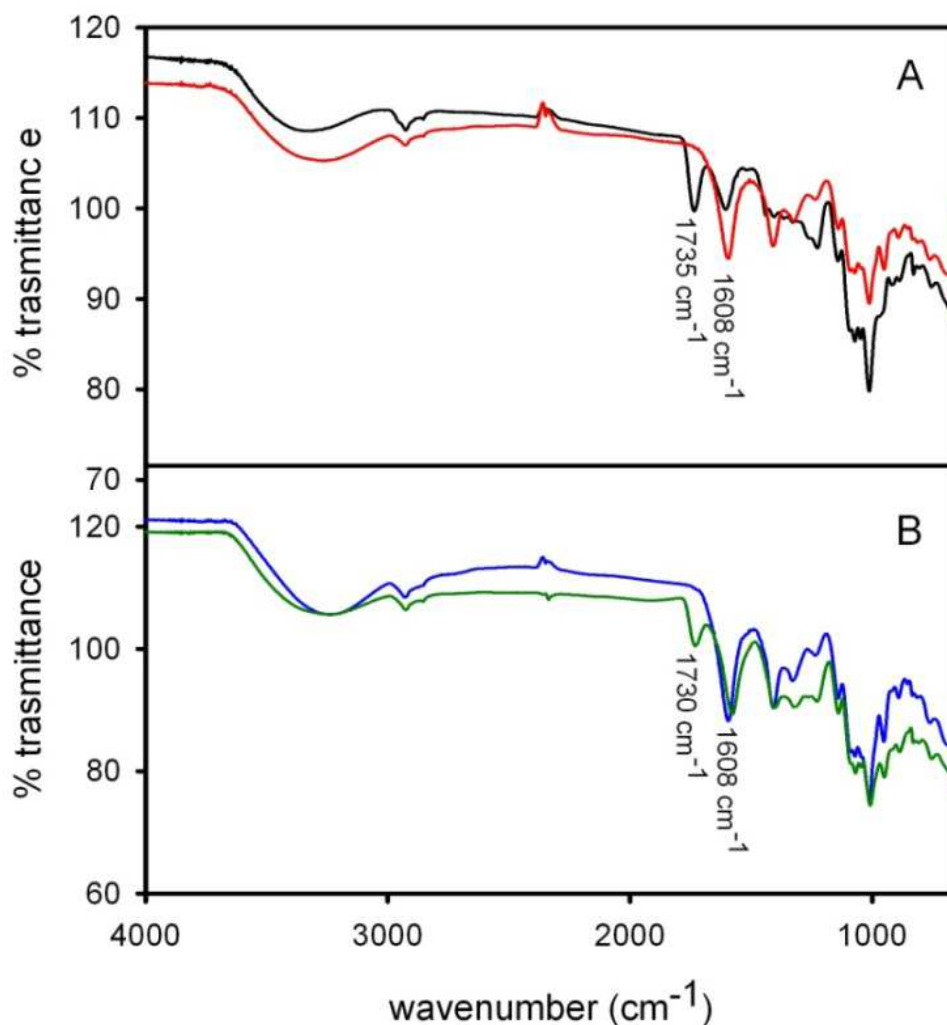
Figure 28 IR spectra. **A**: pectin as such, black; pectin after treatment at pH 12, 50 °C, red. **B**: p-AgNPs product under standard synthetic conditions (Ag$^+$ 0.001 M, 1.0% pectin, 60°C), blue); same, but with excess Ag$^+$ (equimolar with galacturonic acid units), green. The wavenumber of the relevant bands are reported in the figure.

The solid dry p-AgNPs isolated from the standard preparation (1% pectin, 10^{-3}M Ag$^+$, 60 °C) has been examined with coupled DSC and TGA experiments, finding 3.5% weight Ag. In the starting mixture Ag is 1.1% w/w with respect to pectin. The 3-fold increase confirms that pectin is in large excess and most of it does not interact with AgNPs and is eliminated during the isolation work up. Pure pectin sample's thermogravimetric analysis was performed first and is reported in **Figure 29**. It shows a mass loss of about 7.3 wt % below 100 °C, that could be due to the release of the adsorbed water. Starting from 450 °C, a huger mass loss is evident, characterized by three overlapping steps with different kinetics, with the last one not yet ended at the maximum temperature reached in the measurement. At the end of the heating ramp, the total mass loss is

of 95.2 wt %. The residual powder (4.8 wt %), analysed by XRPD, gives a signal characteristic of an amorphous phase and could be constituted by residual carbonaceous materials.
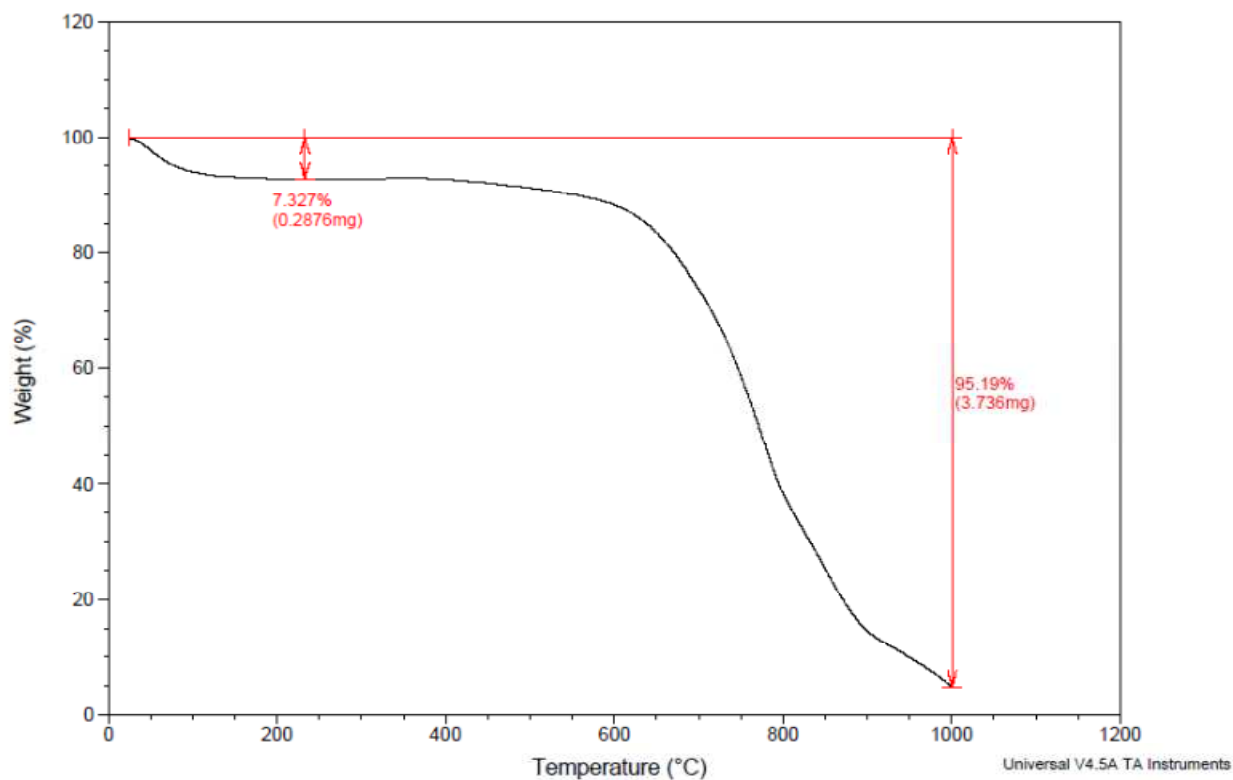

Figure 29 Pure pectin thermogravimetric analysis.

For the TGA-DSC measurements on a p-AgNPs sample, the thermogravimetric curve (black line in **Figure 30**) shows, after the mass loss due to the water adsorbed release (about 13 %), a two steps decomposition process, with the first stage starting fast at 150 °C and ending with a very slow tail at 500 °C and the slower second one from 650 °C to 1000 °C. The residual mass (not constant, like for the pure pectin sample) at the end of the measurement is 8.5 wt %. Considering a residual mass loss for pure pectin of about 5 wt % as seen in **Figure 29** we can estimate an amount of metallic Ag of 3.5 wt%. In the calorimetric profile (blue line in **Figure 30**), a more pronounced exothermic peak and a wide endothermic signal in correspondence of the beginning and the end of the first mass loss step and some small endothermic peaks underlying the second decomposition step are evident. A small endo peak with onset point at 955 °C and centred at 960

°C is evident. Being Ag a calorimetric standard melting at 961.78 °C,[64] the above quoted peak can be attributed to the melting of the small amount of metallic Ag in the preparation. Starting from the melting enthalpy of pure Ag (104.4 J/g; http://www.tainstruments.co.jp/application/pdf/Thermal_Library/Applications_Notes/TN011.PDF) and the measured enthalpy for the above descrive peak (3.5 J/g), an amount of Ag of about 3.35 wt % can be estimated, in very good agreement with the deduction made starting from TGA data. The presence of crystalline metallic Ag is confirmed also by the XRPD analysis performed on the residual powder.
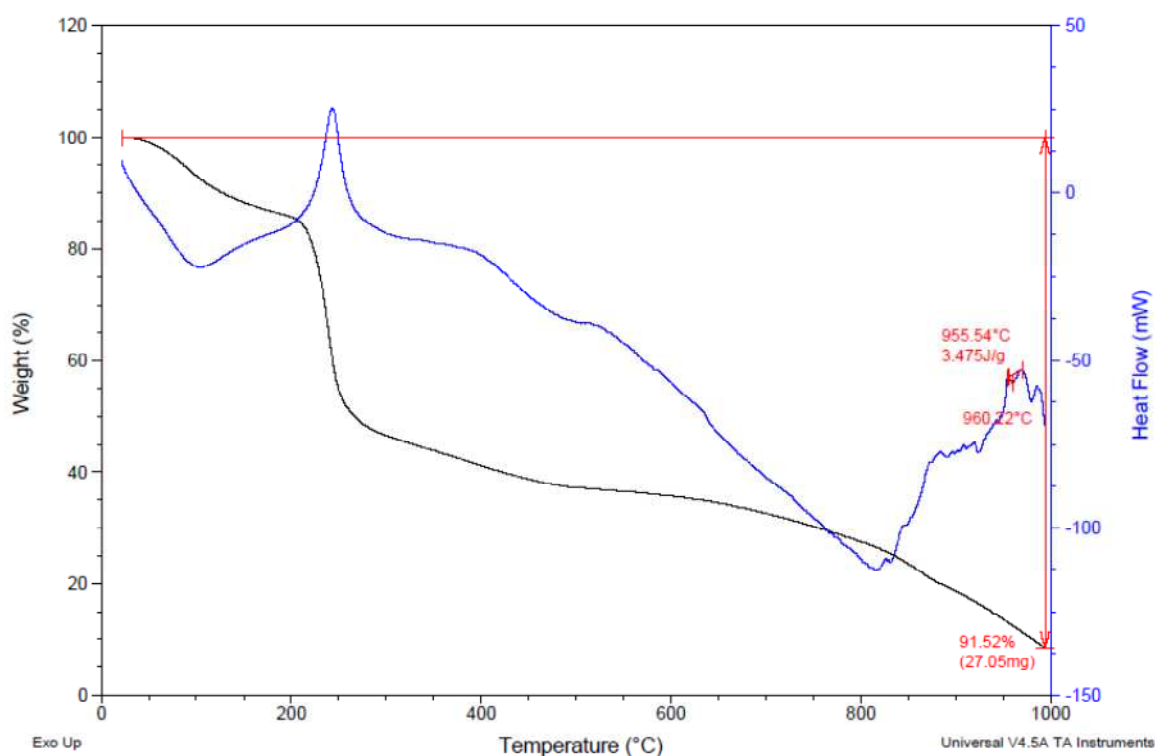
Figure 30 TGA (black line) and DSC (blue line) profiles for dry p-AgNPs.

As reported in **Figure 31**, X ray diffraction fully confirms the nanocrystalline nature of the p-AgNPs in the pectin matrix. Debye–Scherrer analysis and Rietveld refinement found nanocrystallites dimensions of 7.5 nm, in excellent agreement with the p-AgNPs dimensions determined by TEM. Powder x-ray diffraction was run on samples prepared with the standard protocol (0.001M

---

[64] H.P. Thomas, *Metrologia*, 1990, 27, 3.

Ag+/1% pectin/ 60°C) and 1:1 Ag/pectin molar ratio, i.e. 0.5 g pectin ($2.35*10^{-3}$ mol of galacturonic acid) in 50 mL water, with 0.400 g ($2.35*10^{-3}$ mol) $AgNO_3$, at pH 12, 60 °C. Powders were isolated as described in the experimental for the thermal characterization. Nanocrystalline cubic silver was found in both cases (COD 1509146; spatial group F m -3 m; a = 4.071 Å; V = 67.469 Å3). We were able to determine the average crystallite dimension only in the 1:1 sample. Calculation with Debye–Scherrer formula gave 75 Å, a value confirmed also by Rietveld analysis with the MAUD program (74.5 ± 2 Å).
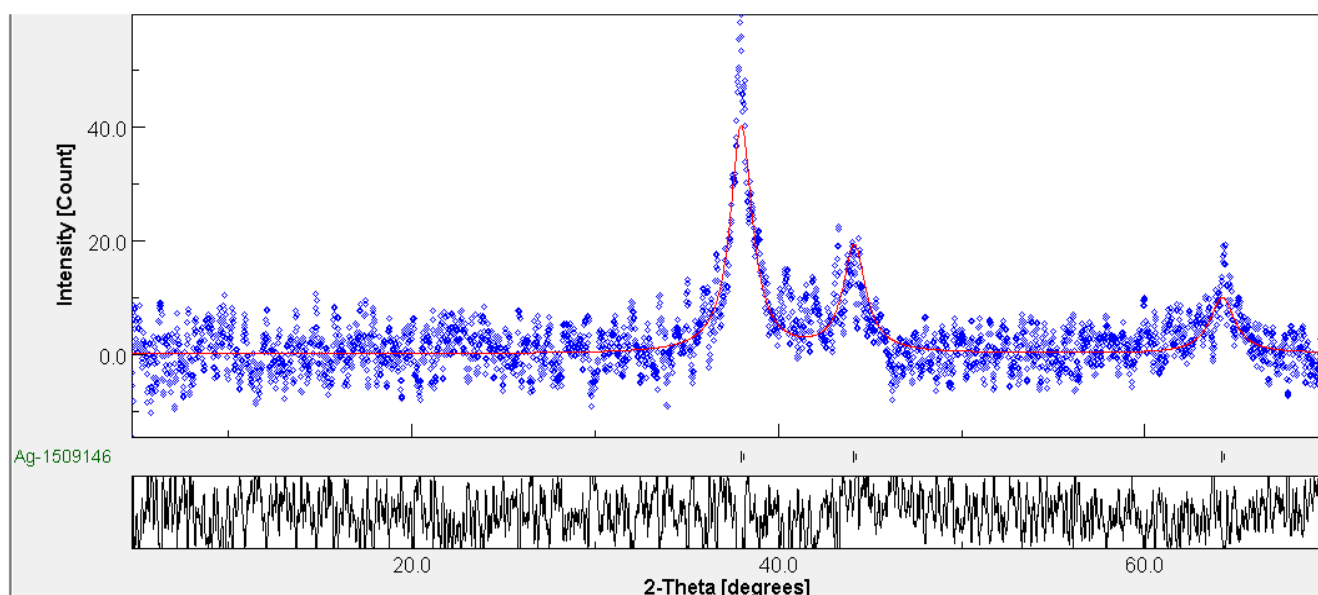
Figure 31 X-ray diffraction for dry p-AgNPs.

Dynamic Light Scattering and P_z measurements carried out on freshly prepared p-AgNPs (0.001 M Ag^+, 1.0% pectin, 60 °C), found instead large objects with average diameters 170-180 nm and with P_z = -50 mV. Examining the TEM images (obtained from p-AgNPs solutions diluted 1:10), see **Figure 9**, grouped AgNPs may be distinguished, although with 2-5 nm inter particle distance (in agreement with the absence of bands at λ > 410 nm), while the poorly electron dense pectin cannot be imaged with TEM. We could hypothesize that the large objects observed with the DLS technique correspond to several AgNPs grouped by one or more pectin polymer chains.

3.2.2.3 Antibacterial and Antibiofilm Activity of p-AgNPs

The effect of p-AgNPs prepared from 1 mM Ag$^+$ in 1% pectin at 60 °C was tested on the viability of two different bacterial strains, *Escherichia coli* PHL628 Gram-negative and *Staphylococcus epidermidis* RP62A Gram-positive. The effect was first evaluated in liquid culture conditions at various concentrations of p-AgNPs. The concentration of Ag(0) in the p-AgNPs solutions was assumed to be 1 mM, following the potentiometric determination of free Ag$^+$ that revealed ~100% Ag+→Ag(0) transformation. Successive geometric v/v dilution of p-AgNPs bulk solutions with TSB allowed treatments at 500, 250, 125, 62.5, 31.25 and 15.625 µM Ag concentration.

The obtained MIC values are summarized in **Table 3**.

	E. coli PHL628		*S. epidermidis* RP62A	
	6h	24h	6h	24h
p-AgNPs[a]	15.62 µM	31.25 µM		500 µM
Ag$^+$ (AgNO₃)	-[b]	125 µM	-[b]	125 µM
gsh-AgNPs[c]	-[b]	140 µM	-[b]	1680 µM[d]

Table 3 MIC values for p-AgNPs and ionic silver in liquid culture conditions. [a]experiments were repeated two times on two different p-AgNPs preparations, with identical results; [b]MIC for Ag$^+$ was not determined at 6h; [c]values from ref[65]; [d]data obtained with *S. aureus*.

The complete trends of viability vs Ag concentration are reported in **Figure 32**.

[65] E. Amato, Y.A. Diaz-Fernandez, A. Taglietti, P. Pallavicini, L. Pasotti, L. Cucca, C. Milanese, P. Grisoli, C. Dacarro, J.M. Fernandez-Hechavarria, V. Necchi, *Langmuir*, 2011, **27**, 9165.
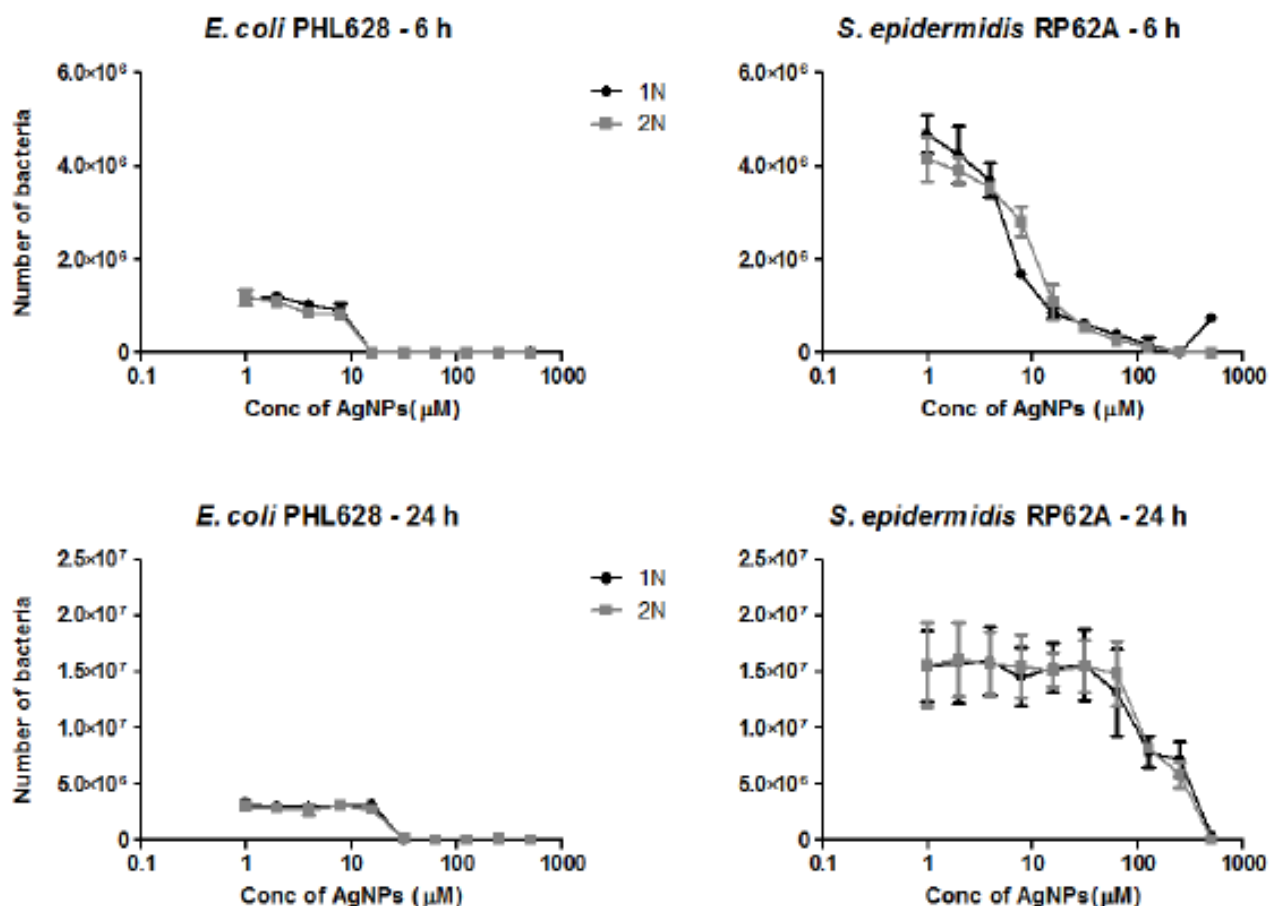
Figure 32 Viability (number of viable bacteria) of *E. coli* PHL628 and *S. epidermidis* RP62A in liquid culture conditions at two different time points (6 hours, upper row, and 24 hours, lower row) as a function of Ag concentration from a 10^{-3}M (in Ag) p-AgNPs solution.

MIC for p-AgNPs was 31.25 µM for *E. coli* PHL628 and 500 µM for *S. epidermidis* RP62A after 24 h incubation. Working on colloidal solutions of glutathione-coated AgNPs (gsh-AgNPs) of comparable dimensions (d = 7 nm), it was previously found in ISB (Iso-Sensitest Broth, Oxoid, England) at pH = 7 a MIC value of 140 µM for *E. coli* ATCC 10536 and of 1680 µM for *S. aureus* ATCC 6538, after 24 h incubation.[65] Values are included in **Table 3** for comparison. While the greater resistance of Gram-positive bacteria to silver is well-known in literature[66,67] and is confirmed in the present work, the lower MIC values found here with respect to gsh-AgNPs prompted us to determine as a control the MIC of ionic silver (from AgNO$_3$ 1 mM aqueous solution) under the same experimental conditions. The MIC for Ag$^+$ was 125 µM for *E. coli* PHL628 and *S. epidermidis* RP62A, on colonies incubated for 24 h.

[66] Q.L. Feng, J. Wu, G. Q. Chen, F.Z. Cui, T. N. Kim, J.O. Kim., *J. Biomed. Mater. Res.*, 2000, **52**, 662.
[67] K.J. Woo, H.C. Koo, K.W. Kim, S. Shin, S.H. Kim, Y.H. Park, *Appl. Environ. Microbiol.*, 2008, **74**, 2171.

Due to the used dilution method for determining MIC, it may be assumed that while 62.5 μM Ag$^+$ is not sufficient to fully inhibit bacteria growth for both strains, 125 μM was shown to be enough. However, the exact MIC values for both strains are comprised between 62.5 and 125 μM. These values fit well with what previously reported for *E. coli* ATCC 10536 and *S. aureus* ATCC 653813 as MIC values for Ag$^+$ (from AgNO$_3$) were 93 μM and 140 μM, respectively, after 24 h incubation time.[62] In the present work, the MIC at 24 h of p-AgNPs for *E. coli* is noticeably lower at the same incubation time, not only in comparison to the MIC of gsh-AgNPs but also to the MIC of ionic Ag$^+$. Negligible Ag$^+$ was released by p-AgNPs, as demonstrated by potentiometric experiments. This is also confirmed by release experiments from p-AgNPs contained in a dialysis membrane immersed in an identical volume of bidistilled water, see **Table 4**. In this experiment, Ag$^+$ concentration was measured in the 20 mL aqueous phase external to a 20 mL sample of p-AgNPs inside an osmosis membrane. Ag$^+$ was determined by ICP-OES analysis on 3.0 mL samples.

sampling time (h)	Ag (mg/L)
0.5	0.04
1.0	0.35
3.0	0.11
6.0	0.09
24	1.20*

Table 4 Ag$^+$ released by p-AgNPs *On the 24 h sample we re-measured the Ag$^+$ concentration after 1:1 dilution with water, finding 1.95 mg/mL concentration (referred to the non-diluted sample). The difference is probably due to a matrix-interfering effect played by pectin and/or by materials released by the slow decomposition of the osmosis membrane, caused by the basic pH (8.5) of the p-AgNPs solution.

After 24 h, 1.95 Ag$^+$ ppm was released in the aqueous phase external to the membrane, corresponding to 1.9% of the silver contained in p-AgNPs. Considering this, a significant role of Ag$^+$ in the antibacterial action of p-AgNPs may be excluded. It may be suggested that with p-AgNPs treatment, the increased antibacterial action towards *E. coli* is connected to AgNPs coating,[68] as nanoparticles have no strongly stabilizing thiolate bonds on their surface like in gsh-AgNPs, thus

---

[68] Y. Xiong, M. Brunson, J. Huh, A. Huang, A. Coster, K. Wendt, J. Fay, D. Qin, *Small*, 2013, **9**, 2628.

being capable to exert a direct nanomechanical disrupting action[69] on the *E. coli* membrane. AgNPs of similar dimensions (d = 7 nm) and coated with a carboxylate (deprotonated gallic acid) showed a comparable MIC of 58 µM at 12 h with *E. coli*.[70] Citrate-coated AgNPs gave a lower MIC for *E. coli*, 2.3 µM, but at a much shorter incubation time, i.e. ≤ 3 h.[71] These values reasonably are comparable to the MIC measured on bacteria incubated for 6 h (**Table 3**). In addition, we may suggest that the effect of the high surface activity and mobility of p-AgNPs is amplified by the delivery-promoting adhesion of pectin to bacteria membrane. Such an effect has already been hypothesized to exist for pectin in combination with different antibacterial agents.[72,73] The greater p-AgNPs antibacterial efficiency over gsh-AgNPs is confirmed also by the MIC comparison on *Staphylococcus* strains, although caution must be used in such comparison, as the two MIC values are obtained with two different staphylococcal species, namely *S. epidermidis* and *S. aureus*. However, in both cases it can be stated that the thick peptidoglycan layer of the Gram-positive cell wall increases the bacteria resistance to the AgNPs nanomechanical action,[69] probably due to prevention of the penetration of AgNPs inside the cytoplasm.

Since both *E. coli* and *S. epidermidis* strains tested for MIC determination are also biofilm producers, their viability in biofilm-forming conditions, i.e. with 0.25% Glucose (Glc) supplement in the medium, was also evaluated. The investigation was performed in two setups: (i) the bacteria were plated in the presence of p-AgNPs or $AgNO_3$ and Glc in the medium (Pre-biofilm formation); (ii) the biofilm was allowed to form and only after that, p-AgNPs or $AgNO_3$ were added (Post-biofilm formation). The exposure time to Ag was always kept constant at 24 h. Results are summarized in **Figure 33**.

[69] A. Taglietti, Y.A. Diaz Fernandez, E. Amato, L. Cucca, G. Dacarro, P. Grisoli, V. Necchi, P. Pallavicini, L. Pasotti, M. Patrini, *Langmuir*, 2012, **28**, 8140.

[70] G.A. Martínez-Castañón, N. Niño-Martínez, F. Martínez-Gutierrez, J.R. Martínez-Mendoza, F. Ruiz, J. *Nanopart. Res*., 2008, **10**, 1343.

[71] S.W. Kim, Y.W. Baek, Y.J. An, *Appl. Microbiol. Biotechnol*., 2011, **92**, 1045.

[72] S. Ravishankar, D. Jaroni, L. Zhu, C. Olsen, T. McHugh and M. Friedman, *J. Food Sci*., 2012, **77**, M377.

[73] G.C. Jayakumar, N. Usharani, K. Kawakami, J.R. Rao, B.U. Nair, *RSC Adv*., 2014, **4**, 42846.
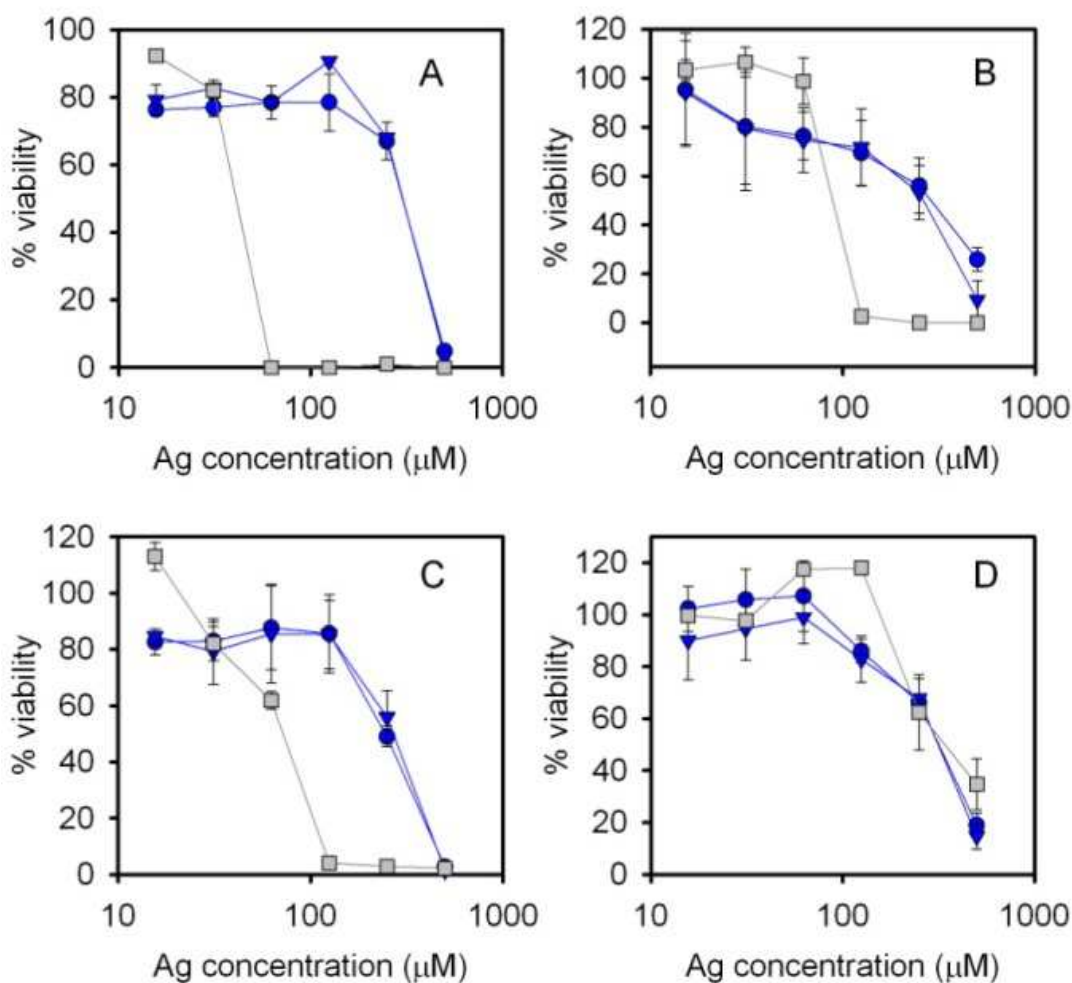
Figure 33 Viability determination as a function of Ag concentration for *E. coli* in pre-biofilm and post-biofilm conditions (**A** and **C**, respectively); same for *S. epidermidis* (**B** and **D**, respectively). Blue points refer to two different experiments carried out with two distinct p-AgNPs preparations. Grey points refer to experiments performed with AgNO$_3$.

In pre-biofilm conditions the concentration of p-AgNPs at which *E. coli* PHL628 viability falls to zero (MIC value) is one order of magnitude larger compared to liquid culture conditions (500 μM compared to 31.5 μM). AgNO$_3$ showed instead a MIC of 6.5μM in pre-biofilm forming condition. It has to be mentioned that in liquid culture conditions 62.5 μM Ag$^+$ reduced vitality to 55%. The slight MIC reduction in pre-biofilm conditions has thus to be attributed to the simultaneous presence of Ag$^+$ and glucose, and may be connected to the easier cell penetration by silver ions in such conditions due to the formation of Ag$^+$-glucose complexes.[74,75] Concerning *S. epidermidis* RP62A (**Figure 33B**), a decrease in viability at the highest concentration tested of p-AgNPs (500

[74] A. Baksi, M. Gandi, S. Chaudhari, S. Bag, S.S. Gupta, T. Pradeep, *Angew. Chem. Int. Ed.*, 2016, **55**, 7777.

[75] L. Boutreau, E. Leon, J.Y. Salpin, B. Amekraz, C. Moulin, J. Tortajada, *Eur. J. Mass Spectrom.*, 2003, **9**, 377.

µM) was observed; the concentration with no bacterial growth (MIC value) could not be determined. Higher Ag concentrations were not tested, as our limiting upper concentration was dictated by the 1000 µM Ag contained in the stock p-AgNPs solution. AgNO$_3$ showed a MIC of 125 µM against *S. epidermidis* RP62A when tested in pre-biofilm forming conditions. Excluding the case of Ag$^+$ and *E. coli*, the overall observed increase in the MIC values is expected, since biofilms are characterized by higher resistance level to any antibacterial substance.[76] In post-biofilm forming conditions, a further overall increase of resistance to both p-AgNPs and Ag$^+$ is observed as expected, due to the mechanical resistance opposed by the extracellular matrix produced by biofilms. The p-AgNPs concentration at which *E. coli* PHL628 viability is affected and reduced to zero is 500µM (**Figure 33C**), while for AgNO$_3$ it is 125 µM. Concerning *S. epidermidis* RP62A (**Figure 33D**), a decrease in viability at the highest p AgNPs concentration (500 µM) was observed; but again the concentration with no bacterial growth could not be determined. This applies also to AgNO$_3$ treatment because a complete inhibition of the bacterial growth at 500 µM was not determined. Also these results were expected, since *S. epidermidis* is well known to form more resistant biofilms with respect to *E. coli*.[77]

These data are further supported by CLSM images as shown in **Figure 34**.

---

[76] R.Y. Pelgrift, A. J. Friedman, *Adv. Drug Delivery Rev.*, 2013, **65**, 1803.
[77] R.M. Donlan, J.W. Costerton, *Clinical Microbiology Reviews*, 2002, **15**, 167.
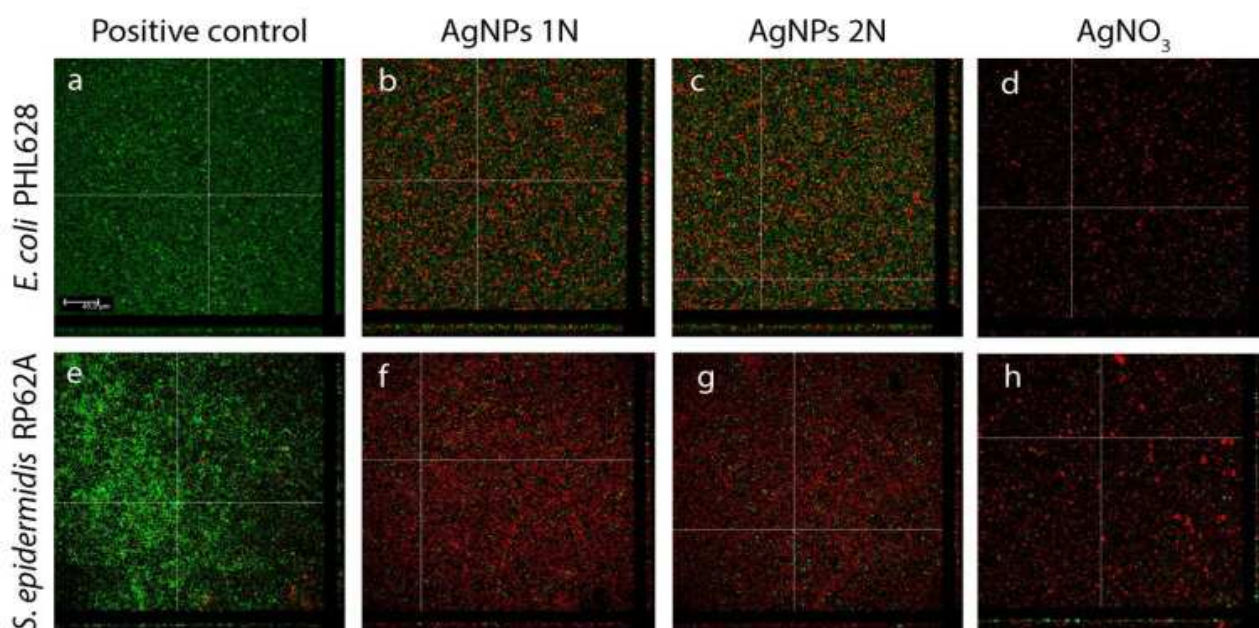
Figure 34 CLSM images of *E. coli* (**a-d**) and *S. epidermidis* (**e-f**) biofilms. Panels a and e are controls (no p-AgNPs or Ag$^+$ treatment). Panels b, c, f and g refer to treatments with p-AgNPs from two different preparations (N1 panels b and f; N2 panels c and g). Panels d and h refer to treatment with ionic silver (from AgNO$_3$). Sagittal sections of the biofilms are shown below and to the right of each panel. Scale bar (see panel a) = 45 µm.

Biofilms were allowed to grow for 24 h, and then incubated with either p-AgNPs or Ag$^+$. After washing and staining, dead cells fluoresced red, while cells fluorescing green were deemed viable. Stained biofilms were examined under CLSM, and optical sections of 0.9 µm were collected over the complete thickness of the biofilm. **Figure 34** shows green-fluorescing viable cells in the control (no p-AgNPs or Ag$^+$ added) for both bacterial strains (panels **a** and **e**). Two p-AgNPs preparations (named 1N and 2N) were examined for both strains with 500 µM p-AgNPs (panels **b**, **c**, **f**, and **g**) and one test was carried out with 500 µM AgNO$_3$ (panels **d** and **h**). While with ionic silver treatment almost complete cellular death was observed, a very significant but partial reduction of viable cells was detected for both biofilms when incubated with p-AgNPs.

3.2.2.4 Cytotoxicity and Cell Proliferation Properties of p-AgNPs

3.2.2.4.1 Assessment of Fibroblasts Viability in the presence of p-AgNPs

NHDF fibroblasts were used to assess the biocompatibility of p-AgNPs. Cells were seeded on a 96-well plate, left in incubator for 24 h and then treated with p-AgNPs or with 1.0% pectin solution.

After further 24h incubation the number of vital cells was determined and expressed in % with respect to incubation in medium without fetal bovine serum (M), to which 100% valued was assigned and in complete medium (CM), i.e. including fetal bovine serum. We tested p-AgNPs preparations obtained from 0.001 M Ag at 60 °C in 1.0% pectin. In addition, the effect of pure 1.0% pectin was examined. Results are graphically summarized in **Figure 35**.
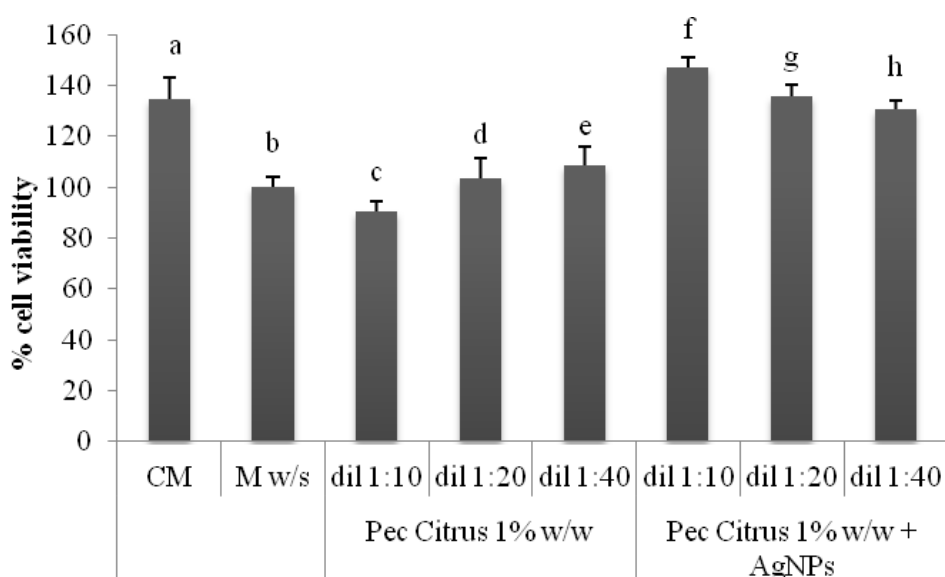

Figure 35 Viability values of 1% pectin and p-AgNPs tested at different dilutions (1:10, 1:20 and 1:40 (v/v)). CM and M (w/s) were used as reference (mean values ± s.e.; n=8). Anova one way – Multiple Range Test (p<0.05): a vs b/c/d/e; b vs f/g/h; c vs f/g/h; d vs f/g/h; e vs f/g/h; f vs h.

First, cells treated with CM showed a higher percent viability with respect to those treated with M, this indicating the discriminating capability of the test. In the case of p-AgNPs and of pectin solution, dilution to 1:10, 1:20 and 1:40 were used with respect to the starting material. Independently of the dilution, no cytotoxic effect was observed in both cases. On the contrary, when using p-AgNPs per cent viability values were higher (120-140%) with respect to the 100% for M and to the 105-110% observed for pure pectin solutions, with values comparable to that observed for CM. Since all the samples tested were diluted in M, the obtained results indicate that the presence of p-AgNPs in pectin solution improve cell viability.

3.2.2.4.1 Cell Proliferation and Wound Healing properties of p-AgNPs

Figure 36 graphically reports also the per cent proliferation values observed for different dilutions of p-AgNPs (1:10, 1:20, 1:40 v/v in M), with M used as reference for 100%. In these experiments cells were immediately treated with p-AgNPs or pure M after being seeded, then incubated for 24 h and subsequently counted.
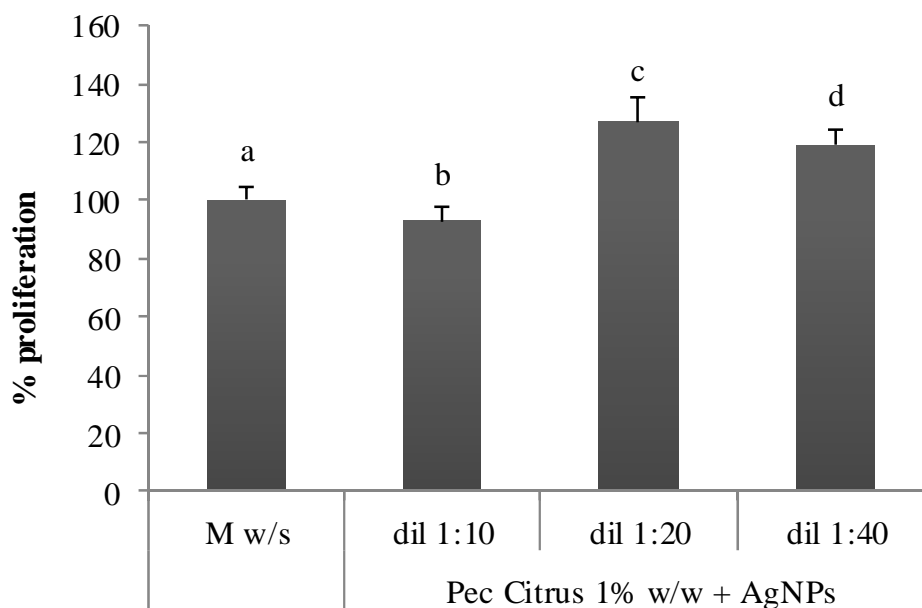

Figure 36 % proliferation values in the presence of p-AgNPs. M (w/s) was used as reference (mean values ± s.e.; n=8). Anova one way, MRT (p < 0.05): a *vs* c/d; b *vs* c/d.

In this case, more diluted p-AgNPs are more effective in promoting fibroblast proliferation, as 120% and 130 % proliferation are found for 1:20 and 1:40 dilutions, respectively. 1:10 dilution leads instead to a proliferation slightly lower than the reference (95%). This prompted us to investigate the wound healing ability of p-AgNPs in an in-vitro test.[78] This is based on a method in which an insert is enclosed in a Petri dish. The insert is made of two chambers with a given area for growth (0.22 cm^2), divided by a septum that mimics the lesion area, allowing a cell-free gap of 500 (±50) μm. After fibroblast growth to confluence the insert is removed yielding two areas of cells divided by the prefixed gap, as reported in **Figure 37A**. In our test, cells were then put in contact with 400 μL of 1:20 p-AgNPs, a dilution chosen on the basis of the viability and

---

[78] M. Mori, S. Rossi, M.C. Bonferoni, F. Ferrari, G. Sandri, F. Riva, C. Del Fante, C. Perotti, C. Caramella, *Int. J. Pharm.*, 2014, **461**, 505.

proliferation results. At given times (24, 48 and 72 h) microphotograph were taken to evaluate the invasion and cell growth in the gap. **Table 5** reports gap width for different contact times of p-AgNPs suspension, M and CM.

	0 h	24 h	48 h	72 h
CM	464 ± 11.5 a	212 ± 34.9 b	128 ± 54.9 c	gap closed
M	539 ± 4.5 a'	532 ± 1.6 b'	496 ± 25.6 c'	469 ± 77.8d'
p-AgNPs	503 ± 5.98 a''	424 ± 28.8 b''	239 ± 17.5 c''	gap closed

Table 5 Width (μm) of cell gap measured after contact with samples for different time intervals (mean values ± s.d.; n=3). Anova one way- Multiple Range Test ($p < 0.05$): a vs b/c/a'; b vs c/b'/b''; c vs c'/c''; a' vs d'; b' vs b/b''; c' vs c/c''; a'' vs b''/c''; b'' vs b/b'/c''; c'' vs c/c'.

After 24 h contact, no sample produced the complete closing of gap. However, it could be observed a significant ($p < 0.05$) decrease of gap width for CM and p-AgNPs suspension with respect to time 0, attributable to an initial invasion of cells. After 48 h, a further significant ($p < 0.05$) decrease of cell width was evident for CM and p-AgNPs suspension. After 72 h, the complete closing of gap is observed for CM and p-AgNPs treatment, see **Figure 37B**, while the presence of a gap persisted for M. Silver nanoparticles (citrate-coated) has already been shown to promote wound healing on animal models (mice) in which both thermal injuries or skin excision was carried out.[24] In such cases not only an antibacterial protective effect was played on the studied wounds, but also a cytokine regulatory role was observed. In our sterile model for wound healing studies the antibacterial properties of p-AgNPs are of course not playing any role. However, we found here that a healing effect holds even on fibroblast colonies, that may as well be caused by cytokine regulation due to p-AgNPs. It has to be stressed that both in our case and in the case of AgNPs are coated by polycarboxylates, i.e. ligands with oxygen atoms weakly interacting with the Ag surface. A related in-vitro increase of fibroblasts viability was reported for AgNPs, also in this case coated with weak O-interacting molecules such as glucose and lactose.[79] On the other hand Ag^+ is a cation well known to be toxic for eukaryotic cells,[80] at least at significant concentrations. As an example,

---

[79] I. Sur, D. Cam, M. Kahraman, A. Baysal, M. Culha, *Nanotechnology*, 2010, **21**, 175104.
[80] S. Chernousova and M. Epple, *Angew. Chem. Int. Ed.*, 2013, 52, 1636.

fibroblast vitality is reduced to 35 % in 10 ppm Ag^{+}.[81] The p-AgNPs product in this work thus is particularly suitable for fibroblast proliferation/wound healing, due to its negligible Ag^{+} release, lower than 2 ppm after 24h.
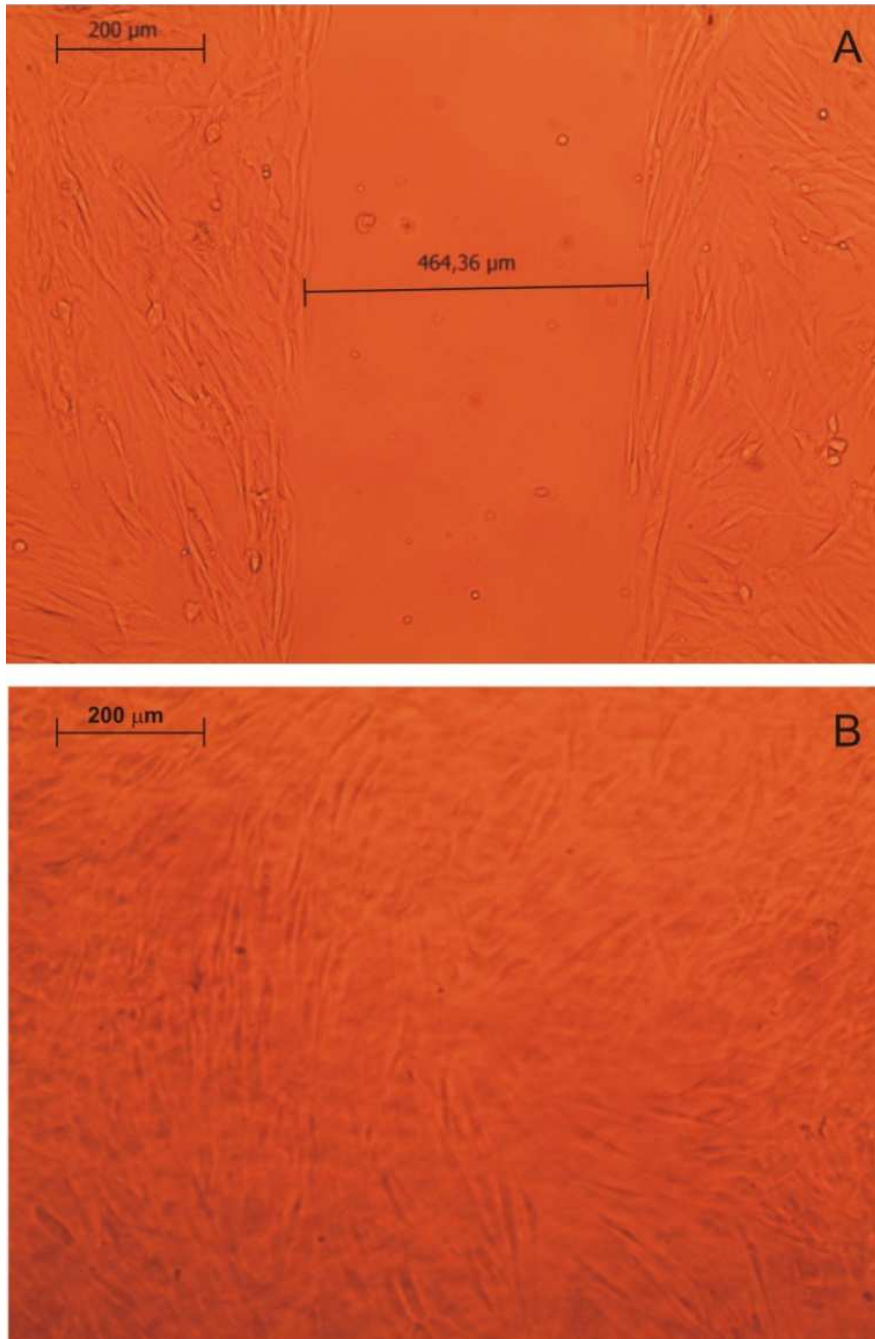

Figure 37 A: microphotographs of cells substrates taken at time 0. **B**: after 72 h contact time with p AgNPs.

[81] A. Milheiro, K. Nozaki, C.J. Kleverlaan, J. Muris, H. Miura, A.J. Feilzer, *Odontology,* 2016, **104**, 136.

3.2.3 Conclusions

A green synthesis for AgNPs was investigated and optimized, in which both the reductant and the protective coating are the same natural product, i.e. pectin from citrus. Under our conditions (water, 1.0%w/w pectin, 0.001M AgNO$_3$, 60 °C for 6 h, 0.025 M OH-) such synthesis brings multiple advantages: 100% Ag+ → Ag(0) conversion, with a negligible concentration of the toxic Ag$^+$ cation in the product (<1 ppm); excellent reproducibility and stability (>> 2 weeks) of the product; short synthesis time (6 h) with a straightforward procedure. Moreover, single-shape (spherical) AgNPs sare obtained, with a narrow dimensional distribution (d = 8.0 ± 2.6 nm). Although no significant Ag$^+$ is released, the pectin matrix allows a nanomechanical action of AgNPs against bacteria. We tested this on biofilm-forming *E. coli*, Gram-negative, and *S. epidermidis* Gram-positive. On these two strains, p-AgNPs expresses excellent antibacterial properties, comparable or superior to those of ionic Ag$^+$, both against planktonic cells and either on forming or preformed biofilms. Moreover, p-AgNPs is capable of promoting fibroblast proliferation and wound healing on model cultures. The combined negligible toxicity, antibacterial properties and wound healing abilities are new and candidate p-AgNPs as an efficient green medication for repairing wounds and to treat the vulnerable surgical site tissues. Combating the infections acquired during surgery is the most important target in preventing implants failure. Owing to the increasing antibiotic-resistance in biofilm-forming bacteria that cause implant-infections, particularly early infections, antibiotic prophylaxis and therapy turn out frequently ineffective. In this connection, as resistance to silver has been rarely seen, local pre-treatment of implants with p-AgNPs may be imagined as an additional, effective prophylaxi in implant (orthopaedic) surgery.

3.3 Cationic Antimicrobial Peptide (AMPs)

The increasing emergence of multidrug-resistant pathogenic microorganism and of nosocomial infections has become one of the most pressing alarms in modern medicine. Recently, cationic antimicrobial peptides (AMPs) has attracted increasing attention. Antimicrobial peptides are short (typically consisting of 20 to 100 amino acid residues in length), generally exhibit rapid and efficient antimicrobial toxicity against a range of pathogens[82] and constitute critical effector molecules in the innate immune system of both prokaryotic and eukaryotic organisms.[83]

Antimicrobial peptides (AMPs) are important constituents of the innate immune response for all species of life. Because many peptides may exert microbekilling properties and thus can fall into the category of AMPs, the field of AMPs is wide and generic. In fact, they are found in eukaryotes, including mammals, amphibians, insects and plants, and also in prokaryotes.[82] Furthermore, these peptides can display other activities like antitumor activity, mitogen activity and signalling molecule activity[82,84] thanks to their pathogen-lytic properties, and frequently they have low toxicity to mammals.[82] In many cases they are effective against pathogens, which are resistant to conventional antibiotics.[85] AMPs have a broad target spectrum that includes Gram-positive and Gram-negative bacteria, yeasts and fungi, and even certain enveloped viruses and protozoa.[86]

More than 1700 endogenous AMPs have been isolated and studied until now and a lot of synthetic analogues are produced. Even if, they share some common characteristics, such as usually being cationic and amphipathic, they are highly diversified from the structural point of view.[85] Although a huge amount of scientific work, a consensus understanding of AMPs antimicrobial mechanism is still lacking. Generally, it is believed that their activity against microorganisms is primarily governed by the charge and hydrophobicity and that the main target is the negatively charged bacterial and fungal cell membrane.[87] The recognized mechanisms of action can be divided in two groups:

(i) transmembrane pore models of AMPs membrane activity: the simplest models of membrane permeation by peptides, which involve the formation of membrane-spanning pores. According to

---

[82] W. van't Hof, E.C. Veerman, E.J. Helmerhorst, A.V. Amerongen, *Biol. Chem.*, 2001, **382**, 597.
[83] R.E. Hancock, G. Diamond, *Trends Microbiol*, 2000, **8**, 402.
[84] M. Brahmachary, S.P.T. Krishnan, J.L.Y. Koh, *Nucleic Acids Research*, 2004.
[85] T. Ganz, R.I. Lehrer, *Mol. Med. Today*, 1999, **5**, 292.
[86] R.E. Hancock, R. Lehrer, *Trends Biotechnol.*, 1998, **16**, 82.
[87] W. Wimley, K. Hristova, *The Journal of Membrane Biology*, 2011, **239**, 27.

the barrel stave pore model, reported by Rapaport and Shai[88], peptides interact laterally with one another to form a specific structure enclosing a water-filled channel, such as protein ion channel. On the other hand, Ludtke et al.[89] proposed the toroidal pore model: peptides affect the local curvature of the membrane forming a peptide-lipid toroid of high curvature;

(ii) non-pore models of AMPs activity: supported by a greater number of scientific evidence, many researchers have proposed that the mechanism of action of AMPs is based on creating a non-specific imbalance of the packaging and organization of membrane lipids once bound to the membrane. There are different models proposed to explain in detail this mechanism: the carpet model described by Shai Gazit et al.[90]; the detergent model proposed by Ostolaza et al.[91] or finally the cluster model by Epand et al.[92]

The bioavailability of AMPs, through an oral administration, emerges to be strongly reduced; however, with injection and topical application, this is very high.[93] For such reason, AMPs are considered products of interest against bacterial and fungal infections associated with catheters[94] and triggering systems.[95] Moreover, due to their interactions with microbial components do not involve specific protein binding, they do not induce resistance.[96]

However, AMPs have a big disadvantage: their production is much more expensive than the normal chemical antibiotics. One of the major factors which makes uneconomical the production process is the length and the high number of amino acids which constitute these peptides[97]. But, thanks to extensive SAR and the mechanism studies, it has been possible to begin to synthesize ultrashort peptides with simple structure and, simultaneously, as powerful as the previous ones.[98]. The ultra short peptide, as the name implies, are shorter than AMPs: they are made from 3 to 7 amino acids and prepared via established facile, solid phase synthetic protocols at lower costs respect to their natural peptide counterparts.[99] They are able to carry out their high antimicrobial activity due to the presence of cationic amino acids (such as lysine). The combinations of possible

[88] D. Rapaport, Y. Shai, *J Biol Chem*, 1991, **266**, 23769.
[89] S.J. Ludtke, *Biochemistry*, 1996, **35**, 13723.
[90] E. Gazit E, *J Mol Biol*., 1996, **258**, 860.
[91] H. Ostolaza H, *Biochim Biophys Acta*, 1993, **1147**, 81.
[92] R.F. Epand, Biochemistry, 2010, **49**, 4076.
[93] Demegen Pharmaceticals, Candidiasis Wedsite, (2010).
[94] M.N. Melo, D. Dugourd, M.A. Castanho, *Recent Pat Antiinfect Drug Discov*., 2006, **1**, 201.
[95] M. Kazemzadeh-Narbat, *Biomaterials*, 2010, **31**, 9519.
[96] R.E. Hancock, H.G. Sahl, *Nat Biotechnol*,2006, **24**, 1551.
[97] K. Hilpert, M.R. Elliott, R. Volkmer-Engert, P. Henklein, O. Donini, Q. Zhou, R.E.W Hancock, *Chemistry and Biology*, 2006, **13**, 1101.
[98] G.S. Bisht, D.S. Rawat, A.Kumar, R. Kumar, S. Pasha, *Bioorg Med Chem Lett*, 2007, **17**, 4343.
[99] R.P. Hicks, H.B. Bhonsle, D. Venugopal, B.W. Koser, A.J. Magill, *J Med Chem*, 2007, **50**, 3026.

ultrashort peptide are varied, but the research team of Laverty et al., examining many products found that the ultrashort NapFFKK peptide, **Figure 38**, had excellent anti bacterial activity.[100,101]
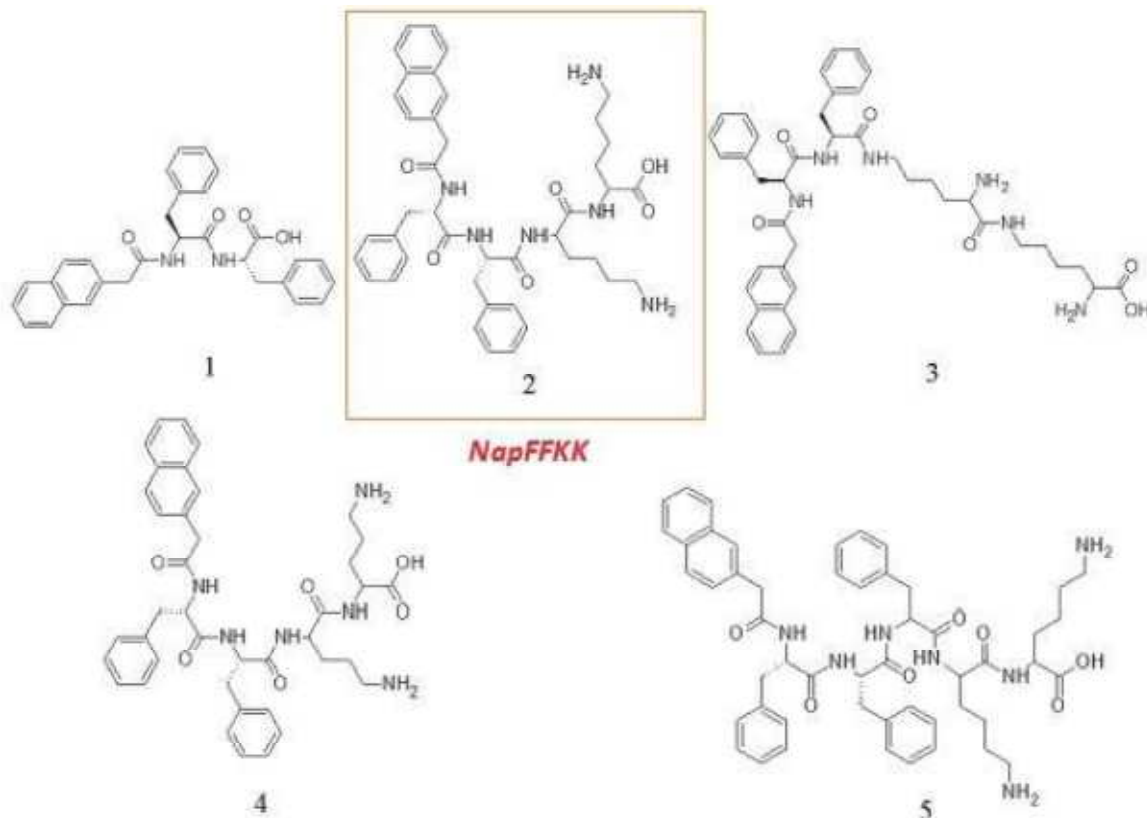

Figure 38 Chemical structures of naphthalene peptide derivatives investigated: (1) NapFF, (2) NapFFKK, (3) NapFFK'K', (4) NapFFOO, (5) NapFFFKK.

NapFFKK is composed of a peptide sequence of phenylalanine-phenylalanine-lysine-lysine and a naphthalene linked to the N-terminal region of the peptide. The choice to add aromatic moieties moities, such as naphthalene and phenylalanine, was made to confer the ability to self-assemble into gel within an aqueous solution. In addition to the antibacterial activity of the hydrogel itself, this feature is very interesting for biomaterials and drug delivery vehicles.[99]

[100] G. Laverty, M. McLaughlin, C. Shaw, S.P. Gorman, B.F. Gilmore, *Chemical Biology and Drug Design*, 2010, **75**, 563.
[101] G. Laverty, A.P. McCloskey, B.F. Gilmore, D.S. Jones, J. Zhou,B. Xu, *Biomacromolecules*, 2014, **15**, 3429.

3.3.1 Visiting Research

During my third year, I have spent two months at School of Pharmacy of Queen's University of Belfast (UK) for a Visiting Research under Supervision of Professor Garry Laverty. My objectives was to synthesize a peptide with the ability to form a bioactive antimicrobial material associated with the majority of biomaterial related infections (e.g. intravascular catheter related infections).[99] This process would replicate the evolutionary advantage awarded to organisms such as amphibians that secrete a thin peptide mucus on their skin to protect against infection; to evaluate antimicrobial activity of spherical silver nanoparticles (AgNPs) against Gram-positive and Gram-negative bacteria and to evaluate antimicrobial activity of spherical silver nanoparticles mixed with the peptide (AgNPs plus) against Gram-positive and Gram-negative bacteria.

I have performed the following experimental methods:

-synthesis of C_{12}-Lys-Thr-Lys-Cys-Lys-D-Phe-Leu-Lys-Lys-Cys peptide;

-synthesis of silver Nanoparticles (AgNPs) and characterization with UV-Vis spectroscopy;

-synthesis of AgNPs plus (mixture of colloidal suspension of AgNPs and peptide in PBS) and characterization with UV-Vis spectroscopy, evaluation of interactions between AgNPs and peptide;

-Minimum inhibitory/bactericidal concentration (MIC/MBC) determination of AgNps and AgNPs plus;

-rate of reduction in viability of biofilms using Alamar Blue assay of AgNPs and AgNPs plus;

-preliminary Haemolysis assays for evaluation of AgNps citotoxity.

3.3.2 Experimental Details: Synthesis and Characterization

All solvents and reagents were purchased from the suppliers indicated and they were used without further purification. For all the treatments and synthesis was used doubly distilled water to prevent any possible form of pollution of the samples.

3.3.2.1 Synthesis of Silver Nanoparticles (AgNPs)

Material

Silver nitrate 99% ($AgNO_3$) (Sigma Aldrich, Dorset U.K.), Sodium citrate ($Na_3C_6H_5O_7$) (Sigma Aldrich, Dorset U.K.), Sodium borohydride 96% (Sigma Aldrich, Dorset U.K.)

Equipment

UV visible spectrophotometer Cary 50 (VARIAN PTY LTD, Australia), Transmission Electron Microscopy TEM (Joel JEM-1200 EX II 140), Quartz cuvette optical path 1 cm

Briefly, to 100 mL of distilled water at 4 °C the following solutions were added in sequence under vigorous stirring: a)1 mL of 1% (w/v) $AgNO_3$ solution, after a minute b) 1 mL of 1% (w/v) $Na_3C_6H_5O_7$ and, after a further minute, 0.500 mL of a ice-cooled solution 0.075% (w/v) in $NaBH_4$ and 1% (w/v) in sodium citrate. After the last addition, stirring was immediately stopped, in order to avoid coagulation. The colloidal suspensions were stored in the preparation flask at 25°C.

3.3.2.3 Synthesis of C_{12}-Lys-Thr-Lys- Cys-Lys-D-Phe-Leu-Lys-Lys-Cys Peptide

Material

Fmoc-Lysine-Wang resin; mesh size 100 – 200, 0.64 mmol/g; Fmoc protected amino acids Lysine K Tyrosine Thr, Cysteine Cys, Leucine Leu and Phenylalanine F from (Novabio-c(Novabio-chemMerk KGaA, Darmstadt Germany), Methanol (Sigma Aldrich, Dorset U.K.), N,N-dimethylformamide (DMF) (Sigma Aldrich, Dorset U.K.), Dichloromethane (DCM) (Sigma Aldrich, Dorset U.K.), Diethyl

ether (Sigma Aldrich, Dorset U.K.), O-(benzotriazol-l-yl)-*N,N,N',N'*tetramethyluroniumhexaflourophosphate HBTU (Sigma Aldrich, Dorset U.K.), N,Ndiisopropylethylamine (DIPEA) (Sigma Aldrich, Dorset U.K.), Triflouroacetic acid (TFA) (Sigma Aldrich, Dorset U.K.), Triisopropylsline (TIPS) (Sigma Aldrich, Dorset U.K.), Thioanisole (Sigma Aldrich, Dorset U.K.), Piperidine (Sigma Aldrich, Dorset U.K.) Phenol (Sigma Aldrich, Dorset U.K.), Ethanol (Sigma Aldrich, Dorset U.K.), Potassiumcyanide (Sigma Aldrich, Dorset U.K.), Pyridine (Sigma Aldrich, Dorset U.K.), Ninhydrin (Sigma Aldrich, Dorset U.K.), Acetonitrile (Sigma Aldrich, Dorset U.K.)

Peptides were synthesized manually from a MBHA rink amide resin by carrying out solid-phase synthesis using a sintered glass funnel attached to a nitrogen bubbler apparatus. The Rink amide MBHA resin (0.74 mmol/g, 200-400 mesh) was swollen with DCM for 30 minutes, followed by three times washes with DMF. Then, the Fmoc group was removed by treating the resin with 20% v/v piperidine/DMF for 1-2 hours followed by three 5 minutes washes with DMF. Couplings were conducted using three equivalents of the corresponding Fmoc-protected amino acid, which was mixed with three equivalents HBTU and six equivalents DIPEA in DMF. The mixture was added to the resin and stirred for 2-4 hours at room temperature under bubbling nitrogen. Then the reaction mixture was removed and followed again by three 5 minutes washes with DMF. The completion of the reactions was checked by the Kaiser test to evaluate the presence of free amino group. A few resin beads from the washed reaction were placed in eppendorf tube with addition of 2 drops phenol/ethanol, 2 drops potassium cyanide/pyridine and 2 drops of 5% ninhydrin/ethanol. The tube then was placed in an oven and heated for 5 minutes at 95˚C. A bluish colour of solution and beads indicated the presence of free amino group, while light yellow to colourless indicated a complete coupling. Peptide elongation was performed by repeated cycles of Fmoc group removal and coupling. After each deprotection and coupling step, the resin was washed with DMF for 5 minutes. Once the sequence was assembled, it was washed with DMF three times for 5 minutes each, DCM also three times for 5 minutes each and finally methanol three times for 5 minutes. Once the chain assembly was completed, cleavage of the peptides from the resin was carried out in a round-bottom flask equipped with a stirrer using TFA/TIPS/thioanisole (95:2.5:2.5 v/v) for 2 hours at room temperature. Then the cleavage mixture was filtered by vacuum filtration under reduced pressure and the resin rinsed with the cleavage cocktail followed by DCM to obtain any remaining mixture. Excess solvent was removed under

reduced pressure by rotary evaporation. The oily residue was treated with cold diethyl ether to obtain the peptide precipitate. The solid peptide was isolated by centrifugation. This process was repeated three times. The solid peptide was stored at -20˚C until needed.

All solvents and reagents were purchased from the suppliers indicated and they were used without further purification. For all the treatments and synthesis was used doubly distilled water to prevent any possible form of pollution of the samples. Silver nitrate 99% (Sigma Aldrich, Dorset U.K.)Sodium citrate (Sigma Aldrich, Dorset U.K.) Sodium borohydride 96% (Sigma Aldrich, Dorset U.K.)

3.3.2.2 Preparation of AgNPs plus

Material

C_{12}-KTKCKFLKKC peptide, colloidal solution of AgNPs, PBS.

Equipment

UV visible spectrophotometer Cary 50 (VARIAN PTY LTD, Australia), quartz cuvette optical path 1 cm

To a solution of antimicrobial C_{12}-KTKCKFLKKC peptide 850 μg/mL in PBS were added AgNPs colloidal suspension in order to obtain a final concentration of 425 μg/mL .

3.3.2.3 Minimum Inhibitory /Bactericidal Concentration Determination

Broth microdilution tests were carried out according to NCCLS guidelines. A working solution of AgNPs (102 μg/mL) and AgNPs plus (50.96 μg/mL) was prepared in MHB (Mueller Hinton Broth) and 0.22 μl sterile filtered. From this stock solution, serial twofold dilutions in MHB were carried out in 96-well microtitre plates. All microbial strains tested, *Escherichia coli* (NCTC 11303), *Pseudomonas aeruginosa* (PAO1), *Staphylococcus epidermidis* (ATCC 35984), *Staphylococcus aureus* (ATCC 29213), were grown over 18–24 h at 37°C in MHB, from which an inoculum was taken and adjusted to optical density 0.3 at 550 nm which is the equivalent to $1*10^8$ CFU/mL. This suspension was further diluted to give a final inoculum density of $2*10^5$ CFU/mL, as verified by

total viable count. All controls and test concentrations were prepared as six replicates. The microtitreplates were then incubated for 24 h at 37°C in a stationary incubator. Following determination of the MIC for each compound, the minimum bactericidal concentrations (MBC) were derived by transferring 20 µl of the suspension from the wells that displayed no signs of growth to MHB plates. The MHB plates were then incubated in a stationary incubator at 37 °C for 24 h and examined for ≥ 99.9% killing (MBC).

3.3.2.4 Rate of Reduction in Viability of Biofilms using Alamar Blue Assay[102]

Microorganism under investigation *Escherichia coli* (NCTC 11303) *Pseudomonas aeruginosa* (PAO1) *Staphylococcus epidermidis* (ATCC 35984) and *Staphylococcus aureus* (ATCC 29213) were grown over 24 hours at 37°C in MHB (Mueller Hinton Broth) in a Gallenkamp gyrorotary incubator. Upon visual confirmation of the growth the inolculum was taken and adjusted to optical density 0.3 at 550 nm in PBS solution, which is the equivalent of $1*10^8$ colony forming unit per milliliter (CFU/mL). This suspension was further diluted in MHB (0.1 mL in 50 mL) and dispensed aseptically in 100 µL aliquots to each well of the microtitre plate. Biofilm are formed on the surface of the well under shear stress provided by Gallenkamp gyrorotary incubator. After inoculation period of 24 h cultures are decanted and the plates irrigated twice with 200 µL of sterile autoclaved 0.9% w/v sodium chloride in each well. Washed plates are tapped gently upside down on a sterile paper towel to remove residual wash. The pepared biofilm is treated for evaluation viability using Alamar blue in a method similar to that used by Pettit and colleagues[103]. The viability of established biofilms in assessed by re-charging wells from above immediately after washing and without dryng, with 0.1 mL fresh MHB containing 20% v/v alamarBlue®, incubating the plate at 37°C for one hour followed by spectrophotometric measurement of absorbance at a wavelength of 570 nm. Alamar blue is Resazurin, a redox indicator which is reduced by metabolic activity of viable microbial cells to pink fluorescent Resorfurin. Each control has 4 replicates. Blank determinations (100% viability: Positive control) are conducted using sterile distilled water, representing a composition of excipients without active ingredient in the case of formulations. Immediately following incubation, the exposed wells are washed twice by irrigation with sterile 0.9% w/v sodium chloride and recharged with fresh MHB containing 20% v/v Alamar Blue and 3% w/v

[102] M. Mateescu, S. Baixe, T. Garnier, L. Jierry, V. Ball, Y. Haikel, P. Lavalle, Plos One, (2015). 10(12).
[103] Pettit , *Microbiol. Antimicrob*., 2009, 8, **28.**

Tween 80 (polysorbate), incubated at 37°C approximately 1 hour and development of ultraviolet absorbance measured spectrophotometically at 570 nm. A positive control (100% microbicidal effect) is also included in the assay using an empty well /no biofilm) and the test item. Reduction in viability of biofilm following exposure to 50.96 µg/mL, 25.48 µg/mL, 12.74 µg/mL, 6.37 µg/mL, 3.18 µg/mL, 1.59 µg/mL and 0.796 µg/mL of AgNPs and AgNPs plus is expressed as a percentage based on percent reduction between untreated blank wells and treated wells using the following equation:

$$\% \text{ reduction in viability} = \text{Abs AgNPs}_{570} - \text{Abs Blank}_{570} / \text{Abs Ethanol}_{570}\ 70\%\ \text{Abs Blank}_{570} *100$$

3.3.2.5 Haemolysis Assay[104]

AgNPs were assayed spectrophotometrically for their ability to induce haemoglobin release from fresh equine erythrocytes according to the method of Shinet al. (24). Fresh defibrinated equine erythrocytes (Laboratory Supplies& Instruments Ltd, Antrim, UK), were washed one times with equal volumes of PBS (20 mL of erythrocytes and 20 mL of PBS). After centrifugation for 15 min at 3000 g, erythrocytes were resuspended in 4% (v/v) in PBS (2 mL of erythrocytes suspension in 20 mL of PBS). Equal volumes (100 µl) of the erythrocyte suspension were added to each well of a 96-well microtitre plate. Erythrocytes were subsequently exposed to AgNPs concentrations (50.96 µg/mL, 25.48 µg/mL, 12.74 µg/mL, 6.37 µg/mL, 3.18 µg/mL, 1.59 µg/mL and 0.796 µg/mL) incubated at 37°C for 1 h and centrifuged at 1000 *g*. Aliquots of the supernatant were transferred to a fresh 96-well microtitre plate, and haemoglobin release measured spectrophotometrically at 450 nm. As a positive control (100% haemolysis), erythrocytes were treated with 1% Triton X-100, whilst PBS (0% haemolysis) acted as a negative control. All AgNPs concentrations are reported as the mean of six replicates. Percentage haemolysis was calculated as follows:

$$\% \text{ Haemolysis} = (\text{Abs}_{450}\ \text{AgNPs}) - (\text{Abs}_{450}\ \text{PBS}) / (\text{Abs}_{450}\ 1\%\ \text{Triton X100}) - (\text{Abs}_{450}\ \text{PBS})$$

[104]S.Y. Shin, S.T. Yang, E.J.Park, S.H. Eom, W.K. Song, J.I. Kim, Y. Kim, *The Journal of Peptide Research*, 2001, **58**, 504.

Statistical Analysis

Statistical analyses were conducted using GraphPad Prism 6. They were employed using a Dunn's multiple comparisons test was used to identify individual differences between the reduction in planktonic cells viability for each hydrogel and the negative control (0% reduction); and it was also utilized for statistical analysis of tissue culture cytotoxicity data by comparison of percentage viability for the AgNPs employed to the negative control (100% viability), with significant reduction in viability reported. Haemolysis data was compared by the same statistical method with percentage haemolysis compared to the PBS, nonhaemolytic, control (0% haemolysis). In all cases, a probability of $P < 0.05$ denoted significance.

3.3.3 Results and Discussion

3.3.3.1 Silver Nanoparticles (AgNPs)

Silver nanoparticles (AgNPs) display the Localized Surface Plasmon Resonance (LSPR) band observed in absorption spectroscopy for colloidal suspensions. Interaction with light of AgNPS causes the collective coherent oscillation of their free conduction band electrons, or LSPR.[105] The intensity, the shape and the position of the LSPR bands depend on the size and shape of the nanoparticles, on the stabilizing agents covering the nanoparticles surface, and on the dielectric constant of the surrounding environment. In the case of spherical AgNPs with size <50 nm of diameter, this band is around 400 nm. In our preparations, the spectra of citrate-stabilized AgNPs showed an LSPR peak centered at 394 nm in aqueous solutions, **Figure 39**. This synthetic procedure yielded spherical AgNPs with a large size distribution of 7 ± 4 nm diameter determinate by Trasmission Electron Microscopy (TEM), **Figure 40**.

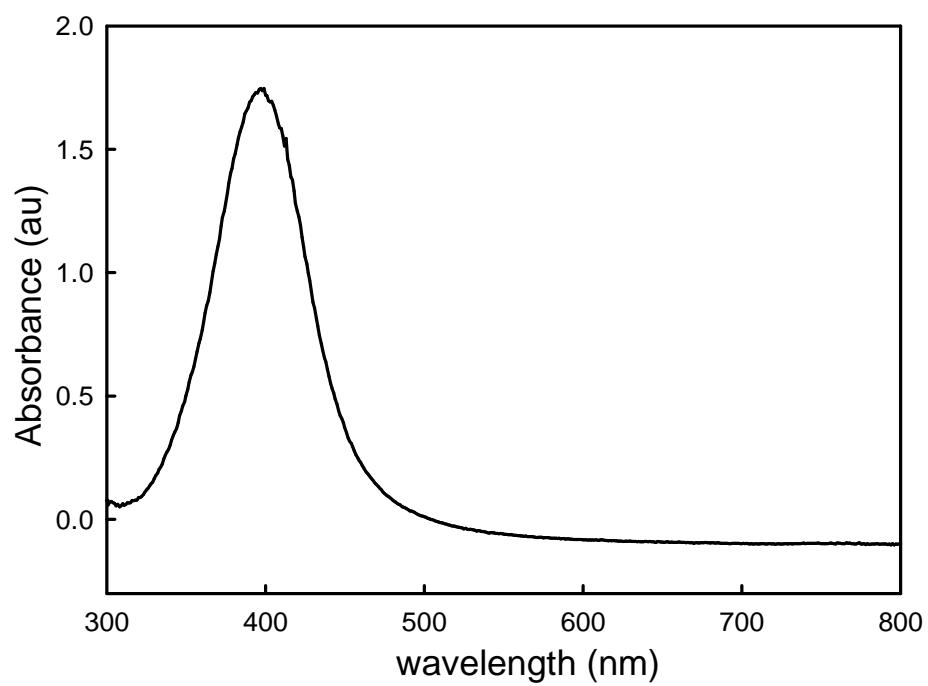[105] G. Mie, *Ann Phys*, 1908, **25**, 377.

Figure 39 UV-Vis absorbance spectrum of colloidal suspensions of AgNPs centered at 394 nm.
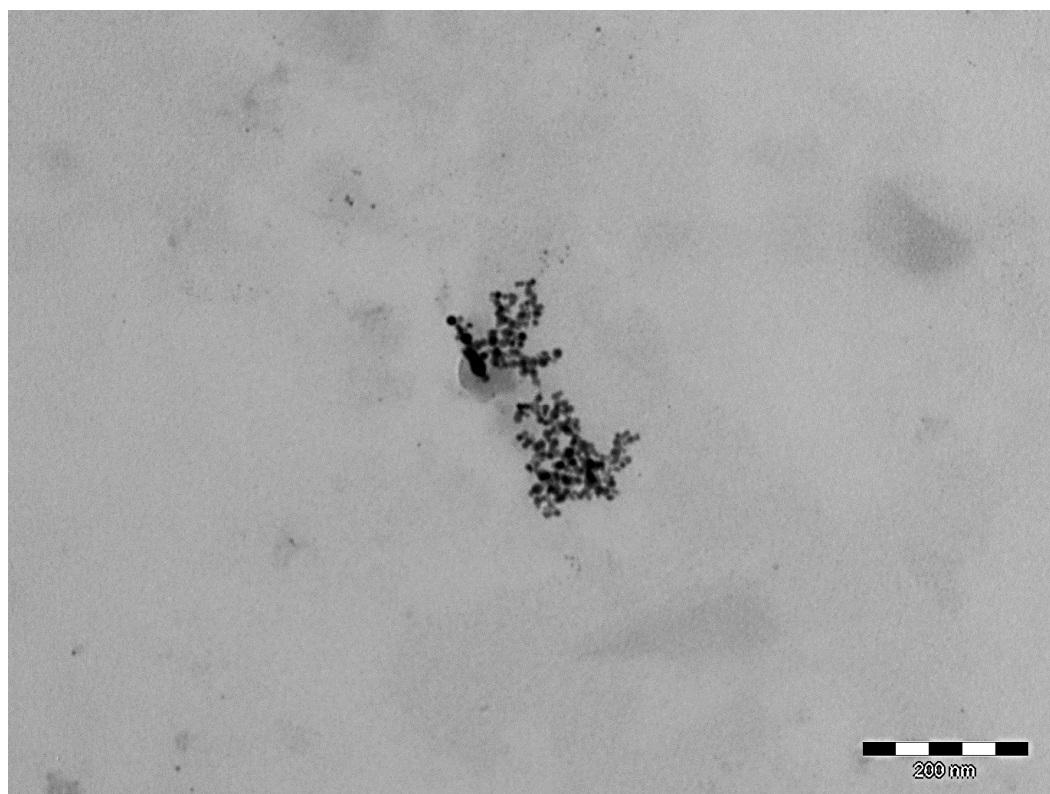

Figure 40 TEM image of colloidal suspensions of AgNPs.
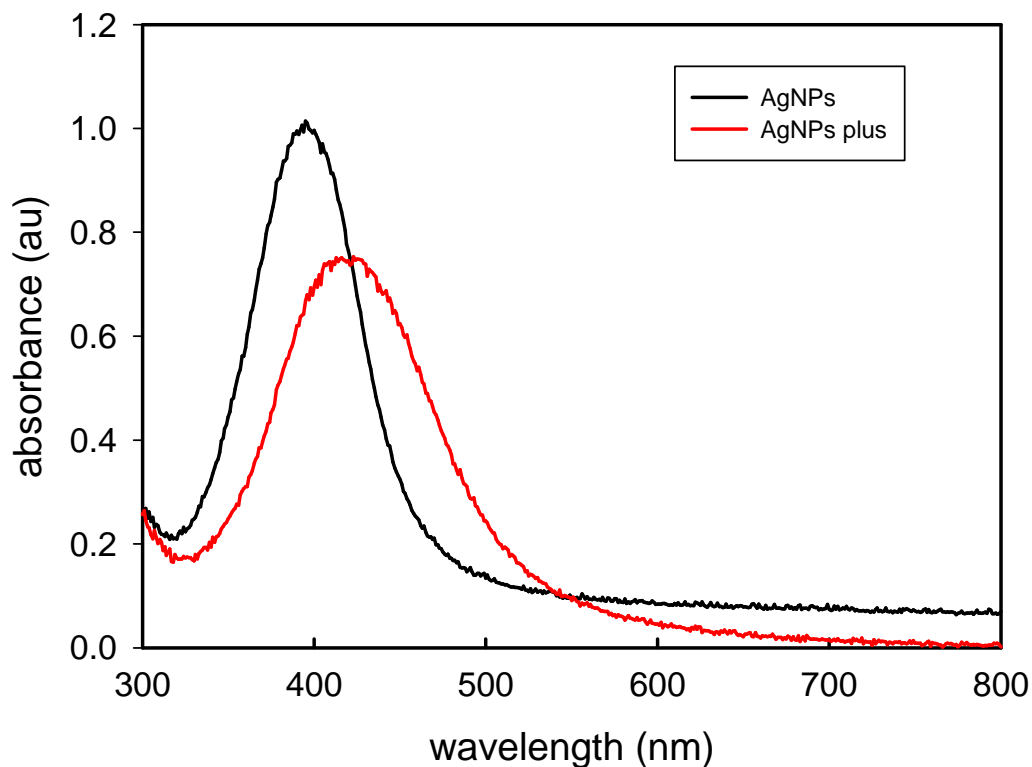
3.3.3.2 AgNPs plus

Figure 41 UV-Vis spectra of AgNPs centered at 394 nm, black line, and AgNPs plus, red line, centered at 430 nm.

In **Figure 41** spectra of AgNPs and AgNPs plus are reported. In this case a red shift of the LSPR peak of AgNPs plus is observed which is due to the presence of antimicrobial peptide and also to the different dielectric constant of the surrounding environment (from distilled water to PBS).

3.3.3.3 Minimum Inhibitory /Bactericidal Concentration Determination

		AgNPs	AgNPs plus
E.coli	MIC	12.74	3.185
	MBC	50.96	12.74
P.aeuriginosa	MIC	6.37	12.74
	MBC	12.74	12.74
S.epidermidis	MIC	12.74	6.37
	MBC	50.96	12.74
S.aureus	MIC		12.74
	MBC		12.74

TABLE 6 Antimicrobial activity of AgNPs, AgNPs plus. Minimum inhibitory concentration (MIC) and minimum bactericidal concentrations (MBC) are given in μg/mL and are quoted as the mean of 6 replicates.

The antimicrobial activity (MIC/MBC values) of the AgNPs and AgNPs plus against a different pathogenic micro-organism are detailed in **TABLE 6**. AgNPs exhibit an activity for Gram-negative bacteria strains. They even show an antimicrobial activity against Gram-positive bacteria *S. epidermidis*, but don't exhibit activity against *S. aureus*. Usually microbicidal activity of AgNPs is higher for Gram-negative bacteria and lower for Gram-positive bacteria which are more resistant to antibacterial action of silver ions (Ag^+) and AgNPs because of the peculiar structure of their membranes. However AgNPs plus not only exert an antimicrobial broad-spectrum activity against the range of organism tested, but also MIC values are lower than MIC of only AgNPs in general. This effect could be explained by a synergic effect of both AgNPs and antimicrobial peptide.

Bactericidal effects of AgNPs is due to the aerobic release of silver ions, which are the primary cause of toxicity to microorganisms. However, from a typical molecular microbiology point of view, a clear and definitive knowledge of the effects of AgNPs on microorganism is still lacking. There are some hypothesized mechanisms, mainly regarding direct Ag^+ induced membrane damage, Ag^+ related oxygen radicals (ROS) production, and cellular uptake of Ag^+ ions or even AgNPs, due to membrane poration, with consequent disruption of ATP production and hindering of DNA replication activities.[106] The direct membrane damage by Ag^+ ions was carried out by Taglietti e*t al*. where imaging investigations, mostly based on TEM analyses, revealed pits or even large holes within the bacterial membrane.[66] Moreover other coordination modes of Ag^+ with aminoacids/peptides have been proposed to explain antibacterial effects of AgNPs.

---

[106] L.Rizzello, P.P. Pompa, *Chem. Soc. Rev.*, 2014, **43**, 1501.

Silver ions may interact with sulfur containing membrane proteins (e.g., with the thiol groups of respiratory chain proteins), causing physical damage to the membrane. All these Ag^+–membrane proteins interactions may lead, in turn, to a drastic change in membrane permeability, by a progressive release of lipopolysaccharides (LPS) and membrane proteins resulting in the dissipation of proton motive force and depletion of intracellular ATP levels.[103] The surface charge of AgNPs may play an important role, as it can affect the possibility of AgNPs binding to bacteria, due to electrostatic interactions. For instance, positive surface charge of AgNPs may promote their binding to negatively charged areas present on bacterial membrane, leading to a higher effective dose available, with a consequent higher local ions release. At the same time, silver ions release is strongly promoted in the close proximity of the external membrane of bacteria, because of the proton motive force that induces a local strong decrease of pH (down to values of 3).

3.3.3.4 Rate of reduction in Viability of Biofilms using Alamar Blue Assay

The ability of AgNPs and AgNPs plus to exert anti biofilm activity have been demonstrated against four species of bacteria associated with biomaterial related infection: Gram-negative pathogens *Escherichia coli* (NCTC 11303) *Pseudomonas aeruginosa* (PAO1) and Gram-positive *Staphylococcus epidermidis* (ATCC 35984) and *Staphylococcus aureus* (ATCC29213).

AgNPs displayed the most significant ($P< 0.001$) antibiofilm activity at the higher concentration tested against *E. coli* strains (110.7%), whereas they do not show any significant effect concerning *Pseudomonas aeruginosa* biofilm. In addition, AgNPs exhibit a significant antimicrobial activity against *Staphylococcus epidermidis* at 50.96 µg/mL (92.01%), in the meanwhile they do not display a significant antibacterial activity against *Staphylococcus aureus.* Concerning AgNPs plus, we can observe significant reduction for all species of biofilm studied. Particularly, AgNPs plus show the most significant destruction of *Pseudomonas aeruginosa* at 50.96 µg/mL (98.44%).
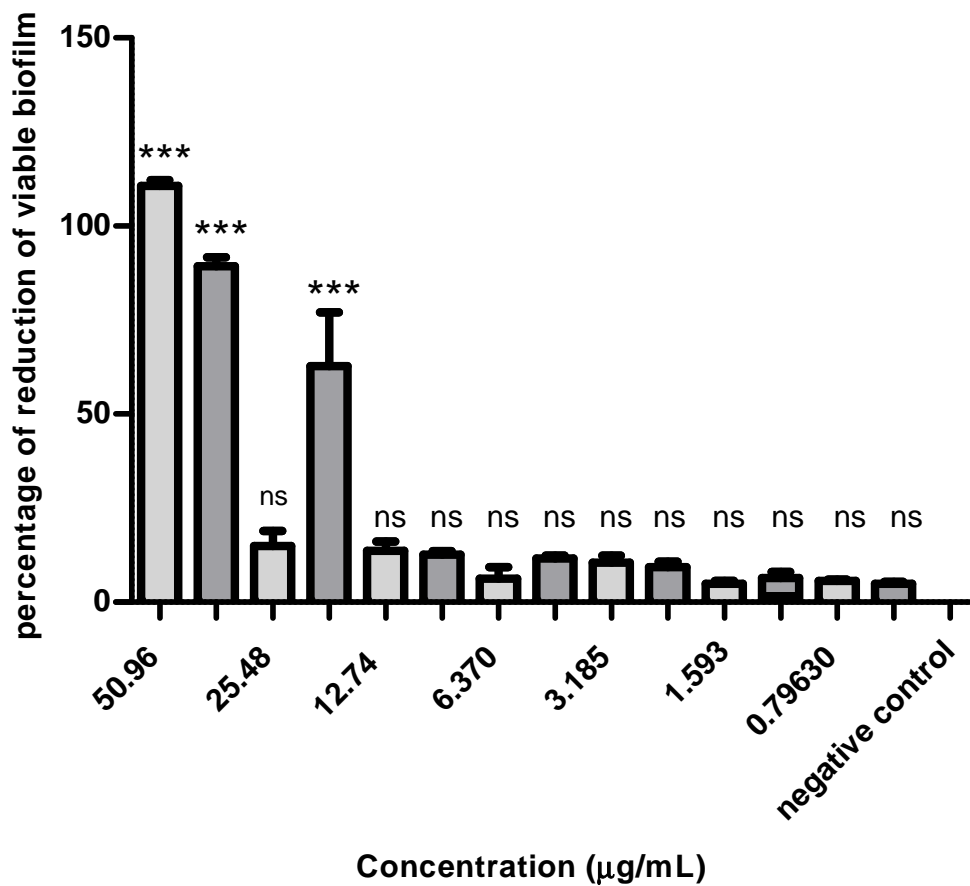
Figure 42 Percentage reduction of mature 24 hour biofilm *Escherichia coli* (NCTC 11303) after 24 h incubation with AgNPs and AgNPs plus utilizing an Alamar Blue assay. Results are displayed as a mean of 4 replicates. Key: AgNPs light gray, AgNPs plus dark gray NS = no significant difference (P ≥ 0.05), * P < 0.05, ** P < 0.01, *** P < 0.001, **** P <0.0001 significant difference between AgNPs and AgNPS plus at each concentration and negative control PBS (no AgNPs and no AgNPs plus).
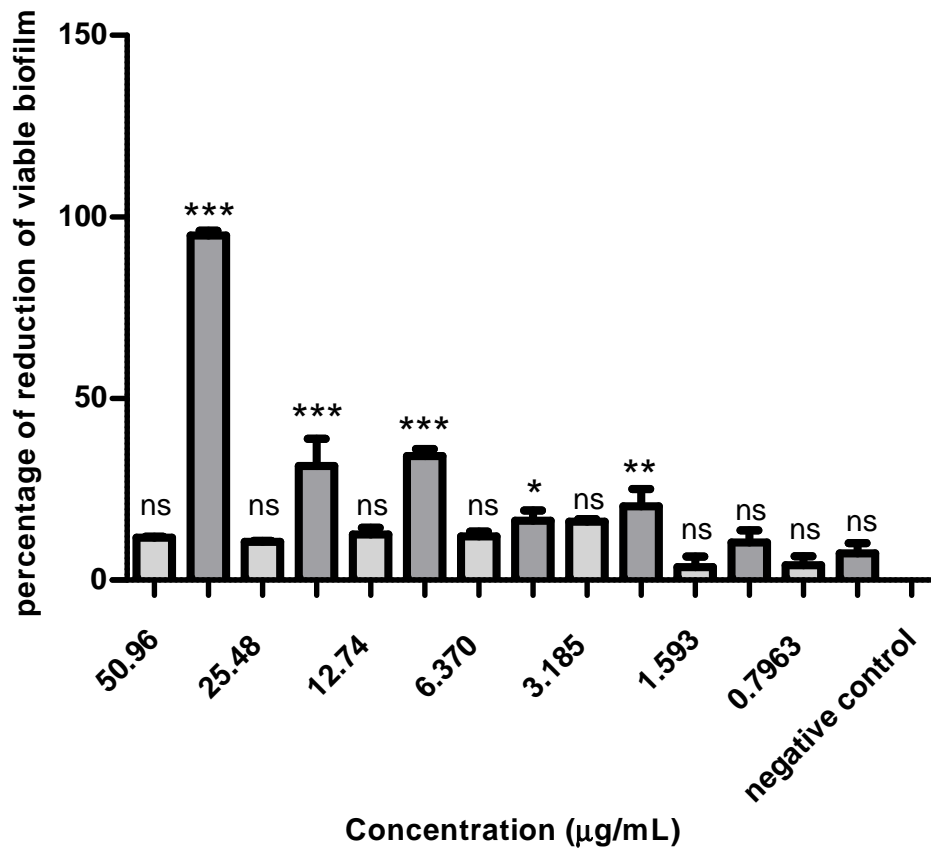
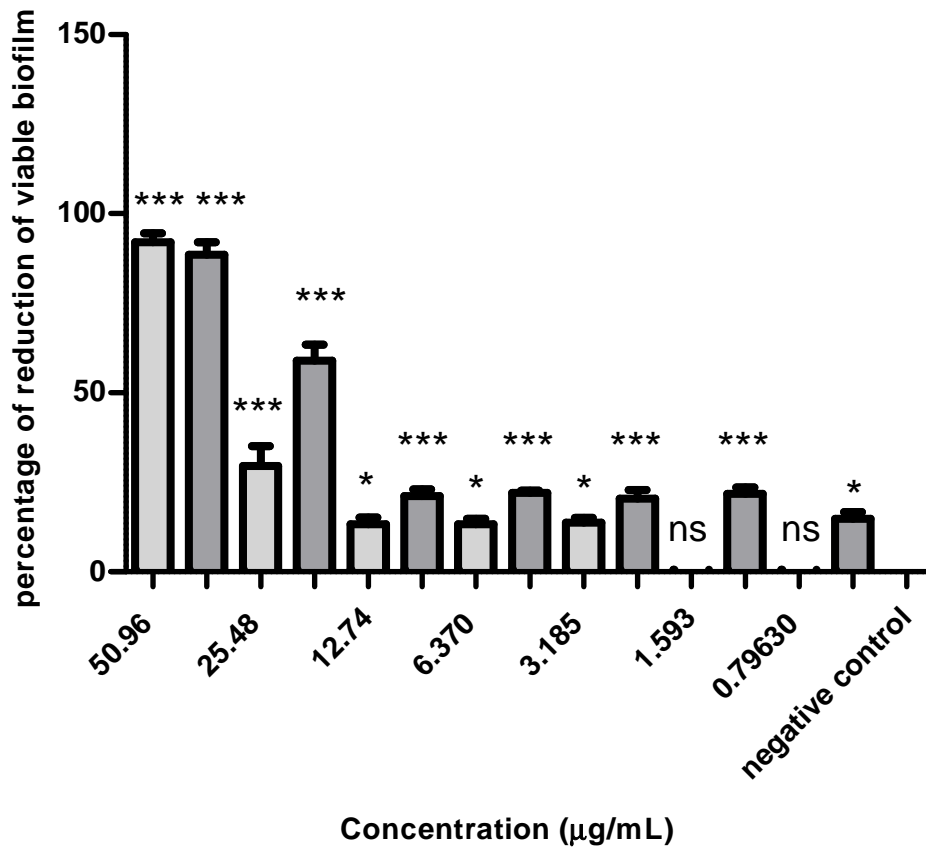**Figure 43** Percentage reduction of mature 24 h *Pseudomonas aeruginosa* (PAO1) biofilm after 24 h incubation with AgNPs and AgNPs plus utilizing an Alamar Blue assay. Results are displayed as a mean of 4 replicates. Key: AgNPs light gray, AgNPs plus dark gray NS = no significant difference (P ≥ 0.05), * P < 0.05, ** P < 0.01, *** P < 0.001, **** P <0.0001 significant difference between AgNPs and AgNPS plus at each concentration of and the negative control PBS (no AgNPs and no AgNPs plus).
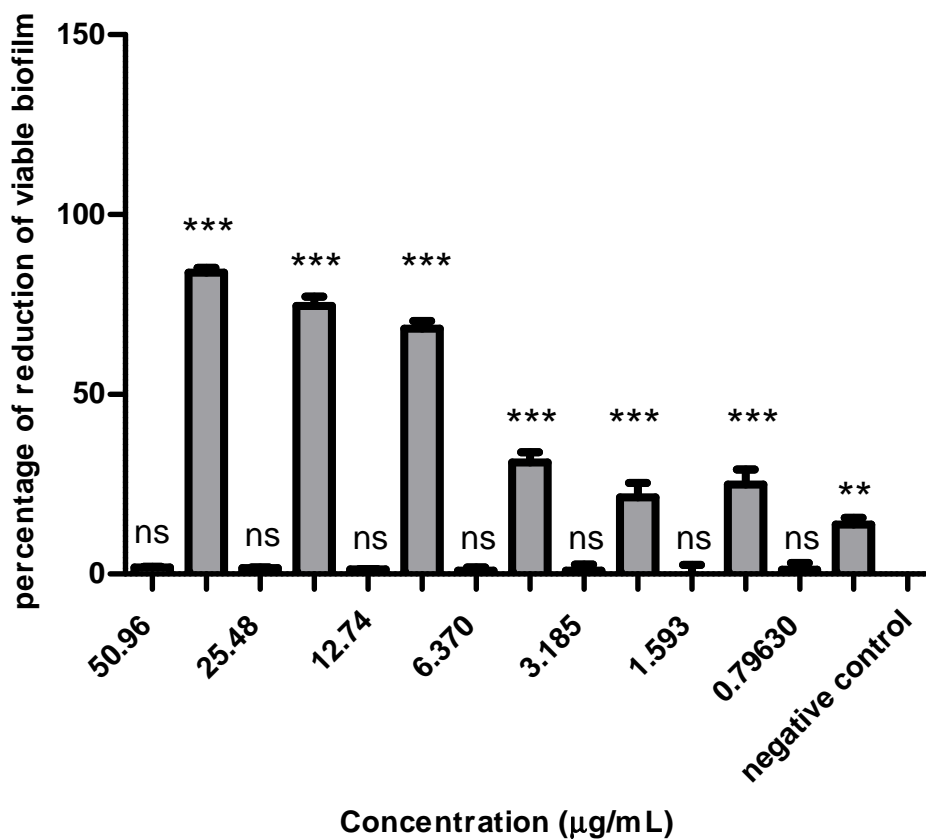
Figure 44 Percentage reduction of mature 24 h *Staphylococcus epidermidis* (ATCC 35984) biofilm after 24 h incubation with AgNPs and AgNPs plus utilizing an Alamar Blue assay. Results are displayed as a mean of 4 replicates. Key: AgNPs light gray, AgNPs plus dark gray NS = no significant difference (P ≥ 0.05), * P < 0.05, ** P < 0.01, *** P < 0.001, **** P <0.0001 significant difference between AgNPs and AgNPs plus at each concentration and the negative control PBS (no AgNPs and no AgNPs plus).

Figure 45 Percentage reduction of mature 24 h *Staphylococcus aureus* (ATCC 29213) biofilm after 24 h incubation with AgNPs and AgNPs plus utilizing an alamar Blue assay. Results are displayed as a mean of 4 replicates. Key: AgNPs light gray, AgNPs plus dark gray NS = no significant difference (P ≥ 0.05), * P < 0.05, ** P < 0.01, *** P < 0.001, **** P <0.00,1 significant difference between AgNPs and AgNPs plus at each concentration and the negative control PBS (no AgNPs and no AgNPs plus).
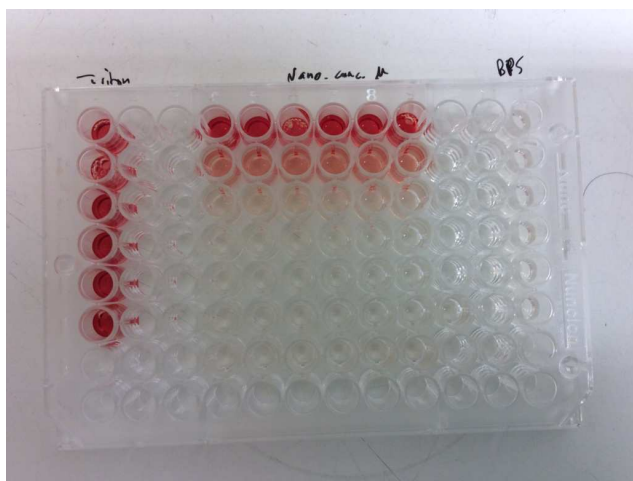
3.3.3.5. Haemolysis Assay

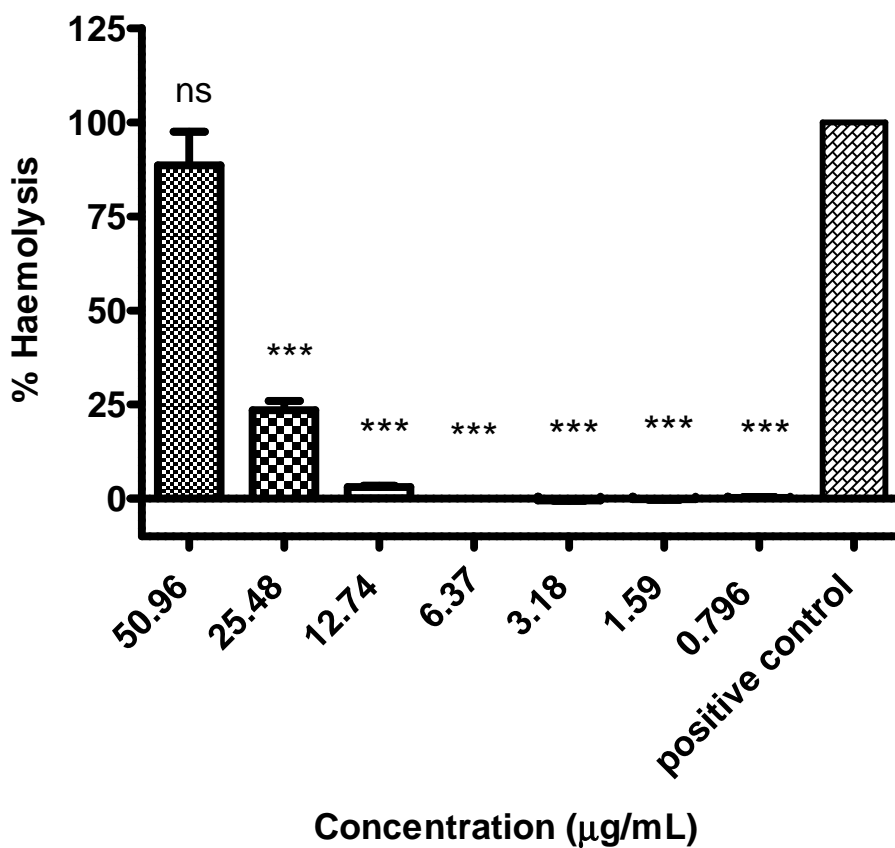**Figure 46** 96-well microtitre plate used during haemolysis assay .

Figure 47 Percentage haemolysis of the AgNPs against equine erythrocytes. Each value is expressed as the mean of six replicates incubated at 37 °C for 1 h. NS = no significant difference ($P \geq 0.05$), * $P < 0.05$, ** $P < 0.01$, *** $P < 0.001$, **** $P < 0.0001$ significant difference between AgNPs and the positive control (100% haemolysis).

To evaluate the potential of AgNPs to cause cellular toxicity, the ability of a range concentration of AgNPs to cause lysis of equine erythrocytes was assayed by colorimetric haemolysis assay, the results of which are shown in **Figure 47**. AgNPs exhibited significant haemolysis at the highest concentration tested (50.96 µg/mL), whereas treatment of erythrocytes with a reduced concentration (25.48 µg/mL) show a low haemolytic activity (24±6 %). Mostly, we can observe a decreasing of haemolytic activity at decreasing of concentration of AgNPs. This indicated that AgNPs could be safely used at its MIC values for all organism tested in this study.

3.3.4 Conclusions

UV-Vis spectroscopy shows that AgNPs remains stable in presence of the peptide and suggested the coating of AgNPs with the peptide by means of formation of S-Ag bounds between thiolic residues of Cys monomers in the peptide.

The antimicrobial activity (MIC/MBC values) of the AgNPs and AgNPs plus against different pathogenic micro-organisms have been evaluated. AgNPs exhibit an activity for both Gram-negative bacteria strains investigated (*E. coli* and *P. aureginosa*). They even show an antimicrobial activity against Gram-positive bacteria *S. epidermidis*, but don't exhibit activity against *S. aureus*. However AgNPs plus not only exert an antimicrobial broad-spectrum activity against the whole range of organism tested, but also their MIC values are lower than MIC of "plane" AgNPs tested. This effect could be explained by a synergic effect between AgNPs and antimicrobial peptide, and we are planning to investigate this in the immediate future.

The ability of AgNPs and AgNPs plus to exert antibiofilm activity have been tested against the same four species of bacteria, which are associated with biofilm growth responsible of biomaterial related infection: Gram-negative pathogens (*E. coli P. aeruginosa)* and Gram-positive pathogens (*S. epidermidis* and *S. aureus)*. AgNPs displayed the most significant antibiofilm activity against *E. coli* strains (complete removal) when used at the higher concentration tested, whereas they do not show any significant effect towards *P. aeruginosa* biofilm. In addition, AgNPs exhibit a significant antimicrobial activity against *S. epidermidis* (92.01%), in the meanwhile they do not display a significant antibacterial activity against *S. aureus.* On the other side, for AgNPs plus we can observe significant reduction for all species of biofilm studied. Particularly, AgNPs plus show the most significant destruction of *P. aeruginosa* biofilm.

Moreover, to evaluate the risk of AgNPs to cause cellular toxicity, we tested the ability of a range concentration of AgNPs to cause lysis of equine erythrocytes, using a colorimetric haemolysis assay. AgNPs exhibited significant haemolysis at the highest concentration tested, whereas treatment of erythrocytes with a lesser concentration show a low haemolytic activity (24±6 %): we can observe a decreasing of haemolytic activity with the decreasing of concentration of AgNPs. This fact suggests that AgNPs plus could probably be safely used at their MIC values for all organism tested in this study, as these concentrations are lower than concentrations causing significant haemolysis. A careful investigation of health risks connected to concentration of AgNPs plus should be completed.

CHAPTER 4: CONCLUSIONS

Conclusions relating to each one of the parts of the work reported in this thesis can be found at the end of each chapter which describes the investigation (see **Paragraphs 2.2.3**, **2.3.3**, **3.2.3** and **3.3.4**).

Anyway, the path I have followed with enthusiasm in these three years of PhD research deserves a few conclusive words.

Silver *allure* started in ancient times, it never came out of fashion, and is experiencing an exciting *renaissance* in the last years. One of the reasons of this renewed success comes from the wide revival of silver use for biomedical applications, propitiated by the explosion of nanotechnology.

In the first two parts of the work (**Chapters 2.2** and **2.3**), the (nowadays) classical AgNPs antibacterial action was coupled with the innovative photothermal action, which is peculiar of anisotropical nano-objects (nanoplates), which can be tailored to fulfill the desired features. In chapter 2.4 we also showed how these kinds of new materials can be used for a completely different task, i.e. for the realization of prototypes of SERS sensing chips.

In the following chapter, we started from the consideration that green synthesis of AgNPs has been one of the most investigated nanotechnology in the last decade, while wound healing properties of AgNPs has begun to gain attention only very recently: we demonstrated (**Chapter 3.2**) that the two approaches can be coupled to start to build a new class of powerful pharmaceutical preparations.

Going back to antibacterial applications, a promising novelty comes from the use of Antimicrobial peptides (AMPs): preliminary investigations conducted during my research period in Belfast (**Chapter 3.3**) seem to indicate that a synergy between AMPs and AgNPs is possible and fruitful.

To conclude, learning from the lessons of Prof. Feynman, I believe that in this work it was demonstrated that as expected "there is plenty of room at the bottom". In the same time silver related nanotechnologies are showing that there is a plethora of new possible applications at the top.

Acknowledgement